The Institution of Engineering and Technology

Model Predictive Control for Microgrids

From power electronic converters to energy management

Jiefeng Hu, Josep Guerrero and Syed Islam



IET ENERGY ENGINEERING SERIES 199

Model Predictive Control for Microgrids

Other volumes in this series:

Volume 1 **Power Circuit Breaker Theory and Design** C.H. Flurscheim (Editor)

Volume 4 **Industrial Microwave Heating** A.C. Metaxas and R.J. Meredith

Volume 7 **Insulators for High Voltages** J.S.T. Looms

Volume 8 **Variable Frequency AC Motor Drive Systems** D. Finney

Volume 10 **SF6 Switchgear** H.M. Ryan and G.R. Jones

Volume 11 **Conduction and Induction Heating** E.J. Davies

Volume 13 **Statistical Techniques for High Voltage Engineering** W. Hauschild and W. Mosch

Volume 14 **Uninterruptible Power Supplies** J. Platts and J.D. St Aubyn (Editors)

Volume 15 **Digital Protection for Power Systems** A.T. Johns and S.K. Salman

Volume 16 **Electricity Economics and Planning** T.W. Berrie

Volume 18 **Vacuum Switchgear** A. Greenwood

Volume 19 **Electrical Safety: a guide to causes and prevention of hazards** J. Maxwell Adams

Volume 21 **Electricity Distribution Network Design, 2nd Edition** E. Lakervi and E.J. Holmes

Volume 22 **Artificial Intelligence Techniques in Power Systems** K. Warwick, A.O. Ekwue and R. Aggarwal (Editors)

Volume 24 **Power System Commissioning and Maintenance Practice** K. Harker

Volume 25 **Engineers' Handbook of Industrial Microwave Heating** R.J. Meredith

Volume 26 **Small Electric Motors** H. Moczala *et al.*

Volume 27 **AC-DC Power System Analysis** J. Arrillaga and B.C. Smith

Volume 29 **High Voltage Direct Current Transmission, 2nd Edition** J. Arrillaga

Volume 30 **Flexible AC Transmission Systems (FACTS)** Y-H. Song (Editor)

Volume 31 **Embedded generation** N. Jenkins *et al.*

Volume 32 **High Voltage Engineering and Testing, 2nd Edition** H.M. Ryan (Editor)

Volume 33 **Overvoltage Protection of Low-Voltage Systems, Revised Edition** P. Hasse

Volume 36 **Voltage Quality in Electrical Power Systems** J. Schlabbach *et al.*

Volume 37 **Electrical Steels for Rotating Machines** P. Beckley

Volume 38 **The Electric Car: Development and future of battery, hybrid and fuel-cell cars** M. Westbrook

Volume 39 **Power Systems Electromagnetic Transients Simulation** J. Arrillaga and N. Watson

Volume 40 **Advances in High Voltage Engineering** M. Haddad and D. Warne

Volume 41 **Electrical Operation of Electrostatic Precipitators** K. Parker

Volume 43 **Thermal Power Plant Simulation and Control** D. Flynn

Volume 44 **Economic Evaluation of Projects in the Electricity Supply Industry** H. Khatib

Volume 45 **Propulsion Systems for Hybrid Vehicles** J. Miller

Volume 46 **Distribution Switchgear** S. Stewart

Volume 47 **Protection of Electricity Distribution Networks, 2nd Edition** J. Gers and E. Holmes

Volume 48 **Wood Pole Overhead Lines** B. Wareing

Volume 49 **Electric Fuses, 3rd Edition** A. Wright and G. Newbery

Volume 50 **Wind Power Integration: Connection and system operational aspects** B. Fox *et al.*

Volume 51 **Short Circuit Currents** J. Schlabbach

Volume 52 **Nuclear Power** J. Wood

Volume 53 **Condition Assessment of High Voltage Insulation in Power System Equipment** R.E. James and Q. Su

Volume 55 **Local Energy: Distributed generation of heat and power** J. Wood

Volume 56 **Condition Monitoring of Rotating Electrical Machines** P. Tavner, L. Ran, J. Penman and H. Sedding

Volume 57 **The Control Techniques Drives and Controls Handbook, 2nd Edition** B. Drury

Volume 58 **Lightning Protection** V. Cooray (Editor)

Volume 59 **Ultracapacitor Applications** J.M. Miller

Volume 62 **Lightning Electromagnetics** V. Cooray

Volume 63 **Energy Storage for Power Systems, 2nd Edition** A. Ter-Gazarian

Volume 65 **Protection of Electricity Distribution Networks, 3rd Edition** J. Gers

Volume 66 **High Voltage Engineering Testing, 3rd Edition** H. Ryan (Editor)

Volume 67 **Multicore Simulation of Power System Transients** F.M. Uriate

Volume 68 **Distribution System Analysis and Automation** J. Gers

Volume 69 **The Lightening Flash, 2nd Edition** V. Cooray (Editor)

Volume 70 **Economic Evaluation of Projects in the Electricity Supply Industry, 3rd Edition** H. Khatib

Volume 72 **Control Circuits in Power Electronics: Practical issues in design and implementation** M. Castilla (Editor)

Volume 73 **Wide Area Monitoring, Protection and Control Systems: The enabler for Smarter Grids** A. Vaccaro and A. Zobaa (Editors)

Volume 74 **Power Electronic Converters and Systems: Frontiers and applications** A. M. Trzynadlowski (Editor)

Volume 75 **Power Distribution Automation** B. Das (Editor)

Volume 76 **Power System Stability: Modelling, analysis and control** B. Om P. Malik

Volume 78 **Numerical Analysis of Power System Transients and Dynamics** A. Ametani (Editor)

Volume 79 **Vehicle-to-Grid: Linking electric vehicles to the smart grid** J. Lu and J. Hossain (Editors)

Volume 81 **Cyber-Physical-Social Systems and Constructs in Electric Power Engineering** S. Suryanarayanan, R. Roche and T.M. Hansen (Editors)

Volume 82 **Periodic Control of Power Electronic Converters** F. Blaabjerg, K.Zhou, D. Wang and Y. Yang

Volume 86 **Advances in Power System Modelling, Control and Stability Analysis** F. Milano (Editor)

Volume 87 **Cogeneration: Technologies, Optimisation and Implentation** C. A. Frangopoulos (Editor)

Volume 88 **Smarter Energy: from Smart Metering to the Smart Grid** H. Sun, N. Hatziargyriou, H. V. Poor, L. Carpanini and M. A. Sánchez Fornié (Editors)

Volume 89 **Hydrogen Production, Separation and Purification for Energy** A. Basile, F. Dalena, J. Tong and T.N.Veziroğlu (Editors)

Volume 90 **Clean Energy Microgrids** S. Obara and J. Morel (Editors)

Volume 91 **Fuzzy Logic Control in Energy Systems with Design Applications in Matlab/Simulink®** İ. H. Alta

Volume 92 **Power Quality in Future Electrical Power Systems** A. F. Zobaa and S. H. E. A. Aleem (Editors)

Volume 93 **Cogeneration and District Energy Systems: Modelling, Analysis and Optimization** M. A. Rosen and S. Koohi-Fayegh

Volume 94 **Introduction to the Smart Grid: Concepts, technologies and evolution** S.K. Salman

Volume 95 **Communication, Control and Security Challenges for the Smart Grid** S.M. Muyeen and S. Rahman (Editors)

Volume 96 **Industrial Power Systems with Distributed and Embedded Generation** R Belu

Volume 97 **Synchronized Phasor Measurements for Smart Grids** M.J.B. Reddy and D.K. Mohanta (Editors)

Volume 98 **Large Scale Grid Integration of Renewable Energy Sources** A. Moreno-Munoz (Editor)

Volume 100 **Modeling and Dynamic Behaviour of Hydropower Plants** N. Kishor and J. Fraile-Ardanuy (Editors)

Volume 101 **Methane and Hydrogen for Energy Storage** R. Carriveau and D. S-K. Ting

Volume 104 **Power Transformer Condition Monitoring and Diagnosis** A. Abu-Siada (Editor)

Volume 106 **Surface Passivation of Industrial Crystalline Silicon Solar Cells** J. John (Editor)

Volume 107 **Bifacial Photovoltaics: Technology, applications and economics** J. Libal and R. Kopecek (Editors)

Volume 108 **Fault Diagnosis of Induction Motors** J. Faiz, V. Ghorbanian and G. Joksimović

Volume 110 **High Voltage Power Network Construction** K. Harker

Volume 111 **Energy Storage at Different Voltage Levels: Technology, integration, and market aspects** A.F. Zobaa, P.F. Ribeiro, S.H.A. Aleem and S.N. Afifi (Editors)

Volume 112 **Wireless Power Transfer: Theory, Technology and Application** N.Shinohara

Volume 114 **Lightning-Induced Effects in Electrical and Telecommunication Systems** Y. Baba and V. A. Rakov

Volume 115 **DC Distribution Systems and Microgrids** T. Dragičević, F.Blaabjerg and P. Wheeler

Volume 116 **Modelling and Simulation of HVDC Transmission** M. Han (Editor)

Volume 117 **Structural Control and Fault Detection of Wind Turbine Systems** H.R. Karimi

Volume 119 **Thermal Power Plant Control and Instrumentation: The control of boilers and HRSGs, 2nd Edition** D. Lindsley, J. Grist and D. Parker

Volume 120 **Fault Diagnosis for Robust Inverter Power Drives** A. Ginart (Editor)

Volume 121 **Monitoring and Control using Synchrophasors in Power Systems with Renewables** I. Kamwa and C. Lu (Editors)

Volume 123 **Power Systems Electromagnetic Transients Simulation, 2nd Edition** N. Watson and J. Arrillaga

Volume 124 **Power Market Transformation** B. Murray

Volume 125 **Wind Energy Modeling and Simulation Volume 1: Atmosphere and plant** P.Veers (Editor)

Volume 126 **Diagnosis and Fault Tolerance of Electrical Machines, Power Electronics and Drives** A.J. M. Cardoso

Volume 128 **Characterization of Wide Bandgap Power Semiconductor Devices** F. Wang, Z. Zhang and E.A. Jones

Volume 129 **Renewable Energy from the Oceans: From wave, tidal and gradient systems to offshore wind and solar** D. Coiro and T. Sant (Editors)

Volume 130 **Wind and Solar Based Energy Systems for Communities** R. Carriveau and D. S-K. Ting (Editors)

Volume 131 **Metaheuristic Optimization in Power Engineering** J. Radosavljević

Volume 132 **Power Line Communication Systems for Smart Grids** I.R.S Casella and A. Anpalagan

Volume 139 **Variability, Scalability and Stability of Microgrids** S. M. Muyeen, S. M. Islam and F. Blaabjerg (Editors)

Volume 145 **Condition Monitoring of Rotating Electrical Machines** P. Tavner, L. Ran, C. Crabtree

Volume 146 **Energy Storage for Power Systems, 3rd Edition** A.G. Ter-Gazarian

Volume 147 **Distribution Systems Analysis and Automation 2nd Edition** J. Gers

Volume 152 **Power Electronic Devices: Applications, failure mechanisms and reliability** F Iannuzzo (Editor)

Volume 153 **Signal Processing for Fault Detection and Diagnosis in Electric Machines and Systems** Mohamed Benbouzid (Editor)

Volume 155 **Energy Generation and Efficiency Technologies for Green Residential Buildings** D. Ting and R. Carriveau (Editors)

Volume 156 **Lithium-ion Batteries Enabled by Silicon Anodes** Chunmei Ban and Kang Xu (Editors)

Volume 157 **Electrical Steels, 2 Volumes** A. Moses, K. Jenkins, Philip Anderson and H. Stanbury

Volume 158 **Advanced Dielectric Materials for Electrostatic Capacitors** Q Li (Editor)

Volume 159 **Transforming the Grid Towards Fully Renewable Energy** O. Probst, S. Castellanos and R. Palacios (Editors)

Volume 160 **Microgrids for Rural Areas: Research and case studies** R.K. Chauhan, K. Chauhan and S.N. Singh (Editors)

Volume 166 **Advanced Characterization of Thin Film Solar Cells** N Haegel and M Al-Jassim (Editors)

Volume 167 **Power Grids with Renewable Energy** Storage, integration and digitalization A. S. Sallam and O. P. Malik

Volume 171 **Utility-scale Wind Turbines and Wind Farms** A. Vasel-Be-Hagh and D. S.-K. Ting

Volume 172 **Lighting interaction with Power Systems, 2 volumes** A. Piantini (Editor)

Volume 193 **Overhead Electric Power Lines: Theory and practice** S. Chattopadhyay and A. Das

Volume 905 **Power system protection, 4 volumes**

Model Predictive Control for Microgrids

From power electronic converters to energy management

Jiefeng Hu, Josep Guerrero and Syed Islam

The Institution of Engineering and Technology

Published by The Institution of Engineering and Technology, London, United Kingdom

The Institution of Engineering and Technology is registered as a Charity in England & Wales (no. 211014) and Scotland (no. SC038698).

© The Institution of Engineering and Technology 2021

First published 2021

This publication is copyright under the Berne Convention and the Universal Copyright Convention. All rights reserved. Apart from any fair dealing for the purposes of research or private study, or criticism or review, as permitted under the Copyright, Designs and Patents Act 1988, this publication may be reproduced, stored or transmitted, in any form or by any means, only with the prior permission in writing of the publishers, or in the case of reprographic reproduction in accordance with the terms of licences issued by the Copyright Licensing Agency. Enquiries concerning reproduction outside those terms should be sent to the publisher at the undermentioned address:

The Institution of Engineering and Technology
Michael Faraday House
Six Hills Way, Stevenage
Herts, SG1 2AY, United Kingdom

www.theiet.org

While the authors and publisher believe that the information and guidance given in this work are correct, all parties must rely upon their own skill and judgement when making use of them. Neither the author nor publisher assumes any liability to anyone for any loss or damage caused by any error or omission in the work, whether such an error or omission is the result of negligence or any other cause. Any and all such liability is disclaimed.

The moral rights of the author to be identified as author of this work have been asserted by him in accordance with the Copyright, Designs and Patents Act 1988.

British Library Cataloguing in Publication Data
A catalogue record for this product is available from the British Library

ISBN 978-1-83953-397-6 (hardback)
ISBN 978-1-83953-398-3 (PDF)

Typeset in India by Exeter Premedia Services Private Limited
Printed in the UK by CPI Group (UK) Ltd, Croydon

Contents

List of figures
List of tables
About the authors
Abbreviations

1 Introduction
1.1 Microgrid fundamentals
1.2 Operation considerations
1.2.1 Power sharing
1.2.2 Power balancing
1.2.3 Power quality
1.2.4 Seamless mode transition
1.2.5 System stability
1.3 Key technologies and challenges
1.3.1 New semiconductor devices
1.3.2 Power electronic converters and control
1.3.3 Renewable intermittency
1.3.4 Lack of systematic approaches
1.3.5 Large-scale grid integration and its impact on the main grid
1.3.6 Energy storage
1.3.7 Smart sensors
1.3.8 Information and communication technology
References

2 Power electronic converters and control
2.1 Power electronic converters in energy conversion
2.1.1 DC–DC converters
2.1.2 DC–AC converters (inverters)
2.1.2.1 Grid-forming inverters
2.1.2.2 Grid-feeding inverters
2.1.2.3 Grid-supporting inverter
2.2 Control of a single converter
2.2.1 Voltage-oriented control

2.2.2 Direct control
2.2.3 Fuzzy logic control
2.2.4 Sliding mode control
2.2.5 Predictive control
2.2.5.1 Deadbeat-based predictive control
2.2.5.2 VPC
2.2.5.3 MPC
2.3 Control of parallel inverters
2.3.1 Centralized control
2.3.2 Circular chain control
2.3.3 Master-slave control
2.3.4 Average load sharing
2.3.5 Droop control
References
Further reading

3 Distributed renewable power generation
3.1 Distributed generation
3.2 Wind power generation
3.2.1 Wind turbine characteristics
3.2.2 Constant speed constant frequency system
3.2.3 VSCF system
3.2.3.1 Wound field synchronous generator
3.2.3.2 Permanent-magnet synchronous generator
3.2.3.3 Doubly fed induction generator
3.2.3.4 Squirrel cage induction generator
3.2.4 Recent advances in wind power generation
3.3 Solar PVs generation
3.3.1 Principle and configuration of PV systems
3.3.2 Power converters and recent advance of MPC for PV systems
3.3.2.1 Single-phase single-stage
3.3.2.2 Single-phase multiple-stage
3.3.2.3 Three-phase single-stage
3.3.2.4 MPPT control of PV system
3.3.2.5 Grid-side inverter control of PV system
References
Further reading

4 Modeling and hierarchical control of microgrids
4.1 Modeling of MGs
4.2 Hierarchical control architecture of MGs
4.2.1 Primary control
4.2.2 Secondary control
4.2.2.1 Centralized secondary control
4.2.2.2 Distributed secondary control

4.2.2.3 Decentralized secondary control
4.2.3 Tertiary control
References
Further reading

5 MPC of PV-wind-storage microgrids
5.1 Introduction
5.2 Modeling of PV system and its control structure
5.3 Modeling of wind turbine system and its control structure
5.4 Modeling of ESS and its control structure
5.5 Modeling of the AC subgrid and its control structure
5.6 System level control
5.6.1 Mode 1 operation
5.6.2 Mode 2 operation
5.6.2.1 Low wind speed, low solar irradiation, and heavy load
5.6.2.2 High wind speed, high solar irradiation, and light load
5.6.3 Mode 3 operation
5.7 Case studies
5.7.1 Fluctuation output from renewable energy
5.7.2 Grid-connected operation
5.7.3 Islanded operation
5.7.4 Grid-synchronization and connection
5.8 Conclusion
References
Further reading

6 MPC of PV-ESS MGs with voltage support
6.1 Introduction
6.2 Model predictive power control scheme
6.3 Voltage support
6.4 Verification
6.4.1 Flexible power injection from PV-ESS
6.4.2 Grid voltage support by PV-ESS
6.5 Conclusion
References
Further reading

7 MPC of parallel PV-ESS microgrids
7.1 Introduction
7.2 MPCC for solar PVs
7.3 MPPC of BESS DC–DC converters
7.4 MPVC of parallel inverters
7.5 Verification
7.5.1 MPPT of PV system

7.5.2 Charging and discharging processes of BESS
7.5.3 Power sharing between parallel inverters
7.6 Conclusion
References
Further reading

8 MPC of MGs with secondary restoration capability
8.1 Background and system configuration
8.2 Washout filter-based power-sharing method
8.3 Improved model predictive voltage control scheme
8.4 Results
8.5 Conclusion
References
Further reading

9 MPC of MGs with tertiary power flow optimization
9.1 Tertiary control of MGs and MPC
9.2 MPC for economic dispatch and optimal power flow in MGs
9.3 MPC for networked MGs
9.4 Future trend
9.4.1 New mathematical formulation
9.4.2 Holistic and intelligent MPC approaches
9.4.3 MPC in DC MGs
9.4.4 Distributed and decentralized control
9.5 Conclusion
References
Further reading

Index

List of figures

Figure 1.1 A typical MG structure
Figure 1.2 A laboratory MG integrated with DGs and loads
Figure 1.3 AC-coupled MG
Figure 1.4 DC-coupled MG
Figure 1.5 AC–DC-coupled MG
Figure 1.6 A DC MG
Figure 1.7 Networked MGs. (a) Interconnected via a common power highway, (b) interconnected via a sparse power network
Figure 2.1 Control methods of power converters
Figure 2.2 Block diagram of VOC
Figure 2.3 Schematic diagram of the conventional linear control of an inverter
Figure 2.4 Block diagram of DPC
Figure 2.5 Voltage vectors and the sector division
Figure 2.6 Block diagram of fuzzy logic control
Figure 2.7 Block diagram of SMC
Figure 2.8 Block diagram of deadbeat-based predictive control
Figure 2.9 Structure of an AC–DC conversion system
Figure 2.10 Experimental results of AC–DC conversion using SDPC: (a) DC-link voltage, active power, and reactive power, (b) grid voltage and three-phase line currents
Figure 2.11 Experimental results of AC–DC conversion using deadbeat-based predictive control: (a) DC-link voltage, active power, and reactive power, (b) grid voltage and three-phase line currents
Figure 2.12 Block diagram of VPC
Figure 2.13 Schematic illustration of a symmetric 3+3 vectors sequence
Figure 2.14 Active and reactive power derivatives against the input voltage vector position
Figure 2.15 The schematic diagram of the improved VPC
Figure 2.16 Comparison of system performance with P^* = 900 W and Q^* = 0 VAR. (a) SDPC, (b) conventional VPC, (c) improved VPC

Figure 2.17 Block diagram of MPC
Figure 2.18 Experimental results of AC–DC conversion using SDPC. (a) DC-link voltage, active power, and reactive power, (b) power source voltage and line currents, (c) harmonic spectrum of line current
Figure 2.19 Experimental results of AC–DC conversion using MPC. (a) DC-link voltage, active power, and reactive power, (b) power source voltage and line currents, (c) harmonic spectrum of line current
Figure 2.20 Schematic of the FCS-MPC applied to inverters
Figure 2.21 System-level MPC
Figure 2.22 Block diagram of centralized control
Figure 2.23 Block diagram of 3C scheme
Figure 2.24 Block diagram of master-slave control
Figure 2.25 Block diagram of ALS control, (a) average current sharing, (b) average power sharing
Figure 2.26 Block diagram of the conventional droop control
Figure 3.1 Configurations of DG systems. (a) Wind energy conversion system, (b) solar PV system
Figure 3.2 Wind energy conversion system with power flow path
Figure 3.3 Example of cost distribution of a wind energy conversion system
Figure 3.4 Turbine output power characteristics for different wind speeds
Figure 3.5 CSCF system with SCIG
Figure 3.6 WFSG system
Figure 3.7 PMSG system
Figure 3.8 Doubly fed wound induction generator system
Figure 3.9 BDFTSIG system
Figure 3.10 SCIG system
Figure 3.11 Schematic illustration of MPPT strategies: (a) wind speed measurement, (b) power versus rotor-speed characteristic
Figure 3.12 Solar PV output in two different days
Figure 3.13 Current versus voltage characteristic of a solar PV module
Figure 3.14 Centralized PV configuration
Figure 3.15 PV configuration with individual string inverters
Figure 3.16 PV configuration with module inverters
Figure 3.17 Single-phase single-stage PV power electronics
Figure 3.18 Single-phase multiple-stage PV power electronics
Figure 3.19 Three-phase PV topology with line-frequency transformer
Figure 3.20 Example of a control scheme for PV systems
Figure 4.1 Equivalent circuit of a parallel-inverters-based MG
Figure 4.2 Hierarchical control structure of MGs

Figure 4.3 Illustration of droop mechanism in MG primary control. (a) *P–f* droop and (b) *Q–V* droop
Figure 4.4 Primary control for parallel inverters
Figure 4.5 Three main structures of secondary control: (a) centralized secondary control, (b) distributed secondary control, and (c) decentralized secondary control
Figure 5.1 A hybrid AC–DC MG
Figure 5.2 A solar PV power electronic system
Figure 5.3 Output characteristics of a solar module
Figure 5.4 Wind power system structure
Figure 5.5 Control scheme of the generator-side converter
Figure 5.6 ESS
Figure 5.7 Control of the ESS
Figure 5.8 AC side of the MG
Figure 5.9 Proposed control for the interlinking converter, (a) MPPC and (b) MPVC [4]
Figure 5.10 Energy management—system level control
Figure 5.11 PMSG performance under wind speed variation
Figure 5.12 PV output under variable solar irradiation
Figure 5.13 MG performance under variable wind power and load demand condition in grid-connected mode. The waveforms from top to bottom are (a) wind power, (b) battery power, (c) total load demand, (d) power exchanged between micro and utility grid, (e) current flow between micro and utility grid, and (f) DC-bus voltage
Figure 5.14 MG performance under variable PV power and load demand condition in islanded mode. The waveforms from top to bottom are (a) PV power, (b) battery power, (c) total load demand, (d) SOC, (e) AC-bus voltage, and (f) DC-bus voltage
Figure 5.15 MG performance in grid synchronization and connection
Figure 6.1 A PV-ESS configuration
Figure 6.2 Schematic diagram of the ESS
Figure 6.3 Equivalent circuits of (a) boost and (b) buck modes
Figure 6.4 Currents flowing in the MG
Figure 6.5 Block diagram of MPPC to control the DC–DC bidirectional converter [58]
Figure 6.6 AC-side of MG
Figure 6.7 Block diagram of MPPC for the DC–AC converter connected to the grid [58]
Figure 6.8 Single-line diagram of power flows
Figure 6.9 PV inverter active and reactive capacity

Figure 6.10 The performance of MPPC for DC–DC bidirectional converter under variable PV generation and load demand condition: (a) PV power, (b) battery power, (c) DC-bus voltage, (d) SOC
Figure 6.11 The performance of MPPC for grid-connected inverter under variable PV generation and load demand condition: (a) active power at PCC, (b) reactive power at PCC, (c) total load, (d) active power from grid, (e) grid current
Figure 6.12 VS performance of the proposed method. (a) Using active power flow control. (b) Using reactive power flow control
Figure 7.1 Topology of a PV-battery-based AC MG
Figure 7.2 Simplified schematic of the PV DC–DC boost converter
Figure 7.3 Simplified flowchart for selecting the optimal switching signal in MPCC-based DC–DC boost conversion
Figure 7.4 Block diagram of the combination of MPPT and MPCC to control the DC–DC boost converter
Figure 7.5 Illustration of the current flow within the system. (a) Charging process, (b) discharging process
Figure 7.6 Block diagram of MPPC to control buck-boost converters
Figure 7.7 Simplified flowchart for selecting the optimal switching signal in MPC-based buck-boost conversion
Figure 7.8 Block diagram of the combination of droop and MPVC for inverters [37]
Figure 7.9 Overall control strategy for the parallel PV-ESS MG
Figure 7.10 PV system performance under variations of solar irradiation and ambient temperature
Figure 7.11 Charging and discharging processes of BESS
Figure 7.12 Step response of DC-bus voltage when changing DC bus references
Figure 7.13 The DC-bus voltage under load variation and varying PV outputs
Figure 7.14 MG response to load variations
Figure 7.15 DG output voltage and current
Figure 8.1 A MG with PV-BESS and multiple converters
Figure 8.2 AC-subgrid circuitry
Figure 8.3 Voltage-tracking trajectory
Figure 8.4 Block diagram of the conventional overall control scheme
Figure 8.5 Proposed overall control strategy of inverters (improved MPVC and improved washout filter-based power-sharing strategy) [41]
Figure 8.6 Performance of the DC side of the MG using the proposed control strategy under varying solar irradiation and ambient temperature and variable load demand. (a) Solar irradiation, (b) ambient temperature, (c) electrical power generated by PVs, (d) DC-link

voltage by using MPPC scheme, (e) DC-link voltage using conventional cascaded loops control structure

Figure 8.7 Performance of AC side of the MG using the proposed control strategy. (a) DG1 active power output, (b) DG1 reactive power output, (c) DG1 frequency using proposed washout filter-based power-sharing method, (d) DG1 output voltages using proposed washout filter-based power-sharing method, (e) DG1 frequency using conventional droop control, (f) DG1 output voltage using conventional droop control

Figure 8.8 Voltage quality when the MG supplies linear loads [41]. (a) DG1 output voltage using improved cost function (8.25), (b) DG1 output voltage using conventional cost function (8.20)

Figure 8.9 Voltage quality when the MG supplies nonlinear loads [41]. (a) DG1 output voltage using improved cost function (8.25), (b) DG1 output voltage using conventional cost function (8.20)

Figure 9.1 Hierarchical control pyramid of a MG [3, 4]

Figure 9.2 Considerations in MG tertiary control

Figure 9.3 A MG structure with various DERs and different types of loads

Figure 9.4 Schematic illustration of the tertiary level MPC for MGs

Figure 9.5 Control objectives of the tertiary level MPC in MGs

Figure 9.6 System-level MPC

Figure 9.7 Hierarchical control architecture in [28]

Figure 9.8 Physical connection and digital communication of networked MGs

List of tables

Table 2.1 Quantitative comparison of DPC methods in experiment
Table 2.2 Improved vector selection of VPC
Table 3.1 Comparison of different VSCF wind generators
Table 5.1 Distributed generation and load parameters
Table 6.1 System parameters
Table 7.1 System parameters
Table 8.1 System parameters
Table 8.2 Load profile

About the authors

Jiefeng Hu is an associate professor in power electronics and smart microgrids, and the program coordinator (electrical engineering) of the School of Engineering, Information Technology and Physical Sciences at Federation University Australia. Previously, he was an assistant professor at The Hong Kong Polytechnic University, where he led an international team to develop renewable energy technologies for smart cities. He has published more than 100 research papers, and serves as editor/associate editor on prestigious IET and IEEE journals.

Josep Guerrero is a professor with the Department of Energy Technology, Aalborg University, Denmark. He is responsible for the Microgrid Research Program, and the founder and director of the Centre for Research on Microgrids (CROM). Prof. Guerrero's research interests focus on different microgrid aspects, including power electronics, distributed energy-storage systems, control, energy management, metreing and the use of the IoT. From 2014 to 2018 he was awarded a Highly Cited Researcher by Thomson Reuters.

Syed Islam is a professor and the dean for the School of Engineering, Information Technology and Physical Sciences at Federation University Australia. His awards include the Curtin University inaugural award for Research Development and two Sir John Madsen medals. He has published over 270 technical papers on condition monitoring of transformers, wind energy and smart power systems, and serves on prestigious committees and boards, and in editorial capacities of key journals.

Abbreviations

3C	Circular Chain Control
AC	Alternating Current
ALS	Average Load Sharing
BDFTSIG	Brushless Doubly Fed Twin Stator Induction Generator
BESS	Battery Energy Storage System
BS	Bypass Switch
CB	Circuit Breaker
CCS-MPC	Continuous Control Set MPC
CHP	Combined Heat and Power
CSCF	Constant Speed Constant Frequency
CSI	Current Source Inverter
DC	Direct Current
DER	Distributed Energy Resource
DFIG	Doubly-Fed Induction Generator
DG	Distributed Generation
DMPC	Distributed Model Predictive Control
DNO	Distribution Network Operator
DPC	Direct Power Control
DSVM	Discrete Space-vector Modulation
DTC	Direct Torque Control
DVR	Dynamic Voltage Restorer
EMS	Energy Management System
ESS	Energy Storage System
EV	Electric Vehicle
FACTS	Flexible AC Transmission System
FCS-MPC	Finite Control Set MPC
GCC	Global Central Controller
GMPF	Generalized Microgrid Power Flow
HEMS	Home Energy Management System

HV	high voltage
HVDC	High Voltage Direct Current
IoT	Internet of Things
KCL	Kirchhoff’s Current Law
KVL	Kirchhoff’s Voltage Law
LV	low voltage
MAS	Multi-agent System
MG	Microgrid
MGC	Microgrid cluster
MGCC	Microgrid Central Controller
MILP	Mixed-integer Linear Programming
MIMO	Multiple-input–multiple-output
MPC	Model Predictive Control
MPCC	Model Predictive Current Control
MPP	Maximum Power Point
MPPC	Model Predictive Power Control
MPPT	Maximum Power Point Tracking
MPVC	Model Predictive Voltage Control
MV	Medium Voltage
NPC	Neutral-Point-Clamped
NPP	Neutral Point Potentials
OLTC	On-load Tap Changer
PCC	Point of Common Coupling
PID	Proportional-integral-derivative
PLL	Phase-locked Loop
PMSG	Permanent Magnet Synchronous Generator
PV	Photovoltaics
PWM	Pulse Width Modulation
QCQP	Quadratically Constrained Quadratic Program
RES	Renewable energy sources
RLC	Resistor-inductor-capacitor
SCIG	Squirrel-Cage Induction Generator
SDPC	Switching Table-based Direct Power Control
SMC	Sliding Mode Control
SoC	State of Charge
SP	Smith Predictor
SPWM	Sinusoidal Pulse Width Modulation
STATCOM	Static Synchronous Compensator

STS	Static Transfer Switch
SVM	Space Vector Modulation
THD	Total Harmonic Distortion
TSO	Transmission System Operator
TSR	Tip-Speed Ratio
UPFC	Unified Power Flow Controller
UPS	Uninterruptable Power Supply
VC	Vector Control
VOC	Voltage Oriented Control
VPC	Vector-sequence-based Predictive Control
VS	Voltage Support
VSC	Voltage Source Converter
VSCF	Variable Speed Constant Frequency
VSI	Voltage Source Inverter
WFSG	Wound Field Synchronous Generator
WRIG	Wound-Rotor Induction Generator
ZSCC	Zero Sequence Circulating Current

Chapter 1
Introduction

This chapter gives a brief review of microgrid (MG) fundamentals and technical aspects. The advantages and challenges of MGs will be revealed. Their future forms and key technologies will also be discussed.

1.1 Microgrid fundamentals

The fast depletion of traditional fossil fuels and the urge for the reduction of greenhouse gas emission are the key factors driving the growing use of distributed generation (DG) units, including both renewable and nonrenewable energy sources such as solar photovoltaics (PVs) fuel cells, wind turbines, wave generators, and gas- or steam-powered combined heat and power (CHP) stations [1]. Meanwhile, traditional power grid is getting more and more stressed because of the ongoing increase in power demand, limited power delivery capability of the power network, and the costly reinforcement of the existing transmission-distribution lines [2]. In this context, the existing electrical power network is going through a major transformation from traditional centralized architecture to a decentralized and distributed form [3].

The basic units of the decentralized and distributed power grid are the aforementioned DGs. Such DGs, consisting of renewable energy sources (RESs) and energy storage systems (ESSs), provide electricity as individual power supplies for electric appliances. Among them, solar PV systems and wind turbines are the most popular DG types. In such an energy system, the major portion of the electrical power generated by a DG is consumed locally, and the surplus will be exported to the grid. If the load demand is larger than local generation, more power can be drawn from the grid. Besides, a DG can operate in islanded mode in which electrical power can continue to be supplied to local loads, similar to uninterruptible power supply devices. Despite the benefits provided by DGs, there are technical issues in actual applications on the degree to which DGs can be interconnected. The direct connection of DGs causes profound impacts on the traditional power distribution network, such as a decrease in reliability, stability, and power quality [4].

To explore a better alternative to realize the emerging potentials of DGs, a

new paradigm known as microgrids (MGs) has been proposed [5–7]. As the building blocks of smart grids, MGs have attracted much attention over the past decade. A MG is a local power system integrated with multiple DGs and the associated power electronic devices for power control and measurement, thus, to meet various load demands. Specifically, a MG is a cluster of local loads and DGs that can offer many merits over the existing power grid in terms of power autonomy and the ability to integrate renewable and nonrenewable energy sources. The main objectives of MGs are to (1) exploit renewable energy efficiently and at the same time to smooth out the intermittent output of RESs with appropriate control methods; (2) integrate various types of DGs into the power network effectively; (3) reduce the burden of the traditional power system and provide ancillary services to the existing power grid; (4) supply electrical power to remote areas where the utility power grid is not available. Figure 1.1 depicts a typical structure of a MG. It can be seen that various DGs and loads are connected to a common bus through their power electronic interfaces. Such DGs can be solar PVs, wind turbines, ESS, etc. The loads can be categorized into critical and noncritical forms. ESSs are usually used to absorb the surplus energy from power generators, while they will provide additional power to the loads when power demand is greater than power generation, thus playing a peak-load shifting role. By the proper arrangement of various power converters (direct current (DC)–DC, alternating current (AC)–AC, and AC–DC), common voltage buses can be established and maintained by the converter-interfaced DGs. A common voltage bus is also called a point of common coupling (PCC). The loads can be fed by the common bus, and the noncritical ones can be shed according to the command sent from the microgrid central controller (MGCC) [8]. The MGCC coordinates and dispatches the loads, DGs, and energy storage devices according to demand response and load management.

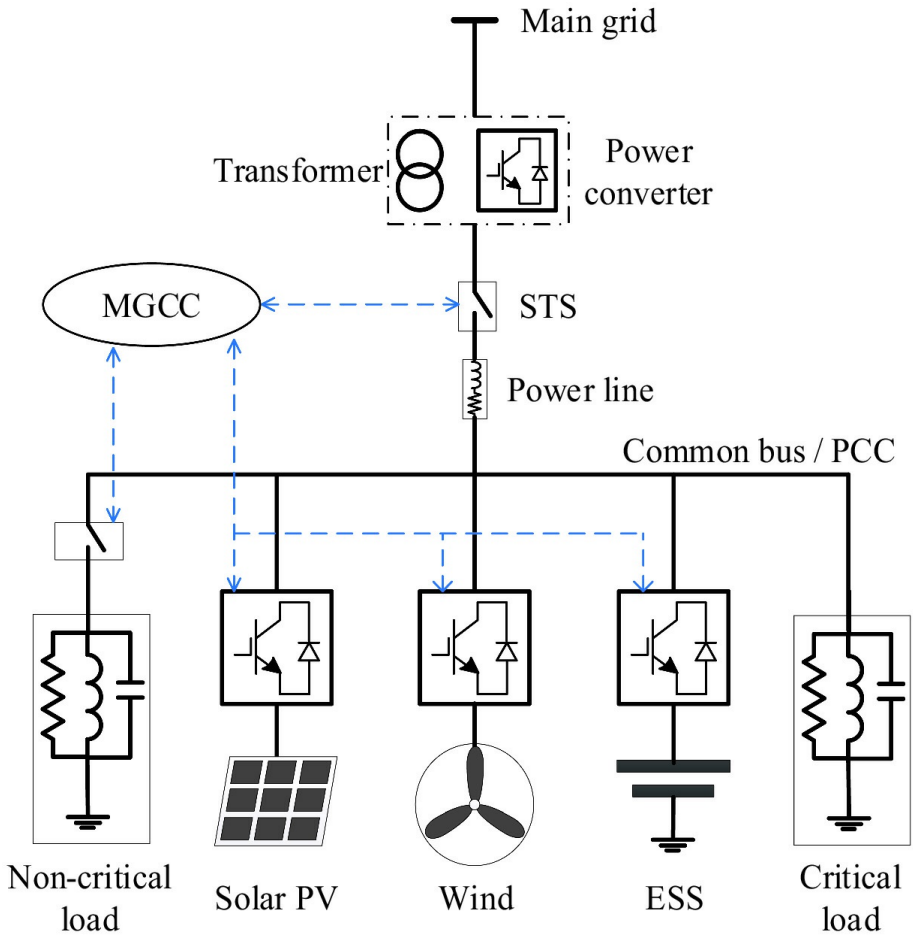


Figure 1.1 A typical MG structure

Figure 1.2 shows a laboratory MG, which consists of a 30 kW gas micro-turbine (MT), a 20 kW solar PV array, a programmable load bank (LB), and an electric motor, all connected to a common AC bus with a nominal line–line voltage of 415 V and nominal frequency of 50 Hz. Each series of PV panels in the array are connected in the form of a single string, with each string connected to a SMA Sunny Boy single-phase inverter. These inverters are then distributed evenly across the three-phase common AC bus. The gas MT is actually a synchronous generator driven by a MT via a gearbox ranged from 50 000 to 12 000 rpm. The generator supplies electric power to the common AC bus through a back-to-back converter. The high-frequency AC power generated by the synchronous generator is first rectified to DC and then converted to AC. Both the amplitude and the frequency of the MT system output voltage are controllable,

and it can supply customer-based-load requirements or can be used for standby, peak shaving, and cogeneration applications. In this work, when the MG is operating in islanded mode, the MT system is used to establish a stable common AC bus voltage and provided a voltage signal to which the PV inverters can synchronize to. The LB comprises a 63 kW resistive load, a 63 kVAR inductive load, and a 63 kVAR of capacitive load, which are arranged in a binary fashion. The control of the DGs, loads, and data acquisition is fulfilled through a supervisory control and data acquisition system. To design a proper controller for this MG, it is necessary to study the characteristic of each component of the MG.

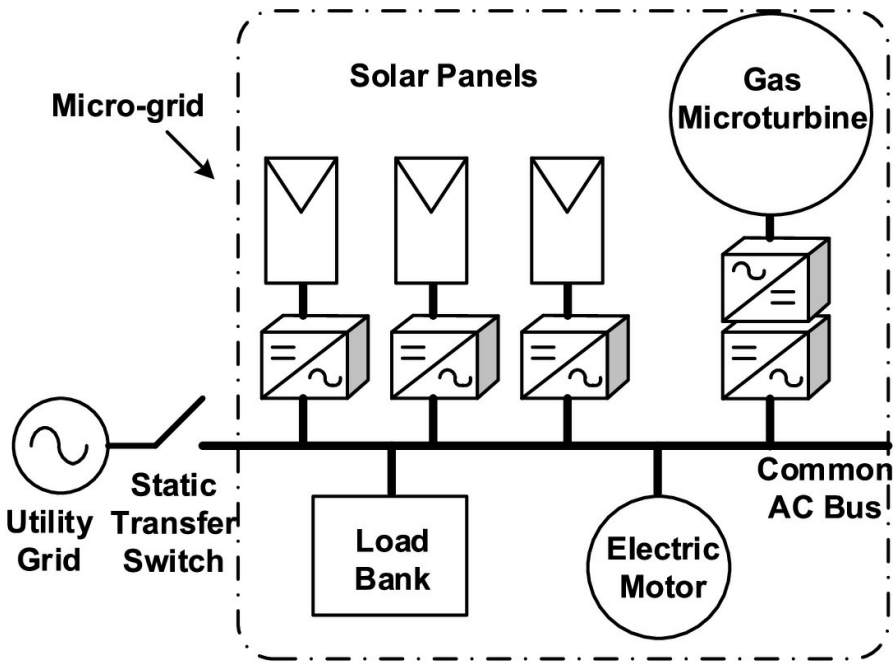


Figure 1.2 A laboratory MG integrated with DGs and loads

In a steady state, a MG usually has two operating modes, i.e., islanded mode and grid-connected mode [9]. The transition between operation modes can be achieved by operating a static transfer switch (STS). The MGCC makes the decision of switching on or off the STS either according to an intentional schedule or subject to an unintentional event. When the STS opens, the MG operates in the islanded mode. By contrast, when the STS closes, the MG transits back to grid-connected mode. In islanded mode, the MGCC can decide whether or not to detach or reattach the noncritical load and hence, guarantee a continuous supply to the critical load. Once STS is closed, the MG exchanges power with the main grid through transformers or power converters in a transformerless manner,

depending on the voltage level of the PCC. This flexible operation has been proved to be feasible in actual implementation. Compared to a power supply unit with only one distributed energy resource (DER), a MG presents obvious technical advantages in terms of reliability and easy integration of multiple DERs. Compared to a large power grid with generation, transmission, and distribution, MGs feature more control flexibilities [10]. The main challenge is, due to the intermittent nature of these DERs, their output powers are not stable and therefore cause power quality issues and damage the electric appliances. For the proliferation of renewable energy on the demand side, MGs should be equipped with facilities that can absorb the fluctuation. In addition, because of the complexity of such a small power system including different kinds of energy sources, energy storage systems, and loads, the coordinated control of these DGs to obtain optimal power flow and ensure high power quality has become a critical task. From the perspective of energy utilization and revenue, the power converters should be controlled to output the maximum real power and export the excess into the utility. On the other hand, from the utility or grid viewpoint, the power electronic interface should also be able to provide ancillary grid services with reactive capability to improve power quality and enhance grid stability.

As already pointed out by researchers and engineers, MGs would and should coexist with the existing electricity grid, and it is required to be resilient with self-healing capability [11]. Large-scale renewable distributed-power-generation plants such as wind turbines and solar PV farms will supply electrical power to the grid together with conventional power stations. In a power network with central power stations and distributed power plants, with the help of intelligent power electronic devices such as soft open points and solid-state transformers, power transmission and distribution network will be able to regulate the power flow and balance to achieve power generation and consumption effectively. On the power demand side, prosumers not only can enjoy high-quality power but also feed the surplus power back to the grid. To achieve flexible grid integration and provide power to various electric appliances, MGs can be distinguished as AC, DC, or hybrid (having both AC and DC) MGs in correspondence with the voltage type of the common bus [12].

In an AC-coupled MG, as shown in Figure 1.3, various DERs and ESSs are connected to the common AC bus through the associated power electronic converters [13]. This configuration is commonly adopted when most of the power sources in the MG generate AC voltages that can match the grid level through interfacing power converters. In such an AC-coupled local power system, the main power management requirement is to ensure power generation meets the load requirement. Especially in islanded operation mode, the main control objective becomes the stabilization of AC bus voltage in terms of both frequency and amplitude. In this configuration, DERs and ESSs operate in a manner similar to AC voltage sources or current sources in parallel. In a current control mode, which is commonly utilized in grid-tied operations, DG's output current is regulated according to the power exchanged reference with the main grid. Apparently, in this case, the output voltage and frequency are fixed by the stiff

utility grid. In a voltage control mode, which can be used in both grid-connected and islanded operation modes, DG's output voltage is controlled to regulate its output power. In this scenario, to produce the dispatched MG output power, power balancing schemes in the central control center are used to share dispatched power among distributed power sources that behave like a synchronous generator.

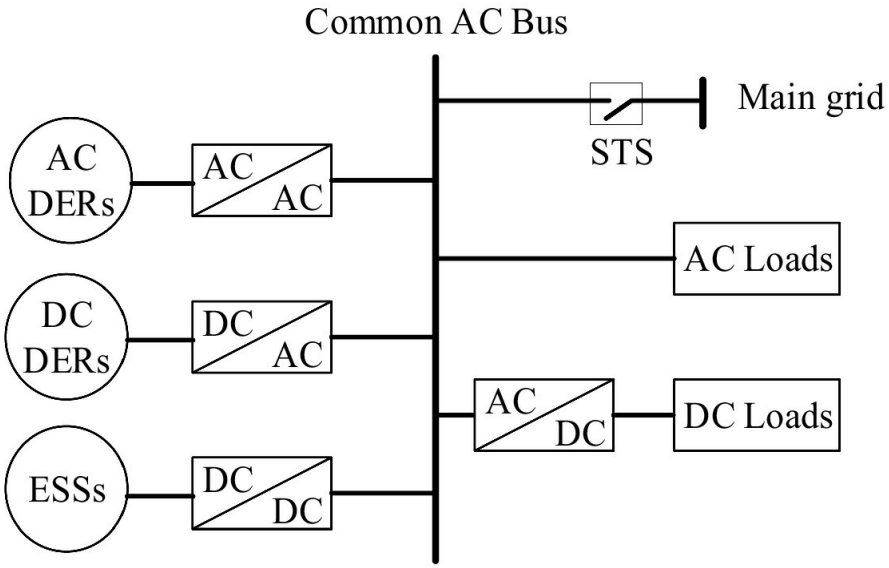


Figure 1.3 AC-coupled MG

Figure 1.4 shows a DC-coupled MG, where DERs and ESSs are connected to a common DC bus. Interlinking converters are then used to interlink the DC and AC buses [14]. This structure can be applied if DC power sources are the major power generation units in the MG. It is noted that in this structure, all the DERs and ESSs are attached to the DC common bus. In this DC-coupled hybrid MG, some AC loads can be connected directly to the AC bus, whereas other AC loads such as adjustable-speed induction motors can be connected to the AC bus through DC to AC converters with variable frequency voltage outputs. In an AC-coupled MG, interlinking converters facilitate bidirectional power flow between AC and DC buses. Depending on the power exchange requirement such as power rating and reliability, more interlinking converters can be added in parallel between DC and AC buses. DC-coupled MGs feature relatively simple structures and do not require any synchronization when integrating different DGs. Nevertheless, the control and power management of parallel interlinking converters, and their output voltage synchronization, either with each other or with the grid for grid-connected operation, can pose some challenges. Moreover,

voltage control and power management are needed for both DC and AC sides in a DC-coupled MG.

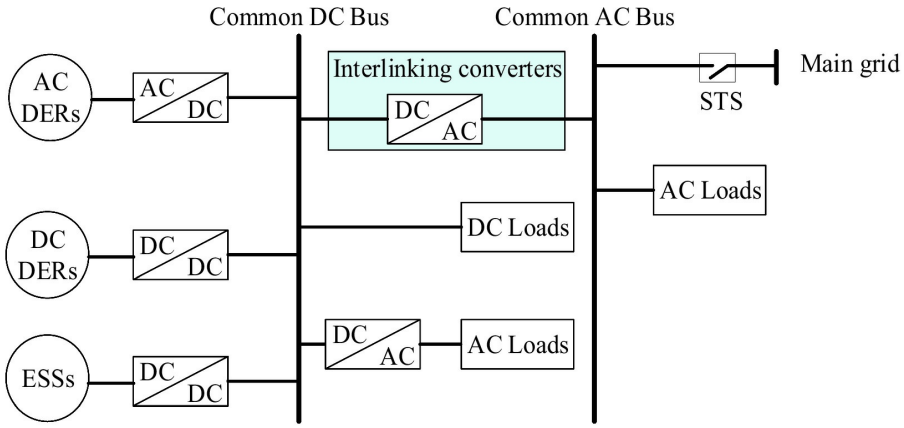


Figure 1.4 DC-coupled MG

The structure of an AC–DC-coupled hybrid MG is depicted in Figure 1.5. As seen from this diagram, both DC and AC buses can be attached with DERs and ESSs, and these buses are interconnected by interlinking converters [15]. Different from the DC-coupled system, the AC–DC-coupled hybrid MG has DERs and ESSs on an AC bus as well, which therefore requires more complicated coordination for the voltage and power control between the DC and AC subsystems. Meanwhile, similarly to the DC-coupled MG, parallel interlinking converters are needed to interconnect AC and DC buses to increase capacity and reliability. In general, this configuration is considered if most of the power sources include a combination of DC and AC power types. In this case, this structure improves overall efficiency and reduces the system cost. This is because by connecting sources and loads to the AC and DC buses, the number of power converters, and hence, the power conversion requirements, can be minimized. Considering these benefits, AC–DC-coupled hybrid MGs could be the most suitable MG structures for a region with rich DC and AC power sources and a combination of DC and AC loads. In some remote areas, in which electrical power is generated from various DC and AC power sources such as offshore wind turbines and large-scale floating solar PVs, AC–DC-coupled hybrid MG could be an effective option for power management and transmission.

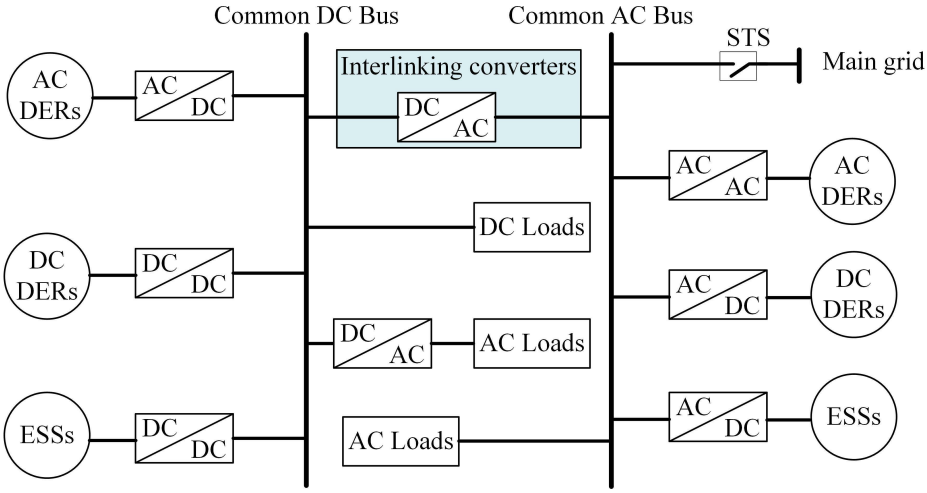


Figure 1.5 AC–DC-coupled MG

Over the past few years, the concept of DC MG has been increasingly popular in smart-grid research due to its efficiency, reliability, and simplicity [16]. A large number of RESs with DC characteristics in nature, such as solar PV panels and electric vehicles (EVs), have been increased steadily in smart cities. In this context, it is more convenient and efficient to connect the DC sources and DC loads to form a DC MG instead of an AC MG. Compared with AC MGs, DC MGs do not present reactive power and harmonic components [17]. As a result, it can assure higher power quality and its control complexity can be eased. Figure 1.6 shows a DC MG. It can be either connected to the traditional AC distribution network through DC to AC conversion or to the high-voltage DC distribution network. While remarkable improvement has been made in obtaining better performance of AC MGs over the past decades, it has been gradually recognized that DC MGs are more attractive for numerous uses, thanks to their distinct merits such as higher efficiency, more natural interface to many types of DERs and ESS, and better compliance with consumer electronics. It has been reported by researchers that the higher voltage rating of the order of 1 kV in the DC distribution system leads to smaller currents power losses compared to an equivalent AC system. Again, when DGs and loads are coupled to a DC bus, there are no problems with reactive power flow, power quality, and frequency regulation, leading to a less complex control system [18]. In summary, DC MGs offer potential advantages over AC MGs as follows.

- No control is required for reactive power and frequency regulation.
- Grid synchronization issues are avoided.
- No issue of inrush current due to the absence of a transformer.
- Conversion losses of an inverter are reduced.
- Fault ride-through capability of its own.

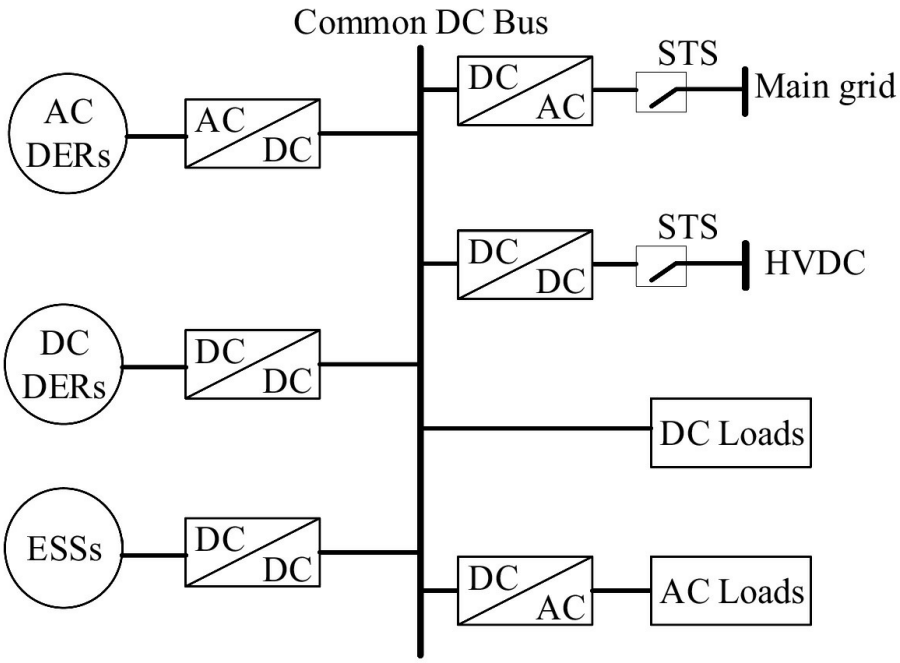


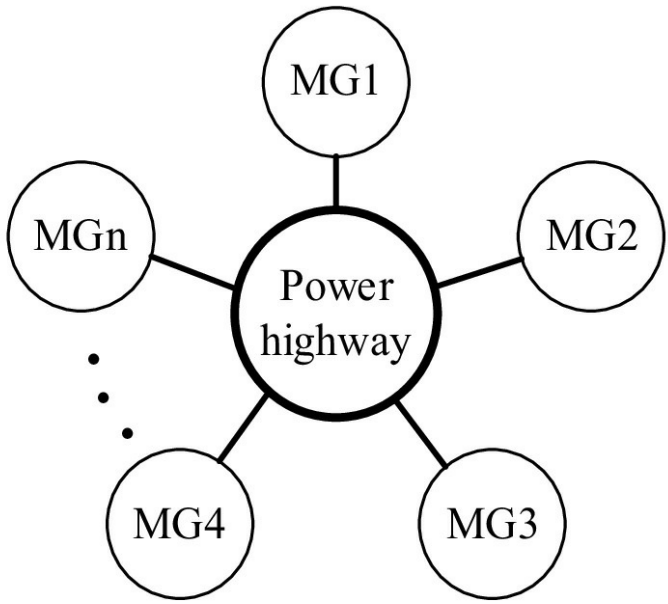
Figure 1.6 A DC MG

However, drawbacks of DC MGs are:

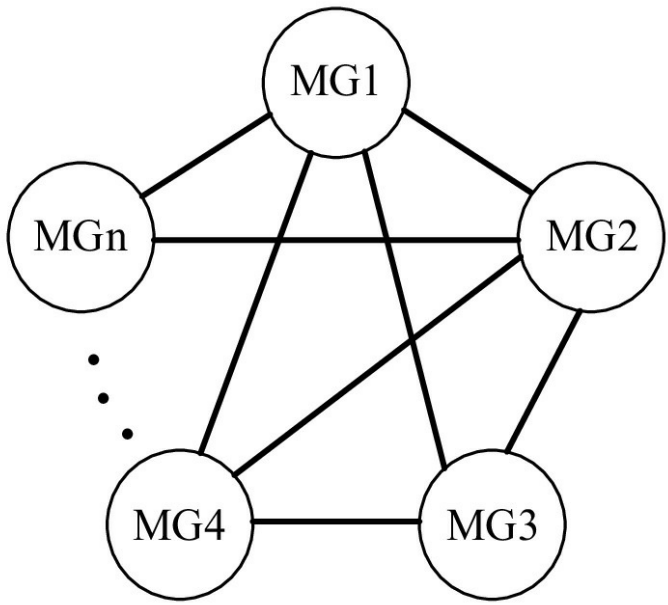
- Construction of private DC distribution lines is required.
- Protection of a DC system is more challenging than an AC system due to the absence of a zero-crossing point of current in the DC system.
- Voltage stability is affected by active power flow alone, while AC system voltage can be regulated using reactive power without affecting active power.

While development in MGs has been witnessed over the decade, their interconnection still needs further investigation. In existing research, although many control methods have been developed for individual MGs, the interconnection between multiple MGs has not yet been satisfactorily studied. With the increasing penetration of solar PVs and wind turbines, the next-generation power grid is most likely to be a decentralized infrastructure with networked MGs [19]. The effective utilization of DERs can be achieved through networked MGs where power shortfall in one MG can be compensated by the excess power available from its neighbors. In this sense, networked MGs have been proposed as the interconnection of two or more MGs with an ability to exchange power among the MGs and/or the distributed system at the PCC within the distributed power network [20]. Figure 1.7 presents two configurations of networked MGs. In the first structure, MGs exchange power through a common

power highway. In the second configuration, MGs are interconnected through a sparse network. It can provide suitable electric infrastructure to utilize cost-effective and environment-friendly electric power generated from DERs. Networking of multiple self-governed MGs is emerging as one of the promising alternatives to improve the resiliency, reliability, and scalability of the power network. The operation of clusters of MGs in the form of networked MGs is possibly the best way to utilize DERs. Also, during emergencies, this can extend the duration of supply to the critical loads and supports black start to nearby generating stations [21]. Thus, the resiliency and reliability of the overall system are enhanced significantly.



(a)



(b)

Figure 1.7 Networked MGs. (a) Interconnected via a common power highway, (b) interconnected via a sparse power network.

The control and operation of networked MGs is a challenging task, as several issues pertaining to reliability, coordination, and uncertainties are involved [22, 23]. The networked MGs are not the same as the traditional power-distribution network. The flow of power is bidirectional from one MG to another, and the change in configuration is frequent due to the plug-and-play operation of DGs and even MGs [24]. So far, most of the research on networked MGs is focused on energy management and optimized control algorithms among interconnected MGs on a very high level [25–27]. For example, to coordinate power exchange between MGs and distribution network, a two-stage decentralized energy management framework based on the alternating direction method of multipliers has been discussed in [26]. In [27], a discounted in-consensus algorithm is proposed to discover the optimal electrical power trading route within networked MGs for power loss minimization. To date, complete implementation of networked MGs, including physical connection, power electronic interfacing, coordination control strategies, and energy management schemes, has not yet been fully realized.

1.2 Operation considerations

Due to the intermittent nature of the renewable sources and fluctuation of the load profile, the output power is unstable and may cause a negative influence on the quality of electricity and affect the performance of electric appliances. To ensure a MG operates properly, there are several issues in operation that must be addressed.

1.2.1 Power sharing

To avoid overload of some DGs and to ensure economical operation of MGs, the active and reactive powers should be shared among DGs simultaneously. In a single MG, obviously, power sharing refers to the load sharing among DGs. In other words, the converter interfaced DGs in a MG should pick up the load changes according to their capacity to avoid overload or power deficiency. In existing power-sharing methods, the droop control is the widely used control approach without requiring communication lines. It can be used to achieve load sharing by mimicking the steady-state characteristics of synchronous generators in islanded MGs [28]. It is noted that there is a trade-off between power-sharing accuracy and mitigation of voltage deviation [29]. Much research effort has been paid to address this issue. Last, it is necessary to point out that, in a MG cluster with multiple MGs interconnected through power and communication networks, power sharing refers to both load sharing among DGs within each MG and the

power exchange among MGs.

1.2.2 Power balancing

Due to the intermittent nature of renewable energy, power generation may not necessarily meet the load demand. For instance, on the one hand, variable energy generation of solar PVs because of stochastic sun radiation, and, on the other hand, the mismatch between generation and load peaks in most of the network can cause voltage rise during the peak PV period as well as voltage drop while meeting the peak power demand [30]. This problem would be more serious when PVs are connected to a low-voltage power grid at the distribution level. The mismatch between power generation and consumption within a MG should be eliminated under a proper power management mechanism, including energy storage, load shedding, power curtailment, and power exchange with the main grid. Moreover, different constraints should be considered such as battery state of charge (SoC) and maximum charging/discharging current in power-management-system design for power balancing.

1.2.3 Power quality

Some control strategies of MGs such as droop control will cause voltage and frequency deviations [31]. Also, fluctuating power output from DGs, nonlinear loads, and unbalanced grid conditions would be a challenge for stabilization of the frequency and voltage and minimization of the total harmonic distortion of injecting current. DGs are often connected to the MG through a power electronic interface converter. The main role of an interface converter is to achieve power conversion. Power electronic converters themselves are the major sources of harmonics that pollute the power grid due to the high-frequency switchings. Nevertheless, if controlled properly, they can be used to contribute to the power-quality improvement. Some advanced control strategies have been developed to address power quality problems, such as voltage harmonics and spikes [32]. For instance, by controlling the DG unit to emulate a resistance at harmonic frequencies, voltage harmonic compensation approaches can be utilized to compensate those harmonics. Voltage unbalances could appear when single-phase loads are switched into the MG. Such voltage unbalances can usually be compensated by injecting negative sequence voltage through active power filters in series with the power distribution line. Meanwhile, shunt active power filters can also be used for voltage unbalance compensation. In these works, voltage unbalances caused by unbalanced loads are eliminated by injecting negative sequence currents [33]. In severe scenarios where voltage is highly unbalanced and distorted, a large amount of current is needed. Hence, DGs must be oversized. Otherwise, the compensation would interfere with the active and reactive power supplies by the DG. To address this problem, static synchronous compensators can be used in MGs.

1.2.4 Seamless mode transition

The isolation of a MG, either intentional islanding or subject to an unintentional event, should not cause major influences on both local loads and the utility grid. Furthermore, the re-synchronization of the MG to the utility should be conducted smoothly and quickly. Transition between grid-connected and islanded modes of a MG can be done either by enabling seamless transition or by implementing a black start [34]. Transition choice has a major impact on the MG system protection and control design. To enable seamless islanding transition, first, it is necessary to design reliable and secure islanding detection. It is highly demanded to ensure a smooth transition to avoid disruption in the stable power supply to the loads. If care has not been taken, power disruption or power oscillation between sources can happen.

1.2.5 System stability

From the perspective of power flow, the movement of the low-frequency oscillations to new location influences the relative stability of the system. In addition, from the system control viewpoint, the variations of control parameters affect system stability as well as sensitivity analysis. In distribution systems with multiple DG units, the main factors that influence stability are the control strategies of the DG units, the energy storage systems, the types of load in the system, the location of faults, and the inertia constant of motors [35]. As the deployment of DGs continues, an increasing number of DC or AC power inverters will be interfaced into the electric grid. MGs may be more vulnerable to voltage instability due to various types of source generation injected in such systems as well as the reactive power limits, load dynamics, and low inertia. At present, the research on MG stability is progressing in areas such as the development of mathematical models for MG stability analysis, methods of MG stability analysis, and methods of improving the stability of MGs. A lot of attention is paid to the small-signal stability analysis and transient stability simulation analysis [36–38]. For example, in [36], small-signal stability analysis of a single-phase grid-connected inverter is presented. Small-signal stability analysis of islanded MGs is covered in [37]. Influences of droop-control gains, line impedance, and load fluctuations on the MG voltage and frequency characteristics are also discussed. Using small-signal stability analysis of MG, better droop-control gains can be obtained.

In conventional power plants, the kinetic energy reservoir in the rotating mass of synchronous generators can stabilize the frequency throughout the power network. However, most MGs with a high penetration level of power electronic converters have low inertia. As a result, converter control methods in MGs such as droop control usually cannot provide enough inertia support. Subject to a large disturbance, e.g., connection or disconnection of a large load, the frequency of the MG may fluctuate too fast to be maintained within the acceptable range by frequency restoration control. Meanwhile, due to the stochastic nature of RESs and frequent load changes, nearly all the modern MGs are associated with dynamic frequency stability issues. Thus, it restricts the maximum number of renewable energy systems that can be penetrated to the MG. To increase the

penetration of low-inertia sources to the MG, the frequency stability issues need to be addressed. The frequency stability issues of a typical MG are addressed by the addition of extra inertial support from the power sources using power converters and an appropriate control loop.

1.3 Key technologies and challenges

Although many research efforts have been paid to MGs, their actual implementation is still under development. Now the situation is that there are still many technical challenges relating to power electronics at the component level, and power flow optimization challenges at the system level need to be addressed to support the smart-grid pyramid. And, there are still many technical gaps that need to be filled before we can fully enjoy the benefits of renewable energy.

1.3.1 New semiconductor devices

The basic components of power electronic converters are semiconductor devices. With the increasing penetration of renewable energy and larger capacity with a higher power level, the semiconductor devices are required to operate under new conditions. Existing semiconductor devices using silicon are reaching their physical limits in power capacity and switching frequency [38]. It is necessary to break through such limits by replacing conventional semiconductor with new materials technology for high-power applications and faster switching performance. As renewable energy together with energy storage technologies have grown in recent years, power-switching devices with high-voltage, high-frequency, low switching loss, and high-temperature operation capability are essential in MGs and smart grids.

1.3.2 Power electronic converters and control

The power converters, as the electronic interface between the local distribution network and the DGs, are playing vital roles in reliable power delivery and high power quality. So far, many researchers have developed various techniques for grid integration. These include couple inductor method [39], instantaneous current-sharing method [40], voltage droop method [41], as well as other categories. To their credit, these methods can integrate the DGs into a local small-power system with proper load sharing. Specifically, the droop method has become popular and has been widely used because it only uses local power measurements while the communication between inverters is avoided. However, these methods typically consist of an outer loop for voltage control and an inner loop for current regulation as the inverter output control. A common approach to the design of the control loops is the use of proportional-integral-derivative controllers with additional feed-forward compensation (if required) [6]. This structure complicates the control systems and much tuning effort is needed. Consequently, system performance and stability are usually comprised. So far, conventional control methods such as cascaded linear control still lack sufficient

control flexibility and intelligence to handle these fluctuations, resulting in stability problems and power quality issues. Therefore, advanced control algorithms with fast transient response and flexibility in considering different constraints are highly desired in MG applications. Another technical aspect of power converter control is reactive capability. Power companies and distributors are seeing inverters' ancillary services to support grid stability. It is now necessary to expand the degree of inverter control flexibilities to make renewable power generation more grid-friendly. Although reactive capacities of PV inverters have been widely recognized and incorporated to enable some level of "smart operation," so far, research detailing advanced power converter techniques to obtain such flexibilities is still under development.

1.3.3 Renewable intermittency

MGs have emerged as a promising solution to facilitate the integration of renewable energy resources. Meanwhile, the intermittent outputs from renewable energy resources and fluctuating power demand have posed many challenges such as voltage or frequency variations. Power and energy balance issues due to the intermittent and randomness of renewable energy cannot be ignored. It tends to impact the planning and operation of power systems as well as the investment of renewable energy plants. The stochastic production simulation can simulate the production of electricity in the power grid. It is an important means to evaluate the production of different types of energy sources in power grids and the responding cost. Accurately predicting energy production and consumption has become a need because of the continuous demand for expansion and interconnection. To reduce the uncertainty inherent in demand and generation, system operators rely upon load and generation forecasts to balance electricity supply and demand. Accurate forecasts not only support the safe and reliable operation of the grid but also encourage cost-effective operation by improving the scheduling of generation and reducing the use of reserves.

1.3.4 Lack of systematic approaches

With the increasing penetration of renewable energy resources and the associated electronic interfaces, the development of high-performance control strategies has attracted much attention in global academic and industry communities. Now the situation is that, on the one hand, some researches focus on the power converters and their control methods at the bottom level, but the power flow optimization on the grid level is seldom considered. On the other hand, some researchers have studied the impact of distributed resources on the electric grid, and high-level power flow control of the network has been investigated. Nevertheless, how to control the power converters to achieve system-level optimal power flow is not detailed. For instance, a systematic approach of developing converters that are fed by PV cells to satisfy multiple requirements is still missing. To sum up, practical strategies of large-scale grid integration of distributed energy sources at both converter level and grid level (power flow) have not been developed, and a

systematic way to design the optimum converters by imposing the practical requirements needs further investigation.

1.3.5 Large-scale grid integration and its impact on the main grid

There is ongoing research on the grid integration of RESs. Much work has been done to integrate distributed energy sources, energy storage systems, and loads into small local power grids. However, existing techniques are mainly concerned with islanded (stand-alone) operation without considering the utility grid. Grid voltage quality can deteriorate due to the power flow between DG sources and loads; this is widely recognized [42]. But the relationship between power injected by DG sources and the grid voltage profile is still unclear. Recently, the utilization of the potential reactive power capacity of grid-tied inverters for grid support has been put forward [43]. However, how to control these inverters in a coordinated way and how much reactive power each inverter should produce are still under discussion. Only limited discussion has been offered to date on the impact of further integration of such small power systems into the distribution grid. A greater penetration level of RESs into existing systems will lead to major challenges such as grid voltage dip and rise. One way of improving the grid voltage is to limit the power injection. However, such capacity limitation baffles the effective utilization of green energy.

1.3.6 Energy storage

It is well known that within an envisioned MG, various types of DGs and customers create and demand varying active and reactive power profiles that may challenge the stability of the system. The ESS, therefore, plays a critical role in stabilizing the voltage and frequency of the MG for both short- and long-term applications. From device to system level, the ESS is a crucial element in the integration of DG into the MG. Following rapid cost reductions and significant improvement in capacity and efficiency, ESS has been seen as a key factor worldwide in the development of future smart grids with the capability of maintaining power balance and providing voltages. There are currently several types of energy-storage technologies with different characteristics, e.g., energy and power density, efficiency, cost, lifetime, and response time. Examples of ESS are ultracapacitors, superconducting magnetic ESS, flywheels, batteries, compressed air, pumped hydro, fuel cells, and flow batteries [44, 45].

Energy storage with newer battery technologies has become a reality. The lead-acid battery-based technology has been replaced by lithium-ion technology and many other alternatives. Initially, batteries are used to absorb surplus energy and increase local consumption in peak generation periods. For instance, using the SoC and power allocation as real-time information, a strategy was presented for smoothing the fluctuating output from renewable energy [46]. The load can be shared among ESS units consistently while the SoC can be controlled within a specified range. In [47], the battery ESS is controlled in a ramp limiting manner

so that the oscillating PV output power can be mitigated. In addition, this method is able to reduce the ESS size, and, hence, the system overall performance can be enhanced.

Planning the best locations and sizes for ESS can have a significant impact on the power system, including enhancing the power system reliability and power quality, reducing the power system cost, controlling high-energy cost-imbalance charges, minimizing power loss, improving voltage profiles, serving the demand for peak load, and correcting the power factor. Meanwhile, with the proliferation of EVs, such new electric loads will trigger extreme surges in demand at rush hours, and therefore, threaten the stability of the power grid [48]. This is a major challenge that must be addressed in the development of a smart grid and smart city. Nowadays all the EV chargers in the market feature the "plug-and-charge" mode regardless of the status of the utility grid. Usually, people will charge their EVs when they arrive at workplaces in the morning or return home in the evening. The simultaneous charging of thousands of EVs will result in a massive peak energy demand, which, in turn, will damage the stability of the power grid. But at the same time, EVs can be regarded as portable ESS. EVs can be endowed with an improved charging system with "plug-and-time-shift charge" characteristics [49, 50]. Instead of starting to charge right away, the charging power is adjusted online based on an optimal schedule that is computed by considering both the real-time status of the power grid and the demand of the EV owners. With this smart charging, the peak load on the grid can be "shaved" and "shifted" in time, so that the bulk of charging is done when the demand is normally low, particularly overnight. Moreover, we can feed the electric energy deposited in EV batteries back to the grid. Under the strategy of "plug-and-time-shift charge," the EVs can be used as the energy sources to supply electricity to the grid when peak demand occurs. In this way, the peak demand is managed, and little investment needs to be made in upgrading the grid to boost capacity.

1.3.7 Smart sensors

To enable an intelligent power grid, smart sensors and smart meters are used to monitor the real-time status of the system such as current, voltage, and power flow for proper operation and control. Due to the high penetration level of DGs with bidirectional power-flow feature, smart sensors with two-way communication capability are of high importance to monitor the real-time status of different nodes within the power network. For instance, an interesting concept called Sensformer is recently proposed by Siemens. It merges physics and information—turning transformers into information and power hubs [51]. Compared to traditional passive transformers, this device actively measures real-time information such as oil temperature, winding current, voltage, and location, based on which operators are able to coordinate the power flows along the distribution feeders, paving the way toward a high renewable energy penetration network.

1.3.8 Information and communication technology

With the increased penetration of smart meters into the power grid, huge amounts of data will be generated, which will need to be transferred, processed, and delivered back with control signals. Thus, information and communication technologies with powerful data processing capability and high-level data transmission security will become significant to deal with data and information explosion. Nowadays, increasing number of smart-grid deployments are based on Internet technologies, broadband communication, and nondeterministic communication environments. Advanced techniques of huge data processing are essential in information collection and energy management within the smart grid. To better enable data and information communication among different key components, Internet of Things has been proposed to further extend itself to integrate smart meters, sensors, RESs and loads, customers, and energy into an information grid under the future smart-grid framework [52].

In the future, MGs are likely owned by private companies or individuals to manage the electrical power within a small region and community. As the power grid incorporates smart metering and load management, user- and corporate privacy are increasingly becoming a concern. Some major questions that need to be answered include: Will the individual power consumption data be stolen or modified by cyber-hacker with illegal motivation? Will the power utilities be able to control end users' loads without the customers' prior permission? Could the electricity consumption behaviors lead to disclosure of not only how much energy a household uses but also when they are at home, at work, or going on holiday? These are the security and privacy issues that need to be considered carefully under the construction of the next-generation smart grid.

As to actual MG implementation, although experimental studies for MG research have been conducted for many years, the validation and design involving real communication networks are still in the beginning stage. In the existing literature, the communication structure and controller parameters are taken as two basic aspects for the category of control system design, where the former indicates the measurement communication among subsystems whereas the latter determines the controller gains of subsystems [53]. It is generally acknowledged that both of the two aspects play significant impacts on the dynamic performance of the overall system. With the extensive usage of open communication mechanisms, the topology of the data network is not necessarily the same as the physical power network. The network topology can be rendered flexible as a tunable variable to adapt the scalability of MGs with plug-and-play capability.

References

[1] Farhangi H., Iravani M.R. 'Power management strategies for a microgrid with multiple distributed generation units'. *IEEE Transactions on Power Systems*. 2006, vol. 21(4), pp. 1821–31.

[2] Farhangi H. 'The path of the smart grid'. *IEEE Power and Energy Magazine*.

2010, vol. 8(1), pp. 18–28.
[3] Hu J., Li Z., Zhu J., Guerrero J.M. 'Voltage stabilization: a critical step toward high photovoltaic penetration'. *IEEE Industrial Electronics Magazine*. 2019, vol. 13(2), pp. 17–30.
[4] Walling R.A., Saint R., Dugan R.C., Burke J., Kojovic L.A. 'Summary of distributed resources impact on power delivery systems'. *IEEE Transactions on Power Delivery*. 2008, vol. 23(3), pp. 1636–44.
[5] Li Z., Chan K.W., Hu J., Guerrero J.M. 'Adaptive droop control using adaptive virtual impedance for microgrids with variable PV outputs and load demands'. *IEEE Transactions on Industrial Electronics*. 2020, p. 1.
[6] Guerrero J.M., Vasquez J.C., Matas J., de Vicuna L.G., Castilla M. 'Hierarchical control of droop-controlled AC and DC microgrids—a general approach toward standardization'. *IEEE Transactions on Industrial Electronics*. 2011, vol. 58(1), pp. 158–72.
[7] Shan Y., Hu J., Liu M., Zhu J., Guerrero J.M. 'Model predictive voltage and power control of Islanded PV-battery microgrids with washout-filter-based power sharing strategy'. *IEEE Transactions on Power Electronics*. 2020, vol. 35(2), pp. 1227–38.
[8] Meng L., Luna A., Díaz E.R., *et al*. 'Flexible system integration and advanced hierarchical control architectures in the Microgrid research laboratory of Aalborg university'. *IEEE Transactions on Industry Applications*. 2016, vol. 52(2), pp. 1736–49.
[9] Blaabjerg F., Teodorescu R., Liserre M., Timbus A.V. 'Overview of control and grid synchronization for distributed power generation systems'. *IEEE Transactions on Industrial Electronics*. 2006, vol. 53(5), pp. 1398–409.
[10] Shan Y., Hu J., Guerrero J.M. 'A model predictive power control method for pv and energy storage systems with voltage support capability'. *IEEE Transactions on Smart Grid*. 2020, vol. 11(2), pp. 1018–29.
[11] Lasseter R.H. 'Smart distribution: coupled microgrids'. *Proceedings of the IEEE*. 2011, vol. 99(6), pp. 1074–82.
[12] Nejabatkhah F., Li Y.W. 'Overview of power management strategies of hybrid AC/DC microgrid'. *IEEE Transactions on Power Electronics*. 2015, vol. 30(12), pp. 7072–89.
[13] Wu X., Xu Y., He J., Wang X., Vasquez J.C., Guerrero J.M. 'Pinning-based hierarchical and distributed cooperative control for AC microgrid clusters'. *IEEE Transactions on Power Electronics*. 2020, vol. 35(9), pp. 9865–85.
[14] Shan Y., Hu J., Chan K.W., Fu Q., Guerrero J.M. 'Model predictive control of bidirectional DC–DC converters and AC/DC interlinking converters—a new control method for PV-wind-battery microgrids'. *IEEE Transactions on Sustainable Energy*. 2019, vol. 10(4), pp. 1823–33.
[15] Fairley P. 'Germany jump-starts the supergrid'. *IEEE Spectrum*. 2013, vol. 50(5), pp. 36–41.
[16] Kakigano H., Miura Y., Ise T. 'Low-voltage bipolar-type DC microgrid for super high quality distribution'. *IEEE Transactions on Power Electronics*. 2010, vol. 25(12), pp. 3066–75.

[17] Sahoo S.K., Sinha A.K., Kishore N.K. 'Control techniques in AC, DC, and hybrid AC-DC microgrid: a review'. *IEEE Journal of Emerging and Selected Topics in Power Electronics*. 2017, vol. 15(3), pp. 1238–50.
[18] Meng L., Shafiee Q., Trecate G.F., *et al*. 'Review on control of DC microgrids and multiple microgrid clusters'. *IEEE Journal of Emerging and Selected Topics in Power Electron*. 2017, vol. 5(3), pp. 928–48.
[19] Alam M.N., Chakrabarti S., Ghosh A. 'Networked microgrids: state-of-the-art and future perspectives'. *IEEE Transactions on Industrial Informatics*. 2019, vol. 15(3), pp. 1238–50.
[20] Li Z., Shahidehpour M., Aminifar F., Alabdulwahab A., Al-Turki Y. 'Networked Microgrids for enhancing the power system resilience'. *Proceedings of the IEEE*. 2017, vol. 105(7), pp. 1289–310.
[21] Hans C.A., Braun P., Raisch J., Grune L., Reincke-Collon C. 'Hierarchical distributed model predictive control of interconnected microgrids'. *IEEE Transactions on Sustainable Energy*. 2019, vol. 10(1), pp. 407–16.
[22] Liu K., Liu T., Tang Z., Hill D.J. 'Distributed MPC-based frequency control in networked microgrids with voltage constraints'. *IEEE Transactions on Smart Grid*. 2019, vol. 10(6), pp. 6343–54.
[23] Yazdanian M., Mehrizi-Sani A. 'Distributed control techniques in microgrids'. *IEEE Transactions on Smart Grid*. 2014, vol. 5(6), pp. 2901–9.
[24] Liu G., Starke M.R., Ollis B., Xue Y. Networked microgrids scoping study. ORNL/TM-2016/294. Oak Ridge National Laboratory Report; 2016.
[25] Shahnia F., Bourbour S., Ghosh A. 'Coupling neighboring microgrids for overload management based on dynamic multicriteria decision-making'. *IEEE Transactions on Smart Grid*. 2017, vol. 8(2), pp. 969–83.
[26] Gao H., Liu J., Wang L., Wei Z. 'Decentralized energy management for networked microgrids in future distribution systems'. *IEEE Transactions on Power Systems*. 2018, vol. 33(4), pp. 3599–610.
[27] Xu Y., Sun H., Gu W. 'A novel discounted min-consensus algorithm for optimal electrical power trading in Grid-connected DC microgrids'. *IEEE Transactions on Industrial Electronics*. 2019, vol. 66(11), pp. 8474–84.
[28] Hu J., Zhu J., Platt G. 'A droop control strategy of parallel-inverter-based microgrid'. *International Conference on Applied Superconductivity and Electromagnetic Devices*; Sydney, New South Wales, Australia; 2011. pp. 1–6.
[29] Simpson-Porco J.W., Shafiee Q., Dorfler F., Vasquez J.C., Guerrero J.M., Bullo F. 'Secondary frequency and voltage control of islanded microgrids via distributed averaging'. *IEEE Transactions on Industrial Electronics*. 2015, vol. 62(11), pp. 7025–38.
[30] Hu J. 'Coordinated control and fault protection investigation of a renewable energy integration facility with solar PVS and a micro-turbine'. *Energies*. 2017, vol. 10(4), pp. 423–13.
[31] Gupta Y., Doolla S., Chatterjee K., Pal B.C. 'Optimal DG allocation and Volt–Var dispatch for a droop-based microgrid'. *IEEE Transactions on Smart Grid*, vol. 12(1), pp. 169–81.

[32] Guerrero J.M., Loh P.C., Lee T.-L., Chandorkar M. 'Advanced control architectures for intelligent microgrids—Part II: power quality, energy storage, and AC/DC microgrids'. *IEEE Transactions on Industrial Electronics*. 2013, vol. 60(4), pp. 1263–70.
[33] Lu D., Wang S., Yao J., Yang T., Hu H. 'Cluster voltage regulation strategy to eliminate negative sequence currents under unbalanced grid for star-connected cascaded H-bridge STATCOM'. *IEEE Transactions on Power Electronics*. 2019, vol. 34(3), pp. 2193–205.
[34] Hu J., Zhu J., Dorrell D.G. 'Model predictive control of inverters for both islanded and grid-connected operations in renewable power generations'. *IET Renewable Power Generation*. 2014, vol. 8(3), pp. 240–8.
[35] Venkatesan A.K., Subramaniam U., Bhaskar M.S., *et al*. 'Small-signal stability analysis for microgrids under uncertainty using MALANN control technique'. *IEEE Systems Journal*, pp. 1–11.
[36] Muyeen S.M., Islam S.M., Blaabjerg F. *Variability, Scalability and Stability of Microgrids*. IET; 2019.
[37] Milošević D., Đurišić Ž. 'Technique for stability enhancement of microgrids during unsymmetrical disturbances using battery connected by single-phase converters'. *IET Renewable Power Generation*. 2020, vol. 14(9), pp. 1529–40.
[38] Wang Y., Luo H., Liu G., li K. 'Recent advances and trend of HEV/EV-oriented power semiconductors – an overview'. *IET Power Electronics*. 2020, vol. 13(3), pp. 394–404.
[39] Ewanchuk J., Member S., Salmon J. 'Three-limb coupled inductor operation for voltage sourced inverters'. *IEEE Transactions on Industrial Electronics: A Publication of the IEEE Industrial Electronics Society*. 2013, vol. 60(5), pp. 1979–88.
[40] Sun X., Lee Y.-S., Xu D. 'Modeling, analysis, and implementation of parallel multi-inverter systems with instantaneous average-current-sharing scheme'. *IEEE Transactions on Power Electronics*. 2003, vol. 18(3), pp. 844–56.
[41] Ma T., Cintuglu M.H., Mohammed O.A. 'Control of a hybrid AC/DC microgrid involving energy storage and pulsed loads'. *IEEE Transactions on Industry Applications*. 2017, vol. 53(1), pp. 567–75.
[42] Wang Y., Syed M.H., Guillo-Sansano E., Xu Y., Burt G.M. 'Inverter-based voltage control of distribution networks: a three-level coordinated method and power hardware-in-the-loop validation'. *IEEE Transactions on Sustainable Energy*. 2020, vol. 11(4), pp. 2380–91.
[43] Available from https://www.sma-australia.com.au/partners/knowledgebase/sma-shifts-the-phase.html.
[44] Ter-Gazarian A.G. *Energy Storage for Power Sysetms*. 3rd edition. IET; 2020.
[45] Khaligh A., Li Z. 'Battery, ultracapacitor, fuel cell, and hybrid energy storage systems for electric, hybrid electric, fuel cell, and plug-in hybrid electric vehicles: state of the art'. *IEEE Transactions on Vehicular*

Technology. 2010, vol. 59(6), pp. 2806–14.
[46] Li X., Hui D., Lai X. 'Battery energy storage station (BESS)-based smoothing control of photovoltaic (PV) and wind power generation fluctuations'. *IEEE Transactions on Sustainable Energy*. 2013, vol. 4(2), pp. 464–73.
[47] Lam R.K., Yeh H.-G. 'PV ramp limiting controls with adaptive smoothing filter through a battery energy storage system'. *IEEE Green Energy and Systems Conference*; Long Beach, California, USA; 2014. pp. 55–60.
[48] Qiu J., Hu J. 'Yen's algorithm-based charging facility planning considering congestion in coupled transportation and power systems'. *IEEE Transactions on Transportation Electrification*. 2019, vol. 5(4), pp. 1134–44.
[49] Qian T., Shao C., Wang X., Shahidehpour M. 'Deep reinforcement learning for EV charging navigation by coordinating smart grid and intelligent transportation system'. *IEEE Transactions on Smart Grid*. 2020, vol. 11(2), pp. 1714–23.
[50] Chan C.C., Jian L., Tu D. 'Smart charging of electric vehicles – integration of energy and information'. *IET Electrical Systems in Transportation*. 2014, vol. 4, pp. 89–96.
[51] Available from https://www.siemens.com/global/en/home/products/energy/high-voltage/transformers/sensformer.html.
[52] Zanella A., Bui N., Castellani A., Vangelista L., Zorzi M. 'Internet of things for smart cities'. *IEEE Internet of Things Journal*. 2014, vol. 1(1), pp. 22–32.
[53] Lou G., Gu W., Wang J., Sheng W., Sun L. 'Optimal design for distributed secondary voltage control in islanded microgrids: communication topology and controller'. *IEEE Transactions on Power Systems*. 2019, vol. 34(2), pp. 968–81.

Chapter 2
Power electronic converters and control

This chapter lays the foundation of this book from the perspective of power converters and their control, particularly, model predictive control algorithms.

2.1 Power electronic converters in energy conversion

Power electronic converters, as the electronic interface between the local distribution network and the distributed generations (DGs), play vital roles in reliable power supply and high power quality. In DG interfacing, either connected to the grid or a local load, the key components during the power conversion process are the power electronic converters, which provide flexible interfaces between the energy sources and the end users. Particularly in microgrids (MGs), the following converter topologies have been widely applied.

2.1.1 DC–DC converters

DC–DC converters are involved in providing easier interconnection and reliability of various distributed energy resources (DERs) by stepping down or stepping up the voltage from the generated voltage of the power source to another voltage level. In MGs, the DC–DC converters mainly aim to interface various renewable energy resources to the DC bus or the loads. Some popular types are boost converters, buck converters, and buck-boost converters [1]. Since most of the voltages generated from renewable energy resource units are relatively low, it is usually necessary to step up the low voltage obtained from the renewable source to a level suitable for the DC bus/load. Actually, DC–DC converters can be further categorized into isolated and non-isolated converters [2]. Isolated converters use a high-frequency transformer to isolate electrically the input and the output sides of the power conversion stage. In contrast, non-isolated converters present their distinct advantages such as lower cost, size, and no core-saturation-related problems.

The selection of an appropriate DC–DC converter becomes significant as the overall system efficiency is highly dependent on the converter's performance [3]. For a DERs-fed DC distribution system, a DC–DC converter capable of featuring a higher voltage step-up ratio is more attractive because electricity distribution at

a low voltage level is inefficient due to higher transmission loss. Renewable sources such as solar panels and fuel cells typically output power in the voltage range of 20–45 V. A high-voltage-gain DC–DC converter would be an effective solution for integrating low-voltage renewable energy sources onto a higher-voltage DC bus, e.g., 400 V. High-voltage-gain DC–DC converters make it feasible for connecting such sources to the high-voltage bus by boosting the low voltage from the sources to higher voltages [4]. Theoretically, conventional boost and boost-derived converters can offer higher voltage step-up ratios. In practice, however, they suffer from practical issues such as unstable operation in extreme duty ratio, large-voltage stress on the switch, diode reverse-recovery problems, and low efficiency. In this context, nowadays, high-voltage-gain DC–DC converters have become an important research stream attracting much research effort [5].

Another promising configuration is the multiport DC–DC converters. Traditionally, multiple DC–DC converters are used to connect multiple renewable energy sources to a grid or load. Nevertheless, multiple DC–DC converter option causes problems, such as low efficiency because of using an independent DC–DC converter for each source, big architecture, lower power density, and high cost. For example, photovoltaic (PV) systems having rechargeable batteries are prone to be complex and costly because multiple converters are necessary to individually regulate a load, PV panel, and battery. To overcome the above drawbacks, multiport DC–DC converters have been used. This kind of converter has multiple input ports for combining various DC energy sources [6]. The primary purpose is to integrate multiple ports into a single power stage allowing power flow between each port. It has the advantages of low losses, high power density, compact structure, and low cost. To date, a number of alternative designs have been reported in the open literature that combine all stages into a single power stage with integrated multiple ports resulting in a multiport converter. Multiport DC–DC converters help in efficiently managing power and integrating load with multiple sources. There is a single controller for multiple input and output ports [7]. In a multiport DC–DC power converter, there are fewer power components required, which reduces the cost of the power converter, thus making it a cheaper option. Additionally, the transformation steps are minimized, which results in higher productivity. Multiport DC–DC converters show promising applications particularly in solar systems due to the merits of high power density, low cost, and compact structure. Besides, power flow among different ports can be controlled more easily than that with multiple individual converters because no board-to-board communication is required [8]. There are two categories of multiport converters. One is the non-isolated multiport converter, which does use transformers; the other is isolated multiple converters and they are preferable owing to the advantage of electrical isolation and high step-up voltage ratio.

2.1.2 DC–AC converters (inverters)

As to DC–AC converters, i.e., inverters, the DC–AC conversion can be achieved by a variety of circuitry topologies available. One of the most popular topologies

is the two-level voltage-source inverter (VSI) [9–11]. Meanwhile, there are also topologies such as the multilevel [12, 13] and interleaved forms that have recently attracted much interest from engineers and scholars in MGs. Other power converters recently proposed for MG applications are the current source inverters (CSIs) [14, 15], matrix inverters [16], and solid-state transformers [17]. Inverters have two main functions: to regulate the active (P) and reactive (Q) powers injected into the AC bus and to manage the connection of the DERs to the MGs AC bus.

Particularly, multilevel inverters have drawn much attention in recent years. Multilevel converters have been developed usually for medium-voltage high-power applications. They have become a mature solution for the increasing power demand of multiple applications such as renewable energy systems. However, the maximum nominal power of three-phase converters (mainstream converter topology for a vast number of applications) is limited by these maximum ratings. If the nominal power of the application is above this physical limit, it would be required to install several power units to manage all the power. To overcome this issue, for more than decades, researchers have focused on developing new power converter topologies with higher nominal power using the existing limited-power devices. This fact is achieved by a clever serial connection of power devices increasing the voltage managed by the converter. Based on this principle, various multilevel converter topologies have been developed. Such multilevel converters show advantages including improved output waveform quality, reduced output filter, medium-voltage high-power operation, and fault-tolerance capability [18]. On the other hand, higher complexity of control and modulation techniques, voltage isolation requirements, DC voltage balance needs, and complex switching-signals routing can be regarded as potential disadvantages.

Regardless of topologies, inverters can be categorized into three types, depending on their functionality. They are grid-forming inverters, grid-feeding inverters, and grid-supporting inverters [19].

2.1.2.1 Grid-forming inverters

A grid-forming inverter can be equivalent to an ideal AC voltage source connected in series with a small impedance output. Using a proper control loop, a voltage with specified voltage amplitude and frequency can be generated for the local grid. They have two main objectives, one for grid connection and another for islanded operation. In grid-connected operation, grid-forming inverters regulate the active and reactive powers injected into the AC bus to maintain the power balance and, in some cases, to improve the power quality. In islanded operation, its main task is to form or generate the sinusoidal voltage on the bus. In this case, it can be represented as a controlled voltage source with a low impedance in series. Parallel grid-forming inverters typically have droop control to adjust both the output voltage frequency and magnitude to regulate the active and reactive power, respectively. As voltage sources, they present a low output impedance and, hence, need an extremely accurate synchronization system to operate in parallel with other grid-forming converters. In a MG, the AC voltage

generated by a grid-forming power converter will be used as a reference to which the rest of grid-feeding power converters synchronize. In fact, a grid-forming inverter usually operates specifically in an islanded mode in MGs where synchronous generators are not available to produce the main grid AC voltage.

2.1.2.2 Grid-feeding inverters

Grid-feeding inverters are controlled as current sources with high output impedance in parallel [20]. Due to the nature of the current source, such power converters can therefore operate in parallel with other grid-feeding power converters in grid-connected mode. Actually, most of the power converters associated with DG systems operate in grid-feeding modes, such as in PV or wind power systems. Grid-feeding power converters cannot operate in stand-alone mode if there are no grid-forming or grid-supporting power converters, or local synchronous generators to maintain the voltage amplitude and frequency of the AC MG. In this sense, a grid-feeding power converter, controlled as a current source, needs a generator or a power converter to form the grid voltage for normal operation. Therefore, this kind of converter cannot operate independently in islanded mode. The grid-feeding inverters are mainly aimed to deliver power to an energized grid.

2.1.2.3 Grid-supporting inverter

A grid-supporting power inverter, as the name indicates, provides support to the regulation of the grid frequency and the voltage. It acts in between a grid-feeding and a grid-forming power converter to deliver a proper amount of active and reactive powers to the energy system [21]. Due to the limited amount of energy in DGs and ESSs, a grid-forming inverter may not be able to maintain the voltage frequency and amplitude of the AC bus within the desired ranges. Thus, dispatchable generators and/or additional ESS associated with grid-supporting inverters are able to help, or support, grid-forming inverters in islanding operation. In islanded mode, grid-supporting inverters usually operate as a controlled voltage source. Meanwhile, they can be also controlled to follow the grid and then inject a given amount of current to provide assistance to grid-forming converters. During grid-connected operation, those grid-supporting inverters can be idle or may be used to improve the power quality of the AC bus.

It is noted that while various power converters can be utilized in MGs, the three-phase two-level bidirectional AC–DC converter is used as an application example in this book.

2.2 Control of a single converter

In power electronics and electric drives, a large variety of pulse width modulation (PWM) converters have been built, and ongoing effort has been paid by researchers to develop the associated control strategies over the last few decades. Recently, due to the fast growth in the exploitation of renewable energy sources

such as wind power, solar PV, and wave energy, more and more power converters have been utilized to interface the power sources with the AC and/or DC common buses in distributed energy systems and MGs. In a power-electronics-rich power grid, power converters are required to present high efficiency and operate effectively to improve power quality and maintain dynamic stability [22]. To fulfill these requirements, advanced control techniques are highly desired.

As illustrated in Figure 2.1, several control schemes have been developed for the control of a single power converter. The classic linear controllers, which usually include PWM, and nonlinear controllers based on hysteresis comparators, are the widely utilized control approaches for power converters. Among various schemes, the voltage-oriented control (VOC) and direct control are the most commonly used methods. At the same time, other advanced control techniques such as predictive control, fuzzy logic, and sliding mode control (SMC) were developed with rapid evolution of digital signal processors in computational capacity. Here, these control methods will be reviewed with a three-phase two-level AC–DC converter as an implementation example. Particularly, the model predictive control (MPC) strategy, which is the main focus of this book, will be investigated in more detail.

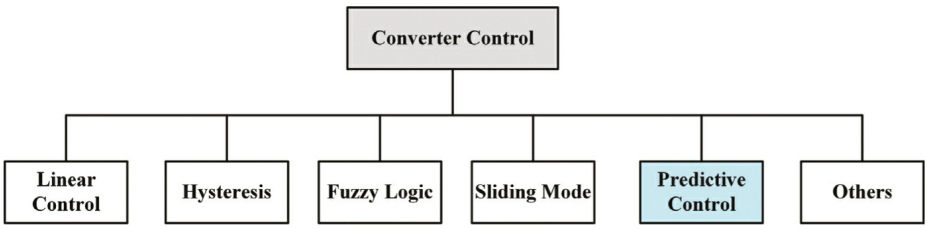


Figure 2.1 Control methods of power converters

2.2.1 Voltage-oriented control

The classic scheme of VOC is illustrated in Figure 2.2. Since the line current vector, $\boldsymbol{i} = i_d + ji_q$, follows the phase voltage vector, $\boldsymbol{v} = v_d + jv_q$, of the power source supplying the converter, a revolving reference frame aligned with $\boldsymbol{v}$ can be used. Under this reference frame, the converter active power output can be controlled by adjusting the reference value, i_d^*, of the quadrature component of $\boldsymbol{i}$, while the converter reactive power output can be controlled by setting the reference value, i_q^*, of the quadrature component of $\boldsymbol{i}$ [23]. Usually, i_q^* is set to zero for unity power factor operation. The actual converter currents, the components in both d-axis and q-axis, are compared with their references. After that, the errors are delivered to the proportional–integral (PI) controllers to generate the converter voltage references. Once the voltage reference is obtained, the corresponding switching signals for individual phases of the rectifier can be generated by PWM techniques such as a classic space vector modulation (SVM).

VOC approaches present several merits including fixed switching frequency and insensitivity to the line inductance variation. However, the requirement of coordinate transformation, decoupling between active and reactive components, and proportional-integral-derivative (PID) regulator tuning result in complex algorithms and compromised transient performance.

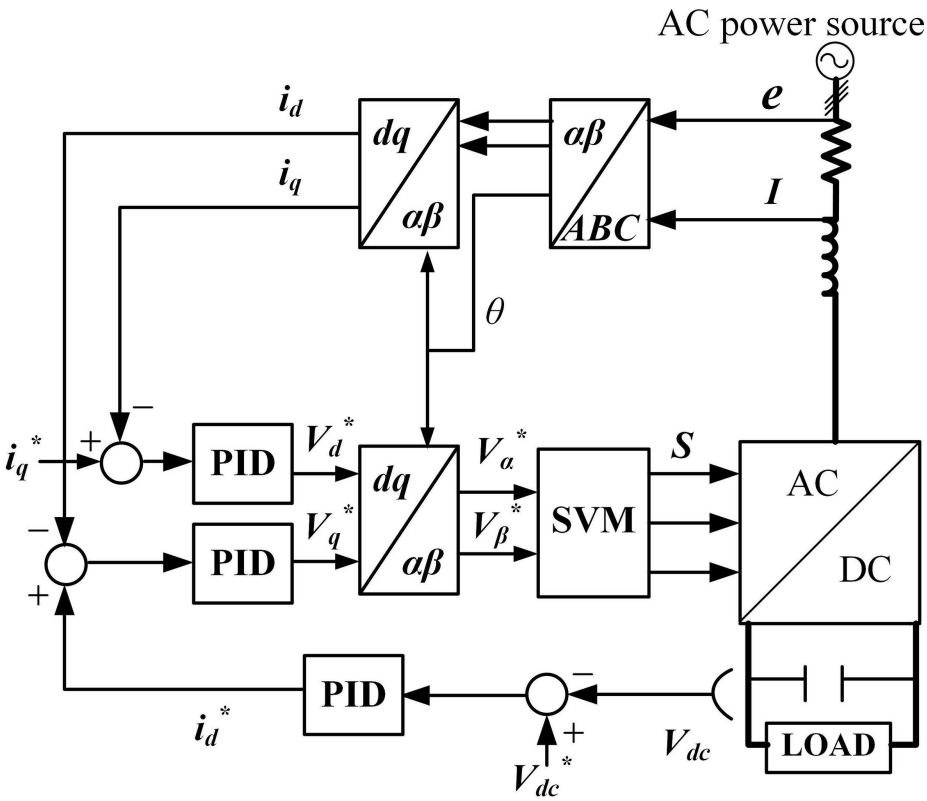


Figure 2.2 Block diagram of VOC

As to inverter control in applications such as uninterruptable power supply (UPS), the cascaded inner-current outer-voltage control structure has been widely used [24]. The schematic diagram of the conventional linear control structure is presented in Figure 2.3, which is used to produce signals to drive converters. It is shown that the cascaded control structure consists of an outer voltage loop tracking the reference voltage and providing a current reference for the inner current loop and an inner current loop generating the voltage reference for the pulse width modulator.

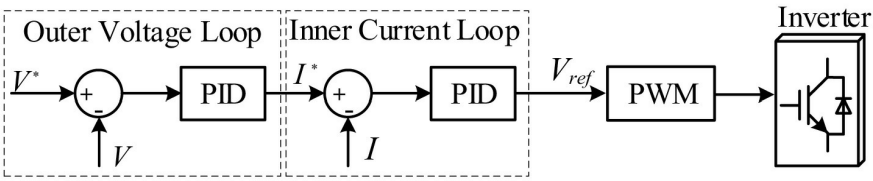


Figure 2.3 Schematic diagram of the conventional linear control of an inverter

While the linear control technique has been used to control power converters, some drawbacks appear.

1. The control architecture becomes complicated when using multiple feedback loops and PWM generator to produce PWM signals, which also results in a slow dynamic response.
2. PID modules are generally adopted. However, the PID parameter-tuning procedure based on extensive trial-and-error tests is time-consuming, which leads to a difficult implementation.
3. In a real MG that contains diverse renewable energy source (RESs), fluctuant power generation is unavoidable, which can bring in possible oscillations if there are no rapid and active reactions. In this sense, traditional linear control methods may no longer be competent to meet the new requirements.

2.2.2 Direct control

Over the past few years, the direct control strategy has been emerging as a simple but effective control approach. Depending on the directly controlled control objectives, this control strategy can be expanded into various applications. One of the most commonly used approaches in DG systems and MGs is direct power control (DPC) [22]. The conventional direct switching table-based direct power control (SDPC) based on switching table stems originally from the direct torque control for AC machine drives, and it has now become one of the most popular control strategies because of its excellent transient performance, robustness, and simplicity [25, 26]. In the SDPC, according to the output signals of hysteresis active and reactive power controllers as well as the position of grid voltage vector or virtual-flux vector, the proper switching state of controlling the converter is selected from a predefined switching table. Since then, several improved switching tables have been proposed, trying to achieve better system performance such as reduced power ripples and faster dynamic response [27, 28].

Different from VOC, SDPC has a totally different principle in selecting control signal for the converter by replacing traditional coordinate transformation, pulse width modulators, and inner current loops with a switching table. The disadvantages of SDPC are variable switching frequencies and relatively large

ripples on the controlled variables.

Figure 2.4 illustrates the SDPC scheme applied to an AC–DC converter. It has been seen as a milestone in power converter control, and it is often regarded as a benchmark to which new DPC strategies are compared. The referenced active power, P^*, is produced from the PID regulator of the outer DC voltage loop while the referenced reactive power, Q^*, is usually set to zero for unity power factor control. The digitized signals, d_P and d_Q, are then generated by two fixed bandwidth hysteresis comparators using the tracking errors between the estimated and referenced values of active and reactive power. The converter switching states are selected based on a look-up switching table according to d_Q, d_P, and the position of power source voltage, which is located in an α-β plane divided into 12 sectors, as depicted in Figure 2.5. This algorithm is derived based on the stationary reference frame without involving any modulation. The major disadvantages include large power ripples and variable switching frequency. To achieve a satisfactory performance, a relatively high sampling frequency and hence, a high switching frequency is needed.

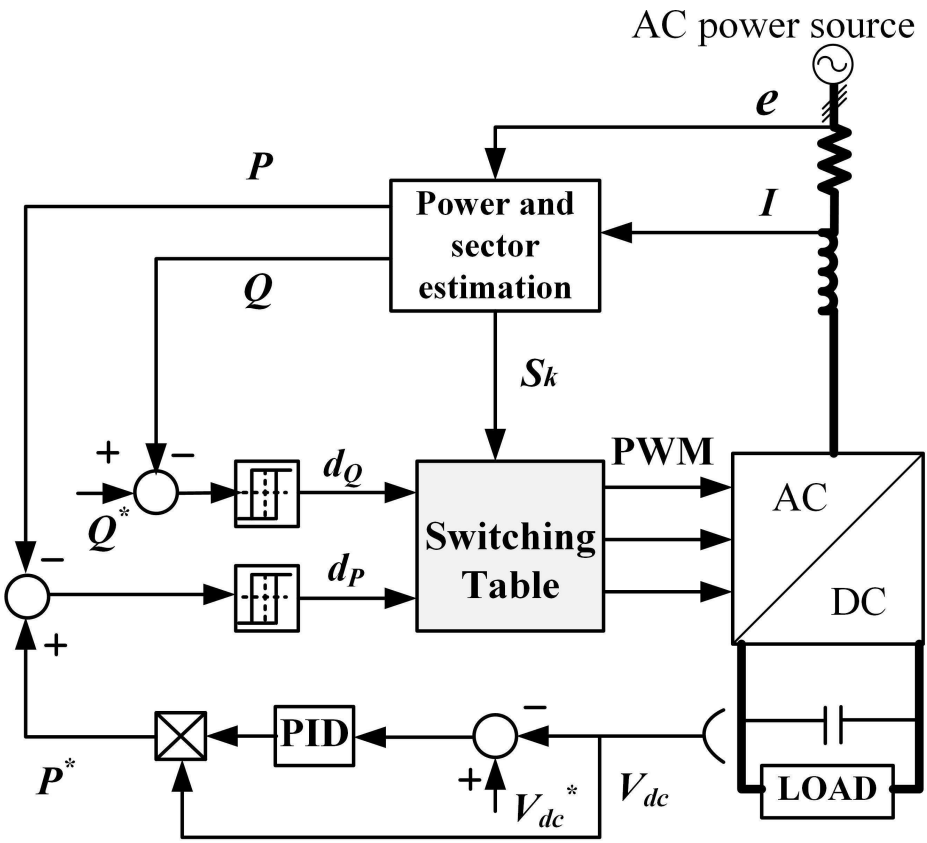


Figure 2.4 Block diagram of DPC

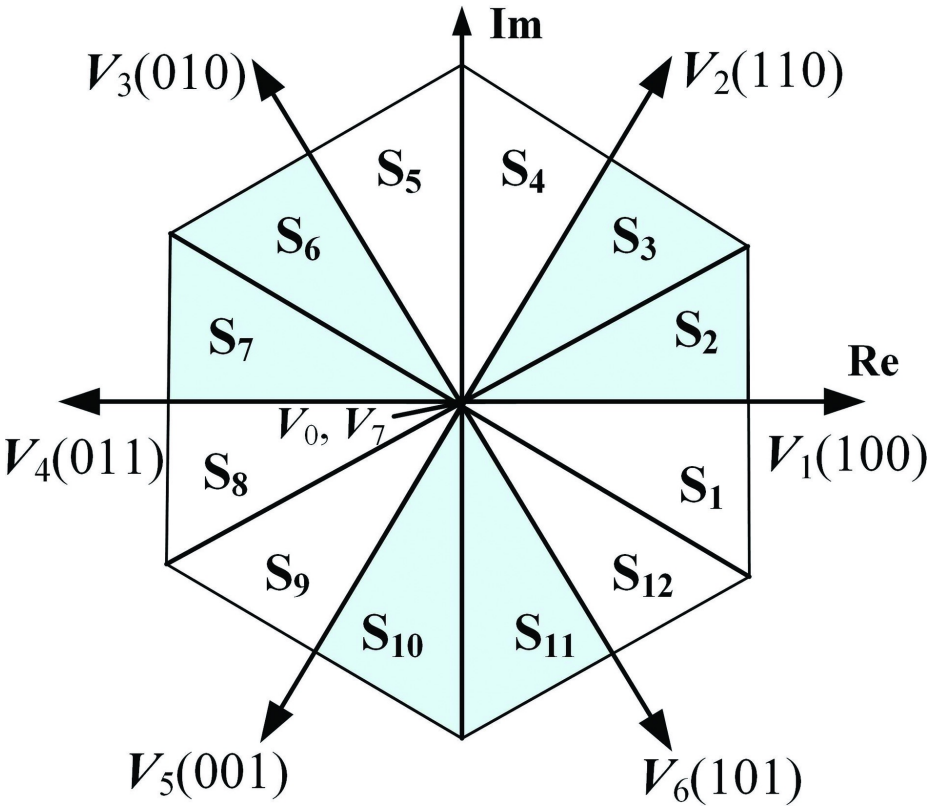


Figure 2.5 Voltage vectors and the sector division

2.2.3 Fuzzy logic control

Fuzzy logic control features adaptive characteristics in nature, which means it has the ability of robust response subject to external load disturbance, system parameter variation, and uncertainty. It has been widely used in the field of power electronic converters. Figure 2.6 shows the schematic diagram of fuzzy logic control applied to an AC–DC conversion system. Different from the SDPC discussed in Subsection B of Section 2.2, this method determines the control action for the converter by means of fuzzy logic rules according to the instantaneous errors of active and reactive power, εP and εQ, respectively. At each control instant, the deviation between the reference and the actual performance, $\varepsilon P(k)$ and $\varepsilon Q(k)$, is converted to the corresponding fuzzy variables, which are used to determine the desired switching state [29].

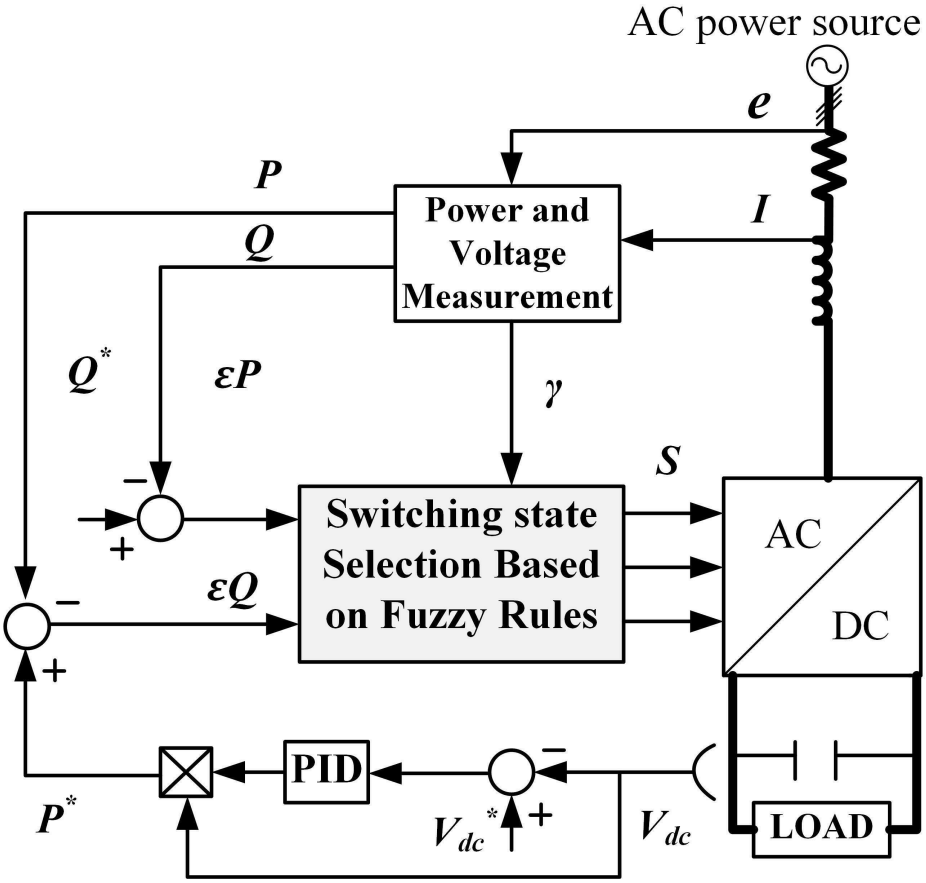


Figure 2.6 Block diagram of fuzzy logic control

2.2.4 Sliding mode control

The basic principle of the SMC method is to enforce the trajectories of the system variables onto a sliding surface (or hyperplane) using a relatively high-frequency switching control signal. After a finite time, the system trajectories remain at the vicinity of the sliding surface and eventually toward the equilibrium point [30]. Since the system will move toward the equilibrium point, the sliding surface can be designed carefully to achieve desired specifications according to the applications and the control objectives. SMC is robust with respect to matched internal and external disturbances. On the other hand, undesired chattering produced by the high-frequency switching may be considered as a problem when SMC approaches are implemented in practical applications.

The SMC theory is illustrated in Figure 2.7 with the AC–DC conversion as an example. The error between the DC-bus voltage reference V_{dc}^{*} and the measured

DC-bus voltage V_{dc} is processed by SMC, which produces the active power reference, P^*, and reactive power reference, Q^*. They are then compared with the actual power values. The errors are further delivered to the hysteresis comparators, and the output is used to select an appropriate switching state or voltage vector for the converter. A SMC controller contains two fundamental components, i.e., the sliding surface and the SMC law. As mentioned in Subsection E of Section 2.2, the sliding surface is employed to predefine the trajectories of the control objective. To improve the transient response and minimize the steady-state error, the switching surfaces can be designed in integral forms. Alternatively, they can also be established using back-stepping and nonlinear damping techniques. As to the design of the SMC law, a Lyapunov approach is usually sufficient to derive conditions on the control law that will enforce the system state to orbit around the equilibrium [31, 32].

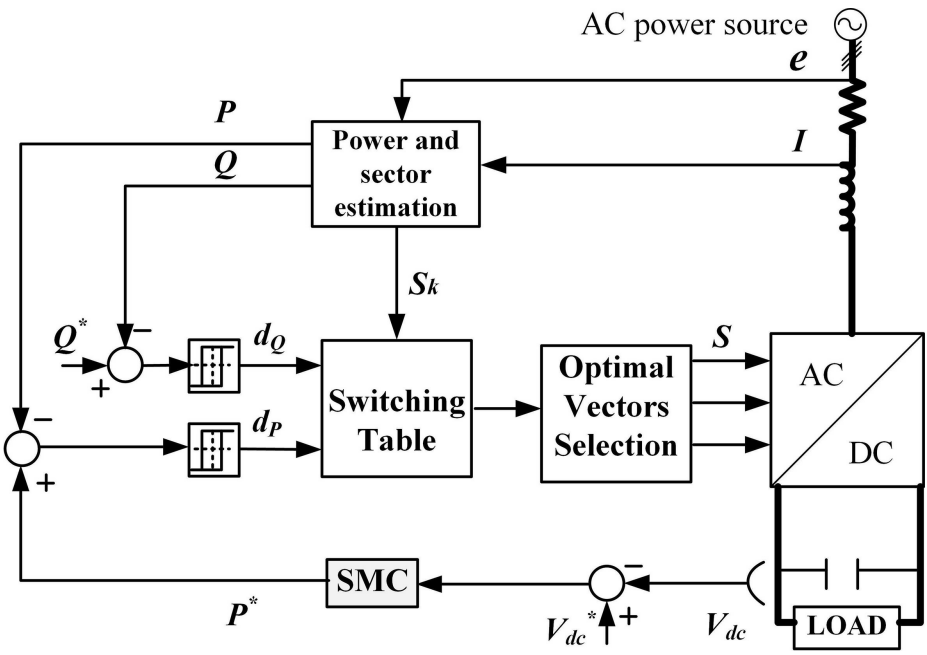


Figure 2.7 Block diagram of SMC

2.2.5 Predictive control

More recently, predictive control has emerged as an attractive approach for controlling power converters and DGs [33–35]. Different types of control methods have been developed under the name of predictive control. The most important types are deadbeat control [36, 37], vector-sequence-based predictive control (VPC) [38, 39], and MPC [40–46]. Deadbeat control uses the system

model to predict the required voltage vector that can enforce the controlled variable to track the reference in every sampling period. This required voltage vector is then generated using a modulator such as SVM. The principle of the VPC is to force the system variables onto the pre-calculated trajectories, in which several voltage vectors are typically used within each control period. In the MPC, the system model and the possible control options are used to predict the system behavior over a certain time horizon. After that, a cost function as the criterion is used to evaluate the possible control options, and the one that minimizes the cost function will be selected to control the converter. MPC is the focus of this book. It will be investigated comprehensively and its applications on MGs will be studied.

2.2.5.1 Deadbeat-based predictive control

The deadbeat-based predictive control approach takes advantage of system models to compute, once at the beginning of every control period, the required control action that enables the controlled variable to reach the reference value at the end of every control period [36, 37]. The required control action, or the desired voltage vector, can be synthesized by a SVM to obtain the PWM signal. The utilization of this approach has been seen in various applications, such as current and power control in inverters and rectifiers, harmonics elimination in active filters and power factor correctors, voltage regulation in DC–DC converters and uninterruptible power supplies, as well as electromagnetic torque and flux control of electric drives.

In a renewable power DG system, besides the utilization of inverters where DC power is converted to AC power such as grid-connected PV inverters and rotor-side inverter of doubly-fed induction generator (DFIG)-based wind power system, there is also AC–DC conversion, for instance, grid-side converter control of DFIG-based wind power system, generator-side converter control of PMSM-based wind power system, and battery bank-based energy storage system (ESS) connected to the common AC bus in MGs. Figure 2.8 illustrates the working principle of the deadbeat-based predictive control in AC–DC conversion. To mitigate the active and reactive power-tracking errors at the end of a sampling period, the controller uses the system model to estimate, once every sampling period, the required reference voltage that can make P and Q reach their reference values in the next sampling instant. This required voltage vector is then produced using an SVM to generate the relevant switching signals. The advantages of this approach include a better steady-state performance with fewer ripples in the controlled variables. Nevertheless, as the prediction depends on the system model, variations in the parameter values of the model, one-step delays, and other errors in the model often deteriorate the system performance and may lead to instability. Another limitation of these deadbeat control schemes is that constraints of system variables and nonlinearities are difficult to incorporate.

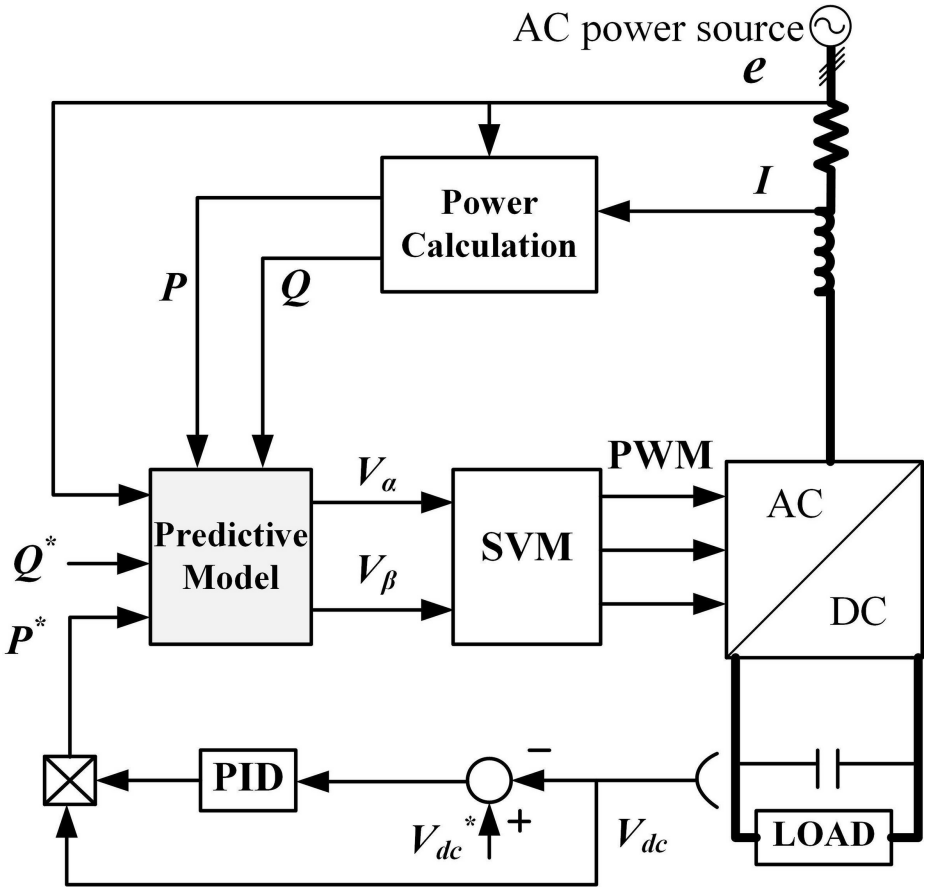


Figure 2.8 Block diagram of deadbeat-based predictive control

Here, the feasibility of the deadbeat predictive control strategy is tested in an AC–DC conversion system, as shown in Figure 2.9. Three insulated-gate bipolar transistor (IGBT) bridges are connected to the AC source with a choke including inductors L and resistors R. At the DC side, a purely resistive load R_L is connected parallel to a capacitor C. Figures 2.10 and 2.11 show the experimental results. To demonstrate the effectiveness of the deadbeat-based predictive control, SDPC is used here as a benchmark for comparison. It can be observed that the active and reactive powers are poorly controlled in the case of SDPC with large ripples, particularly in reactive powers, thus leading to severely distorted line currents. However, after using the deadbeat-based predictive control method, the power ripples are significantly reduced with much more sinusoidal line currents and more stable DC-link voltage.

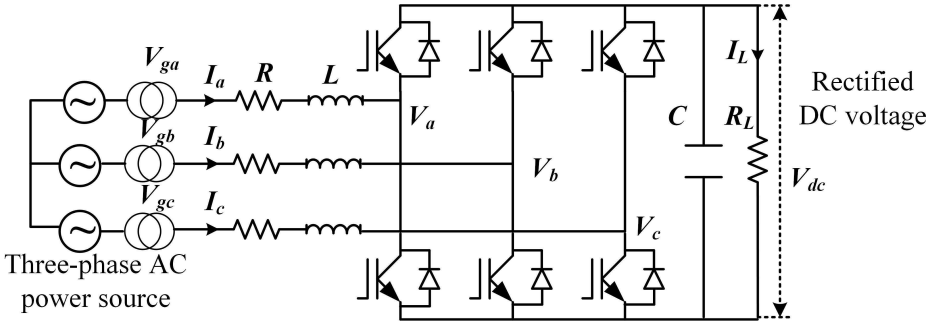
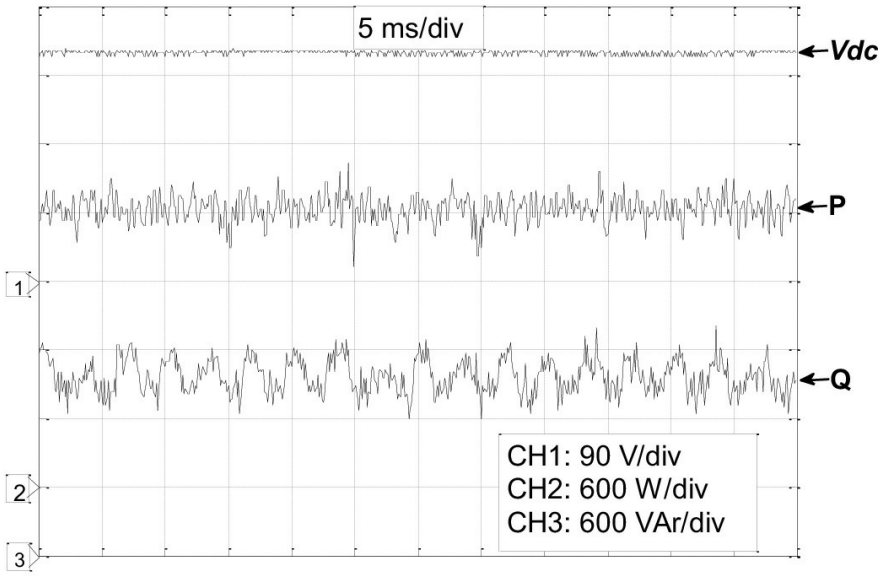
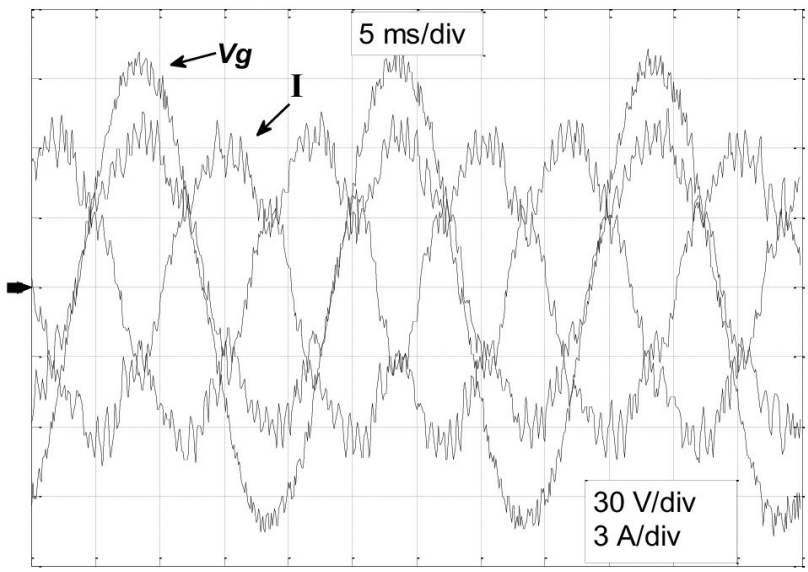


Figure 2.9 Structure of an AC–DC conversion system

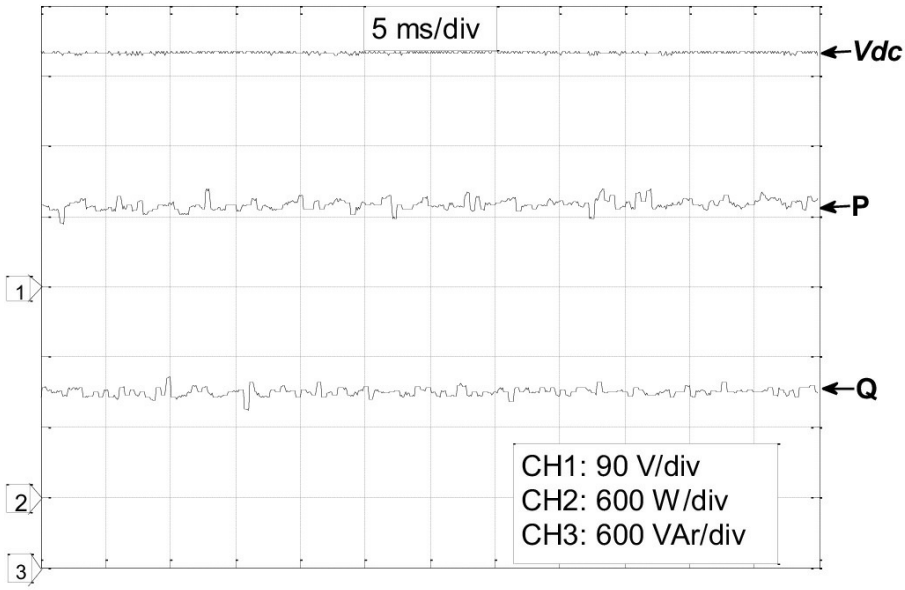

5 ms/div
Vdc
P
Q
1
2
3
CH1: 90 V/div
CH2: 600 W/div
CH3: 600 VAr/div

(a)

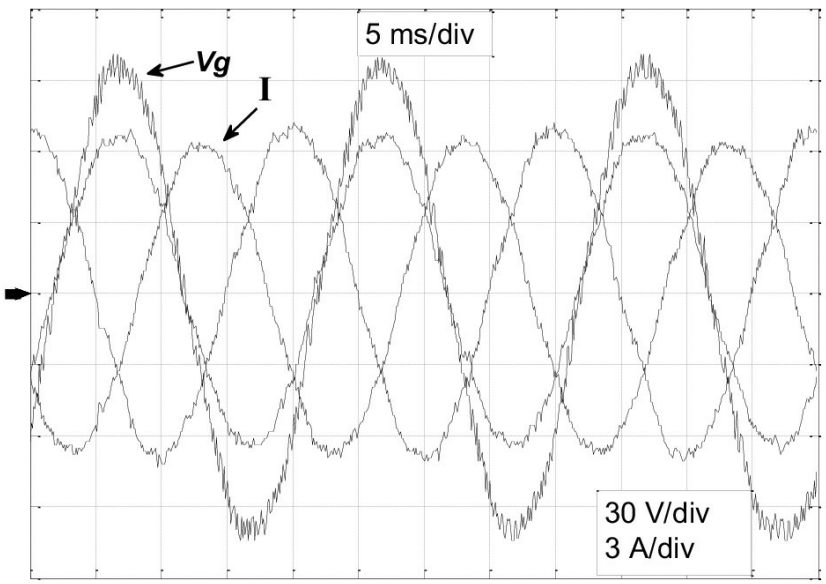

5 ms/div
Vg
I
30 V/div
3 A/div

(b)

Figure 2.10 Experimental results of AC–DC conversion using SDPC: (a) DC-link voltage, active power, and reactive power, (b) grid voltage and three-phase line currents


5 ms/div
Vdc
P
Q
1
2
3
CH1: 90 V/div
CH2: 600 W/div
CH3: 600 VAr/div

(a)


5 ms/div
Vg
I
30 V/div
3 A/div

(b)

Figure 2.11 Experimental results of AC–DC conversion using deadbeat-based predictive control: (a) DC-link voltage, active power, and reactive power, (b) grid voltage and three-phase line currents

For better comparison, the quantitative index of the sampling frequency, average switching frequency, power ripples, DC-link voltage ripple, and line current total harmonic distortion (THD) are listed in Table 2.1. It can be seen that the deadbeat predictive control strategy presents an overall better performance than that of SDPC, in terms of active and reactive power ripples, DC-link voltage ripple, and line current THD, with almost the same switching frequencies.

Table 2.1 Quantitative comparison of DPC methods in experiment

Strategy	f_s **(kHz)**	f_{sw} **(kHz)**	P_{rip} **(W)**	Q_{rip} **(VAR)**	V_{dc_rip} **(V)**	**THD (%)**
SDPC	20	5.06	68.60	107.58	1.25	12.08
Deadbeat-based predictive control	20	5.00	41.91	33.78	0.79	5.60

2.2.5.2 VPC

This predictive approach chooses an optimal set of concatenated voltage vectors that force the controlled variables to converge toward the reference values within a fixed predefined switching period [38, 39]. The difference from deadbeat control is, for deadbeat control, the reference voltage, V^*, is calculated in every sampling period directly from the predictive model and generated using modulators. For VPC, the required control action is not determined directly from the predictive model, instead, by predefined criteria, and thus no modulators are needed. And this control action is usually a set of concatenated voltage vectors rather than one single voltage vector.

Figure 2.12 illustrates the principle of the VPC of rectifiers. The instantaneous active and reactive power slopes (or the derivative of active and reactive powers with respect to time), f_p and f_q, for different voltage vectors can be calculated. Under the condition that the power source voltage is unchanged and the line current variations are small during each sampling period, the power slopes can be assumed constant for this period. By applying different voltage vectors, the active and reactive powers can be controlled differently as they have different effects on the P and Q. Taking the symmetrical 3+3 vectors sequence as an example, within every control period, the active and reactive powers can increase or decrease in

three different rates of change. Figure 2.13 shows the schematic waveform of the symmetric 3+3 VPC. The vector selection is based on specified criteria by evaluating the effects of the vectors on the control objective y. These criteria vary with different applications, e.g., forcing y equal to y_{ref} at the end of the period (i.e., deadbeat control), or making the mean value of y equal to y_{ref} over the entire period, or making the root mean square value of y over one period to be minimal. The key of this approach is to calculate the proper duration for each voltage vector according to the specified criteria such as power ripple minimization and a deadbeat manner. Because of the utilization of an optimal sequence of vectors in each period, i.e., more than one voltage vector, the system objectives can be well controlled, thus resulting in excellent steady-state performance. The drawbacks include complicated control structure and high sensitivity to system parameter variations due to the complexity in the calculation of "slopes." To obtain an intuitive view of the active and reactive power derivatives (or "slopes"), Figure 2.14 graphically illustrates the evolutions of active and reactive power slopes versus powersource voltage vector position for an AC–DC rectifier.

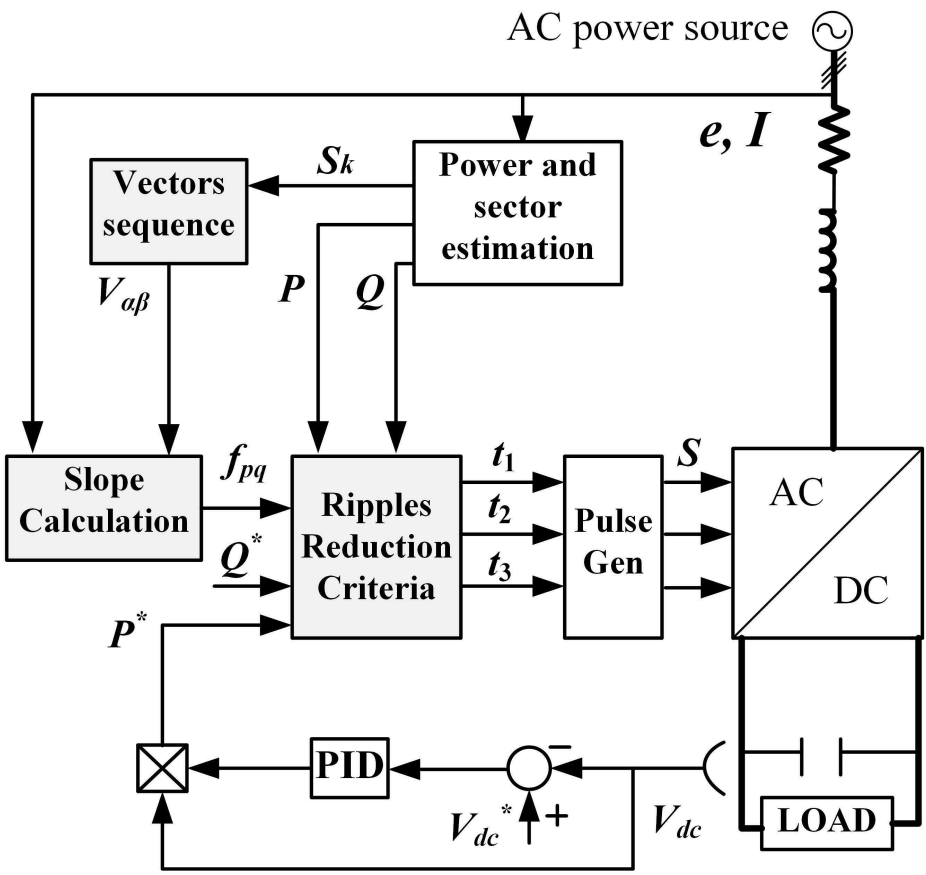


Figure 2.12 Block diagram of VPC

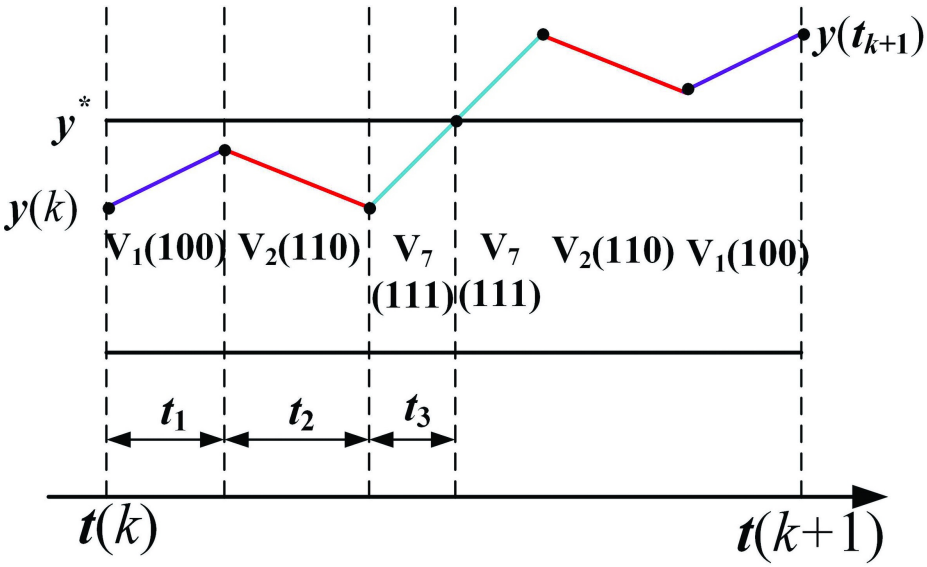


Figure 2.13 Schematic illustration of a symmetric 3+3 vectors sequence

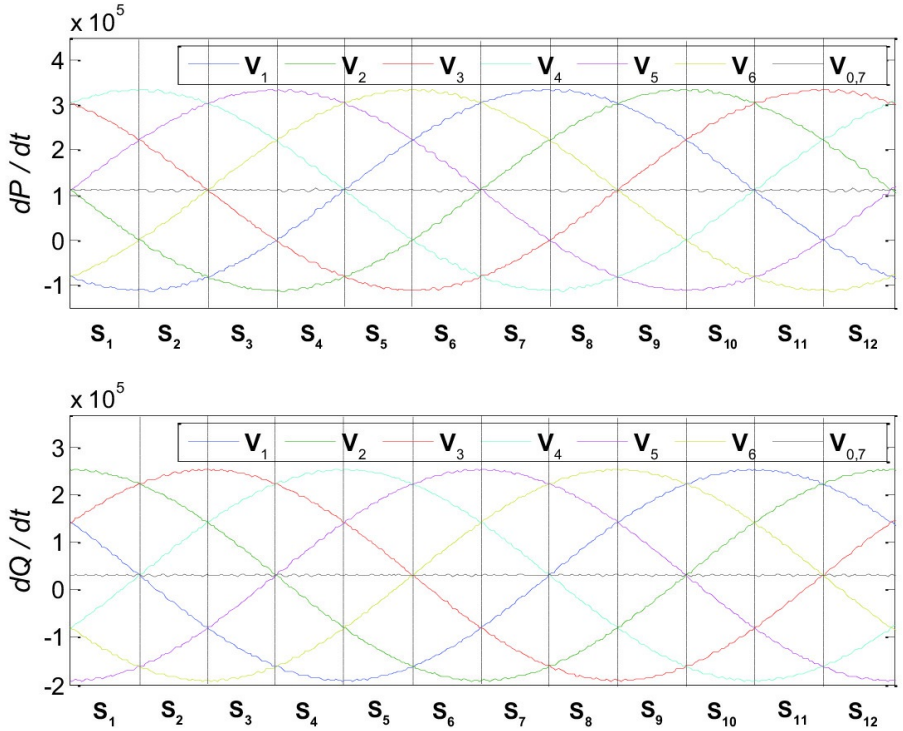


Figure 2.14 Active and reactive power derivatives against the input voltage vector position

In VPC, in addition to the duration for each voltage vector, another important factor that determines the controller performance is the selection of voltage sequence in every control period. Taking the three-phase two-level AC–DC conversion, for example, in sector S_2, the instantaneous input power of the rectifier can be regulated properly using vector sequence $\mathbf{V}_1$-$\mathbf{V}_2$-$\mathbf{V}_7$ in every sampling period [38, 39]. This is because these three selected vectors can increase and decrease the active power (or reactive power) within the sector. However, an in-depth analysis of the power slopes in Figure 2.14 reveals that all three vectors produce positive dQ/dt during the initial part of S_2 because $\mathbf{V}_1$ actually generates positive dQ/dt at the very beginning, resulting in large reactive power ripples. Furthermore, using the least-squares method as the ripple reduction criterion to calculate the duration of each vector, a negative period for the second vector $\mathbf{V}_2$ is generated. In practical implementation, this will generally be forced to be zero, and thus an unexpected failure will occur [28]. Also, a negative duration indicates that another active vector that decreases Q is required to replace $\mathbf{V}_2$ to control the power more effectively ($\mathbf{V}_5$ or $\mathbf{V}_6$, generally $\mathbf{V}_6$ should be selected with the

purpose of reducing commutation frequency). In a similar manner for other even sectors, the second vector of the vector sequences should be replaced by another appropriate and active vector. Based on this analysis, an improved vector sequence for the rectifier is proposed in Table 2.2, and its overall control scheme is illustrated in Figure 2.15.

Table 2.2 Improved vector selection of VPC

		S1	S2	S3	S4	S5	S6	S7	S8	S9	S10	S11	S12
V_a		V_1	V_1	V_2	V_2	V_3	V_3	V_4	V_4	V_5	V_5	V_6	V_6
V_b	$t_2 > 0$	V_6	V_2	V_1	V_3	V_2	V_4	V_3	V_5	V_4	V_6	V_5	V_1
	$t_2 < 0$		V_6		V_1		V_2		V_3		V_4		V_5
V_c		V_7	V_7	V_0	V_0	V_7	V_7	V_0	V_0	V_7	V_7	V_0	V_0

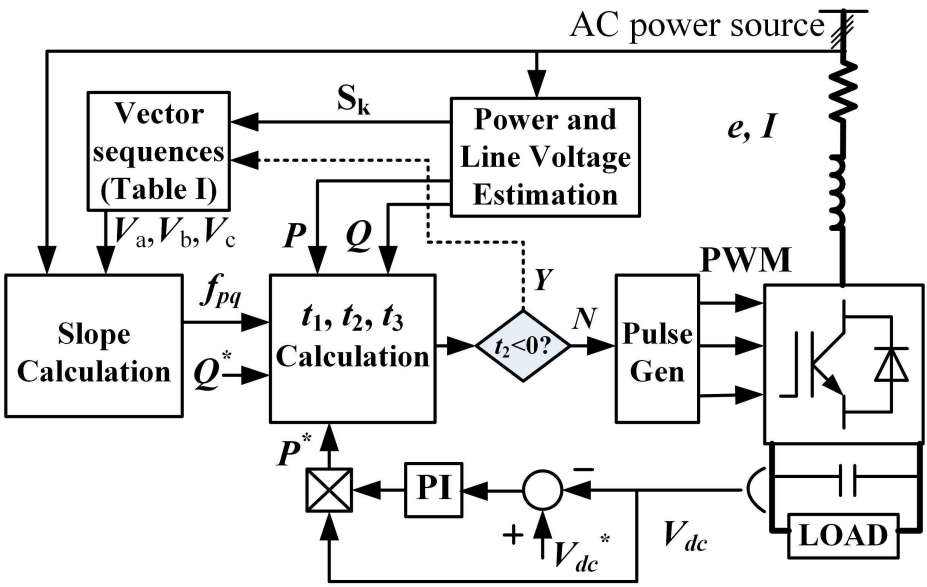
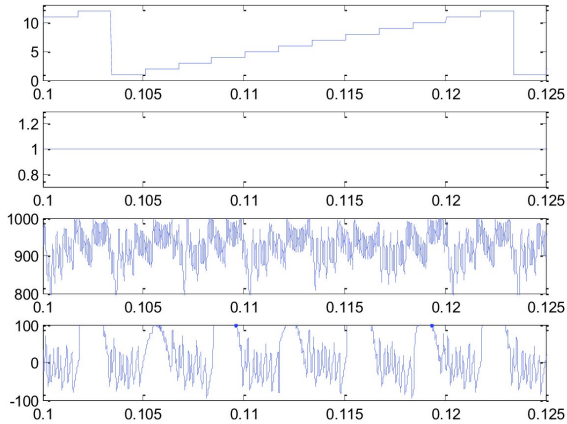


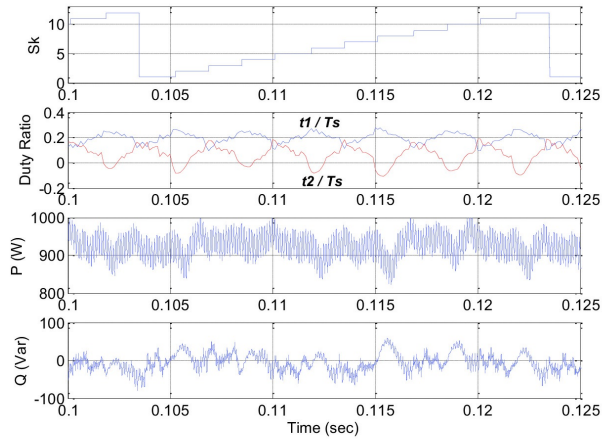
Figure 2.15 The schematic diagram of the improved VPC

The simulation results compared with SDPC and conventional VPC are presented in Figure 2.16, where t_1 and t_2 denote the duration of the first voltage vector and the second voltage vectors, respectively, whereas T_S means the sampling period. Since only one voltage vector is selected in every sampling period according to a predefined switching table, i.e., duty ratio being one, P and Q cannot be regulated satisfactorily, showing large oscillations and ripples, as

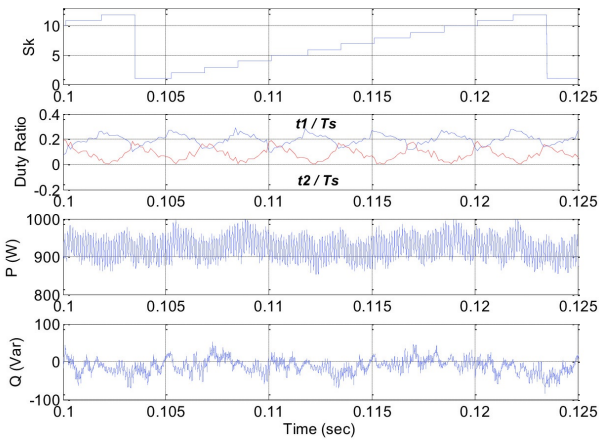
demonstrated in Figure 2.16(a). After that, VPC is applied and the results are presented in Figure 2.16(b). It can be seen that P and Q can track their references better compared with SDPC. Then, further observation reveals that t_2 is smaller than zero at the beginning of the even sectors. This means the second voltage vector selected is actually not effective to control the P and Q at the beginning of the even sectors. To address this problem, an improved vector sequence selection strategy depicted in Table 2.2 is applied. After using improved sequences, both active and reactive powers were regulated more smoothly and their ripples are reduced further, as proved in Figure 2.16(c).


10
5
0
0.1
0.105
0.11
0.115
0.12
0.125
1.2
1
0.8
1000
900
800
100
0
-100

(a)


Sk
Duty Ratio
t1 / Ts
t2 / Ts
P (W)
Q (Var)
Time (sec)

(b)


Sk
Duty Ratio
t1 / Ts
t2 / Ts
P (W)
Q (Var)
Time (sec)

(c)

Figure 2.16 Comparison of system performance with P = 900 W and Q* = 0 VAR. (a) SDPC, (b) conventional VPC, (c) improved VPC.*

2.2.5.3 MPC

MPC has drawn more and more attention, ever since it originated around the 1970s. As an entirely different control principle and structure, MPC is based on the knowledge of system modeling and the prediction of the system behavior. MPC itself is not strictly limited to one specific control method. In fact, control methods that involve the model of a process or a system with the predictive action can all be categorized as the MPC. In general, based on the type of the optimization problem, the MPC methods are classified into finite control set-MPC (FCS-MPC) [40–43] and continuous control set-MPC (CCS-MPC) [44, 45].

The MPC uses the system model to predict system behaviors over an N-step time horizon in the future and a cost function subsequently as the criterion for choosing appropriate switching states. Generally, the design of a MPC controller can include three steps: system predictive model, cost function formulation, and parameter design. First, the system model can be discretized into a state-space model. With the present state of the model, the discrete interval and the possible control actions as the inputs, the output of this discrete model can be calculated. Using this method, the future state of the system can be predicted in a certain horizon of time. Second, a selection criteria over a finite horizon of length N is then designed to evaluate each control action, and the one resulting in the least error between $\boldsymbol{x}(t)$ and $\boldsymbol{x}^*$ will be chosen to control the converter during the next control period. What this cost function aims to achieve is the determination of the most suitable control action that will force a specific system variable, $\boldsymbol{x}(t)$, as close as possible to the reference value, $\boldsymbol{x}^*$. Third, system constraints and nonlinearities are formulated into the cost function. Notice that the weighting factors can be used to prioritize different control objectives to obtain satisfactory performance.

Figure 2.17 depicts the essential principle of the MPC strategy, where one-step prediction is applied. The essential concept of this MPC scheme is to predict the power at the $(k+1)$th instant for all the control possibilities. Obviously, the effects of each voltage vector on the active and reactive powers are different, which will be evaluated according to a specific cost function. After that, the voltage vector that produces the least power ripple can be identified. In AC–DC conversion using rectifiers, the rectified DC voltage across the DC-link capacitor and the power factor of the AC input are the major concerns. They can be controlled by means of active power, P, and reactive power, Q, respectively. Once again, to validate the effectiveness of the MPC strategy, the AC–DC conversion system shown in Figure 2.9 is utilized, and its performance is also compared with that of SDPC. As shown in Figure 2.18, large ripples and oscillations can be

observed in the converter input power, particularly in reactive power, leading to distorted line currents with a large number of harmonics, which is aligned well with the simulation result presented previously. By contrast, using MPC scheme, the optimal voltage vector is chosen according to a cost function to control the active and reactive powers. Therefore, better performance can be achieved, as shown in Figure 2.19.

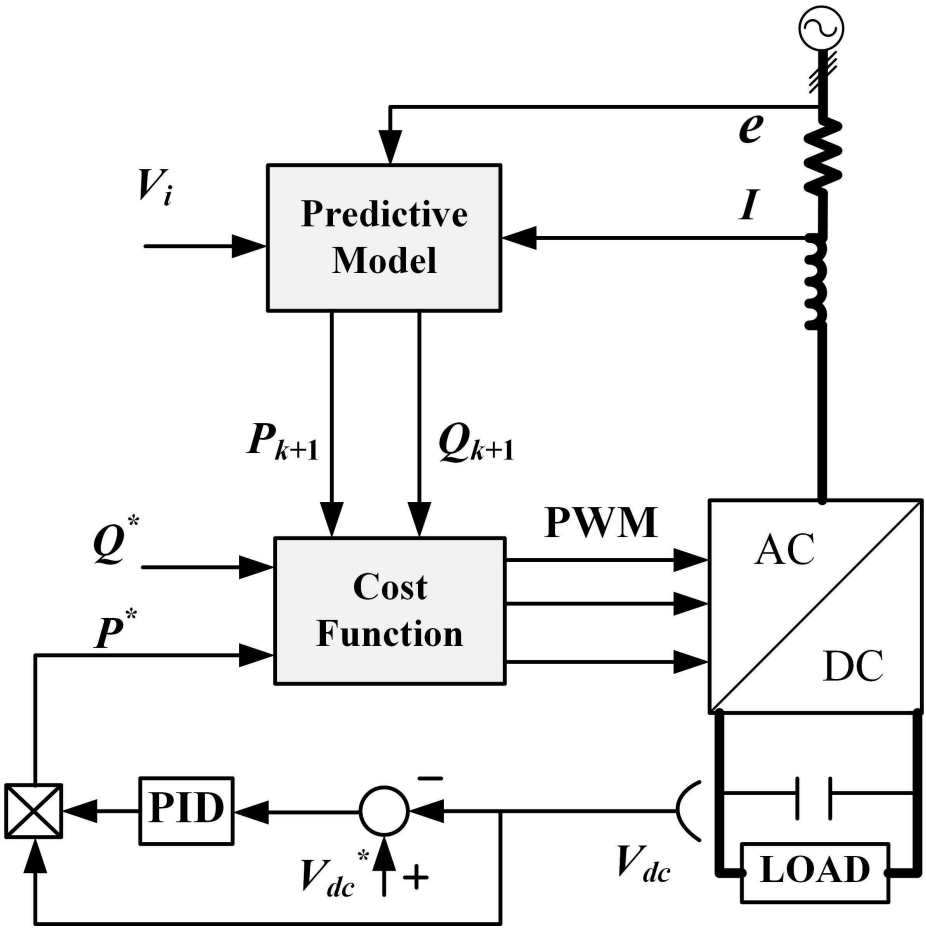


Figure 2.17 Block diagram of MPC

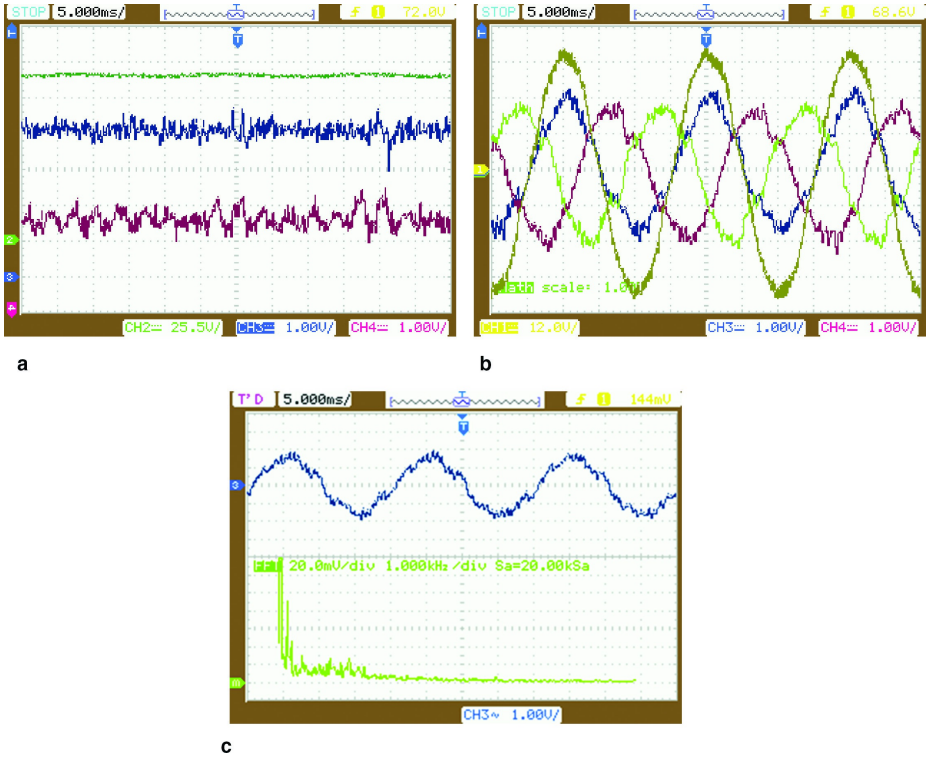


Figure 2.18 Experimental results of AC–DC conversion using SDPC. (a) DC-link voltage, active power, and reactive power, (b) power source voltage and line currents, (c) harmonic spectrum of line current.

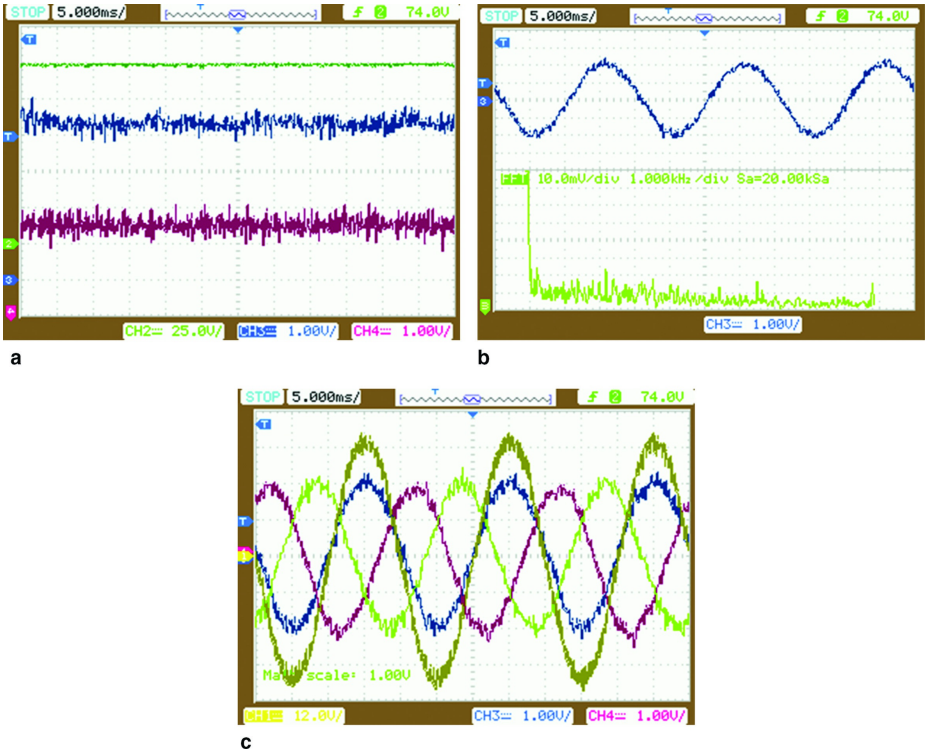


Figure 2.19 Experimental results of AC–DC conversion using MPC. (a) DC-link voltage, active power, and reactive power, (b) power source voltage and line currents, (c) harmonic spectrum of line current.

In the MPC control family, FCS-MPC is an important branch, which uses the discrete-time properties of the system. FCS-MPC has been extensively applied to the field of converter control. For an FCS-MPC-controlled converter, the optimal switching state is determined according to a prespecified cost function and the predictive model is built based on the system states and the converter switching states. The cost function can be solved over some future certain intervals. While the principle of MPC has been explained in detail for AC–DC converters, i.e., rectifiers previously, it has also been widely applied in DC–AC converters, i.e., inverter. Generally, the schematic of the FCS-MPC applied to inverters can be described as shown in Figure 2.20.

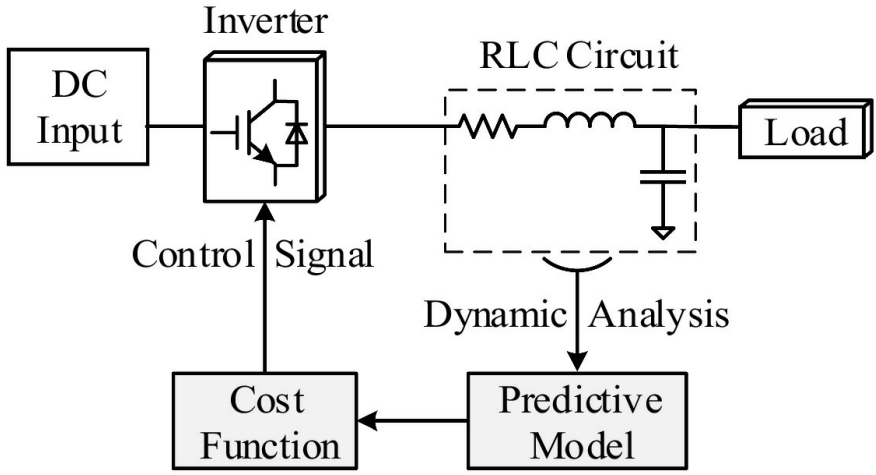


Figure 2.20 Schematic of the FCS-MPC applied to inverters

It can be seen that the predictive model and cost function are the two important ingredients for FCS-MPC-controlled converters. The predictive model is built upon the dynamic analysis of the RLC circuit. Then through a discretization process that facilitates the implementation in processors, the future variables can be obtained by computing state formulas at the current time. The cost function, as an evaluation criterion or an expected control effect, is repeatedly and periodically solved, resulting in the optimal control signals, which will be sent to the switching devices of converters. The multiple objectives can be included in the cost function.

It is noted that there has been ongoing research on FCS-MPC of power converters, resulting in a variety of improved strategies with different functionalities, including long prediction horizon MPC and duty ratio MPC. MPC with a long prediction horizon improves the system's performance and stability as compared with short prediction horizons. One of the challenges in long prediction horizon MPC is the computational burden. This is because FCS-MPC optimization problem is usually solved by an exhaustive search algorithm that computes the cost function's value for each of the possible switching vectors or sequences. When the prediction horizon increases, the computational burden grows exponentially. In duty ratio MPC, the optimal voltage vector selected based on the cost function is integrated with one or two zero-voltage vectors in actual implementation in every control period. The duty ratio is calculated according to some specified criteria such as ripple minimization or deadbeat fashion. This scheme is mainly aimed to improve system steady-state performance.

Besides FCS-MPC, another important stream under MPC of power electronic converters is CCS-MPC, in which a continuous control signal is first calculated,

and then a modulator is used to generate the corresponding switching signals to control the power converter for the desired output voltage. The modulation strategy can be anyone that is valid for the converter topology under study. The main advantage of CCS-MPC is that it results in a fixed switching frequency. In addition, as part or all of the optimization problem can be computed offline, CCS-MPC usually has a lower computational burden than FCS-MPC. For this reason, long prediction horizon problems can be better addressed using CCS-MPC.

There is another line of research, i.e., system-level MPC or grid-level MPC. It is similar to converter-level MPC in terms of control structure. The grid-level MPC also consists of a predictive model, cost function, and solving algorithm. Grid-level MPC functions as an optimization algorithm that is suitable to optimize the performance of constrained systems with multiple objectives. Nevertheless, grid-level MPC aims to control system-level operations rather than power electronic converter-switching states (e.g., power flows within a MG or among networked MGs, ESS capacity, load management). The block diagram of grid-level MPC is presented in Figure 2.21. It can be seen that the prediction model is built upon the system states with possible forecasts, which formulates an expression for the future state prediction usually based on current/past states. More specifically, the forecasts/predictions of the predictive model can be various system variables on a certain time-interval basis, such as PV generations, load demands, and electricity prices. Based on the past and present status and the possible optimal control actions, a prediction model is utilized to predict the future outputs in the plant. Considering the complicated computational process, an optimizer is needed to calculate these control actions, taking the cost function as well as the system constraints into account. The optimizer is another fundamental tool to support the MPC strategy as it is responsible for control action calculation. If the cost function is design in a quadratic format, its minimum can be solved as an explicit function (linear) based on past inputs and outputs and the future reference trajectory. In the presence of inequality constraints in the cost function, however, the solution will need to be gained by more computationally powerful algorithms [46–48].

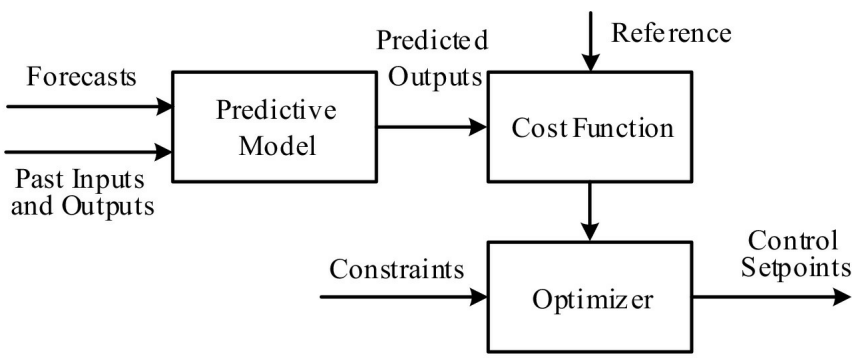


Figure 2.21 System-level MPC

When we design the cost function, it is important to bear in mind that the control objectives together with system constraints should be reflected and weighted properly, i.e., to ensure the predictions generated from the prediction plant and all the possible desired targets are formulated into this cost function. Generally, the terms formulated in a cost function are in line with the multiple control or optimization targets in priority order with weighting factors. In every control period, the optimal control/command sequence is computed over a certain time horizon. Then, a group of system states is refreshed, resulting in an updated control sequence, waiting for another round of calculation to move the horizon one step forward. Taking advantage of the feedback mechanism and the receding prediction horizon, grid-level MPC can effectively reduce the impacts of parameter uncertainties and external disturbances, leading to a robust control structure.

In MGs, constraints involved in DGs, power electronics, and power transfer limit power lines and the utility grid should be considered. Given that the constraints are well integrated into the controller, the system performance can be guaranteed with an ability to operate within or near the constraint boundaries safely. With the time horizon window moving forward, the optimization problems taking constraints into account will be solved and updated again once new predictions are available. Compared to the converter-level MPC, the sampling interval Δt of a grid-level MPC is often larger, ranged from several seconds, several hours, and days. The time horizon is often selected according to multiple factors. For instance, if the PV power output is measured on a 1-min period basis, while the PV generation is predicted every 30 min. In this case, the sampling interval for the MPC is expected to be multiples of 30 min for a better match and precision.

The steps to implement the grid-level MPC can be summarized as follows: (1) system states and targets are utilized to establish a receding model; (2) under a certain control horizon, an optimal control/command sequence is computed for the next control period based on the past, present, and future system states; (3) implement the first step of the MPC considering all variables and constraints; and (4) update all available states for the next period while moving one step ahead and repeating the optimization.

Owing to its control principle and structure, MPC has many attractive characteristics:

1. As a control objective, the cost function of MPC can be designed in a very explicit and intuitive way.
2. Multiple constraints that are derived from either the control demand or object-oriented limitation can be easily involved.
3. Dynamic performance is good and the controlled system is robust.
4. For FCS-MPC used in power converters, control signals can be directly produced, eliminating the signal modulator.

In many regards, although MPC has so many advantages over conventional linear control, it has these major disadvantages:

1. MPC depends on the predictive model of the target system to perform predictive control but sometimes the predictive model is not easy to develop and the accuracy is difficult to guarantee.
2. Since there involves both mathematical modeling and online solution running in the processor, sometimes the computational burden is heavy and cannot be underestimated.
3. For FCS-MPC, sometimes the switching frequency is not constant and keeps changing, which makes the filter parameter difficult to set.

2.3 Control of parallel inverters

In a MG system, DGs are usually connected in parallel to a common voltage bus through power electronic converters. The common bus is then connected to the utility grid or other MGs via a static transfer switch. Proper operation of the MG in both the grid-connected and islanded modes needs the implementation of high-performance power flow control and voltage regulation algorithms. For example, under load variation conditions, instead of supplying the additional power from one DG, all the DGs with sufficient energy capacity should be able to adjust their power outputs to compensate for the change in power demand. The parallel operation of converters is a challenging problem that is more complex than controlling an individual converter because every converter must properly participate in load sharing. In this sense, appropriate control strategies for parallel-connected DGs are required.

The control strategies for parallel-connected converters were initially developed for UPS applications, which can be generally categorized as follows [49]:

2.3.1 Centralized control

The centralized control is depicted in Figure 2.22, which is also known as concentrated control. The output current reference from each module is identical, which is obtained by averaging the total load current among modules. Therefore, it is essentially a current averaging method [50]. The current reference value is then compared with the actual current of each module. The errors are sent to inner current control loops with PID regulators. Subsequently, pulse width modulators are employed to produce switching signals.

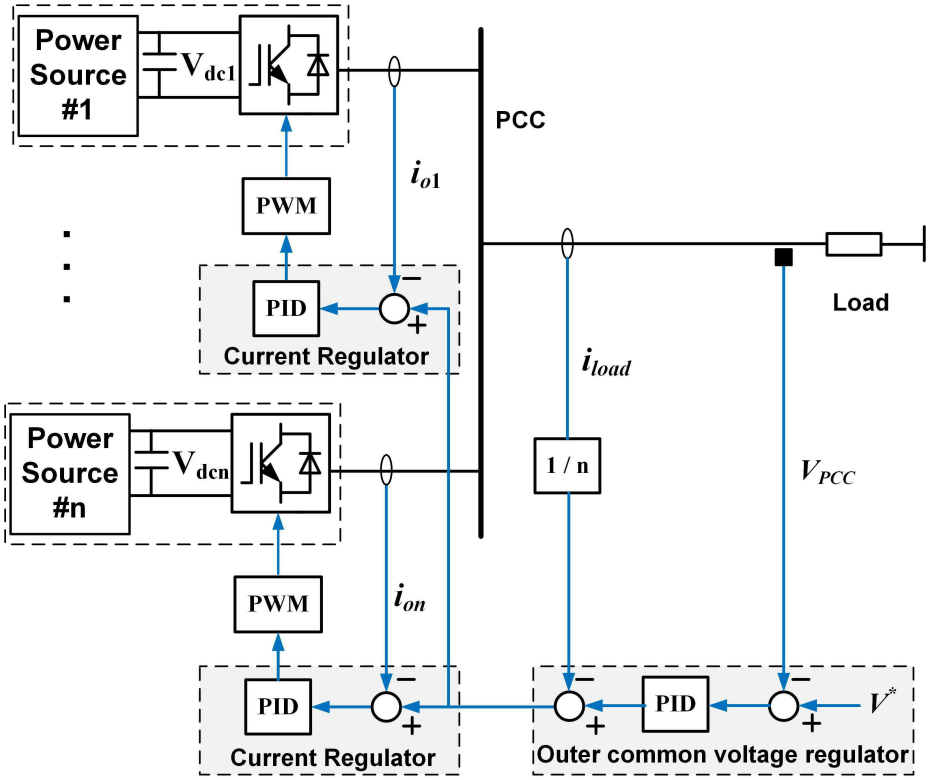


Figure 2.22 Block diagram of centralized control

In addition to the inner current loop described in Subsection A. Centralized control, an outer control loop in the centralized control adjusts the load voltage. Using this method, the measurement of the current at each module and then the calculation of the total load current are required. Hence, this control method is impractical in a large distributed system. Alternatively, a central control board is needed.

In summary, this method can be implemented through three tasks. The measurement of total load current is the first task to figure out the current reference for each inverter. The second task is to obtain the error through comparison between the actual value and the reference, and then decompose the current error into the direct component, Δi_p, and the quadrature component, Δi_q. Finally, Δi_p and Δi_p will be utilized to control the amplitude and phase of the output voltage for every inverter.

2.3.2 Circular chain control

The control diagram of circular chain control (3C) is shown in Figure 2.23.

Different from the centralized control mentioned in Subsection A of Section 2.3, each unit obtains the current reference from the adjacent module to form a control ring. The current reference i_k^* for the kth module is obtained from the $(k-1)$th unit. In other words, the current control in the kth module is achieved by comparing its own output current with the current from the $(k-1)$th module. At the terminals of this chain, the current reference of the first module is obtained from the last unit to form a circular connection [51]. In this way, the successive unit tracks the current of its previous one. Thus, this strategy can achieve equal current distribution among modules.

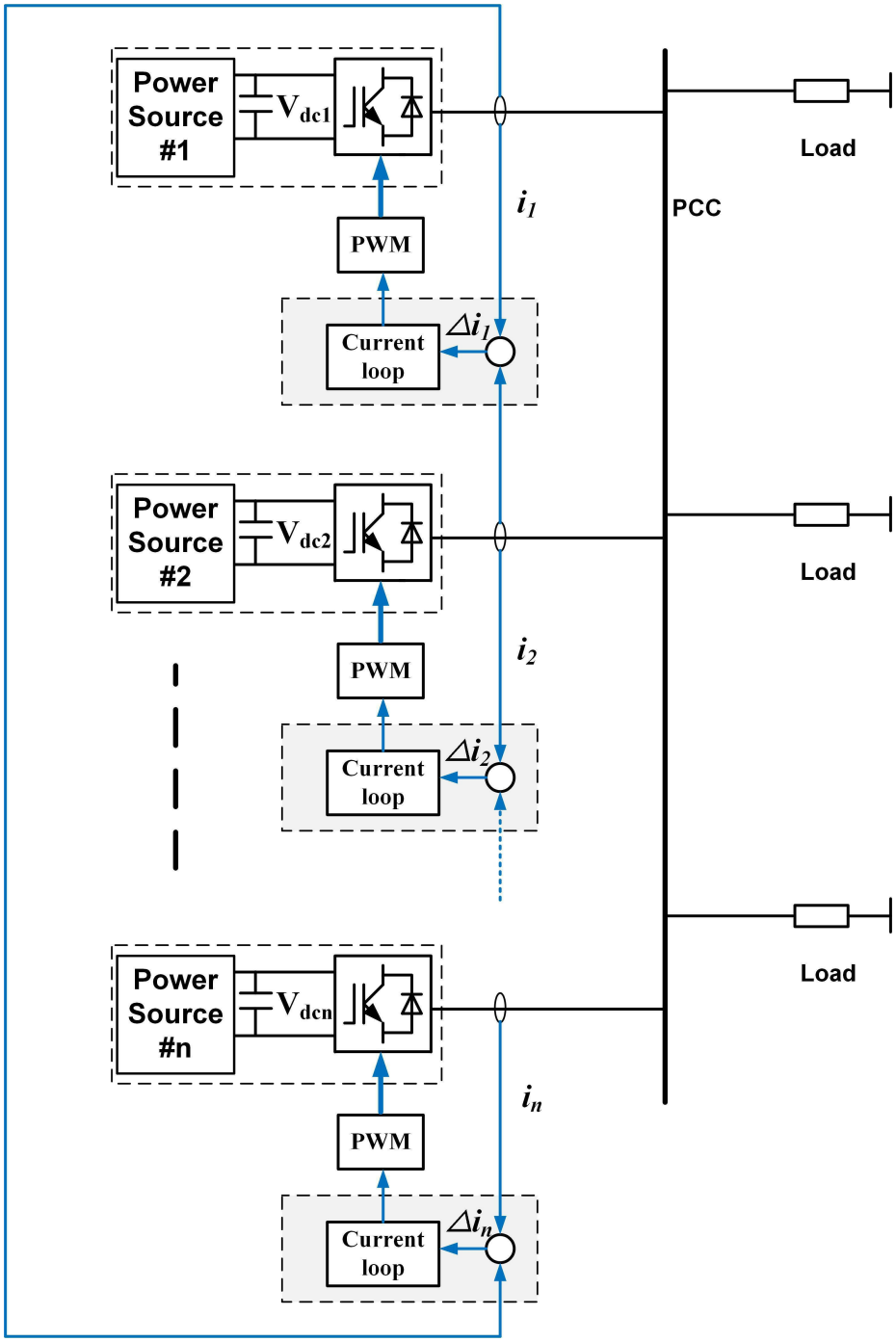


Figure 2.23 Block diagram of 3C scheme

In this approach, all the DG units have the same circuit structure, and each unit includes an inner current control loop and an outer voltage control loop where PI regulators can be employed to adjust the steady-state and dynamic response. Due to its specific structure, this approach can be quite suitable for DG systems where DGs are arranged in a power ring manner through the distribution of the power lines.

2.3.3 Master-slave control

In this method, as depicted in Figure 2.24, the master module acts as a VSI while the slave modules work as CSIs. Specifically, the master module regulates the load voltage, and it determines the current references for the rest of the modules.

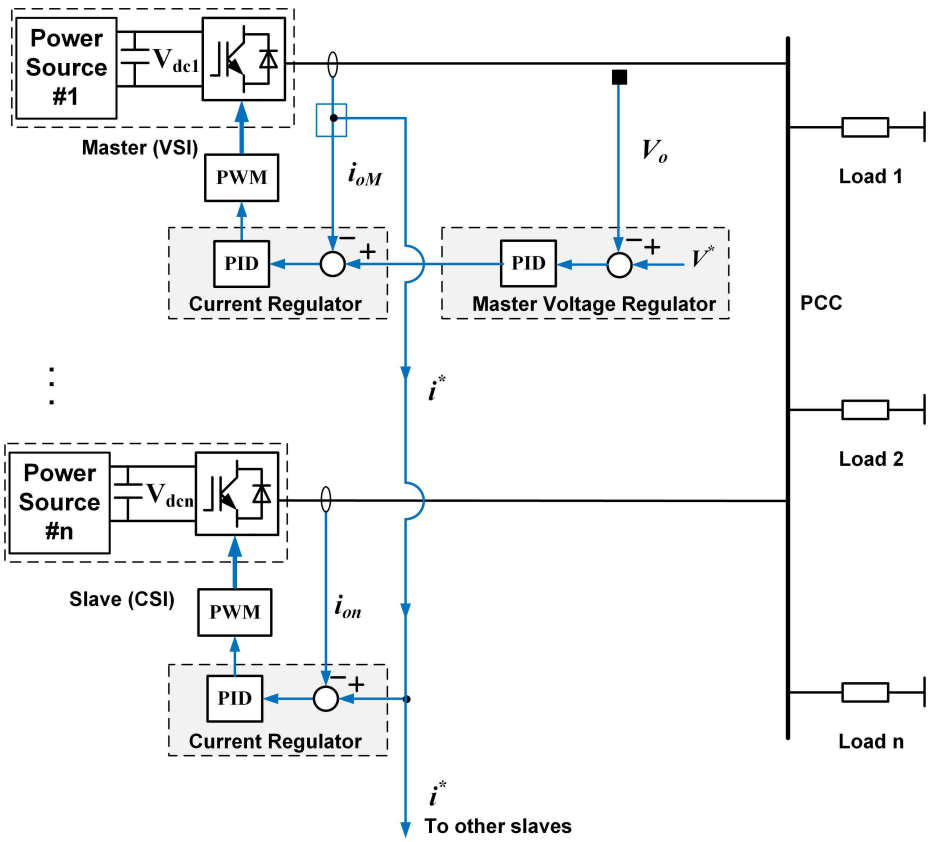


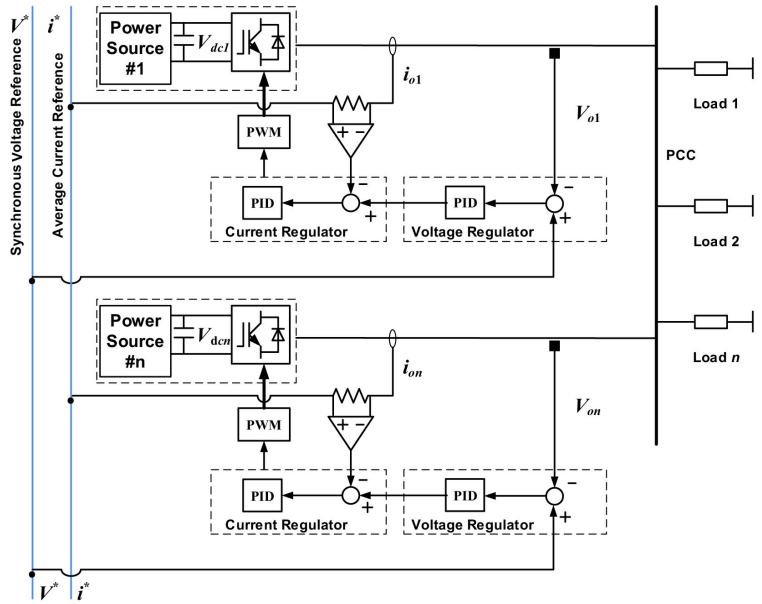
Figure 2.24 Block diagram of master-slave control

In the energy system, one VSI operates as the master to supply a stable sinusoidal AC voltage for the loads. The remaining modules, serving as CSIs, receive the current reference from the power distribution center for current

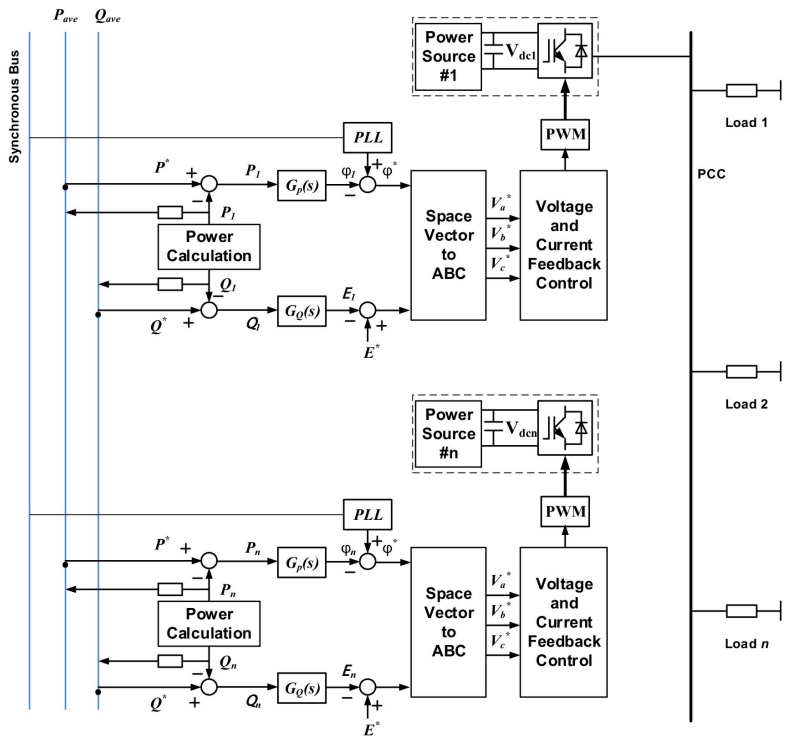
sharing among modules. To mitigate the impacts of voltage disturbance and improve current-sharing response, a voltage feed-forward loop and a current feed-forward loop can be included in the current controller for each CSI. Consequently, the load current sharing can track closely to the references from the power distribution center [52]. In this configuration, to avoid the overall failure of the system, one of the slave modules will take the role of the master if the original master unit fails.

2.3.4 Average load sharing

The average load sharing (ALS) approach can be implemented using average current or average power approach, as illustrated in Figure 2.25(a), where the ALS using the average current scheme is presented. In the average current-based ALS, the average current reference is generated by a resistor connected to the current sensor of every inverter. This current reference will be distributed among modules through a communication line. By changing the resistor, the power rating of the parallel-connected converters can be adjusted to a different value. It is worth mentioning that the average current delivered through the communication line is the reference for all units. Consequently, this method is relatively reliable because every converter tracks the average current calculated by all the active converters [53]. Also, this method is highly modular and robust, making it very easy to use in practical applications.


Synchronous Voltage Reference
Average Current Reference
Power Source #1
Power Source #n
PWM
PID
Current Regulator
Voltage Regulator
PCC
Load 1
Load 2
Load n

(a)


Synchronous Bus
Power Source #1
Power Source #n
PWM
PLL
Power Calculation
Space Vector to ABC
Voltage and Current Feedback Control
PCC
Load 1
Load 2
Load n

(b)

Figure 2.25 Block diagram of ALS control, (a) average current sharing, (b) average power sharing

This average current strategy can be implemented using either an inner or an outer current loop. Since the voltage loop has a narrow bandwidth, a compensator is needed in the inner current loop. Otherwise, system instabilities may occur. In addition, the narrow bandwidth in the control loop causes poor current sharing, particularly during load variations.

Another ALS technology is to use the active and reactive power information rather than the current to control the phase and magnitude of the inverter output voltage [54]. Figure 2.25(b) illustrates the principle of the average power-sharing method. The active and reactive powers are first calculated through the active and reactive components of the output current and voltage. Then, the average active and reactive power references are obtained by dividing the measured power by the number of converters, *N*. Same as the average current scheme mentioned in Subsection D. Average load sharing, the average active and reactive power references are set as the power reference for each converter. Using this method, by regulating the output voltage amplitude and phase, each converter module is able to match its output power to the average active and reactive powers of the entire system. In this technique, obviously, each module participates actively in load sharing without division between master units and slave units. Moreover, good *P* and *Q* sharing is achieved while only low-bandwidth digital communications are needed. One problem remaining is the nonlinear load sharing because this method only considers the fundamental component of the output current. As a result, large circulating harmonic currents among parallel converter units can be induced due to the mismatch between the power stages and the power lines.

The control strategies discussed in Subsections A-D for the coordination of parallel converters can be regarded as active load-sharing methods. Even though these techniques can guarantee good output-voltage control and equal current sharing, they need critical intercommunication lines among modules. Any communication interruptions or delays in these communication lines can affect the current sharing, thus degrading system reliability and scalability.

2.3.5 Droop control

For the operation of multiple DG units with various converters, such as in a MG, the control algorithms applied should preferably require no communication links. This is because the DG units could be located far apart, which causes additional system cost in long communication lines. Hence, it would be highly desired if only local feedback variables are measured for local controllers. Different from the active load-sharing techniques discussed in Subsections A-D, another group of control schemes for distributed parallel inverters, namely droop control, is

introduced here. This concept mimics the characteristic of a synchronous generator in power system, in which frequency is decreased when the load consumption increases. Using this approach, the active and reactive powers provided by individual inverters are changed automatically because their output voltage frequency and amplitude are adjusted according to a predefined droop manner. Critical communication links can be avoided, which can improve the reliability without restricting the physical location of the modules [55–57].

Figure 2.26 presents the block diagram of the droop control method, which consists of an inner voltage control loop and an outer power droop controller. In the droop controller, the instantaneous P and Q are calculated from the measurement of inverter output voltages and output currents and then averaged through low-pass filters. These measured powers together with the power references, $P^*$and Q^*, are input to a predefined droop curve to generate the voltage reference, E^*, which will be used for the inner voltage control loop. The inner voltage control loop usually includes two cascaded control loops, i.e., voltage tracking and current tracking. In the voltage-tracking loop, a PID compensator is usually used to enable the inverter output voltage to track the voltage reference E^* that has been obtained from the droop controller previously. The outputs of this PID compensator together with the inner filter inductor currents are then compared and fed to another PID compensator to produce modulating signals for the sinusoidal PWM. The droop approach uses system frequency as a global communication link among DGs to share the power supply contribution according to predefined characteristics.

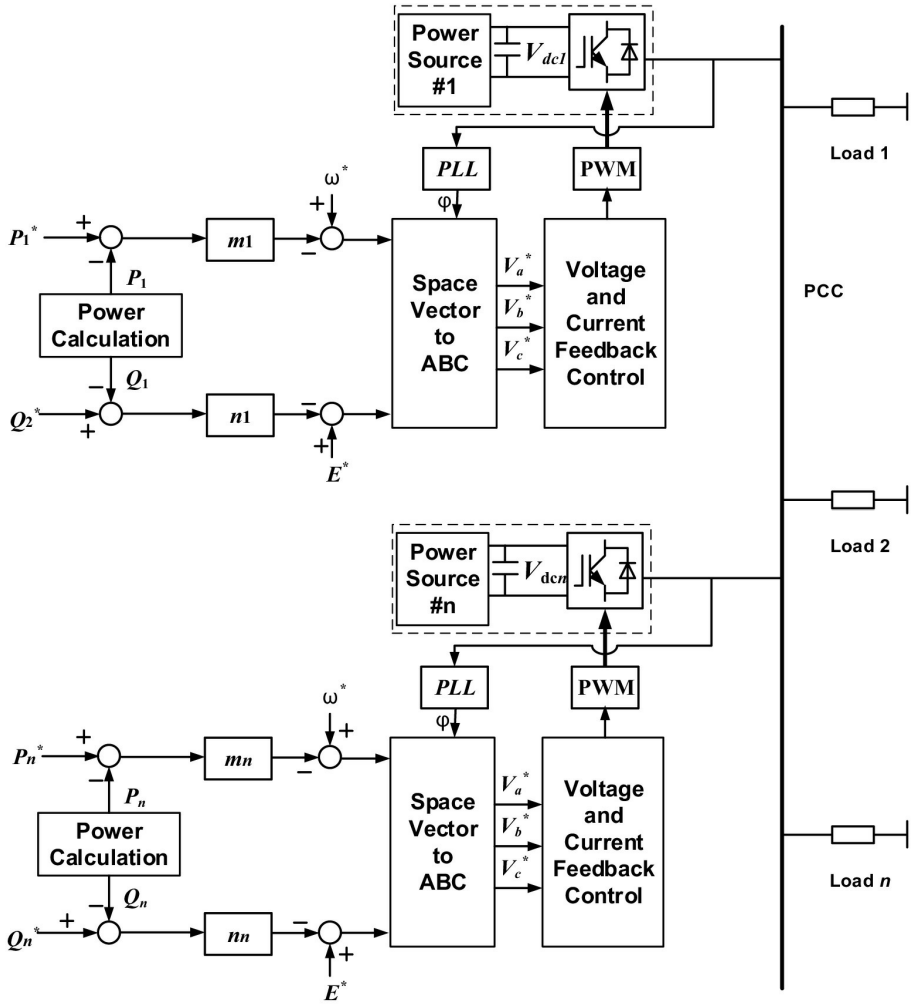


Figure 2.26 Block diagram of the conventional droop control

References

[1] Dahale S., Das A., Pindoriya N.M., Rajendran S. 'An overview of DC-DC converter topologies and controls in DC microgrid'. *2017 7th International Conference on Power Systems (ICPS)*; Pune, India; 2017. pp. 1–6.

[2] Available from https://www.electronicdesign.com/power-management/article/21748916/nonisolated-dcdc-converters.

[3] Prabhakaran P., Agarwal V. 'Novel boost-SEPIC type interleaved DC–DC converter for mitigation of voltage imbalance in a low-voltage bipolar DC

microgrid'. *IEEE Transactions on Industrial Electronics*. 2020, vol. 67(8), pp. 6494–504.
[4] Reddy Baddipadiga B.P. *High-Voltage-Gain DC-DC Power Electronic Converters - New Topologies and Classification [PhD dissertation]*; 2016.
[5] Chen M., Li K., Hu J., Ioinovici A. 'Generation of a family of very high DC gain power electronics circuits based on switched-capacitor-inductor cells starting from a simple graph'. *IEEE Transactions on Circuits and Systems I: Regular Papers*. 2016, vol. 63(12), pp. 2381–92.
[6] Ning J., Zeng J., Du X. 'A four-port bidirectional DC-DC converter for renewable energy-battery-DC microgrid system'. *IEEE Energy Conversion Congress and Exposition (ECCE)*; 2019. pp. 1–6.
[7] Bhattacharjee A.K., Kutkut N., Batarseh I. 'Review of multiport converters for solar and energy storage integration'. *IEEE Transactions on Power Electronics*. 2019, vol. 34(2), pp. 1431–45.
[8] Sato Y., Uno M., Nagata H. 'Nonisolated multiport converters based on integration of PWM converter and phase-shift-switched capacitor converter'. *IEEE Transactions on Power Electronics*. 2020, vol. 35(1), pp. 455–70.
[9] Yazdani A., Iravani R. *Voltage-Sourced Converters in Power Systems: Modeling, Control, and Applications*. New Jersey, US: Wiley-IEEE Press; 2010.
[10] Available from https://au.mathworks.com/help/physmod/sps/examples/two-and-three-level-voltage-source-controllers-vsc.html.
[11] Kazmierkowski M.P., Malesani L. 'Current control techniques for three-phase voltage-source PWM converters: a survey'. *IEEE Transactions on Industrial Electronics*. 1998, vol. 45(5), pp. 691–703.
[12] Leon J.I. 'Multilevel converters: control and modulation techniques for their operation and industrial applications'. *Proceedings of the IEEE*. 2017, vol. 105(11), pp. 2066–81.
[13] Raman S.R., Cheng K.W.E., Hu J. A seven level switched capacitor multilevel inverter with asymmetric input sources for microgrids. *IEEE. 20th International Conference on Electrical Machines and Systems (ICEMS)*; 2017. pp. 1–6.
[14] Xing L., Wei Q. 'Series-connected current source inverters with less switches'. *IEEE Transactions on Power Electronics*. 2020, vol. 35(6), pp. 5553–6.
[15] Anand S., Gundlapalli S.K., Fernandes B.G. 'Transformer-less grid feeding current source inverter for solar photovoltaic system'. *IEEE Transactions on Industrial Electronics*. 2014, vol. 61(10), pp. 5334–44.
[16] Zhang G., Wang H., Yang Y., Su M., Zhang C., Blaabjerg F. 'Common-mode voltage reduction with improved output voltage for three-to-five-phase indirect matrix converters'. *IEEE Journal of Emerging and Selected Topics in Power Electronics*. 2020, vol. 8(3), pp. 2918–29.
[17] Lahooti Eshkevari A., Mosallanejad A., Sepasian M. 'In-depth study of the application of solid-state transformer in design of high-power electric vehicle charging stations'. *IET Electrical Systems in Transportation*. 2020,

vol. 10(3), pp. 310–19.
[18] Wu M., Tian H., Li Y.W., Konstantinou G., Yang K. 'A composite selective harmonic elimination model predictive control for seven-level hybrid-clamped inverters with optimal switching patterns'. *IEEE Transactions on Power Electronics*. 2021, vol. 36(1), pp. 274–84.
[19] Bastidas-Rodríguez J.D., Ramos Paja C.A., Universidad Nacional de Colombia. 'Types of inverters and topologies for microgrid applications'. *Revista UIS Ingenierías*. 2107, vol. 16(1), pp. 7–14.
[20] Rocabert J., Luna A., Blaabjerg F., Rodríguez P. 'Control of power converters in AC microgrids'. *IEEE Transactions on Power Electronics*. 2012, vol. 27(11), pp. 4734–49.
[21] Diaz N.L., Vasquez J.C., Guerrero J.M. 'A communication-less distributed control architecture for islanded microgrids with renewable generation and storage'. *IEEE Transactions on Power Electronics*. 2018, vol. 33(3), pp. 1922–39.
[22] Hu J., Zhu J., Dorrell D.G. 'In-depth study of direct power control strategies for power converters'. *IET Power Electronics*. 2014, vol. 7(7), pp. 1810–20.
[23] Sato A., Noguchi T. 'Voltage-source PWM rectifier–Inverter based on direct power control and its operation characteristics'. *IEEE Transactions on Power Electronics*. 2011, vol. 26(5), pp. 1559–67.
[24] Abdel-Rahim N.M., Quaicoe J.E. 'Analysis and design of a multiple feedback loop control strategy for single-phase voltage-source UPS inverters'. *IEEE Transactions on Power Electronics*. 1996, vol. 11(4), pp. 532–41.
[25] Noguchi T., Tomiki H., Kondo S., Takahashi I. 'Direct power control of PWM converter without power-source voltage sensors'. *IEEE Transactions on Industry Applications*. 1998, vol. 34(3), pp. 473–9.
[26] Liu M., Chan K.W., Hu J., Xu W., Rodriguez J. 'Model predictive direct speed control with torque oscillation reduction for PMSM drives'. *IEEE Transactions on Industrial Informatics*. 2019, vol. 15(9), pp. 4944–56.
[27] Baktash A., Vahedi A., Masoum M. 'Improved switching table for direct power control of three-phase PWM rectifier'. *Australasian Universities Power Engineering Conference*; Perth, Western Australia, Australia; 2007. pp. 1–5.
[28] Bouafia A., Gaubert J.P., Krim F. 'Analysis and design of new switching table for direct power control of three-phase PWM rectifier'. *13th International Power Electronics and Motion Control Conference*; Poznan, Poland; 2008. pp. 703–9.
[29] Bouafia A., Krim F., Gaubert J.-P. 'Fuzzy-logic-based switching state selection for direct power control of three-phase PWM rectifier'. *IEEE Transactions on Industrial Electronics*. 2009, vol. 56(6), pp. 1984–92.
[30] Incremona G.P., Rubagotti M., Ferrara A. 'Sliding mode control of constrained nonlinear systems'. *IEEE Transactions on Automatic Control*. 2017, vol. 62(6), pp. 2965–72.
[31] Raviraj V.S.C., Sen P.C. 'Comparative study of proportional-integral,

sliding mode, and fuzzy logic controllers for power converters'. *IEEE Transactions on Industry Applications*. 1997, vol. 33(2), pp. 518–24.
[32] Hu J., Shang L., He Y., Zhu Z.Q. 'Direct active and reactive power regulation of grid-connected DC/AC converters using sliding mode control approach'. *IEEE Transactions on Power Electronics*. 2011, vol. 26(1), pp. 210–22.
[33] Vazquez S., Rodriguez J., Rivera M., Franquelo L.G., Norambuena M. 'Model predictive control for power converters and drives: advances and trends'. *IEEE Transactions on Industrial Electronics*. 2017, vol. 64(2), pp. 935–47.
[34] Hu J. 'Predictive direct flux control – a new control method of voltage source inverters in distributed generation applications'. *Energies*. 2017, vol. 10(4), pp. 428–11.
[35] Cortes P., Kazmierkowski M.P., Kennel R.M., Quevedo D.E., Rodriguez J. 'Predictive control in power electronics and drives'. *IEEE Transactions on Industrial Electronics*. 2008, vol. 55(12), pp. 4312–24.
[36] Zhi D., Xu L., Williams B.W. 'Model-based predictive direct power control of doubly fed induction generators'. *IEEE Transactions on Power Electronics*. 2010, vol. 25(2), pp. 341–51.
[37] Bouafia A., Gaubert J.-P., Krim F. 'Predictive direct power control of three-phase pulsewidth modulation (PWM) rectifier using space-vector modulation (SVM)'. *IEEE Transactions on Power Electronics*. 2010, vol. 25(1), pp. 228–36.
[38] Hu J., Zhu J., Zhang Y., Platt G., Ma Q., Dorrell D.G. 'Predictive direct virtual torque and power control of doubly fed induction generators for fast and smooth grid synchronization and flexible power regulation'. *IEEE Transactions on Power Electronics*. 2013, vol. 28(7), pp. 3182–94.
[39] Vazquez S., Marquez A., Aguilera R., Quevedo D., Leon J.I., Franquelo L.G. 'Predictive optimal switching sequence direct power control for grid-connected power converters'. *IEEE Transactions on Industrial Electronics*. 2015, vol. 62(4), pp. 2010–20.
[40] Hu J., Zhu J., Lei G., Platt G., Dorrell D.G. 'Multi-objective model-predictive control for high power converters'. *IEEE Transactions on Energy Conversion*. 2013, vol. 28(3), pp. 652–63.
[41] Hu J., Zhu J., Dorrell D.G. 'Model predictive control of grid-connected Inverters for pv systems with flexible power regulation and switching frequency reduction'. *IEEE Transactions on Industry Applications*. 2015, vol. 51(1), pp. 587–94.
[42] Hu J., Zhu J., Dorrell D.G. 'Predictive direct power control of doubly fed induction generators under unbalanced grid voltage conditions for power quality improvement'. *IEEE Transactions on Sustainable Energy*. 2015, vol. 6(3), pp. 943–50.
[43] Chen T., Abdel-Rahim O., Peng F., Wang H. 'An improved finite control set-MPC-based power sharing control strategy for Islanded AC microgrids'. *IEEE Access*. 2020, vol. 8, pp. 52676–86.

[44] Low K.S. ‘Model predictive control of parallel-connected inverters for uninterruptible power supplies’. *IEEE Transactions on Industrial Electronics*. 2008, vol. 55(8), pp. 2884–93.
[45] Ahmed A.A., Koh B.K., Lee Y.I. ‘A comparison of finite control set and continuous control set model predictive control schemes for speed control of induction motors’. *IEEE Transactions on Industrial Informatics*. 2018, vol. 14(4), pp. 1334–46.
[46] Camacho E.F., Bordons C. *Model Predictive Control*. London: Springer; 1995.
[47] Ouammi A., Dagdougui H., Dessaint L., Sacile R. ‘Coordinated model predictive-based power flows control in a cooperative network of smart Microgrids’. *IEEE Transactions on Smart Grid*. 2015, vol. 6(5), pp. 2233–44.
[48] Parisio A., Rikos E., Glielmo L. ‘A model predictive control approach to microgrid operation optimization’. *IEEE Transactions on Control Systems Technology*. 2014, vol. 22(5), pp. 1813–27.
[49] Hu J. *Advanced Control in Smart Microgrids [PhD dissertation]*. University of Technology: Sydney, Australia; 2013.
[50] Martins A.P., Carvalho A.S., Araujo A.S. ‘Design and implementation of a current controller for the parallel operation of standard UPSs’. *Proceedings of IECON '95 - 21st Annual Conference on IEEE Industrial Electronics*; Orlando, Florida, USA; 1995. pp. 584–9.
[51] Wu T.F., Chen Y.-K., Huang Y.-H. ‘3C strategy for inverters in parallel operation achieving an equal current distribution’. *IEEE Transactions on Industrial Electronics*. 2000, vol. 47(2), pp. 273–81.
[52] Holtz J., Werner K.-H. ‘Multi-inverter ups system with redundant load sharing control’. *IEEE Transactions on Industrial Electronics*. 1990, vol. 37(6), pp. 506–13.
[53] Sun X., Lee Y.-S., Xu D. ‘Modeling, analysis, and implementation of parallel multi-inverter system with instantaneous average-current-sharing scheme’. *IEEE transactions on power electronics*. 2003, vol. 18(3), pp. 844–56.
[54] Tao J., Lin H., Zhang J., Ying J. ‘A novel load sharing control technique for paralleled inverters’. *PESC Record - IEEE Annual Power Electronics Specialists Conference*; 2003. pp. 1432–7.
[55] Chandorkar M.C., Divan D.M., Adapa R. ‘Control of parallel connected inverters in standalone AC supply systems’. *IEEE Transactions on Industry Applications*. 1993, vol. 29(1), pp. 136–43.
[56] Guerrero J.M., GarciadeVicuna L., Matas J., Castilla M., Miret J. ‘A wireless controller to enhance dynamic performance of parallel inverters in distributed generation systems’. *IEEE Transactions on Power Electronics*. 2004, vol. 19(5), pp. 1205–13.
[57] Eisapour-Moarref A., Kalantar M., Esmaili M. ‘Power sharing in hybrid microgrids using a harmonic-based multidimensional droop’. *IEEE Transactions on Industrial Informatics*. 2020, vol. 16(1), pp. 109–19.

Further reading

- Sadabadi M.S. ‘A distributed control strategy for parallel DC-DC converters’. *IEEE Control Systems Letters*. 2021, vol. 5(4), pp. 1231–6. doi:10.1109/LCSYS.2020.3025411
- Hassani M.Y., Maalandish M., Hosseini S.H. ‘A new single-input multioutput interleaved high step-up DC–DC converter for sustainable energy applications’. *IEEE Transactions on Power Electronics*. 2021, vol. 36(2), pp. 1544–52. doi:10.1109/TPEL.2020.3011218
- Saadatizadeh Z., Babaei E., Blaabjerg F., Cecati C. ‘Three-port high step-up and high step-down DC-DC converter with zero input current ripple’. *IEEE Transactions on Power Electronics*. 2021, vol. 36(2), pp. 1804–13. doi:10.1109/TPEL.2020.3007959
- De Doncker R.W.A.A., Divan D.M., Kheraluwala M.H. ‘A three-phase soft-switched high-power-density DC/DC converter for high-power applications’. *IEEE Transactions on Industry Applications*. 1991, vol. 27(1), pp. 63–73. doi:10.1109/28.67533
- Qun Zhao., Lee F.C. ‘High-efficiency, high step-up DC-DC converters’. *IEEE Transactions on Power Electronics*. 2003, vol. 18(1), pp. 65–73. doi:10.1109/TPEL.2002.807188
- Wang F., Duarte J.L., Hendrix M.A.M. ‘Grid-interfacing converter systems with enhanced voltage quality for microgrid application—concept and implementation’. *IEEE Transactions on Power Electronics*. 2011, vol. 26(12), pp. 3501–13. doi:10.1109/TPEL.2011.2147334
- Mahmud N., Zahedi A., Mahmud A. ‘A cooperative operation of novel pv Inverter control scheme and storage energy management system based on ANFIS for voltage regulation of grid-tied pv system’. *IEEE Transactions on Industrial Informatics*. 2017, vol. 13(5), pp. 2657–68. doi:10.1109/TII.2017.2651111
- Bayhan S., Abu-Rub H., Balog R.S. ‘Model predictive control of Quasi-Z-source four-leg inverter’. *IEEE Transactions on Industrial Electronics*. 2016, vol. 63(7), pp. 4506–16. doi:10.1109/TIE.2016.2535981
- Liu Z., Liu J., Zhao Y. ‘A unified control strategy for three-phase inverter in distributed generation’. IEEE Transactions on Power Electronics. 2014, vol. 29(3), pp. 1176–91.
- Lazzarin T.B., Barbi I. ‘DSP-based control for parallelism of three-phase voltage source inverter’. *IEEE Transactions on Industrial Informatics*. 2013, vol. 9(2), pp. 749–59. doi:10.1109/TII.2012.2223477
- Salem A., Van Khang H., Robbersmyr K.G., Norambuena M., Rodriguez J. ‘Voltage source multilevel inverters with reduced device count: topological review and novel comparative factors’. *IEEE Transactions on Power Electronics*. 2021, vol. 36(3), pp. 2720–47. doi:10.1109/TPEL.2020.3011908
- Ali A.I.M., Sayed M.A., Takeshita T. ‘New cascaded-transformers multilevel Inverter for renewable distribution systems’. *Proceedings of IEEE ECCE*. 2020, pp. 1–6.

- Rodriguez J., Jih-Sheng Lai., Fang Zheng Peng., Lai, F J. 'Multilevel inverters: a survey of topologies, controls, and applications'. *IEEE Transactions on Industrial Electronics*. 2002, vol. 49(4), pp. 724–38. doi:10.1109/TIE.2002.801052
- Abu-Rub H., Holtz J., Rodriguez J., Ge Baoming. 'Medium-voltage multilevel converters—state of the art, challenges, and requirements in industrial applications'. *IEEE Transactions on Industrial Electronics*. 2010, vol. 57(8), pp. 2581–96. doi:10.1109/TIE.2010.2043039
- Krim Y., Abbes D., Robyns B. 'Joint optimisation of sizing and fuzzy logic power management of a hybrid storage system considering economic reliability indices'. *IET Renewable Power Generation*. 2020, vol. 14(14), pp. 2581–91. doi:10.1049/iet-rpg.2020.0102
- M. Said S., Ali A., Hartmann B. 'Tie-line power flow control method for grid-connected microgrids with SMES based on optimization and fuzzy logic'. *Journal of Modern Power Systems and Clean Energy*. 2020, vol. 8(5), pp. 941–50. doi:10.35833/MPCE.2019.000282
- Hannan M.A., Ghani Z.A.B.D., Hoque M.M., Ker P.J., Hussain A., Mohamed A. 'Fuzzy logic inverter controller in photovoltaic applications: issues and recommendations'. *IEEE Access*. 2019, vol. 7(5), pp. 24934–55. doi:10.1109/ACCESS.2019.2899610
- Shah N., Rajagopalan C. 'Experimental evaluation of a partially shaded photovoltaic system with a fuzzy logic‐based peak power tracking control strategy'. *IET Renewable Power Generation*. 2016, vol. 10(1), pp. 98–107. doi:10.1049/iet-rpg.2015.0098
- Mokhtar M., Marei M.I., El-Sattar A.A. 'An adaptive droop control scheme for DC microgrids integrating sliding mode voltage and current controlled boost converters'. *IEEE Transactions on Smart Grid*. 2019, vol. 10(2), pp. 1685–93. doi:10.1109/TSG.2017.2776281
- Ali M., Aamir M., Khan H.S., Khan A.A., Haroon F. 'Design and implementation of fractional-order sliding mode control for parallel distributed generations units in Islanded microgrid'. *Proceedings of IEEE 28th International Symposium on Industrial Electronics*. 2019, pp. 1–6.
- Baghaee H.R., Mirsalim M., Gharehpetian G.B., Talebi H.A. 'A decentralized power management and sliding mode control strategy for hybrid AC/DC microgrids including renewable energy resources'. *IEEE transactions on industrial informatics*. 2017, p. 1. doi:10.1109/TII.2017.2677943
- Singh S., Fulwani D., Kumar V. 'Robust sliding‐mode control of DC/DC boost converter feeding a constant power load'. *IET Power Electronics*. 2015, vol. 8(7), pp. 1230–7. doi:10.1049/iet-pel.2014.0534
- Yin J., Leon J.I., Perez M.A., Franquelo L.G., Marquez A., Vazquez S. 'Model predictive control of modular multilevel converters using quadratic programming'. *IEEE Transactions on Power Electronics*. 2021, vol. 36(6), pp. 7012–25. doi:10.1109/TPEL.2020.3034294
- Engel S.P., Stieneker M., Soltau N., Rabiee S., Stagge H., De Doncker R.W. 'Comparison of the modular multilevel DC converter and the dual-active

bridge converter for power conversion in HVDC and MVDC grids'. *IEEE Transactions on Power Electronics*. 2015, vol. 30(1), pp. 124–37. doi:10.1109/TPEL.2014.2310656

- Chen X., Xu G., Xie S., *et al*. 'A natural bidirectional Input-series–output-parallel LLC-DCX converter with automatic power sharing and power limitation capability for Li-Ion battery formation and grading system'. *IEEE Journal of Emerging and Selected Topics in Power Electronics*. 2019, vol. 8(4), pp. 3618–32. doi:10.1109/JESTPE.2019.2941583
- Zientarski J.R.R., da Silva Martins M.L., Pinheiro J.R., Hey H.L. 'Evaluation of power processing in series-connected partial-power converters'. *IEEE Journal of Emerging and Selected Topics in Power Electronics*. 2019, vol. 7(1), pp. 343–52. doi:10.1109/JESTPE.2018.2869370
- Wu H., Jia Y., Yang F., Zhu L., Xing Y. 'Two-stage isolated bidirectional DC–AC converters with three-port converters and two DC buses'. *IEEE Journal of Emerging and Selected Topics in Power Electronics*. 2020, vol. 8(4), pp. 4428–39. doi:10.1109/JESTPE.2019.2936145
- Verveckken J., Silva F., Barros D., *et al*. 'Two-stage isolated bidirectional DC–AC converters with three-port converters and two DC buses'. *IEEE Transactions on power del*. 2012, vol. 27(4), pp. 1772–82.
- Zhang J., Liu J., Yang J., Zhao N., Wang Y., Zheng T.Q. 'A modified DC power electronic transformer based on series connection of full-bridge converters'. *IEEE Transactions on Power Electronics*. 2019, vol. 34(3), pp. 2119–33. doi:10.1109/TPEL.2018.2842728
- Wu H., Zhu L., Yang F. 'Three-port-converter-based single-phase bidirectional AC–DC converter with reduced power processing stages and improved overall efficiency'. *IEEE Transactions on Power Electronics*. 2018, vol. 33(12), pp. 10021–6. doi:10.1109/TPEL.2018.2824242
- Yue X., Boroyevich D., Lee F.C., Chen F., Burgos R., Zhuo F. 'Beat frequency oscillation analysis for power electronic converters in DC nanogrid based on crossed frequency output impedance matrix model'. *IEEE Transactions on Power Electronics*. 2018, vol. 33(4), pp. 3052–64. doi:10.1109/TPEL.2017.2710101
- Jang Y., Jovanovic M.M., Dillman D.L. 'Soft-switched pFc boost rectifier with integrated ZVS Two-switch forward converter'. *IEEE Transactions on Power Electronics*. 2006, vol. 21(6), pp. 1600–6. doi:10.1109/TPEL.2006.882966
- Ryu M.-H., Kim H.-S., Baek J.-W., Kim H.-G., Jung J.-H. 'Effective test bed of 380-V DC distribution system using isolated power converters'. *IEEE Transactions on Industrial Electronics*. 2015, vol. 62(7), pp. 4525–36. doi:10.1109/TIE.2015.2399273
- Zientarski J.R.R., Martins M.LdaS., Pinheiro J.R., Hey H.L. 'Series-connected partial-power converters applied to pv systems: a design approach based on step-up/down voltage regulation range'. *IEEE Transactions on Power Electronics*. 2018, vol. 33(9), pp. 7622–33. doi:10.1109/TPEL.2017.2765928

- Zhang Y., Rodriguez M., Maksimovic D. ‘Very high frequency PWM buck converters using monolithic GAN half-bridge power stages with integrated gate drivers’. *IEEE Transactions on Power Electronics*. 2016, vol. 31(11), pp. 7926–42. doi:10.1109/TPEL.2015.2513058
- Ma D., Chen W., Shu L., Qu X., Zhan X., Liu Z. ‘A multiport power electronic transformer based on modular multilevel converter and mixed-frequency modulation’. *IEEE Transactions on Circuits and Systems II: Express Briefs*. 2019, vol. 67(7), pp. 1284–8. doi:10.1109/TCSII.2019.2931529
- Kim K., Cha H., Kim H.-G. ‘A new single-phase witched-coupled-inductor DC–AC inverter for photovoltaic systems’. *IEEE Transactions on Power Electronics*. 2017, vol. 32(7), pp. 5016–22. doi:10.1109/TPEL.2016.2606489
- Raveendhra D., Pathak M.K. ‘Three-phase capacitor clamped boost inverter’. *IEEE Journal of Emerging and Selected Topics in Power Electronics*. 2019, vol. 7(3), pp. 1999–2011. doi:10.1109/JESTPE.2018.2873154
- Zou X., Du X., Wang G., Tai Heng‐Ming., Tai H. ‘Single stationary domain equivalent inverter admittance for three‐phase grid‐inverter system considering the interaction between grid and inverter’. *IET Power Electronics*. 2019, vol. 12(6), pp. 1593–602. doi:10.1049/iet-pel.2018.5856
- Rizzoli G., Mengoni M., Zarri L., Tani A., Serra G., Casadei D. ‘Comparative experimental evaluation of zero-voltage-switching Si inverters and hard-switching Si and SiC inverters’. *IEEE Journal of Emerging and Selected Topics in Power Electronics*. 2019, vol. 7(1), pp. 515–27. doi:10.1109/JESTPE.2018.2831603
- Borrega M., Marroyo L., Gonzalez R., Balda J., Agorreta J.L. ‘Modeling and control of a master–slave PV inverter with N-paralleled inverters and three-phase three-limb inductors’. *IEEE Transactions on Power Electronics*. 2013, vol. 28(6), pp. 2842–55. doi:10.1109/TPEL.2012.2220859
- Qanbari T., Tousi B. ‘Single-source three-phase multilevel Inverter assembled by three-phase two-level inverter and two single-phase cascaded H-bridge inverters’. *IEEE Transactions on Power Electronics*, vol. 36(5) 5204–12. doi:10.1109/TPEL.2020.3029870
- Wang S., Liu Z., Liu J., Boroyevich D., Burgos R. ‘Small-signal modeling and stability prediction of parallel droop-controlled inverters based on terminal characteristics of individual inverters’. *IEEE Transactions on Power Electronics*. 2020, vol. 35(1), pp. 1045–63. doi:10.1109/TPEL.2019.2914176
- Dbeiss M., Avenas Y., Zara H., Dupont L., Shakarchi F.A. ‘A method for accelerated aging tests of power modules for photovoltaic inverters considering the inverter mission profiles’. *IEEE Transactions on Power Electronics*. 2019, vol. 34(12), pp. 12226–34. doi:10.1109/TPEL.2019.2907218
- Kim N., Parkhideh B. ‘PV-Battery series inverter architecture: a solar inverter for seamless battery integration with partial-power DC–DC Optimizer’. *IEEE Transactions on Energy Conversion*. 2019, vol. 34(1), pp. 478–85. doi:10.1109/TEC.2018.2873664

- Nauman M., Hasan A. ‘Efficient implicit model-predictive control of a three-phase inverter with an output LC filter’. *IEEE Transactions on Power Electronics*. 2016, vol. 31(9), pp. 6075–8. doi:10.1109/TPEL.2016.2535263
- Jafarian H., Kim N., Parkhideh B. ‘Decentralized control strategy for AC-stacked PV inverter architecture under grid background harmonics’. *IEEE Journal of Emerging and Selected Topics in Power Electronics*. 2018, vol. 6(1), pp. 84–93. doi:10.1109/JESTPE.2017.2773079
- Roy J., Xia Y., Ayyanar R. ‘High step-up transformerless inverter for AC module applications with active power decoupling’. *IEEE Transactions on Industrial Electronics*. 2019, vol. 66(5), pp. 3891–901. doi:10.1109/TIE.2018.2860538

Chapter 3
Distributed renewable power generation

In a microgrid (MG), the basic power sources are distributed generation (DG) units. In this chapter, DG concept is presented. Particularly, two most popular distributed energy resources, namely, wind generators and solar photovoltaic (PV) systems, are presented in detail.

3.1 Distributed generation

The rapid depletion of conventional energy sources such as coal, increased electricity demand, and ever-tightening government regulations on the reduction of greenhouse gas emissions, together with the inefficiency of traditional electricity grid, causes major transformation in electricity generation, distribution, and consumption patterns all over the world. In the last decade, much attention has been paid to DGs including both nonrenewable and renewable sources, such as solar PV, wind turbine generators, panels, fuel cells, gas microturbine generators, and gas- or steam-powered combined heat and power stations. To some extent, these DG sources can reduce the burden of the existing power grid, and they can offer competitive generation options.

DG is an electrical power generation unit that can be connected to the local distribution network or just supply power to local electric appliances in a manner similar to a uninterruptible power supply (UPS) system. The advantages of DG applications can be described as follows:

- reliable power supply, especially when interruption of service is unacceptable;
- easy to exploit renewable energy sources (RESs);
- alternative power supply options for remote and regional areas where utility grid is unavailable for customers.

Figure 3.1(a) shows the configuration of a doubly fed induction generator (DFIG)-based wind power generation system. The wind turbine captures the kinetic wind energy and converts it into mechanical energy. A gearbox is used to increase the low turbine speed to a higher level for driving the generator. The generator converts the mechanical power into electrical power, which is then supplied to local loads or fed into a grid possibly through power electronic

converters, transformers, and together with circuit breakers and electricity meters. The stator of the DFIG is directly connected to the grid for power output, while a partial-scale power converter draws power from the grid to control the rotor frequency and thus the rotor speed [1].

Figure 3.1(b) shows a typical structure of a solar PV system, where numerous PV panels are assembled in series and/or parallel to form an array to convert the solar energy into electricity via PV conversion. The electricity generated by the PV panels is then supplied to local loads or fed to the utility grid via a centralized inverter that further converts the DC power to AC electricity for consumer use [2]. To maximize the electricity output converted from solar energy, several aspects are of concern. For example, the tilt angle and orientation angle of the PV panel need to be adjusted with respect to the sun position. Given a certain solar irradiance on the PV panel, the performance of the solar cells determines the PV conversion efficiency. Then, on the electrical side, the inverter needs to continuously operate according to the terminal conditions of the PV module(s) so that it maintains the maximum power point tracking (MPPT). In this book, the power electronic inverter operation at the electrical side is focused.

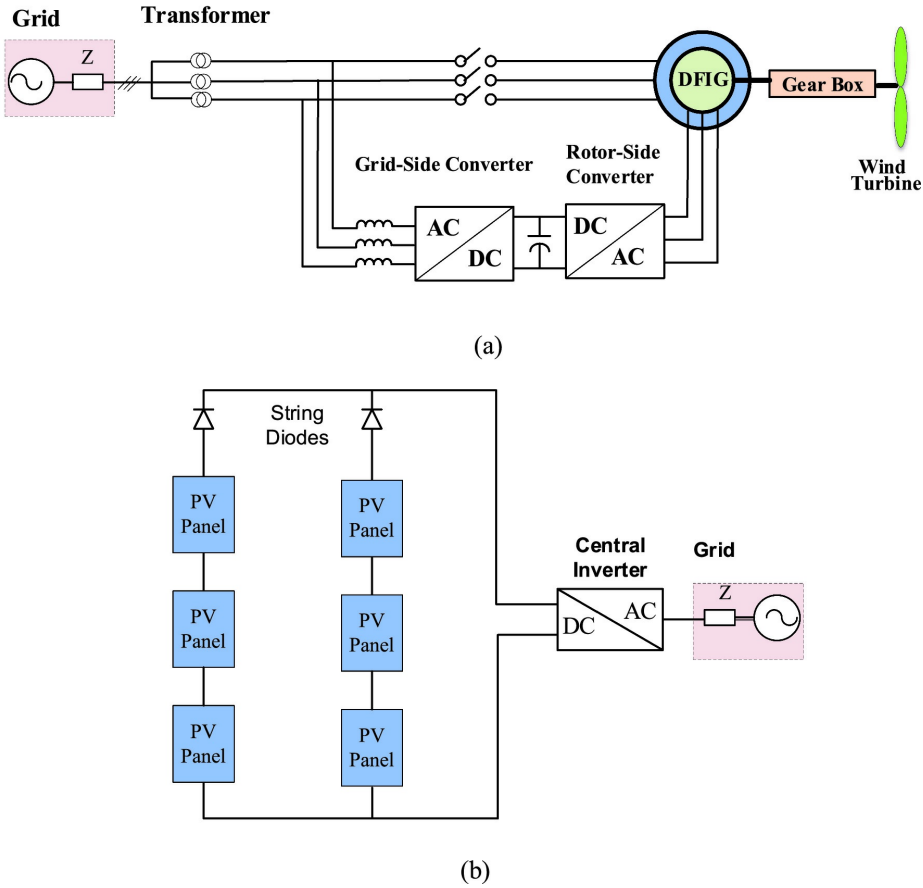


Figure 3.1 Configurations of DG systems. (a) Wind energy conversion system, (b) solar PV system.

Despite the benefits provided by the DGs mentioned in Section 3.1, there are technical challenges that need to be addressed. The main concerns of utilizing DGs can be summarized as the following:

- The transient voltage variations at the point of connection due to the sudden connection or disconnection of a DG.
- The power output of the DG is fluctuating due to the intermittent nature of RESs, which would cause negative impacts on electric appliances. Energy storage is usually needed to compensate for the fluctuation in generation.
- Connecting or disconnecting DGs, particularly in a large-scale manner, will deteriorate the power quality and stability of the utility grid.
- Additional protection mechanism is necessary to address issues such as

breaker reclosing problem, over-current protection relaying interference, etc.

- Unlike the stiff utility grid, DGs present possible power quality problems, such as voltage flickers and harmonics.
- Impact on power system dynamics.
- Safety concerns of islanding operation of a single DG for customers or DG itself.

3.2 Wind power generation

Wind energy is relatively clean and sustainable compared to traditional energy sources such as coals and petrol fuel. It has become one of the most promising and fastest-growing renewable energy resources in the world. Thanks to the ever-growing wind technology and the incentives provided by governments and associations, the cost of electricity from wind energy has been reduced steadily. The global wind power installed capacity has increased from about 198 000 MW in 2010 to 651 000 MW in 2019. In the year 2019, around 621 421 MW were generated from onshore installations, of which 54 206 MW attributed to new installation in that year [3]. A typical wind power system, consisting of RES, wind turbine, gearbox, generator, power converter, control unit, transformer, and certainly electric network, is depicted in Figure 3.2. Cost distribution for the main components of a typical wind generation system is shown in Figure 3.3.

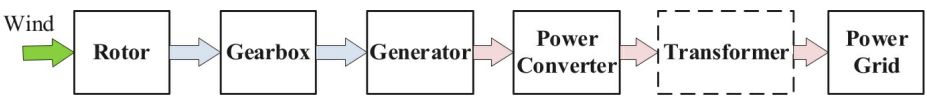


Figure 3.2 Wind energy conversion system with power flow path

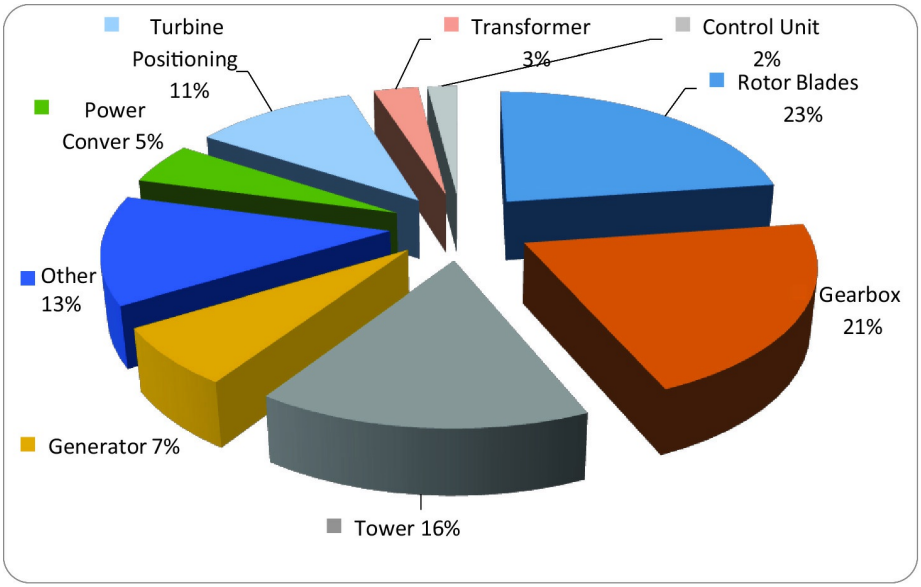


Figure 3.3 Example of cost distribution of a wind energy conversion system

With the rapid development of DGs especially renewable sources, as well as the introduction of new grid code requirements, it is necessary to improve the quality of the electricity generated from individual wind generators or even wind farms. To facilitate the grid integration of wind power systems, MGs and smart grids have been proposed to better manage the available resources by incorporating advanced sensing technologies, control methods, and communication into the current grid. Therefore, important issues are of great concern in wind energy generation systems, including reliability, efficiency, system cost, power quality, and automated fault ride-through capability [4, 5].

3.2.1 Wind turbine characteristics

For a horizontal axis wind turbine, the amount of power that can be captured is given by [6]

$$P = 0.5\rho A C_p v^3 \tag{3.1}$$

where ρ is the air mass density; A the cross-sectional area of the turbine; C_p the power coefficient that is related to the tip speed ratio (TSR) λ and the blade pitch angle β; and v the wind speed. The TSR λ is defined as the ratio of the turbine speed at the tip of a blade to wind velocity, which can be written as

$$\lambda = R\frac{\omega}{v} \tag{3.2}$$

where ω is the turbine rotational speed in radians per second and R the turbine radius. Figure 3.4 shows an example of the relationship between P and ω for a wind turbine. Under different wind speeds, there is only one specific λ enabling maximal C_p so that the turbine is most efficient. For this reason, the rotor rotational speed should be regulated continuously according to the wind speed to achieve MPPT. In reality, the rotor usually will not rotate until the wind speed reaches a minimum value of about 3–5 m/s, which is called the cut-in wind speed. This is because the power generated may not be enough to compensate for the power required by the system to operate under cut-in wind speed. As wind velocity increases, the generated power will then ramp up with respect to the wind speed by following the MPPT curve. When the wind speed is above the rated level, the system then enters a constant-power region through wind shedding. As the velocity continues to increase, at some point, for example, around 25 m/s, the wind turbine system must be shut down to avoid damage due to strong wind.

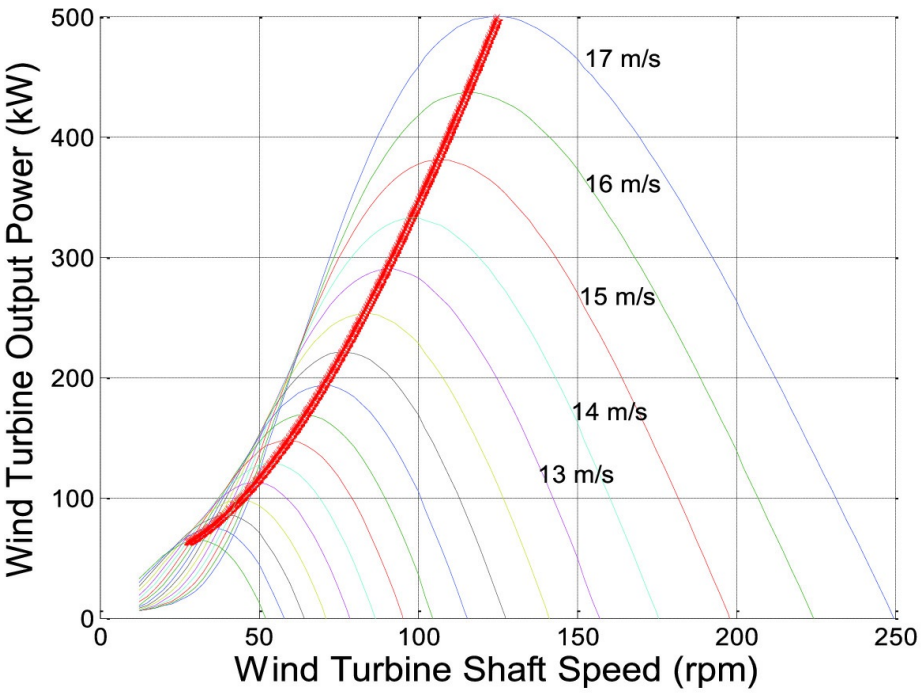


Figure 3.4 Turbine output power characteristics for different wind speeds

3.2.2 Constant speed constant frequency system

Wind energy conversion systems can be categorized into two types, namely constant speed constant frequency (CSCF) system and variable speed constant frequency (VSCF) system. In the CSCF system, the wind turbine rotor speed is constant and fixed by the grid frequency under various wind speeds. Such wind systems are usually equipped with squirrel cage induction generators (SCIGs), soft-starters, and capacitor banks, and they are connected directly to the grid, as depicted in Figure 3.5. During operation, the lagging reactive power is compensated by the capacitor bank [7].

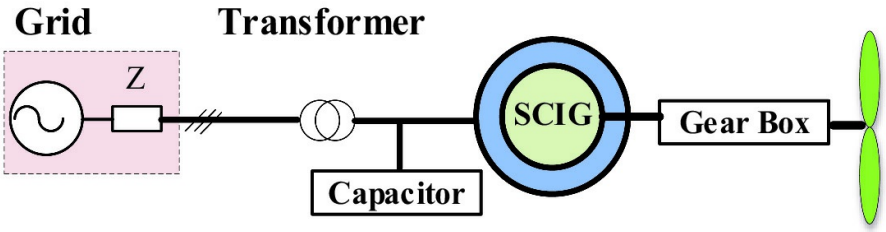


Figure 3.5 CSCF system with SCIG

The CSCF type presents the advantages of being reliable, simple, and robust. Nevertheless, the maximum conversion efficiency can be achieved only at a specified wind speed and will decrease at any other operating points. As a result, with the varying wind speed, the CSCF wind turbine generates highly fluctuating output power, which will become disturbances to the power systems. In addition, this type of turbines also needs a sturdy mechanical design to absorb mechanical stresses.

An evolution of the SCIG-based CSCF system is the limited variable-speed system [8]. The improvement is that wound-rotorinduction generators with variable external rotor resistances controlled by power electronics are used to adjust the rotor speed within a limited range. In this way, since the total rotor resistance is adjustable, the slip of the generator and therefore the slope of the mechanical characteristic can be controlled. As mentioned in Section 3.2.2, usually the control range is small, typically up to 10 percent over the synchronous speed. Another approach to widen the dynamic speed range is to use a generator with switchable poles or use two generators of different sizes. For switchable pole wind generators, obviously, additional devices are needed for pole switching. Notice that the operating speeds are dependent on the number of generator poles and/or the gear ratio. Therefore, this approach is actually a discrete-type control method where the rotor speed cannot be adjusted continuously. For the wind turbine with two generators of different sizes, the smaller generator is activated in low winds and the larger in high winds.

3.2.3 VSCF system

Since the 2000s, variable-speed wind systems have gradually dominated the global wind generation market because they can achieve maximum aerodynamic efficiency over a wider range of wind speeds and, hence, generate more amount of electricity. Specifically, the turbine rotor can continuously adapt its rotational speed to the wind speed. By doing this, the TSR can be maintained at an optimal value for maximum power output using the MPPT technique. In practice, to make the turbine rotor speed adjustable, the generator is normally connected to the utility grid through a power electronic converter system. To obtain an easy comparison with the fixed speed wind turbine systems, the advantages of the VSCF wind are summarized as follows [9]:

- Mechanical stress on different components of the turbine can be released to some extent because wind gusts can be absorbed by the turbine.
- There are fewer fluctuations in the power injected from the wind generators to the main grid because the impacts of variable wind energy can now be buffered in mechanical energy and are not passed directly onto the grid.
- The system efficiency is enhanced by the adjustment of the rotational speed according to the actual wind speed. The maximum output power can be achieved over a wider wind speed range.
- Better revenue or economic return due to the larger amount of power generated on a monthly or yearly basis.

In the following Sections 3.2.3.1, 3.2.3.2, 3.2.3.3, 3.2.3.4, the VSCF systems with different electrical generators are briefly reviewed and compared with necessary discussion.

3.2.3.1 Wound field synchronous generator

Figure 3.6 illustrates a VSCF system with a wound field synchronous generator (WFSG). In this configuration, the stator winding is connected to the power grid through a four-quadrant power converter comprised of two back-to-back pulsewidth modulation (PWM)-VSIs. The stator-side converter regulates the electromagnetic torque, while the supply-side converter manages the real and reactive power. Synchronous generators are generally more expensive than their counterparts in wind systems such as induction generators with a similar size. The good side is the use of a multipole synchronous generator (large diameter synchronous ring generator) has the possibility to avoid the installation of a gearbox. But it can result in a significant increase in weight [10].

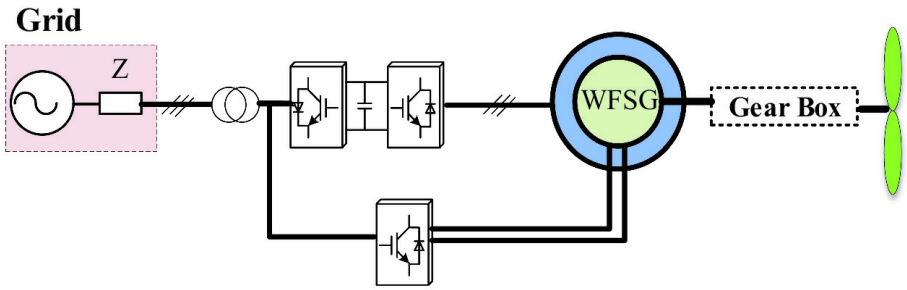


Figure 3.6 WFSG system

3.2.3.2 Permanent-magnet synchronous generator

Figure 3.7 shows a VSCF system in which a permanent-magnet synchronous generator (PMSG) is connected to a three-phase rectifier that controls the electromagnet torque of the generator. At the same time, the grid-side converter maintains the DC-link voltage as well as controlling the output power factor, i.e., active and reactive powers. The PMSG has become an attractive option as a wind turbine generator. Advantages include high efficiency, self-excitation, and high power factor. It is especially suitable for small wind turbines. It is noted that permanent magnet materials are still relatively expensive at present. They are also difficult to handle in manufacture. In the actual application in wind systems as the key element in PMSGs, it is also critical to maintain an operating temperature lower than a threshold temperature, known as the Curie point, as permanent magnets are sensitive to temperature. They would lose magnetism above the Curie point [11, 12].

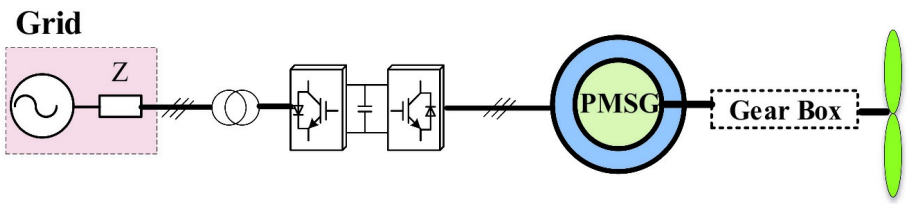


Figure 3.7 PMSG system

3.2.3.3 Doubly fed induction generator

As shown in Figure 3.8, this structure consists of a DFIG. The stator winding is directly connected to the network and the rotor winding is connected to the

network as well through a four-quadrant power converter. Usually, the electromagnetic torque and part of the reactive power to maintain the magnetization of the machine can be regulated by the controller of the rotor-side converter. Meanwhile, the controller of the grid-side converter controls the power factor and maintains a stable voltage across the DC link.

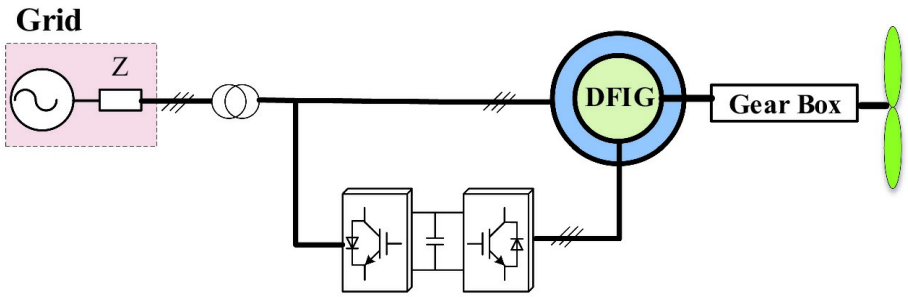


Figure 3.8 Doubly fed wound induction generator system

A distinct characteristic of DFIGs is the two modes of operation, namely sub-synchronous and super-synchronous modes because of the bidirectional power flow in the rotor circuit. During sub-synchronous generation, the rotor absorbs a fraction of the power generated by the stator. In contrast, under a super-synchronous condition, both the stator and rotor feed power to the grid. As the rotor absorbs or supplies only a fraction of the power, converters with a power rating, approximately 20 percent of the total machine power, are sufficient [13, 14].

Based on a similar working principle, DFIGs have evolved into other configurations. Figure 3.9 presents a wind energy configuration using a brushless doubly fed twin stator induction generator (BDFTSIG). This configuration essentially can be constructed by two cascaded induction machines. It is necessary to emphasize that their rotors should be interconnected properly so that the combined generator can act as a DFIG but with the benefit of avoiding brushes [15, 16].

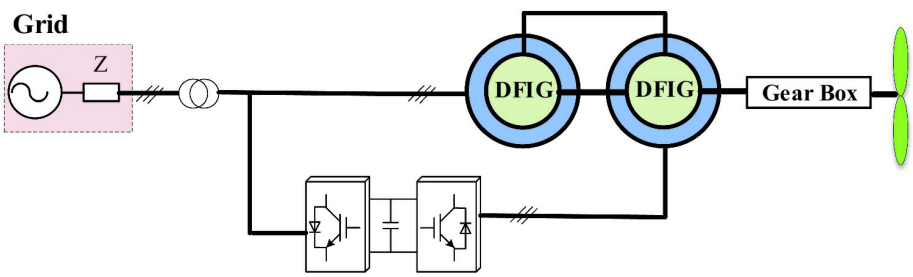


Figure 3.9 BDFTSIG system

3.2.3.4 Squirrel cage induction generator

Another type of wind generator is SCIG. Similar to PMSG, its stator winding is connected to the power network through an AC–DC–AC converter, as depicted in Figure 3.10. The difference is that the rotor is constructed by conductors to form a "squirrel cage" without using permanent magnet. As to power electronic converters, the stator-side converter regulates the electromagnetic torque and provides reactive power to maintain the machine magnetism. The grid-side converter controls the real and reactive power. SCIG is a very popular machine due to its simple structure and robust construction. A major problem is the necessity of obtaining the excitation current from the stator terminals. In addition, issues such as unbalanced three-phase loads, overheating, and torque pulsations may appear when connected to a weak grid [17].

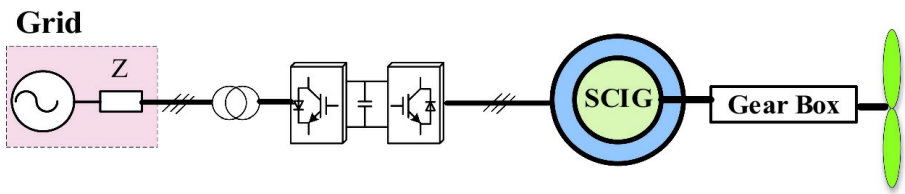


Figure 3.10 SCIG system

Overall, there are different features in these four generator types and they can be commonly used in different systems. Table 3.1 lists the advantages and drawbacks of different generator systems.

Table 3.1 Comparison of different VSCF wind generators

Type	Pros	Cons
WFSG	✓Full speed range ✓Possible to avoid gearbox ✓Complete control of reactive and active power	❖Full-scale power converter ❖Small converter for field
PMSG	✓Full speed range ✓No power converter for field ✓Possible to avoid gearbox ✓Complete control of reactive and active power ✓Brushless (low maintenance)	❖Full-scale power converter ❖Multipole generator (big and heavy) ❖Permanent magnets needed
DFIG	✓Limited speed range around −30% to 30% ✓Inexpensive small capacity converter ✓Complete control of reactive and active power	❖Need for gearbox
SCIG	✓Full speed range ✓Complete control of reactive and active power	❖Full-scale power converter ❖Need for gearbox

3.2.4 *Recent advances in wind power generation*

For maximum energy extraction in a VSCF system, as explained in (3.1) and (3.2), the speed of the turbine rotor should vary with the wind speed so that the optimal TSR is maintained. A control strategy that uses wind speed measurements is illustrated in Figure 3.11(a). In this approach, the wind speed is measured and the required rotor-speed for maximum power generation is computed according to the target TSR [18, 19]. The rotor-speed is also measured and compared to the calculated rotor-speed reference. The error is then sent to the inner torque controller for speed regulation. An improved algorithm for wind speed estimation using support-vector regression was reported in [20]. Neither anemometers nor external memory for power-mapping look-up tables is required. Other methods that could be regarded as sensorless systems were reported in [21, 22]. However, all of these methods still require the use of wind speed detection, which means that there will be a degree of power fluctuation under unstable wind conditions.

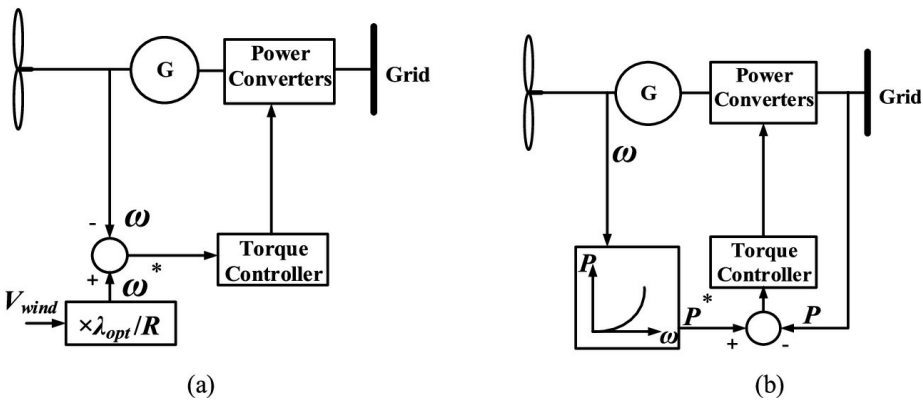


Figure 3.11 Schematic illustration of MPPT strategies: (a)

wind speed measurement, (b) power versus rotor-speed characteristic

Another control group is described in Figure 3.11(b). The actual output power is calculated and the target rotor speed for the required power generation is derived from the pre-mapped power versus rotor-speed characteristic [23]. This approach is also named power signal feedback. Based on this principle, several improved methods have been developed. Hill-climb searching is one of the strategies widely used because the generator parameters are not required, and it is very robust [24]. A further development stemmed from this is the step-changed hill-climb searching algorithm, which also works well for large inertia wind turbines [25]. An advanced technique, which uses a rotor position phase lock loop and thus does not need a tachometer, position encoder, or anemometer, was presented in [26].

In the global wind market, the DFIG has become one of the most popular options in wind turbines. As already mentioned in Section 3.2.3.3, its major merits include low capital cost due to the use of a partially rated converter, maximum power-tracking over a wider speed range, and decoupled active and reactive power control. As the penetration level of DGs is increasing, concerns about system ability and power quality are raised. First, wind-driven generators should meet the grid connection regulations. Second, they should not deteriorate the power system stability when they are connected to the grid. With more advanced control strategies, wind generators can actually participate in grid support. For example, they can be controlled to ride through the grid fault according to the latest grid codes and then help stabilize the grid voltage and frequency [27].

A variety of control strategies have been developed for DFIGs. The most widely used one is field-oriented control, i.e., vector control (VC). It separately regulates the *d*- and *q*-axis components of the rotor current to control the active and reactive power [28, 29]. This method requires complex coordination transformation. A significant amount of work is also required to tune the PI regulators. To overcome these limitations, direct torque control (DTC) [30] and then direct power control (DPC) [31] were proposed for DFIGs. The DTC and DPC approaches are much simpler and more robust than the VC methods. However, the conventional direct control algorithms, which use predefined switching tables, generate large ripples in magnetic flux, electromagnetic torque, and active/reactive power. They also result in a variable switching frequency. To address these issues, several modified strategies have been recently proposed and investigated [32–34]. Recently, a new control strategy, known as predictive control, was introduced in electrical drives. A predictive DPC method, which applies three voltage vectors in every control period to obtain constant switching frequency and reduce power ripples, is proposed in [35] and [36]. The predicted duration time for each vector in predictive DPC is calculated based on the power ripple minimization principle, which makes the calculation complicated. In

addition, the voltage vectors are still selected from a fixed switching table, which cannot guarantee an optimal vector selection. As a different category, model predictive DPC, which selects the optimal voltage vector based on the minimization of cost function rather than a simple fixed switching table, has been validated for application in power converters [37, 38]. In [37], a finite-state model predictive control (MPC) technique is applied to control DFIGs. It shows mitigated power fluctuations and less current harmonics. Besides, the control structure is quite simple without complex coordinate transformation and controller parameter tuning. It has many merits, such as reduced torque, flux and active/reactive power ripples, constant switching frequency, and excellent steady-state and transient responses. Later on, a two-vector-based low-complexity model predictive DPC was proposed [38], which applies a nonzero vector and a zero vector in every control period; the power fluctuation is restrained by regulating the duration of the nonzero vector.

Most existing DFIG control strategies discussed in Section 3.2.4 do not consider the grid synchronization, which is an important and practical issue and runs concurrently with protection [39]. The established methods for grid synchronization using VC like [40] utilize a control structure with an outer voltage loop and an inner rotor current loop to match the frequency, phase, and magnitude between the DFIG and the grid. These methods all inherit the drawbacks of VC and require measurements of rotor currents, rotor position, and grid and stator voltages, leading to heavy hardware requirements in measurement and complicated control algorithms. A direct voltage control scheme using an integral variable control structure without a current control loop was investigated in [41]. Unfortunately, it still requires the measurement of the grid and stator voltages. Besides, because of its complexity, the transient response is compromised.

Grid synchronization using DTC was reported in [42] in 2002. In comparison with the VC, a better transient performance was achieved. In this method, three PI regulators are adopted and the measurement of the rotor position and currents, and the stator and grid voltages are required. Later on, fast grid synchronization was achieved without the need for PI regulators or stator voltage measurement by introducing a virtual torque concept [43]. Although the control structure is simpler and the measurement burden is reduced, the stator voltage waveform is distorted due to large torque and flux ripples caused by the inherent feature of DTC. Also, the switching frequency is variable. These become the major obstacles to a smooth grid connection.

Another important concern in wind energy systems is the power regulation in grid-connected operation. Fast and flexible active and reactive power regulation after grid connection is desired as it can enable wind generators to participate in power quality improvement and energy management of the distribution network. A DPC strategy was studied in 2009. It can not only enable grid synchronization but also achieve smooth grid connection and flexible active and reactive power regulation without changing the controller structure in mode transition [44]. Actually, this control method is almost identical to the one proposed in [43]

except that it uses a virtual power concept rather than the virtual torque. From the perspective of grid synchronization, DPC is not superior to DTC for the following two reasons. First, under the same generator parameters, the effects of power ripples using DPC are larger than that of the torque and flux ripples using DTC. Consequently, more distorted stator voltage waveforms will be induced when DPC strategy is applied. Second, in DTC, the stator and grid voltage magnitudes are matched during synchronization by directly controlling the rotor flux amplitude. In contrast, this condition is fulfilled by imposing zero reactive power in DPC, resulting in an algorithm that is more complex and sensitive to parameter variations. Inspired by the advantages and limitations of [43] and [44] and also the merits of the predictive control, an overall DFIG control strategy by combining predictive direct virtual torque control and predictive DPC was proposed in [1] and [45]. It can be applied for both grid synchronization and grid-connected operation.

In reality, the grid voltage is not a perfect sinusoidal waveform. Instead, it presents distortion to some extent due to the complicated load connection and distribution network. Distorted network conditions such as grid voltage unbalance can influence the wind turbine system. Typically, oscillations can be observed in the electromagnetic torque, and the generator will inject distorted stator current into the main grid. In this case, the wind turbines might have to be disconnected from the distorted network to protect themselves from oscillated torques as well as overcurrents and overvoltages. However, disconnection is generally not allowed by the latest grid codes [46]. Therefore, the system controller must react to the perturbation and mitigate the adverse effects on the wind turbine systems themselves and the utility grid. When the grid voltage is unbalanced, the control performance of various control strategies that are designed with the assumption of normal grid conditions will be affected. To address this issue, different methods are studied to improve the performance of the DPC strategies under unbalanced grid conditions. To overcome the drawbacks mentioned above and enhance the control flexibility of the DFIGs, [14] and [47] propose a model predictive DPC strategy with power compensation schemes. It aims to improve power quality and mitigate torque oscillations under unbalanced grid voltage conditions. In this work, the extraction of negative-sequence components from the stator current is not needed. Switching tables, PI regulators, coordinate transformation, and pulse width modulators are all avoided. Thus, an excellent dynamic response can be obtained.

The variable speed wind energy conversion systems using PMSGs, gearless drive train (direct-drive), and full-scale power converters have generated significant attention in recent years for megawatt (MW) level wind turbine manufacturers. Such direct-drive structures show attractive properties (e.g., higher energy density, heavy gearbox elimination, and reduced maintenance), several direct-drive topologies have been developed. Once again, MPC algorithms find their promising applications in PMSG-based wind systems. In [48], a medium voltage power converter topology, which consists of a diode rectifier, a three-level boost converter, and neutral-point-clamped (NPC) inverter, is studied for a

PMSG-based high-power wind energy conversion system. The MPPT and DC-link capacitor voltage balancing are guaranteed by controlling the generator-side three-level boost converter, while the grid-side NPC inverter controls the DC-bus voltage and manages the reactive power injected into the grid. A significant improvement in the grid power quality is accomplished as the NPC inverter no longer controls the DC-link neutral point voltage. Based on this configuration, a model predictive strategy is proposed to control the overall system. The proposed power electronic converter set is expressed in terms of discrete-time models that are used to predict the future behavior of control variables. Similarly, a direct-drive PMSG with a three-level NPC back-to-back power converter has also attracted research attention in high-power wind energy conversion applications. For such a topology, finite-control set MPC has emerged as a promising alternative. In [49], a robust finite-control set MPC method with revised predictions is proposed and validated for such a system. With the proposed solution, not only the control variables can be better regulated with less steady-state ripples but also the system robustness against parameter variations is enhanced. In [50], a Vienna rectifier connecting to the PMSG is studied for the wind turbine system. Based on this structure, an MPC strategy with the discrete space-vector modulation was developed. The feasible voltage vectors of the Vienna rectifier are extended from 8 to 19. Thus, the torque ripple and vibration can be further eliminated and the neutral-point voltage can be better maintained.

3.3 Solar PVs generation

3.3.1 Principle and configuration of PV systems

Solar PV reaction converts solar energy directly into electrical energy inside solar cells, which are usually manufactured and combined into modules, depending on the output voltage and current of the module. Additionally, the modules can be further grouped in series or parallel to form arrays with unique voltage and current characteristics.

The output of a PV array can be influenced by many factors, such as sunlight density, shading, temperature, etc. Figure 3.12 shows the total power output performance of a PV array from early morning to late evening on a sunny day and a cloudy day, respectively. It can be seen that during a sunny day, the power generated from the PV increased steadily in the morning, climbed up to the peak value of about 19 kW at around 2 pm, decreased gradually afterward, and hit the bottom of 0 kW at about 7 pm. By contrast, the PV output power presents an obvious fluctuating characteristic on a cloudy day. Figure 3.13 shows the V–I characteristic of a solar module under uniform solar irradiation conditions. One important feature of a solar module is the short-circuit current and open-circuit voltage. In addition, it can be seen from the V–I curve that PV panels exhibit a unique operating point corresponding to maximal PV output power.

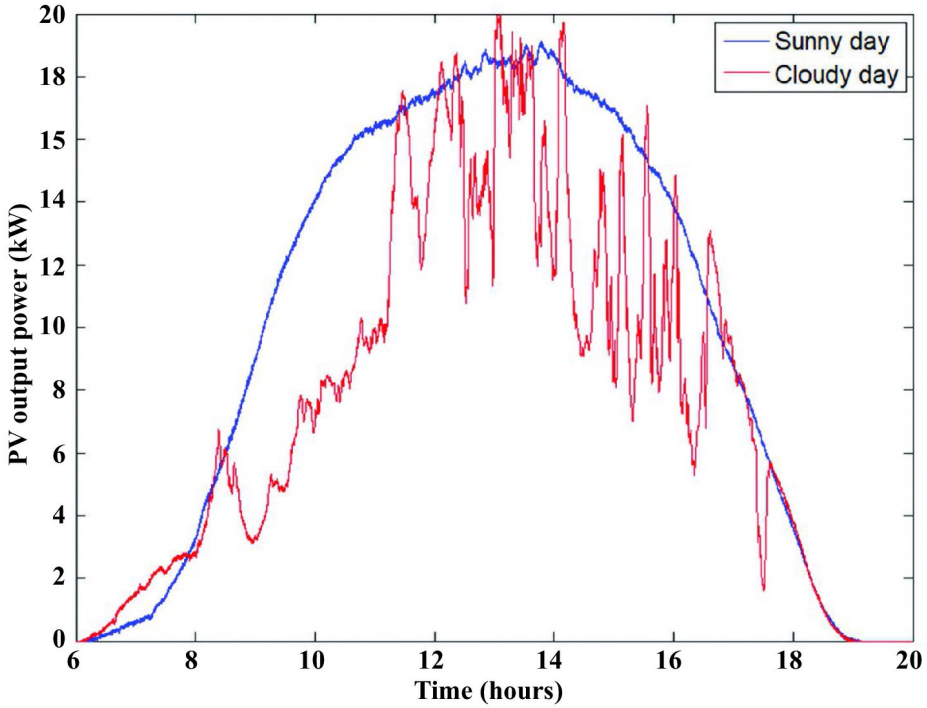


Figure 3.12 Solar PV output in two different days

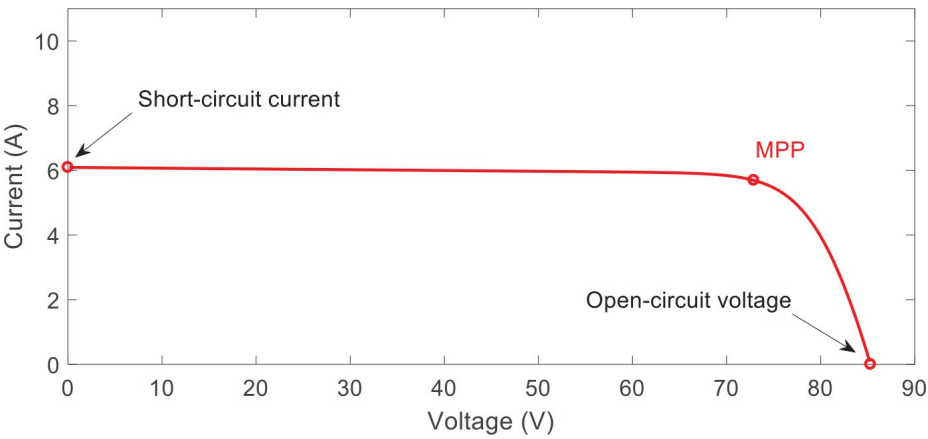


Figure 3.13 Current versus voltage characteristic of a solar PV module

Several topology configurations can be applied in solar PV systems.

Essentially, various configurations distinguish from each other in terms of the power electronic interfaces that interconnect the system to the utility grid [2]. Figure 3.14 presents the structure in which a centralized inverter is utilized. It has been the most common type of PV installation in the past. PV modules are connected in series and/or parallel and the terminal is connected to the centralized DC–AC converter. The main advantage of this structure is the fact that if the inverter accounts for a large portion of the total cost in the installed PV system, this configuration probably requires the lowest investment because of the presence of only one inverter. However, the main drawback of this configuration is that the power losses can be high due to the shading effect difference between the PV strings and the presence of string diodes. Another disadvantage is that this centralized structure shows a single point failure feature at the inverter and thus has less reliability.

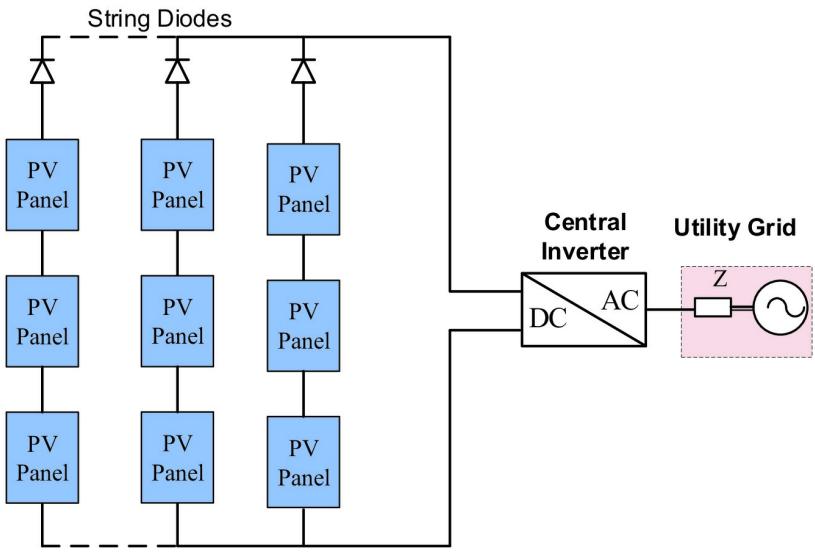


Figure 3.14 Centralized PV configuration

Figure 3.15 shows another configuration named string-array PV systems. The series of PV panels are connected in the form of separate strings that are interconnected to the utility through individual inverters. Without the string diodes, the power losses can be reduced. Most importantly, the MPPT can be implemented on each PV string. Consequently, the overall efficiency is greatly improved compared to the centralized configuration, particularly when multiple strings are mounted on fixed surfaces in different operations. Apparently, one of the disadvantages of this configuration is the increased cost due to additional inverters.

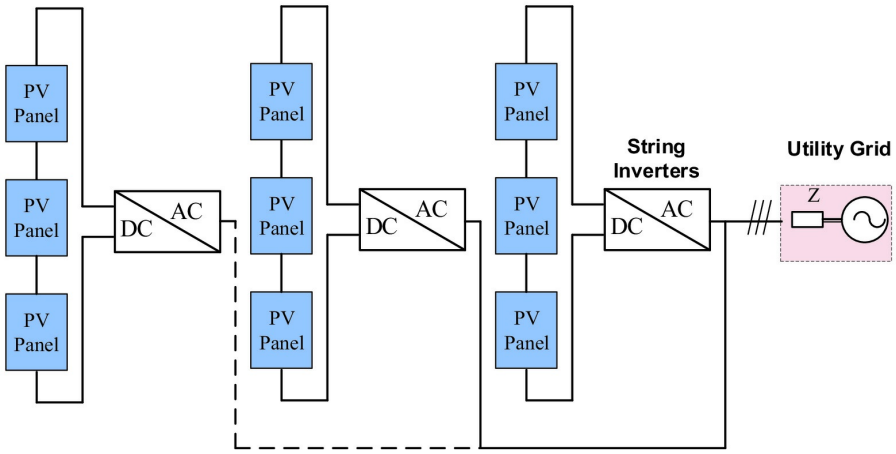


Figure 3.15 PV configuration with individual string inverters

Figure 3.16 shows a solution that each PV module is attached to its own inverter. The advantages of this configuration type include the easy installation of additional modules because each module has its own DC–AC inverter. As to utility grid connection, it can be easily done by connecting the inverter AC field wirings together. The system overall reliability can also be improved as well because there is no single-failure for the system. In addition, the power loss of the system is lower due to the reduced mismatch among the modules and the MPPT on each module. If the size and the cost of power electronic converters can be continuously reduced, this configuration could be a promising option for future smart grid with high PV penetration.

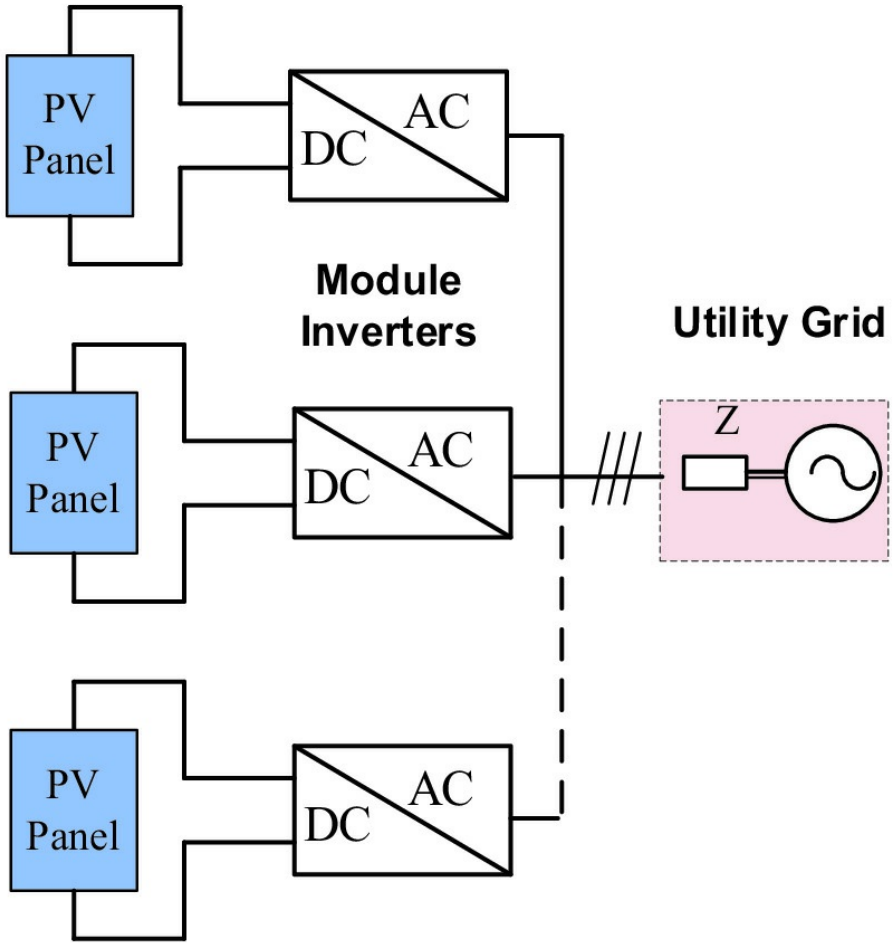


Figure 3.16 PV configuration with module inverters

3.3.2 Power converters and recent advance of MPC for PV systems

For PV systems, there is no standard topology in terms of system structure and power electronic interfaces. To date, a variety of topologies have been studied and applied [51, 52]. Regarding the power electronic interfaces, their main requirement for the PV systems is to implement MPPT and to convert the PV output DC voltage into an appropriate AC for consumer use and utility connection. Usually, due to the relatively low-voltage output from PV modules, the terminal DC voltage from the PV array is required to step up to a higher value using additional converters before converting them to the utility compatible AC.

The DC–AC inverters are then utilized to convert the voltage to AC. Here, it is worth mentioning that MPPT and DC–AC conversion can be implemented in one inverter, depending on the inverter topology and the actual requirement. Overall, the power electronics topologies for the PV systems can be classified according to the number of power processing stages, the types of grid interfaces, the location of power decoupling capacitors, and the utilization transformers.

3.3.2.1 Single-phase single-stage

Figure 3.17 shows the single-phase single-stage setup of the PV connection. It is one of the fundamental options for PV systems in the last decades. The output of the PV array is first connected to a voltage-balancing capacitor, which is used to maintain the DC-link voltage and mitigate the harmonics from the array. The other side of the capacitor is connected to a single-phase full-bridge converter that is connected to an LC filter before connecting to the grid through an isolated transformer. This configuration offers several advantages including low cost, simple structure, and high reliability. However, since all the modules are connected to the same MPPT device, serious power losses during partial shadowing are unavoidable.

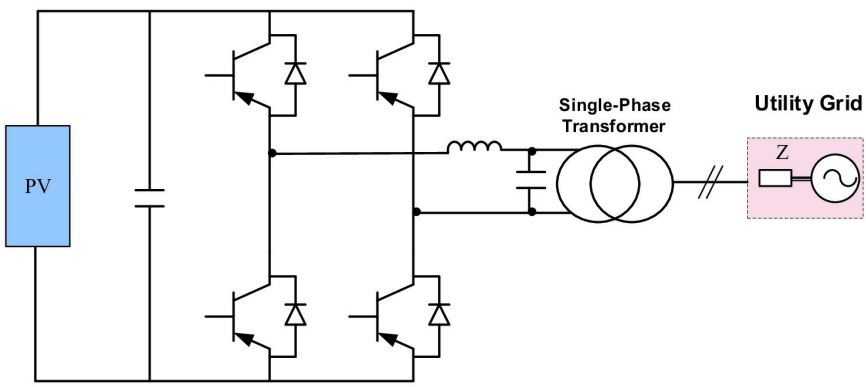


Figure 3.17 Single-phase single-stage PV power electronics

3.3.2.2 Single-phase multiple-stage

Actually, due to the utilization of low-frequency transformers, as shown in Figure 3.17, the single-phase single-stage option described in Section 3.3.2.1 has another drawback that is a relatively large size and low efficiency. To overcome these drawbacks, multistage conversion systems can be utilized. Figure 3.18 presents a single-phase multistage configuration, which employs a high-frequency

transformer for a single-phase connection to the grid. As the secondary side of the transformer generates a high-frequency voltage, it does not match the frequency of the grid voltage. Consequently, a diode-bride rectifier is needed to convert the high-frequency voltage to DC voltage and then convert it back to AC voltage through an inverter for easy grid connection in terms of amplitude, frequency, and phase angle.

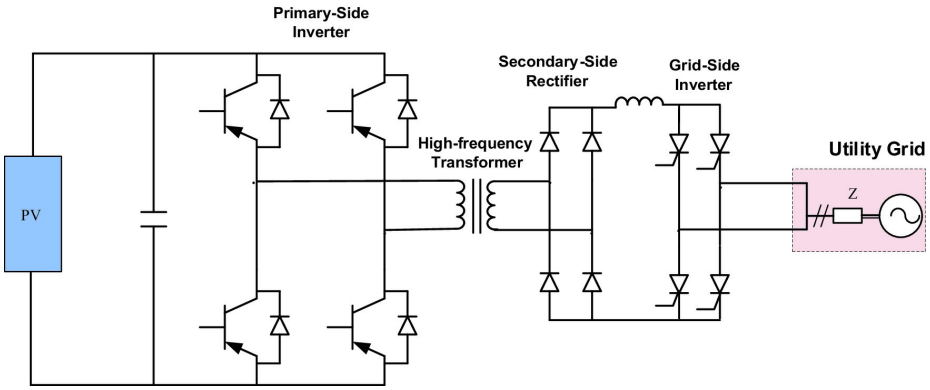


Figure 3.18 Single-phase multiple-stage PV power electronics

3.3.2.3 Three-phase single-stage

Recently, the utilization of three-phase inverters in PV systems has increased for larger PV systems. With the increase in high-voltage high-power renewable power systems, three-phase systems with larger power capacities are more suitable. Besides, compared to single-phase systems, three-phase systems can avoid unbalance issues from the generation side. Figure 3.19 shows the three-phase option for PV systems. The output of the PV array is connected to a capacitor first, before connected to the three-phase inverter. Then, LC filters are employed here to eliminate the high-frequency AC harmonics caused by the PWM. Finally, a low-frequency three-phase transformer is used to step up the voltage for grid connection.

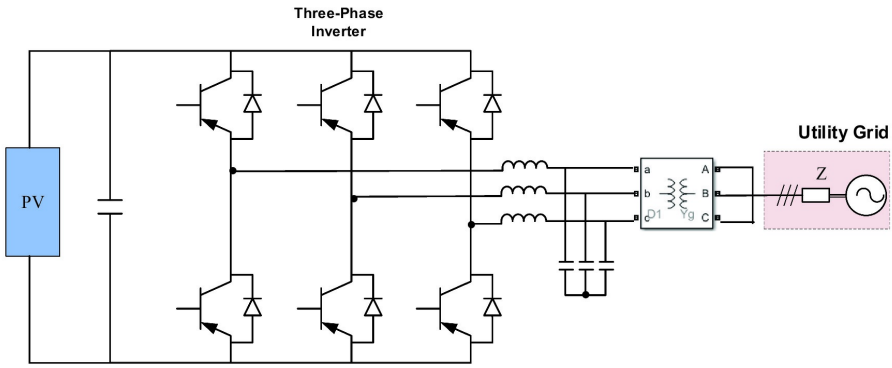


Figure 3.19 Three-phase PV topology with line-frequency transformer

A common PV configuration and the associated control scheme are shown in Figure 3.20. It consists of a DC–DC converter, a three-phase inverter and a three-phase step-up transformer. The DC–DC converter is built by connecting a current-source full-bridge inverter, a high-frequency transformer, and a rectifier in series. The filter capacitor in parallel with the PV system can be avoided by connecting the current-source full-bridge inverter to the PV terminals. The DC voltage from the PV terminals is first inverted into a high-frequency AC through the current-source full-bridge inverter. The induced AC voltage at the transformer secondary side is then converted back to DC using a full-bridge diode rectifier. Subsequently, the rectified DC power is injected into the utility grid through a three-phase voltage-source inverter and a three-phase low-frequency transformer.

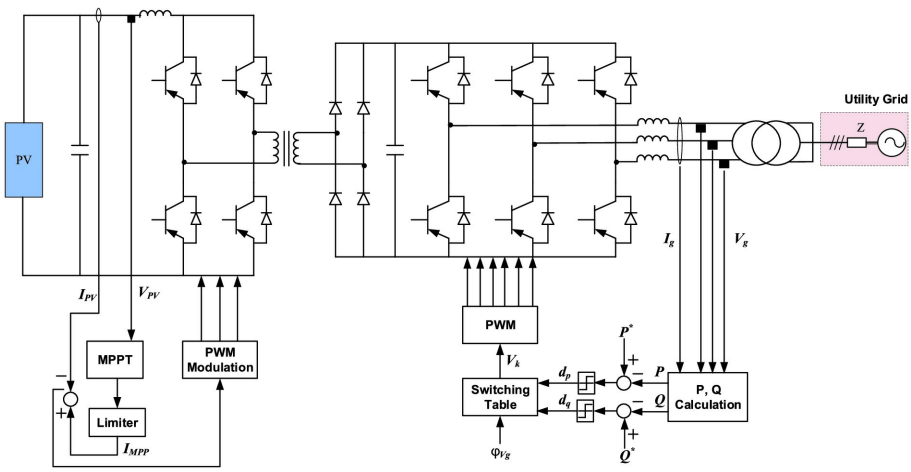


Figure 3.20 Example of a control scheme for PV systems

3.3.2.4 MPPT control of PV system

As explained in Section 3.3.1, the PV actual output varies with the sunlight density and temperature in a nonlinear characteristic. If the PV output voltage is not adjusted accordingly, the extraction of maximum power cannot be achieved. To address this problem, several schemes for extracting maximum power have been developed, which are briefly introduced here. Tracking the maximum power point (MPP) of a PV array is usually an important stage of a PV system as it affects the overall efficiency. MPPT can often be implemented on the D–DC converter. Over the years, many MPPT algorithms have been developed and implemented. These methods show their features in terms of the range of effectiveness, complexity, implementation hardware, required sensors, cost, convergence speed, popularity, etc. The names of some of these methods include perturb and observe, hill climbing, fractional short-circuit current, incremental conductance, fractional open-circuit voltage, fuzzy logic, and neural network control, current sweep, ripple correlation control, dP/dV or dP/dI feedback control, DC-link capacitor droop control, load-current or load-voltage maximization, etc.

- *Constant voltage method*

One of the simple approaches is constant voltage control. In practice, the voltage corresponding to the MPP varies around 70–80 percent of the PV open-circuit voltage. Based on this empirical experience, the MPP can be approximately reached by maintaining the PV output voltage to this specified value. In this method, the control structure is relatively simple because only the PV voltage is measured. However, it is not superior to other MPPT methods in terms of overall energy conversion efficiency as the voltage is not adaptive. Besides, it is noted that this method may not be effective in locations where the temperature varies very significantly due to the change of the voltage at the terminals of the module under temperature variation [53].

- *Fixed duty cycle*

Another conventional and simple approach of MPPT is the fixed duty cycle method. It does not require any feedback, and the load impedance is adjusted only once for the MPP [54].

- *MPP locus characterization*

In fact, even though the output characteristic of the PV modules is nonlinear, the relationship between voltage and current at all MPPs can be approximated as a linear feature. Specifically, this relationship is the tangent line to the MPP locus curve for the PV current in which the minimum irradiation condition satisfies the sensitivity of the method. Generally, the formula expressed in (3.3) can be used to represent the MPP locus curve [55]. Based on this locus curve, the linear

approximation can be made offline for the PV panel, and it should be updated with the temperature.

$$T_L = \left(\frac{\eta V_T}{I_{MPP}} - N \cdot R_s \right) I_{MPP} + \left[V_{oc} - \eta \left(V_{Do} + V_T \right) \right] \quad (3.3)$$

where N is the number of the PV cells. I_{MPP} is the current at MPP. V_T is the temperature voltage, whereas V_{Do} is the differential voltage.

- *Beta method*

The beta method is the approximation of the MPP through (3.4) with an intermediate variable β [56]

$$\beta = \ln \left(\frac{I_{PV}}{V_{PV}} \right) - c \times V_{PV} \quad (3.4)$$

where $c = (q/(\eta \cdot K_B \cdot T \cdot N_S))$ is a constant that depends on several factors including temperature T, the Boltzmann constant K_B, the electron charge q, the number of series PV cells N_S, and the quality factor of the junction panel η.

In this approach, the value of β remains almost constant under various operating conditions. Thus, β can be continuously calculated using the voltage and current of the PV panel and inserted on a conventional closed loop with a constant reference. One shortcoming of this method is the requirement of PV electrical parameters.

- *Temperature method*

To mitigate the temperature effect on the MPPT methods mentioned in Section 3.3.1, one solution is to use a temperature method. To do this, a low-cost temperature sensor can be employed, which modifies the MPP algorithm function, maintaining the accurate tracking of MPP [57].

- *System oscillation and ripple correlation*

This technique uses the disturbance to determine the optimal point of operation, which is similar to the hill-climb searching technique of MPPT for wind power systems, as introduced in Chapter 2. At the MPP, the ratio of the oscillating deviation to the average voltage is constant. To implement this method, the additional low-frequency ripple or doubly grid frequency can be used. Nevertheless, switching frequencies must be filtered before being acquired for the purpose of avoiding wrong switching states and eliminating electromagnetic interference [58]. Similarly, ripple correlation utilizes power oscillations through an all-pass filter to reach the optimal point. In other words, the high-frequency ripples in power and voltage are extracted using high-frequency filters, which are

then used to calculate dP/dV. After that, the sign of this derivative is sent to a signal function to indicate the right region of operation, and an integrator also ensures the MPP.

- *P&O and P&O based on PI*

The basic principle of the P&O method is to periodically increase or reduce the output terminal voltage of the PV cell. Based on this, the power obtained in the current cycle will be compared with the power of the previous one by checking the sign of dP/dV. For example, if the power increases subject to the change of terminal voltage, the control system will change the operating point in that direction. Otherwise, it changes the operating point in the opposite direction. After the direction for the change of voltage is determined, the voltage is varied at a constant rate [59, 60]. A modified operation can be made by varying the steps according to the distance of the MPP, thus resulting in higher efficiency.

It is noted that in steady state, the operation point is not altered unless the PV module ambient environments such as temperature and solar irradiance changes. The key is to reduce the dP/dV to zero using a closed-loop control performing the P&O based on PI.

- *Finite-control set MPC-based MPPT*

In the last few years, intelligent methods such as MPC were developed for better extraction of the maximum power from the PV arrays [61]. In general, the control strategy consists of three steps. The first step is to measure the system variables, i.e., the PV voltage and current. After that, the current and/or voltage reference that can achieve MPPT will be calculated using the P&O method or incremental conductance (INC) method [62], which is considered as an improved P&O method. The second step is to calculate the predicted current and/or voltage based on the system model and the measured data. This calculation should be for all the possible switching states of the converter. The next step is to minimize the cost function based on the predicted values and their references. In a PV system, obviously, the variables are the PV current and voltage. Eventually, the switching states corresponding to the reduced cost function will be applied.

3.3.2.5 Grid-side inverter control of PV system

All the MPPT approaches discussed in Section 3.3.2.4 are relatively mature and already proved in practical application. In this subsection, we concentrate on the grid-side inverter control of the PV system.

In a distributed PV system, there are generally two operations, namely, islanded mode and grid-connected mode. In islanded mode, the PV system and the local loads form an isolated autonomous small power system, in which the loads are totally powered by the PV units. In this case, by establishing a stable voltage at the point of common coupling (PCC), the inverters are controlled to convert the DC power to AC power for the local loads. In islanded operation, generally, an LC filter is required to filter the PWM ripples from the solar inverters to establish a satisfactory voltage waveform. If the power generated

within the DG system is greater than the local load demand, these DG units should inject the surplus energy into the utility grid through grid synchronization and connection. Alternatively, the power mismatch can be absorbed by the energy storage. After the grid connection, solar inverters should be controlled to achieve flexible power regulation. According to some traditional requirements such as relevant IEEE standards, a DG system is not allowed to actively regulate the voltage at the PCC. It is recommended that low-power systems should be disconnected when the grid voltage is lower than 0.85 p.u. or higher than 1.1 p.u., as an anti-islanding requirement [63]. Despite this, according to some recent regulations, if individual DG systems such as MGs can be allowed to contribute to voltage support and power quality improvement by flexibly regulating active and reactive power output at the low-voltage distribution level [64].

The operation of solar inverters in islanded mode with a function such as UPS units has been studied, with a particular research interest in multiloop feedback control, adaptive control, deadbeat control, etc. Most of these methods utilize conventional outer voltage and inner current loops with proportional-integral-derivative regulators. This cascaded control not only requires significant tuning effort to obtain satisfactory performance but also degrades system dynamic response to load changes and solar irradiance variations. To address these shortcomings, a MPC strategy was proposed to control solar inverters in islanded operation [65]. In this work, there is no need for inner current-control loops or modulators, and the approach is easy to implement.

Meanwhile, research effort has also been made to grid-connected operation. Predictive control techniques appear to be an attractive option for the control of power converters, among which MPC has drawn much attention, mainly because of its flexible control principle that allows easy inclusion of system nonlinearities, constraints, and objectives. In the control process, a discrete model representing the system, together with current states and all possible control actions, are used to predict the future states. After that, a cost function is designed as a selection criterion to evaluate the possible control actions. The control objectives formulated in the cost function are dependent on actual requirements. For instance, inverter output voltage is the control objective for a UPS system. In other applications, the control objectives become reactive power and DC-link voltage for rectifiers, output currents for grid-connected inverters, and magnetic flux and electromagnetic torque for electric drives. While many control approaches have been developed to control converters in distributed energy systems, the majority of them only focus on one specific operation mode. General and unified control strategies that deal with different operation modes in MG applications still need further development. In [66], an inverter control method based on MPC algorithm for PV systems is proposed, which enables islanded operation, seamless transfer, and grid-connected operation.

With the increasing penetration of RESs integrated into the power grid, energy conversion efficiency has become one of the major concerns. In conventional control, a high switching frequency can usually guarantee better steady-state performance and faster dynamic response in energy conversion.

However, high switching frequencies will result in a larger amount of power loss, particularly in high-voltage and high-power DGs such as MW wind turbines and solar farms. In this sense, researchers have been trying to reduce the power converter switching frequencies and at the same time to retain the system performance. Taking advantage of the flexible control structure of MPC, [67] proposes a model predictive DPC method of grid-connected inverters for solar PVs. A cost function is designed to reduce active and reactive power ripples, which, in turn, eliminates harmonic currents injection. Next, a model-based prediction scheme is adopted to compensate for a one-step delay, which is a common phenomenon to compromise the system performance. Furthermore, a long horizon prediction algorithm is developed with the purpose of switching frequency reduction. In [68], MPC has been applied to another level for a DC distribution system where multiple PV arrays are connected to the DC common bus through parallel back-to-back DC–DC converters. First, a MPC-based MPPT is developed to control the PV-side converters. Then, a MPC-based droop current regulator for common bus-side converters to achieve load sharing according to power delivery capacities of PV arrays.

References

[1] Hu J., Li Y., Zhu J. 'Multi-objective model predictive control of doubly-fed induction generators for wind energy conversion'. *IET Generation, Transmission & Distribution*. 2019, vol. 13(1), pp. 21–9.

[2] Kramer W., Chakraborty S., Kroposki B., Thomas H. 'Advanced power electronic interfaces for distributed energy systems, part 1: systems and topologies, technical report, NREL/TP-581-42672'. March 2008.

[3] 'GWEC market intelligence'. March 2020.

[4] Yaramasu V., Wu B., Sen P.C., Kouro S., Narimani M. 'High-power wind energy conversion systems: state-of-the-art and emerging technologies'. *Proceedings of the IEEE*. 2015, vol. 103(5), pp. 740–88.

[5] Hu J., Zhu J., Dorrell D., et al. 'A novel control strategy for doubly fed induction generator and permanent magnet synchronous generator during voltage dips'. *Proceeding of 20th Australasian Universities Power Engineering Conference*, 5-8 Dec; 2010. pp. 1–6.

[6] Tafticht T., Agbossou K., Cheriti A., Doumbia M.L. 'utput power maximization of a permanent magnet synchronous generator based stand-alone wind turbine'. *International Symposium on Industrial Electronics*; Montreal, July 9-12; 2006. pp. 2412–16.

[7] Amirat Y., Benbouzid M., Bensaker B., Wamkeue R. 'Generators for wind energy conversion system: state of the art and coming attractions'. *Electrical Systems*. 2007, vol. 3, pp. 26–38.

[8] Li H., Chen Z. 'Overview of different wind generator systems and their comparisons'. *IET Renewable Power Generation*. 2008, vol. 2(2), pp. 123–38.

[9] Blaabjerg F., Liserre M., Ma K. 'Power electronics converters for wind

turbine systems'. *IEEE Transactions on Industry Applications*. 2012, vol. 48(2), pp. 708–19.
[10] Soter S., Wegener R. 'Development of induction machines in wind power technology'. *Electric Machines & Drives Conference, 2007. IEMDC '07. IEEE International*; 2007. pp. 1490–5.
[11] Bhende C.N., Mishra S., Malla S.G. 'Permanent magnet synchronous generator-based standalone wind energy supply system'. *IEEE Transactions on Sustainable Energy*. 2011, vol. 2(4), pp. 361–73.
[12] Haque M.E., Negnevitsky M., Muttaqi K.M. 'A novel control strategy for a variable-speed wind turbine with a permanent-magnet synchronous generator'. *IEEE Transactions on Industry Applications*. 2010, vol. 46(1), pp. 331–9.
[13] Abad G., Marroyo L., Iwanski G., *et al*. *Doubly Fed Induction Machine: Modeling and Control for Wind Energy Generation*. New Jersey, US: Wiley-IEEE Press; 2011.
[14] Hu J J., Zhu Y., Zhang Q.M., Guo Y. 'Simple and robust predictive direct control of DFIG with low constant switching frequency and reduced torque and flux ripples'. *Proceedings of IEEE International Conference on Electric Machines and Drives*, 15–18 May; 2011. pp. 1–6.
[15] Achkar M.E., Mbayed R., Salloum G., Patin N., Monmasson E. 'Voltage control of a stand-alone cascaded doubly fed induction generator'. *IEEE Transactions on Industrial Electronics*. 2018, vol. 66(1), pp. 762–71.
[16] Hu J., Zhu J., Dorrell D.G. 'A new control method of cascaded brushless doubly fed induction generators using direct power control'. *IEEE Transactions on Energy Conversion*. 2014, vol. 29(3), pp. 771–9.
[17] Marques H.P.J., Gründling H.A., Pinheiro J.R., Hey H.L. 'A survey on variable-speed wind turbine system'. 2002, pp. 732–8.
[18] Tan K., Islam S., Island S. 'Optimum control strategies in energy conversion of PMSG wind turbine system without mechanical sensors'. *IEEE Transactions on Energy Conversion*. 2004, vol. 19(2), pp. 392–9.
[19] Chen Z., Guerrero J.M., Blaabjerg F. 'A review of the state of the art of power electronics for wind turbines'. *IEEE Transactions on Power Electronics*. 2009, vol. 24(8), pp. 1859–75.
[20] Abo-Khalil A.G., Dong-Choon Lee. 'MPPT control of wind generation systems based on estimated wind speed using SVR'. *IEEE Transactions on Industrial Electronics*. 2008, vol. 55(3), pp. 1489–90.
[21] Xuemei Z., Lin L., Dianguo X., Platts J. 'Sliding Mode MPPT Control of Variable Speed Wind Power System'. *Power and Energy Engineering Conference, 2009. APPEEC 2009. Asia-Pacific*; 2009. pp. 1–4.
[22] Xie Z., Zhang C.W., Zhang X., Yang S.Y., Cao R.X. 'Study On The Rotor Convertor Of Doubly Fed Induction Generator Used In Wind Turbine System'. *Industrial Electronics and Applications, 2007. ICIEA 2007. 2nd IEEE Conference on*; 2007. pp. 2594–8.
[23] Koutroulis E., Kalaitzakis K. 'Design of a maximum power tracking system for wind-energy-conversion applications'. *IEEE Transactions on Industrial*

Electronics. 2006, vol. 53(2), pp. 486–94.
[24] Datta R., Ranganathan V.T. 'A method of tracking the peak power points for a variable speed wind energy conversion system'. *IEEE Power Engineering Review*. 2002, vol. 22(10), pp. 57–57.
[25] Ping W., Hongyuan L., Cuishuang G., Chenbin T. 'MPPT control algorithms for wind power generation based on voltage disturbance'. *Intelligent Control and Automation, 2008. WCICA 2008. 7th World Congress on*; 2008. pp. 7398–402.
[26] Baike Shen., Mwinyiwiwa B., Yongzheng Zhang., Boon-Teck Ooi. 'Sensorless maximum power point tracking of wind by DFIG using rotor position phase lock loop (PLL)'. *IEEE Transactions on Power Electronics*. 2009, vol. 24(4), pp. 942–51.
[27] Nycander E., Soder L. Review of european grid codes for wind farms and their implications for wind power curtailments. *17th International. Wind Integration Workshop, Stockholm*; Oct. 2018.
[28] Datta R., Ranganathan V.T. 'A simple position-sensorless algorithm for rotor-side field-oriented control of wound-rotor induction machine'. *IEEE Transactions on Industrial Electronics*. 2001, vol. 48(4), pp. 786–93.
[29] De Doncker R.W., Muller S., Deicke M. 'Doubly fed induction generator systems for wind turbines'. *IEEE Industry Applications Magazine*. May/Jun 2002, vol. 8(3), pp. 26–33.
[30] Arnalte S., Burgos J.C., Rodríguez-Amenedo J.L. 'Direct torque control of a doubly-fed induction generator for variable speed wind turbines'. *Electric Power Components and Systems*. 2002, vol. 30(2), pp. 199–216.
[31] Datta R., Ranganathan V.T. 'Direct power control of grid-connected wound rotor induction machine without rotor position sensors'. *IEEE Transactions on Power Electronics*. 2001, vol. 16(3), pp. 390–9.
[32] Zhi D., Xu L., Williams B.W. 'Model-based predictive direct power control of doubly fed induction generators'. *IEEE Transactions on Power Electronics*. 2010, vol. 25(2), pp. 341–51.
[33] Hu J., Zhu J., Zhang Y., Ma Q., Guo Y. 'Simple and robust predictive direct control of DFIG with low constant switching frequency and reduced torque and flux ripples'. *IEEE International Conference on Electric Machines and Drives*. 2011, pp. 781–6.
[34] Xu L., Cartwright P. 'Direct active and reactive power control of DFIG for wind energy generation'. *IEEE Transactions on Energy Conversion*. 2006, vol. 21(3), pp. 750–8.
[35] Abad G., Rodriguez M.A., Poza J. 'Two-level VSC based predictive direct torque control of the doubly fed induction machine with reduced torque and flux ripples at low constant switching frequency'. *IEEE Transactions on Power Electronics*. 2008, vol. 23(3), pp. 1050–61.
[36] Abad G., Rodriguez M.A., Poza J. 'Two-level VSC-based predictive direct power control of the doubly fed induction machine with reduced power ripple at low constant switching frequency'. *IEEE Transactions on Energy Conversion*. 2008, vol. 23(2), pp. 570–80.

[37] Sguarezi Filho A.J., Filho E.R. ‘Model-based predictive control applied to the doubly-fed induction generator direct power control’. *IEEE Transactions on Sustainable Energy*. 2012, vol. 3(3), pp. 398–406.
[38] Sun D., Wang X. ‘Low-complexity model predictive direct power control for DFIG under both balanced and unbalanced grid conditions’. *IEEE transactions on industrial electronics : a publication of the IEEE Industrial Electronics Society*. 2016, vol. 63(8), pp. 5186–96.
[39] Jin Yang., Fletcher J.E., O'Reilly J., Yang J., O’Reilly J. ‘A series-dynamic-resistor-based converter protection scheme for doubly-fed induction generator during various fault conditions’. *IEEE Transactions on Energy Conversion*. June 2010, vol. 25(2), pp. 422–32.
[40] Blaabjerg F., Teodorescu R., Liserre M., Timbus A.V. ‘Overview of control and grid synchronization for distributed power generation systems’. *IEEE Transactions on Industrial Electronics*. 2006, vol. 53(5), pp. 1398–409.
[41] Chen S.Z., Cheung N.C., Wong K.C., Wu J. ‘Grid synchronization of doubly-fed induction generator using integral variable structure control’. *IEEE Transactions on Energy Conversion*. 2009, vol. 24(4), pp. 875–83.
[42] Gomez S.A., Amenedo J.L.R. ‘Grid synchronisation of doubly fed induction generators using direct torque control’. *Proc. IEEE IECON Conf*. 2002, pp. 3338–43.
[43] Arbi J., Ghorbal M.J.-B., Slama-Belkhodja I., Charaabi L. ‘Direct virtual torque control for doubly fed induction generator grid connection’. *IEEE Transactions on Industrial Electronics*. 2009, vol. 56(10), pp. 4163–73.
[44] Manel J.-B.G., Arbi J., Ilhem S.-B. ‘A novel approach of direct active and reactive power control allowing the connection of the DFIG to the grid’. *Proc. IEEE Power Electronics and Applications Conf*. 2009, pp. 1–10.
[45] Hu J., Zhu J., Zhang Y., Ma Q., Guo Y. Simple and robust predictive direct control of DFIG with low constant switching frequency and reduced torque and flux ripples. *IEEE International Electric Machines & Drives Conference*; 2011. pp. 771–6.
[46] Tsili M., Papathanassiou S. ‘A review of grid code technical requirements for wind farms’. *IET Renewable Power Generation*. 2009, vol. 3(3), pp. 308–32.
[47] Hu J., Zhu J., Dorrell D.G. ‘Model-predictive direct power control of doubly-fed induction generators under unbalanced grid voltage conditions in wind energy applications’. *IET Renewable Power Generation*. 2014, vol. 8(6), pp. 687–95.
[48] Yaramasu V., Wu B. ‘Predictive control of a three-level boost converter and an NPC Inverter for high-power PMSG-based medium voltage wind energy conversion systems’. *IEEE Transactions on Power Electronics*. 2014, vol. 29(10), pp. 5308–22.
[49] Lee J.-S., Lee K.-B., Blaabjerg F. ‘Predictive control with discrete space-vector modulation of Vienna rectifier for driving PMSG of wind turbine systems’. *IEEE Transactions on Power Electronics*. 2019, vol. 34(12), pp. 12368–83.

[50] Zhang Z., Li Z., Kazmierkowski M.P., Rodriguez J., Kennel R. 'Robust predictive control of three-level NPC back-to-back power converter PMSG wind turbine systems with revised predictions'. *IEEE Transactions on Power Electronics*. 2018, vol. 33(11), pp. 9588–98.
[51] Kjaer S.B., Pedersen J.K., Blaabjerg F. 'A review of single-phase grid-connected inverters for photovoltaic modules'. *IEEE Transactions on Industry Applications*. 2005, vol. 41(5), pp. 1292–306.
[52] Kouro S., Leon J.I., Vinnikov D., Franquelo L.G. 'Grid-connected photovoltaic systems: an overview of recent research and emerging PV converter technology'. *IEEE Industrial Electronics Magazine*. 2015, vol. 9(1), pp. 47–61.
[53] Pandey A., Dasgupta N., Mukerjee A.K. 'A simple single-sensor MPPT solution'. *IEEE Transactions on Power Electronics*. 2007, vol. 22(6), pp. 698–700.
[54] Tofoli F.L., de Castro Pereira D., de Paula W.J. 'Comparative study of maximum power point tracking techniques for photovoltaic systems'. *International Journal of Photoenergy*. 2015, vol. 2015(3), pp. 1–10.
[55] Scarpa V., Buso S., Spiazzi G. 'Low-complexity MPPT technique exploiting the PV module MPP locus characterization'. *IEEE Transactions on Industrial Electronics*. 2009, vol. 56(5), pp. 1531–8.
[56] Jain S., Agarwal V. 'A new algorithm for rapid tracking of approximate maximum power point in photovoltaic systems'. *IEEE Power Electronics Letters*. 2004, vol. 2(1), pp. 16–19.
[57] Coelho R.F., Concer F.M., Martins D.C. 'A MPPT approach based on temperature measurements applied in PV systems'. *Proc. IEEE ICSET*. 2010, pp. 1–6.
[58] Casadei D., Grandi G., Rossi C. 'Single-phase single-stage photovoltaic generation system based on a ripple correlation control maximum power point tracking'. *IEEE Transactions on Energy Conversion*. 2006, vol. 21(2), pp. 562–8.
[59] Femia N., Petrone G., Spagnuolo G., Vitelli M. 'Optimization of perturb and observe maximum power point tracking method'. *IEEE Transactions on Power Electronics*. 2005, vol. 20(4), pp. 963–73.
[60] Esram T., Chapman P.L. 'Comparison of photovoltaic array maximum power point tracking techniques'. *IEEE Transactions on Energy Conversion*. 2007, vol. 22(2), pp. 439–49.
[61] Lashab A., Sera D., Guerrero J.M., Mathe L., Bouzid A. 'Discrete model-predictive-control-based maximum power point tracking for PV systems: overview and evaluation'. *IEEE Transactions on Power Electronics*. 2018, vol. 33(8), pp. 7273–87.
[62] Elgendy M.A., Zahawi B., Atkinson D.J. 'Assessment of the incremental conductance maximum power point tracking algorithm'. *IEEE Transactions on Sustainable Energy*. 2013, vol. 4(1), pp. 108–17.
[63] IEEE Guide for Monitoring, Information Exchange, and Control of Distributed Resources Interconnected with Electric Power Systems. 'IEEE

1547.3-2007'. 2007.
[64] Bojoi R.I., Limongi L.R., Roiu D., Tenconi A. 'Enhanced power quality control strategy for single-phase inverters in distributed generation systems'. *IEEE Transactions on Power Electronics*. 2011, vol. 26(3), pp. 798–806.
[65] Cortés P., Ortiz G., Yuz J.I., Rodríguez J., Vazquez S., Franquelo L.G. 'Model predictive control of an inverter with output LC filter for UPS applications'. *IEEE Transactions on Industrial Electronics*. 2009, vol. 56(6), pp. 1875–83.
[66] Hu J., Zhu J., Dorrell D.G. 'Model predictive control of inverters for both islanded and grid-connected operations in renewable power generations'. *IET Renewable Power Generation*. 2014, vol. 8(3), pp. 240–8.
[67] Hu J., Zhu J., Dorrell D.G. 'Model predictive control of grid-connected inverters for PV systems with flexible power regulation and switching frequency reduction'. *IEEE Transactions on Industry Applications*. Jan./Feb. 2015, vol. 51(1), pp. 587–94.
[68] Shadmand M.B., Balog R.S., Abu-Rub H. 'Model predictive control of PV sources in a smart DC distribution system: maximum power point tracking and Droop control'. *IEEE Transactions on Energy Conversion*. 2014, vol. 29(4), pp. 913–21.

Further reading

Wind power electronics

- Chinchilla M., Arnaltes S., Burgos J.C. 'Control of permanent-magnet generators applied to variable-speed wind-energy systems connected to the grid'. *IEEE Transactions on Energy Conversion*. 2006, vol. 21(1), pp. 130–5. doi:10.1109/TEC.2005.853735
- Kou P., Liang D., Gao F., Gao L. 'Coordinated predictive control of DFIG-based wind-battery hybrid systems: using non-Gaussian wind power predictive distributions'. *IEEE Transactions on Energy Conversion*. 2015, vol. 30(2), pp. 681–95. doi:10.1109/TEC.2015.2390912
- Datta R., Ranganathan V.T. 'Direct power control of grid-connected wound rotor induction machine without rotor position sensors'. *IEEE Transactions on Power Electronics*. 2001, vol. 16(3), pp. 390–9. doi:10.1109/63.923772
- Sopanen J., Ruuskanen V., Nerg J., Pyrhonen J. 'Dynamic torque analysis of a wind turbine drive train including a direct-driven permanent-Magnet generator'. *IEEE Transactions on Industrial Electronics*. 2011, vol. 58(9), pp. 3859–67. doi:10.1109/TIE.2010.2087301
- Yang B., Zhang X., Yu T., Shu H., Fang Z. 'Grouped grey wolf optimizer for maximum power point tracking of doubly-fed induction generator based wind turbine'. *Energy Conversion and Management*. 2017, vol. 133(9), pp. 427–43. doi:10.1016/j.enconman.2016.10.062
- Zarei M.E., Veganzones Nicolas C., Rodriguez Arribas J. 'Improved predictive direct power control of doubly fed induction generator during

unbalanced grid voltage based on four vectors'. *IEEE Journal of Emerging and Selected Topics in Power Electronics*. 2017, vol. 5(2), pp. 695–707. doi:10.1109/JESTPE.2016.2611004

- Kazmi S.M.R., Goto H., Guo H.-J., Ichinokura O. 'A novel algorithm for fast and efficient speed-sensorless maximum power point tracking in wind energy conversion systems'. *IEEE Transactions on Industrial Electronics*. 2011, vol. 58(1), pp. 29–36. doi:10.1109/TIE.2010.2044732
- Zertek A., Verbic G., Pantos M. 'A novel strategy for variable-speed wind turbines' participation in primary frequency control'. *IEEE Transactions on Sustainable Energy*. 2012, vol. 3(4), pp. 791–9. doi:10.1109/TSTE.2012.2199773
- Errouissi R., Al-Durra A., Muyeen S.M., Leng S., Blaabjerg F. 'Offset-free direct power control of DFIG under continuous-time model predictive control'. *IEEE Transactions on Power Electronics*. 2017, vol. 32(3), pp. 2265–77. doi:10.1109/TPEL.2016.2557964
- Bhende C.N., Mishra S., Malla S.G. 'Permanent magnet synchronous generator-based standalone wind energy supply system'. *IEEE Transactions on Sustainable Energy*. 2011, vol. 2(4), pp. 361–73. doi:10.1109/TSTE.2011.2159253
- Filho A.J.S., Filho M.E.O., Filho E.R. 'A predictive power control for wind energy'. *IEEE Transactions on Sustainable Energy*. 2011, vol. 2(1), pp. 97–105.
- Tanvir A., Merabet A., Beguenane R. 'Real-time control of active and reactive power for doubly fed induction generator (DFIG)-based wind energy conversion system'. *Energies*. 2015, vol. 8(9), pp. 10389–408. doi:10.3390/en80910389
- Morimoto S., Nakayama H., Sanada M., Takeda Y. 'Sensorless output maximization control for variable-speed wind generation system using IPMSG'. *IEEE Transactions on Industry Applications*. 2005, vol. 41(1), pp. 60–7. doi:10.1109/TIA.2004.841159
- Abdullah M.A., Yatim A.H.M., Tan C.W. *'A study of maximum power point tracking algorithms for wind energy system'*. *Proceeding of IEEE Conference on Clean Energy and Technology*; 2011. pp. 321–6.
- Abad G., Rodriguez M.A., Poza J. 'Two-Level VSC-based predictive direct power control of the doubly fed induction machine with reduced power ripple at low constant switching frequency'. *IEEE Transactions on Energy Conversion*. 2008, vol. 23(2), pp. 570–80. doi:10.1109/TEC.2007.914167
- Yaramasu V., Wu B., Sen P.C., Kouro S., Narimani M. 'High-power wind energy conversion systems: state-of-the-art and emerging technologies'. *IEEE Proceedings*. 2015, vol. 103(5), pp. 740–88.
- Yang X., Patterson D., Hudgins J. 'Permanent magnet generator design and control for large wind turbines'. *IEEE Power Electron and Machines in Wind Applications*. 2012, pp. 1–6.
- Wu Y., Tsai C., Li Y. *'Design of wind power generators: summary and comparison'*. *Proceeding of IEEE Conference on Applied System Invention*;

2018. pp. 1–6.
- Terao Y., Sekino M., Ohsaki H. ‘Comparison of conventional and superconducting generator concepts for offshore wind turbines’. *IEEE Transactions on Applied Superconductivity*. 2013, vol. 23(3), pp. 5200904–80. doi:10.1109/TASC.2012.2237223
- Polinder H., Ferreira J.A., Jensen B.B., Abrahamsen A.B., Atallah K., McMahon R.A. ‘Trends in wind turbine generator systems’. *IEEE Journal of Emerging and Selected Topics in Power Electronics*. 2013, vol. 1(3), pp. 174–85. doi:10.1109/JESTPE.2013.2280428
- Brad C., Botezan A., Vadan I. ‘Design aspects of a residential wind generator’. *Journal of Sustainable Energy*. 2017, vol. 8(1), pp. 6–11.
- Ackermann T. *Wind Power in Power Systems*. New Jersey, US: John Wiley & Sons; 2012.
- Fortmann J. *Modeling of Wind Turbines with Doubly Fed Generator System*. New York City, US: Springer; 2015.

Wind review

- Ahmed S.D., Al-Ismail F.S.M., Shafiullah M., Al-Sulaiman F.A., El-Amin I.M. ‘Grid integration challenges of wind energy: a review’. *IEEE Access*. 2020, vol. 8, pp. 10857–78. doi:10.1109/ACCESS.2020.2964896
- Liserre M., Cardenas R., Molinas M., Rodriguez J. ‘Overview of multi-MW wind turbines and wind parks’. *IEEE Transactions on Industrial Electronics*. 2011, vol. 58(4), pp. 1081–95. doi:10.1109/TIE.2010.2103910
- Pena R., Alepuz S., Asher G., Cardenas R. ‘Overview of control systems for the operation of DFIGs in wind energy applications’. *IEEE Ind. Electron*. 2013, vol. 60(7), pp. 2776–98.
- Jin Y., Wu D., Ju P., Rehtanz C., Wu F., Pan X. ‘Modeling of wind speeds inside a wind farm with application to wind farm aggregate modeling considering LVRT characteristic’. *IEEE Transactions on Energy Conversion*. 2019, vol. 35(1), pp. 508–19. doi:10.1109/TEC.2019.2938813
- Feijoo A., Villanueva D. ‘Wind farm power distribution function considering wake effects’. *IEEE Transactions on Power Systems*. 2017, vol. 32(4), pp. 3313–4. doi:10.1109/TPWRS.2016.2614883
- Zhao H., Wu Q., Guo Q., Sun H., Xue Y. ‘Distributed model predictive control of a wind farm for optimal active power control. Part II: implementation with clustering-based piece-wise affine wind turbine model’. *IEEE Transactions on Sustainable Energy*. 2015, vol. 6(3), pp. 840–9. doi:10.1109/TSTE.2015.2418281
- Zeng X., Yao J., Chen Z., Hu W., Chen Z., Zhou T. ‘Co-ordinated control strategy for hybrid wind farms with PMSG and FSIG under unbalanced grid voltage condition’. *IEEE Transactions on Sustainable Energy*. 2016, vol. 7(3), pp. 1100–10.
- Rebello E., Watson D., Rodgers M. ‘Performance analysis of a 10 MW wind farm in providing secondary frequency regulation: experimental aspects’.

IEEE Transactions on Power Systems. 2019, vol. 34(4), pp. 3090–7. doi:10.1109/TPWRS.2019.2891962

- Zhang K., Geng G., Jiang Q. 'Online tracking of reactive power reserve for wind farms'. *IEEE Transactions on Sustainable Energy*. 2020, vol. 11(2), pp. 1100–2.
- Hou P., Hu W., Soltani M., Chen C., Zhang B., Chen Z. 'Offshore wind farm layout design considering optimized power dispatch strategy'. *IEEE Transactions on Sustainable Energy*. 2016, vol. 8(2), pp. 638–47. doi:10.1109/TSTE.2016.2614266
- Howlader A.M., Senjyu T., Saber A.Y. 'An integrated power smoothing control for a grid-interactive wind farm considering wake effects'. *IEEE Systems Journal*. 2014, vol. 9(3), pp. 954–65. doi:10.1109/JSYST.2014.2374311
- Groch M., Vermeulen H.J. 'Modeling high wind speed shut-down events using meso-scale wind profiles and survival analysis'. *IEEE Transactions on Power Systems*. 2019, vol. 34(6), pp. 4955–63. doi:10.1109/TPWRS.2019.2921940
- Wang L., Wang K.-H., Lee W.-J., Chen Z. 'Power-flow control and stability enhancement of four parallel-operated offshore wind farms using a Line-commutated HVDC link'. *IEEE transactions on power delivery*. 2010, vol. 25(2), pp. 1190–202. doi:10.1109/TPWRD.2009.2034915
- Kazda J., Cutululis N.A. 'Model-optimized dispatch for closed-loop power control of waked wind farms'. *IEEE Transactions on Control Systems Technology*. 2020, vol. 28(5), pp. 2029–36. doi:10.1109/TCST.2019.2923779
- Papatheou E., Dervilis N., Maguire A.E., Antoniadou I., Worden K. 'A performance monitoring approach for the novel Lillgrund offshore wind farm'. *IEEE Transactions on Industrial Electronics*. 2015, vol. 62(10), pp. 6636–44. doi:10.1109/TIE.2015.2442212
- Nguyen N., Almasabi S., Mitra J. 'Impact of correlation between wind speed and turbine availability on wind farm reliability'. *IEEE Transactions on Industry Applications*. 2019, vol. 55(3), pp. 2392–400. doi:10.1109/TIA.2019.2896152
- Karaagac U., Faried S.O., Mahseredjian J., Edris A.-A. 'Coordinated control of wind energy conversion systems for mitigating subsynchronous interaction in DFIG-based wind farms'. *IEEE Transactions on Smart Grid*. 2014, vol. 5(5), pp. 2440–9. doi:10.1109/TSG.2014.2330453
- Wu Y.-K., Su P.-E., Su Y.-S., Wu T.-Y., Tan W.-S. 'Economics- and reliability-based design for an offshore wind farm'. *IEEE Transactions on Industry Applications*. 2017, vol. 53(6), pp. 5139–49. doi:10.1109/TIA.2017.2737399
- Li W., Tai-Her Y., We-Jen L., Zhe C. 'Benefit evaluation of wind turbine generators in wind farms using capacity-factor analysis and economic-cost methods'. *IEEE Transactions on Power Systems*. 2009, vol. 24(2), pp. 692–704. doi:10.1109/TPWRS.2009.2016519
- Shrestha G.B., Qiao S., Wang P., Tao T. 'Maximizing profit of a wind Genco

considering geographical diversity of wind farms'. *IEEE Transactions on Power Systems*. 2015, vol. 30(5), pp. 2207–15. doi:10.1109/TPWRS.2014.2361064

- Chen P., Thiringer T. 'Analysis of energy curtailment and capacity over installation to maximize wind turbine profit considering electricity price–wind correlation'. *IEEE Transactions on Sustainable Energy*. 2017, vol. 8(4), pp. 1406–14. doi:10.1109/TSTE.2017.2682820
- Hedayati-Mehdiabadi M., Zhang J., Hedman K.W. 'Wind power dispatch margin for flexible energy and reserve scheduling with increased wind generation'. *IEEE Transactions on Sustainable Energy*. 2015, vol. 6(4), pp. 1543–52. doi:10.1109/TSTE.2015.2455552
- Wang Z., Zhang J., Zhang Y., Huang C., Wang L. 'Short-term wind speed forecasting based on information of neighboring wind farms'. *IEEE Access*. 2020, vol. 8, pp. 16760–70. doi:10.1109/ACCESS.2020.2966268
- Jin Y., Wu D., Ju P., Rehtanz C., Wu F., Pan X. 'Modeling of wind speeds inside a wind farm with application to wind farm aggregate modeling considering LVRT characteristic'. *IEEE Transactions on Energy Conversion*. 2020, vol. 35(1), pp. 508–19. doi:10.1109/TEC.2019.2938813
- Shrestha G.B., Qiao S., Wang P., Tao T. 'Maximizing profit of a wind Genco considering geographical diversity of wind farms'. *IEEE Transactions on Power Systems*. 2015, vol. 30(5), pp. 2207–15. doi:10.1109/TPWRS.2014.2361064
- Opathella C., Venkatesh B. 'Managing uncertainty of wind energy with wind generators cooperative'. *IEEE Transactions on Power Systems*. 2013, vol. 28(3), pp. 2918–28. doi:10.1109/TPWRS.2012.2233502
- Miranda V., Hang P.S. 'Economic dispatch model with fuzzy wind constraints and attitudes of dispatchers'. *IEEE Transactions on Power Systems*. 2005, vol. 20(4), pp. 2143–5.
- Fripp M., Wiser R.H. 'Effects of temporal wind patterns on the value of wind-generated electricity in California and the northwest'. *IEEE Transactions on Power Systems*. 2008, vol. 23(2), pp. 477–85. doi:10.1109/TPWRS.2008.919427
- Lin J., Sun Y., Song Y., Gao W., Sorensen P. 'Wind power fluctuation smoothing controller based on risk assessment of grid frequency deviation in an isolated system'. *IEEE Transactions on Sustainable Energy*. 2012, vol. 4(2), pp. 379–92. doi:10.1109/TSTE.2012.2225853
- Du E., Zhang N., Hodge B.-M., *et al*. 'The role of concentrating solar power toward high renewable energy penetrated power systems'. *IEEE Transactions on Power Systems*. 2018, vol. 33(6), pp. 6630–41. doi:10.1109/TPWRS.2018.2834461
- Abunima H., The J., Jabir H.J. 'A new solar radiation model for a power system reliability study'. *IEEE Transactions Energy Convers*. 2009, vol. 24(2), pp. 442–51.
- Dunn R.I., Hearps P.J., Wright M.N. 'Molten-salt power towers: newly commercial concentrating solar storage'. *Proceedings of the IEEE*. 2012, vol.

100(2), pp. 504–15. doi:10.1109/JPROC.2011.2163739
- Yu D., Ebadi A.G., Jermsittiparsert K., Jabarullah N.H., Vasiljeva M.V., Nojavan S. 'Risk-constrained stochastic optimization of a concentrating solar power plant'. *IEEE Transactions on Sustainable Energy*. 2019, vol. 11(3), pp. 1464–72. doi:10.1109/TSTE.2019.2927735
- Yang Y., Liu X., Wu D. 'Integrated solutions for photovoltaic grid connection: increasing the reliability of solar power'. *IEEE Power and Energy Mag*. 2014, vol. 12(2), pp. 84–91.
- Cabeza L.F., Sole C., Castell A., Oro E., Gil A. 'Review of solar thermal storage techniques and associated heat transfer technologies'. *Proceedings of the IEEE*. 2012, vol. 100(2), pp. 525–38. doi:10.1109/JPROC.2011.2157883
- Strunz K., Abbasi E., Huu D.N. 'DC microgrid for wind and solar power integration'. *IEEE Journal of Emerging and Selected Topics in Power Electronics*. 2014, vol. 2(1), pp. 115–26. doi:10.1109/JESTPE.2013.2294738
- Varma R.K., Rahman S.A., Vanderheide T. 'New control of PV solar farm as STATCOM (PV-STATCOM) for increasing grid power transmission limits during night and day'. *IEEE Transactions on Power Delivery*. 2015, vol. 30(2), pp. 755–63. doi:10.1109/TPWRD.2014.2375216
- Kroposki B., Margolis R., Ton D. 'Harnessing the sun'. *IEEE Power and Energy Mag*. 2009, vol. 7(3), pp. 22–33.
- Ghiassi-Farrokhfal Y., Kazhamiaka F., Rosenberg C., Keshav S. 'Optimal design of solar PV farms with storage'. *IEEE Transactions on Sustainable Energy*. 2015, vol. 6(4), pp. 1586–93. doi:10.1109/TSTE.2015.2456752
- Denholm P., Margolis R., Mai T., *et al*. 'Bright future: solar power as a major contributor to the U.S. grid'. *IEEE Power and Energy Magazine*. 2013, vol. 11(2), pp. 22–32. doi:10.1109/MPE.2012.2234404
- Cordova S., Rudnick H., Lorca A., Martinez V. 'An efficient forecasting-optimization scheme for the intraday unit commitment process under significant wind and solar power'. *IEEE Transactions on Sustainable Energy*. 2018, vol. 9(4), pp. 1899–909. doi:10.1109/TSTE.2018.2818979
- Koraki D., Strunz K. 'Wind and solar power integration in electricity markets and distribution networks through service-centric virtual power plants'. *IEEE Transactions on Power Systems*. 2018, vol. 33(1), pp. 473–85. doi:10.1109/TPWRS.2017.2710481
- Chauhan S., Singh B. 'Grid‐interfaced solar PV powered electric vehicle battery system with novel adaptive digital control algorithm'. *IET Power Electronics*. 2019, vol. 12(13), pp. 3470–8. doi:10.1049/iet-pel.2019.0025
- Mukundan N.., Singh Y., Naqvi S.B.Q., Singh B., Pychadathil J. 'Multi-objective solar power conversion system with MGI control for grid integration at adverse operating conditions'. *IEEE Trans. Sustain. Energy*. 2020, vol. 11(4), pp. 2901–10.

Solar farms

- Aglietti G.S., Redi S., Tatnall A.R., Markvart T. 'Harnessing high-altitude

solar power'. *IEEE Transactions on Energy Conversion*. 2009, vol. 24(2), pp. 442–51. doi:10.1109/TEC.2009.2016026

- Du E., Zhang N., Hodge B.-M., *et al*. 'Operation of a high renewable penetrated power system with Csp plants: a look-ahead stochastic unit commitment model'. *IEEE Transactions on Power Systems*. 2019, vol. 34(1), pp. 140–51. doi:10.1109/TPWRS.2018.2866486
- Das M., Agarwal V. 'Novel high-performance stand-alone solar PV system with high-gain high-efficiency DC–DC converter power stages'. *IEEE Transactions on Industry Applications*. 2015, vol. 51(6), pp. 4718–28. doi:10.1109/TIA.2015.2454488
- Venkatramanan D., John V. 'Dynamic modeling and analysis of buck converter based solar PV charge controller for improved MPPT performance'. *IEEE Transactions on Industry Applications*. 2019, vol. 55(6), pp. 6234–46. doi:10.1109/TIA.2019.2937856
- Anand I., Senthilkumar S., Biswas D., Kaliamoorthy M. 'Dynamic power management system employing a single-stage power converter for standalone solar PV applications'. *IEEE Transactions on Power Electronics*. 2018, vol. 33(12), pp. 10352–62.
- Wang B., Zhang X., Manandhar U., Gooi H.B., Liu Y., Tan X. 'Bidirectional three-level cascaded converter with deadbeat control for HESS in solar-assisted electric vehicles'. *IEEE Transactions on Transportation Electrification*. 2019, vol. 5(4), pp. 1190–201. doi:10.1109/TTE.2019.2939927
- Lodh T., Pragallapati N., Agarwal V. 'Novel control scheme for an interleaved flyback converter based solar PV microinverter to achieve high efficiency'. *IEEE Transactions on Industry Applications*. 2018, vol. 54(4), pp. 3473–82. doi:10.1109/TIA.2018.2818655
- Singh A.K., Badoni M., Tatte Y.N. 'A multifunctional solar PV and grid based on-board converter for electric vehicles'. *IEEE Transactions on Vehicular Technology*. 2020, vol. 69(4), pp. 3717–27. doi:10.1109/TVT.2020.2971971
- Shubhra S., Singh B. 'Three-phase grid-interactive solar PV-battery microgrid control based on normalized gradient adaptive regularization factor neural filter'. *IEEE Transactions on Industrial Informatics*. 2020, vol. 16(4), pp. 2301–14. doi:10.1109/TII.2019.2937561
- Lopez-Lapena O. 'Time-division multiplexing control of multi-input converters for low-power solar energy harvesters'. *IEEE Transactions on Industrial Electronics*. 2018, vol. 65(12), pp. 9668–76. doi:10.1109/TIE.2018.2821622
- Bhattacharjee A.K., Kutkut N., Batarseh I. 'Review of multiport converters for solar and energy storage integration'. *IEEE Transactions on Power Electronics*. 2018, vol. 34(2), pp. 1431–45. doi:10.1109/TPEL.2018.2830788
- Carrasco J.A., de Quiros F.G., Alaves H., Navalon M. 'An analog maximum power point tracker with pulsewidth modulator multiplication for a solar array regulator'. *IEEE Transactions on Power Electronics*. 2019, vol. 34(9), pp.

8808–15. doi:10.1109/TPEL.2018.2886887
- Huang X., Wang K., Fan B., *et al*. 'Robust current control of grid-tied inverters for renewable energy integration under non-ideal grid conditions'. *IEEE Transactions on Sustainable Energy*. 2020, vol. 11(1), pp. 477–88. doi:10.1109/TSTE.2019.2895601

Chapter 4
Modeling and hierarchical control of microgrids

In this chapter, mathematical models of distributed generations (DGs) and the entire microgrid (MG) are presented. These mathematical models are the key elements in designing control schemes for MGs. After that, the hierarchical control framework, i.e., primary control, secondary control, and tertiary control layers are discussed, and the corresponding control objectives are presented.

4.1 Modeling of MGs

Figure 4.1 shows the equivalent circuit of a parallel-inverters-based MG. The active and reactive power flows between DGs and the common voltage bus can be expressed as [1]

$$P = \frac{E^2 cos\varphi_Z - EVcos\left(\varphi_E - \varphi_V + \varphi_Z\right)}{Z} \tag{4.1}$$

$$Q = \frac{E^2 sin\varphi_Z - EVsin\left(\varphi_E - \varphi_V + \varphi_Z\right)}{Z} \tag{4.2}$$

where E and V are the magnitudes of the inverter output voltage and AC common bus voltage. Z is the line impedance. For a distribution line with mainly inductive impedance, the line resistance can be neglected, i.e. $\varphi_Z \approx 90°$. Thus (4.1) and (4.2) become

$$P = \frac{EVsin\left(\varphi_E - \varphi_V\right)}{X} \tag{4.3}$$

$$Q = \frac{E^2 - EV\cos(\varphi_E - \varphi_V)}{X} \tag{4.4}$$

where X is the line reactance. Further, considering that the phase angle difference $\delta = \varphi_E - \varphi_V$ is typically small, one can assume $\sin(\delta) = \delta$ and $\cos(\delta) = 1$. Consequently, (4.3) and (4.5) can be further simplified as

$$P = \frac{EV\delta}{X} \tag{4.5}$$

$$Q = \frac{E(E - V)}{X} \tag{4.6}$$

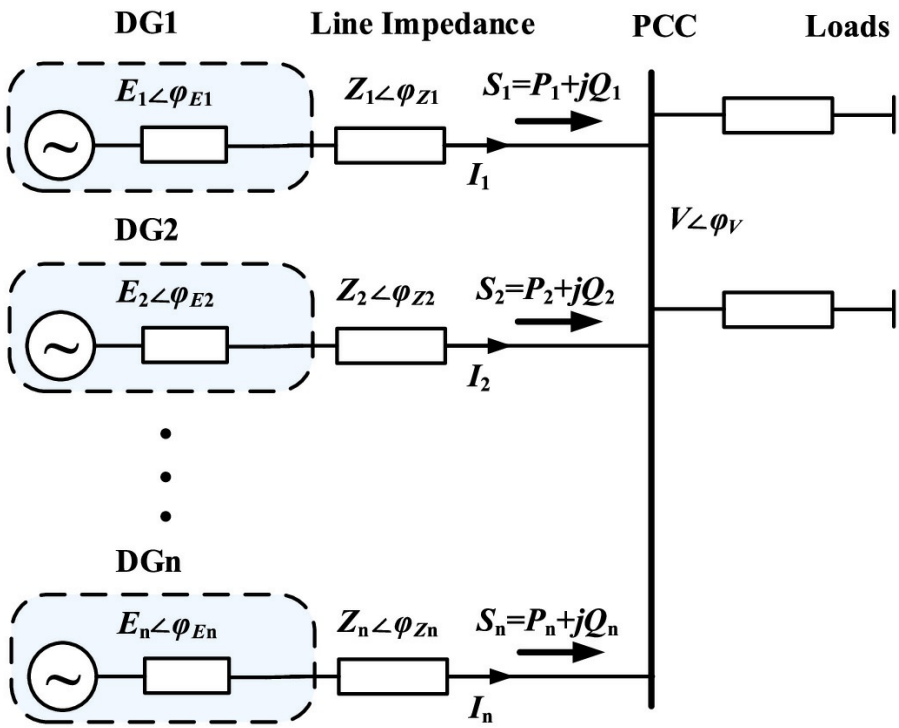


Figure 4.1 Equivalent circuit of a parallel-inverters-based MG

As a result, the flow of active power is linearly dependent on the phase angle difference (δ) and the flow of reactive power is linearly dependent on the voltage magnitude difference ($E - V$). It is noted that (4.5) and (4.6) are developed by assuming highly inductive equivalent impedance between the DG and the common AC bus. However, in low-voltage distribution networks where lines are mainly resistive, (4.5) and (4.6) will not be valid. Instead, active power will be predominately dependent on the DG output voltage amplitude, while reactive power will be mostly dependent on the power angle. In this section, the fundamental power flow model has been revealed. In the following sections and chapters when MG control strategies are reviewed or developed, more accurate models will be needed by considering various aspects in practical applications including line impedance, power converter topologies, renewable power outputs, load variations, etc.

4.2 Hierarchical control architecture of MGs

Conventionally, hierarchical control, or multilayer control, is a common and effective way to govern a complex system such as a power system [2]. It has now been applied in MGs and widely recognized as a standard control framework. In a typical MG with multiple parallel converter-interfaced DGs and diverse bus types as well as different operating modes, a three-level control structure including primary, secondary, and tertiary control can be utilized to coordinate different units [3, 4]. These three levels are differentiated by specified control objectives and bandwidths, as depicted in Figure 4.2. Each level has its own control goals and provides supervisory control over lower-level systems. Thus, the bandwidth is decreased with an increase in the control level.

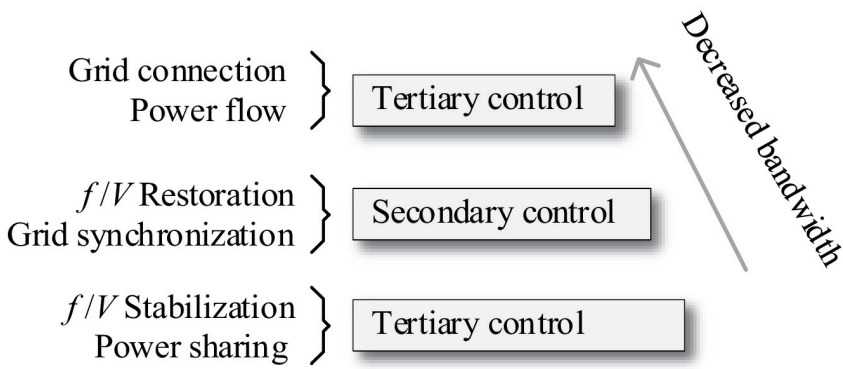


Figure 4.2 Hierarchical control structure of MGs

Primary control, as the name suggests, is the underlying level that stabilizes

the whole system in terms of voltage and frequency within the acceptable ranges, while at the same time, enables load sharing among DGs with fast response. Under the circumstances that the droop control method is used in the primary control, the output voltages of DGs change with respect to load variations. Thus, the frequency/voltage deviations caused may need to be compensated. In steady state, secondary control can restore the deviated frequency/voltage to their rated values. Grid synchronization loop can also be integrated into the secondary controller for grid connection. In general, secondary control can be divided into three categories: centralized, distributed, and decentralized. Upon the MG meets the synchronization requirement, it can connect to the main grid. Tertiary control focuses on regulating the power imported to or exported from the MG. Moreover, associated economic and cost optimization, as well as power planning are all included in the tertiary control regime. So far, many studies have been conducted for the hierarchical control of MGs, particularly for primary control and secondary control.

4.2.1 Primary control

In primary control, the main objective is to control the distributed power converters to establish stable voltage for electric appliances and at the same time to share the power demand properly among DGs. Specifically, the primary control is designed to meet the following requirements:

- To establish the voltage and frequency: Subsequent to an islanding event, without the utility grid support, the MG may lose its stability in voltage and frequency due to the mismatch between the power generation and consumption. How to maintain the voltage and frequency is the main task of primary control, particularly in islanded operation.
- To enable plug-and-play operation for DGs and proper active and reactive power sharing among them, preferably, without any communication links.
- To eliminate circulating currents among DGs that can cause damage and additional power loss on power electronic devices.

The parallel operation of converters is a challenging task that is more complicated than a single DG system because every converter must properly contribute to voltage stabilization and load sharing. Therefore, suitable control strategies for parallel-connected DGs are required. As mentioned in Chapter 2, several typical communication-based control strategies such as centralized and master/slave approaches have been used. In practice, operation without communication links is often preferred to connect inverters, particularly in remote areas such as regional towns and islands. It can avoid complexity and high costs as well as improve redundancy and reliability requirements of a supervisory system. Also, a system without centralized communication infrastructure is easier to expand because of the plug-and-play feature of DGs which allows adding/removing one unit without having to shut down the whole system. In this sense, it is necessary to avoid communication lines especially for MGs with DGs located far away from each other. In existing literature, the control strategies that

operate without interunit communications for power-sharing control are mostly based on the droop concept [5, 6].

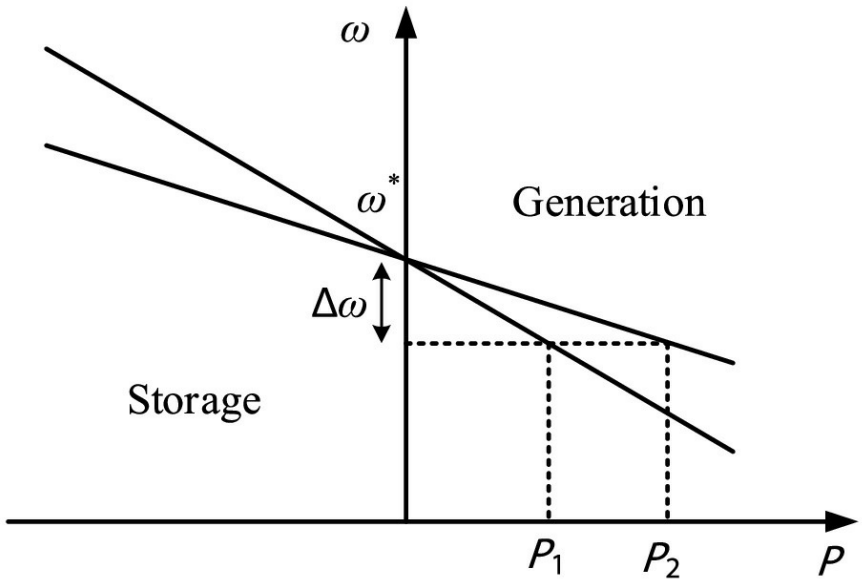
In principle, the droop mechanism regulates frequency and voltage, respectively, to share the active/reactive load demands according to the DG's power ratings. Taking the *f*–*P* and *V*–*Q* droop based on (4.5) and (4.6) for example, the droop mechanism is illustrated in Figure 4.3. The main idea of this control level stems from the behavior of a synchronous generator that reduces the frequency when the active power increases. Similarly, in MG droop, when the load demand increases, DG1 and DG2 will decrease their output frequency and voltage, respectively, to generate more active power and reactive power automatically according to the predefined linear characteristics. This principle can be expressed mathematically as

$$\begin{cases} f_j = f^* - m_j \cdot \left(P_j - P^*\right) \\ U_j = U^* - n_j \cdot \left(Q_j - Q^*\right) \end{cases} \tag{4.7}$$

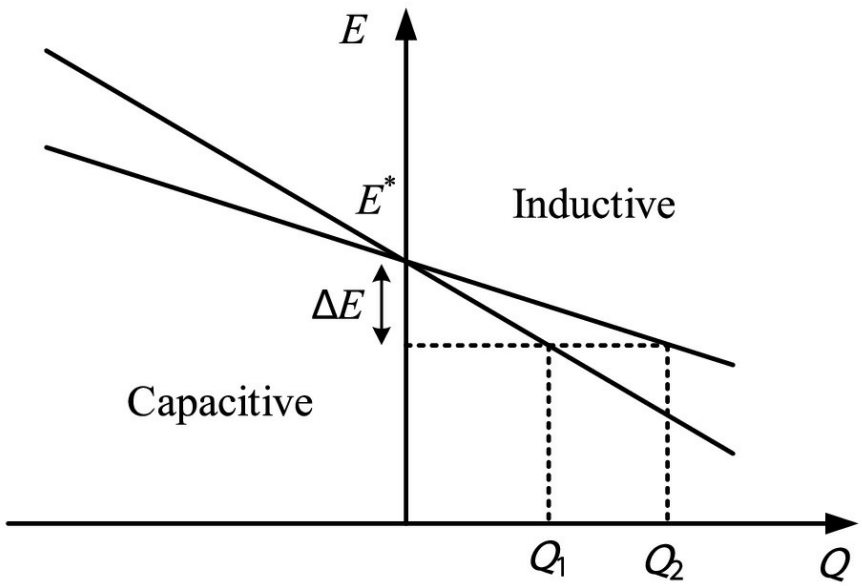
where j is the inverter index number. U_j and f_j are the actual voltage and frequency; U^* and f^* the nominal voltage and frequency; P_j and Q_j the measured active and reactive power after averaging; P^* and Q^* the nominal active and reactive power; and m_j and n_j the droop gains. Conventionally, the droop coefficients can be expressed as

$$m = \frac{\Delta\omega}{S_N}, n = \frac{\Delta V}{S_N} \tag{4.8}$$

where $\Delta\omega$ and ΔV are the maximum allowed deviations of angular frequency and voltage amplitude, respectively. S_N is the DG rated capacity. Figure 4.4 illustrates a complete control structure of primary control. First, the DG output power is calculated and averaged based on the voltage and current measured. Then, the droop scheme adjusts the frequency and amplitude of the voltage that is required to meet the load demand. After the voltage references are generated by the droop controller, an inner dual-loop voltage and current control using proportional and resonant controllers are usually adopted to produce pulse width modulation (PWM) signals to control the inverter.


ω
ω*
Generation
Δω
Storage
P1
P2
P

(a)


E
E*
Inductive
ΔE
Capacitive
Q1
Q2
Q

(b)

Figure 4.3 Illustration of droop mechanism in MG primary control. (a) P–f droop and (b) Q–V droop.

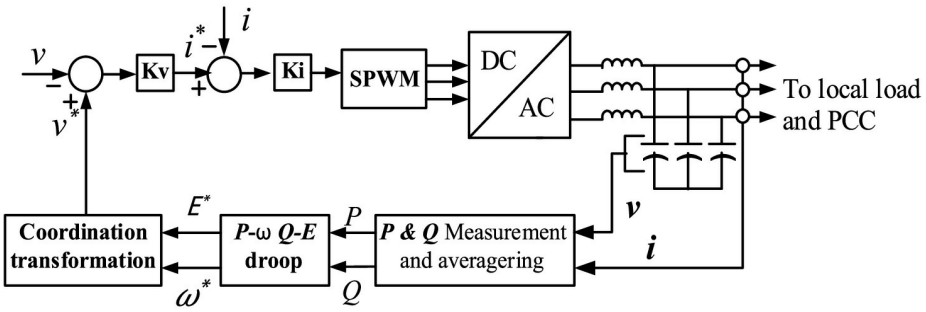


Figure 4.4 Primary control for parallel inverters

Despite its decentralized structure and operational simplicity, droop control has practical limitations: deviations in frequency and voltage, power-sharing inaccuracy in the presence of mixed resistive and inductive distribution line impedance, and poor power quality performance when dealing with nonlinear loads, to name but a few. In addition, as opposed to frequency droop that is capable of accurate active power sharing, voltage amplitude droop typically presents a poor reactive power-sharing performance or even power reversal as well as individual voltage deviations, which are caused by the voltage drop along the distribution line and the inconformity of output impedances and DG parameters. Here, to obtain a better understanding of the droop control and other relevant issues in primary control, the major challenges and the possible solutions are briefly summarized as follows.

- Voltage and frequency deviations

The voltage and frequency of the MG are load-dependent. As mentioned in Section 4.2.1, each DG needs to adjust its output voltage amplitude and frequency for load sharing subject to load variations. Steeper droop or larger droop gain ensures better load sharing, but results in larger frequency and voltage deviations, and even leads to instabilities in the MG in some serious cases. To reduce the frequency deviation, some researchers have proposed the angle droop and virtual flux droop strategies [7–9]. Instead of drooping the frequency, the power angle of the DG is adjusted. The angle droop can also provide proper load sharing among the DGs while mitigating the steady-state frequency deviation in the MG. The main challenge is the synchronization of power angle among DGs. For example, in practice, the frequencies of the crystal oscillators in the digital signal

processors could be slightly different, leading to accumulating phase errors after a certain time. Consequently, this will lead to unsynchronized frequencies between each inverter, resulting in system instability. Certainly, another widely used method to restore the voltage and frequency back to the nominal values is the secondary control, which will be discussed later.

- Trade-off between voltage regulation and load sharing accuracy

As opposed to frequency, voltage is not a global variable in a power network including MGs. There are voltage drops along the distribution lines between DGs and the loads. As a result, the load demand may not be shared properly among DGs according to the predefined droop characteristics, leading to overloading or circulating currents. More specifically, the reactive power is difficult to share between DGs for a MG with mainly inductive line impedance, while inaccuracy active power sharing can be observed for a MG in which distribution lines are mainly resistive. To avoid the active and reactive power coupling, a typical and popular approach is to integrate a virtual output impedance into the droop controller [10]. Specifically, the expected voltage can be modified as [11]

$$V_{ref} = V^* - Z_D(s) \cdot i_0 \tag{4.9}$$

where $Z_D(s)$ is the virtual output impedance and V^* is the output voltage reference under no-load condition. Usually, the output impedance can be generated by emulating an inductive behavior. This can be done by drooping the output voltage in proportional to the derivative of the output current with respect to time. In this way, $Z_D(s)$ will be purely inductive, i.e., $Z_D(s) = sLD$. However, the derivative operation would amplify high-frequency noise, which may deteriorate the effectiveness of the DG voltage control strategy, especially during transients. Recently, it is found that, if the output impedance can be produced by emulating a resistive behavior, the system stability can be improved because resistive impedance does not vary with frequency [12].

- Nonlinear loads

The conventional droop method deals with power sharing for the fundamental components but does not take harmonic sharing into account in presence of nonlinear loads. If it is not coped with properly, it would lead to severe circulating currents and poor power quality. Furthermore, the averaging and smoothing of active and reactive power using low-pass filters cause some delays in time, thus it presents a slow dynamic response. To ensure the DGs equally share the linear and nonlinear loads, one straightforward approach is to calculate the corresponding voltage droop harmonics by sensing the load current harmonics. These calculated voltage harmonics are then compensated to the DG voltage reference that is initially obtained from the conventional droop controller [13]. Another method is to consider droop characteristics in harmonics. The DG output voltage and current are used to calculate not only the fundamental term (P_1, Q_1) but also the

harmonics of DG output active and reactive powers (P_h, Q_h). Each set of droop characteristics determines an additional term to be added to the output voltage reference [14]. To realize better reactive and harmonic power sharing, the virtual impedance concept can also be applied here at the fundamental and specified harmonic frequencies. Similar to virtual output impedance for the fundamental component explained in Section 4.2.1, this enhanced control strategy presents the harmonic virtual impedance. It can achieve better reactive and harmonic power sharing, alleviate the computational burden at the local controller of the DG unit without the need of extracting any fundamental and harmonic components. It can mitigate the point of common coupling (PCC) harmonic voltages by reducing the magnitude of DG unit equivalent harmonic impedance as well [15].

- Mismatch and unknown line impedances

Although the conventional frequency droop control method works well in a MG connected to mainly inductive lines, it would face problems when implemented on a low-voltage network in which the feeder impedance is mainly resistive. In light of (4.1) and (4.2), the line impedances between the paralleled converters affect the power-sharing performance. The conventional droop scheme is derived based on (4.5) and (4.6) under the consumption of similar impedances between distribution lines. However, when the line impedances between the DGs and points of common coupling are various, it could result in a large circulating current and inaccuracy of power sharing among parallel inverters. In addition, if the line impedance is a mix between resistive and inductive, then the active and reactive power will be strongly coupled, as indicated in (4.1) and (4.2). This is quite often in medium voltage (MV) MGs, in which the *R/X* ratio of power lines can be close to one. In [16], improved *P/V* and *Q/f* droop control is proposed to revise the coupled active and reactive power relationships, and a good dynamic performance can be achieved in the case of resistive networks. However, many problems such as mixed *R/X* ratio and different line impedances still cannot be solved. In [17], a virtual frame concept is proposed to transfer the system variables into a new reference frame where the active and reactive powers are independent of the effective line impedance. Consequently, the active power and reactive power can be decoupled. However, the transformation applied needs prior knowledge of the line impedance, which brings in difficulties in actual implementation. In [18], to enable simultaneous active and reactive powers control and regulate the PCC voltage, a *P–Q–V* droop control method is developed. For a MG with complex impedance, both active and reactive powers affect the voltage magnitude. Hence, the droop mechanism for the proposed *P–Q–V* droop method is modified as

$$V = V_{ref} + n_d P + m_d Q \tag{4.10}$$

where V_{ref} is the nominal value of the PCC voltage; n_d and m_d are droop gains of the active and reactive power, respectively. Notice that, these droop gains can be

changed dynamically through a lookup table according to the PCC voltage level. Furthermore, additional loops such as estimator for impedance voltage drops [19], estimator for grid parameters [20], and reactive current loop [21] can be incorporated into the conventional droop control to address line impedance mismatches for improved power-sharing performance.

- Fluctuating outputs from DGs

Another drawback of the conventional droop method is the poor performance with renewable energy resources because the output active power of micro-source is usually fluctuant and changeable. Constant droop gains limit the control flexibility of the droop controller to tackle renewable energy source (RES) uncertainties. The problem is that, if constant coefficients are used corresponding to a constant rated DG capacity, as depicted in (4.8), the load demand may exceed the DG's actual capacity when the RES output fluctuates. As a result, a stable system frequency and the voltage of the DG cannot be retained. To address this problem, an adaptive droop control concept has been proposed [22, 23]. Instead of being kept constant, the droop coefficients are adjusted according to the available capacity of a DG as

$$m = \frac{\Delta\omega}{S_a}, n = \frac{\Delta V}{S_a} \tag{4.11}$$

where S_a is the available power capacity. Using adaptive droop coefficients, proper power sharing among DGs can be achieved even when DGs' capacities vary. It is worth mentioning here that the variable droop gain due to the varying RES outputs can cause stability issues. Adaptive droop coefficients may experience large variations due to the intermittency of RES. For the adaptive droop method, a sudden change in S_a, e.g., from 90 percent to 10 percent of the rated capacity, will lead to a significant variation of m and n, which will degrade the system stability. Such large droop coefficients or significant variations of droop coefficients can make a MG system prone to low-frequency instability [24].

Regarding the primary control layer of MGs, many studies have been conducted over the past years to address the limitations discussed in Section 4.2.1 and to improve the performance. For instance, by introducing power derivative-integral terms into the traditional droop control, faster transient response of power sharing can be achieved [6]. Reactive power-sharing performance of nonlinear loads was improved using adaptive virtual impedance [25]. A modified angle droop control was described to remove the dependence of real power sharing on the output inductance with lower but stable droop coefficients [26]. An enhanced proportional power-sharing method based on adaptive virtual impedance was presented to prevent power coupling [27]. The voltage-shifting and load current feedforward control methods were proposed to eliminate the voltage deviation due to the droop control and improve voltage control dynamics [28]. A new droop

control method based on the Takagi–Sugeno (TS) fuzzy and sliding modes was proposed to improve the current-sharing performance and robustness against the network delays [29]. A novel consensus-based cooperative droop control was introduced to adaptively adjust the droop coefficients to improve the reactive power-sharing accuracy [30]. A new control scheme which includes the islanded, grid-connected, and transient controls was proposed to realize accurate power sharing and eliminate the steady-state voltage bias in islanded mode, and realize accurate power-flow control and restrain the harmonic current injected to grid in grid-connected mode, as well as realize a smooth mode-transfer between above two modes [31]. The cross-circulating current and zero-sequence circulating currents were considered and added to the traditional droop plus virtual impedance control to suppress both cross and zero-sequence circulating currents [32]. The f-P/Q droop control was proposed to autonomously achieve power balance under both resistive-inductive and resistive-capacitive loads [33]. For low-voltage resistive MGs, a V–I droop method was adopted to alleviate traditional droop control shortcomings for the primary control in [34]. A novel voltage stabilization and power-sharing method based on the virtual complex impedance was studied to improve the voltage quality and achieve accurate power sharing without the impact of hardware parameters variations [35].

Despite the continuous efforts made to enhance the performance of primary control for MGs, no significant change in the inner control loops has been seen, i.e., the bottom level of the control hierarchy, in which the traditional cascaded linear control has been used for many years. In fact, the performance of the cascaded linear control at the bottom can considerably influence the effectiveness of higher-level control in the hierarchical control structure. This is usually ignored by many scholars. The main problem in practice is that fluctuating output from RESs can cause oscillations in DG voltage and frequency, which in turn compromises the power quality of the whole MG. The traditional cascaded linear control featuring a relatively slow dynamic response may not be effective to handle these fluctuations. In contrast to the cascaded linear control, the model predictive control (MPC) determines the optimal control action by minimizing a predefined cost function based on the predicted behavior of a power converter over a finite time duration at each time step. Because of its fast dynamics and flexible control scheme in which different constraints can be flexibly integrated, MPC has been recently used in primary control of MGs. One of the trends is the replacement of conventional inner voltage and current feedback loops control loop with an MPC controller [12, 36, 37]. After the voltage reference is determined by the outer droop controller, it will be sent to the inner MPC controller to control the distributed inverters. It has been demonstrated that better voltage quality at steady state and faster power sharing at transients can be obtained by incorporating MPC algorithms with the droop method. Another promising stream of MPC in MG primary control is the droop-free MPC structure. In [38], a new control method for the parallel operation of inverters is presented. A multiple-input–multiple-output (MIMO) state-space model is derived to represent the parallel-connected inverters system, and then a MPC

scheme is proposed for the parallel operation of inverters. In the proposed approach, the control objectives of voltage tracking and current sharing are considered in a cost function with weighting factors. Both proper load sharing among inverters and plug-and-play capability can be achieved. The major limitation of this work is that it assumes no distribution lines between DGs and common voltage bus, and only one common resistor is used as the common load, which is usually not the case in practice. Even there are limitations, this work opens up a new research line in MG control. It is expected that the main challenge of this droop-free MPC is the development of an accurate MIMO state-space model for parallel-connected inverters by considering various practical aspects such as distribution line impedance, resisitive-inductive-capacitive (RLC) loads, nonlinear loads, etc. In [39], an improved finite-control-set (FCS)-MPC of inverters with output LC filter for constant switching frequency and circulating current suppression is presented. In the proposed control scheme, the virtual state vectors are generated in addition to the real state vectors, which are used for the estimation of the future states of voltage and current. In [40], an MPC-based zero common-mode voltage method is presented to reduce the difference of common-mode voltages among the paralleled three-level inverters, meanwhile, an active neutral point potentials (NPP) perturbation-based zero sequence circulating current (ZSCC) feedback control method is proposed to further eliminate the ZSCC. With the proposed method, the ZSCC between paralleled inverters can be eliminated effectively, and both grid current tracking and NPP balance control also can achieve satisfactory performances. This proposed strategy is for grid-connected inverters, but the islanded operation is not considered.

4.2.2 Secondary control

The secondary control is designed to eliminate the deviation of output voltage and frequency caused in the primary control. In other words, the secondary control aims to ensure that the frequency and voltage deviations are regulated toward zero subsequent to any change in generation or consumption within the MG. Grid synchronization for grid connection can also be implemented in the secondary control layer. To connect the MG to the grid, the frequency and voltage of the grid need to be measured as the reference of the secondary control loop. Then, the amplitude, frequency, and phase between the grid and the MG will be synchronized utilizing the synchronization control loop.

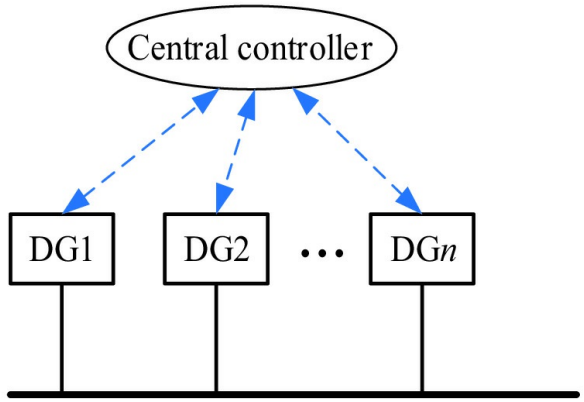
To eliminate the voltage and frequency deviations, a correction term can be added to the droop controller as

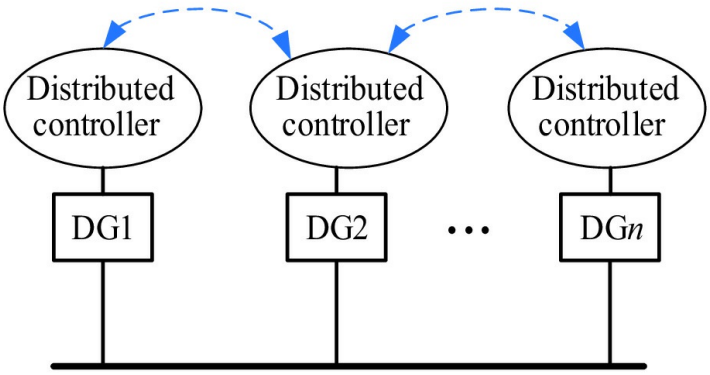
$$\omega = \omega^* - mP + \delta u_\omega \tag{4.12}$$

$$v = v^* - nQ + \delta u_v \tag{4.13}$$

These compensation terms can be produced in a centralized, distributed, or

decentralized manner. Figure 4.5 illustrates the three main secondary control structures.


Central controller
DG1
DG2
DGn
Distribution line
(a)


Distributed controller
Distributed controller
Distributed controller
DG1
DG2
DGn
Distribution line
(b)

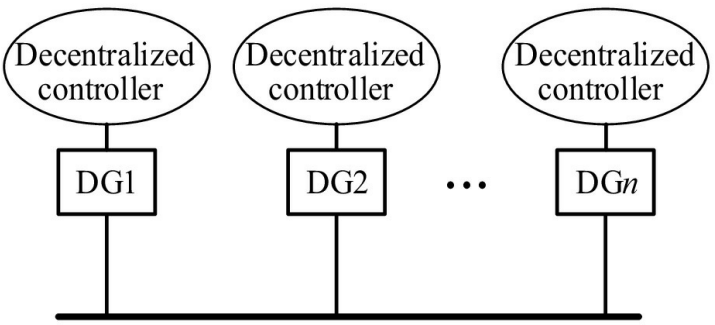

Decentralized controller
Decentralized controller
Decentralized controller
DG1
DG2
DGn
Distribution line
(c)

Figure 4.5 Three main structures of secondary control: (a) centralized secondary control, (b) distributed secondary control, and (c) decentralized secondary control

4.2.2.1 Centralized secondary control

The majority of existing secondary control schemes, either for frequency and voltage restoration, reactive power sharing, or voltage unbalance/harmonic compensation, are designed based on a centralized structure. In the centralized structure, a central controller on top coordinates different DGs and restores their frequency and voltage amplitudes to the nominal values, as depicted in Figure 4.5a. In addition to voltage and frequency restoration, active power management, reactive power management, and harmonic cancelation are the main purposes of the centralized secondary control [41–44]. In this structure, all measured data, i.e., the voltage, current, and frequency are generally transmitted through a high-data-rate communication network.

This structure requires point-to-point communication between the central controller and all local controllers, which increases system complexity and compromises its scalability. It will increase the total cost in both communication and computation when the number of distributed power sources increases. Most importantly, the central controller suffers from a single point of failure, i.e., any failure whether in the communication infrastructure or the central controller itself affects the overall stability and performance of the MG. Therefore, any deficiency in the communication network or failure degrades MG efficiency.

4.2.2.2 Distributed secondary control

Distributed secondary control schemes have become attractive alternatives over centralized control because of distinct attributes such as sparse network, scalability, and improved resiliency to faults or unknown parameters. DGs in an MG are heterogeneous and spatially distributed, which makes distributed control or multiagent system (MAS) network control a natural fit in MGs, addressing reliability and enhancing the scalability of MGs. In such kind of distributed control strategies, local secondary control is to generate setpoints of the droop control for each DG to restore the deviations produced by the primary control, as depicted in Figure 4.5b. Initially, an averaging-based structure was adopted, in which each DG measures its frequency and voltage amplitudes and then communicates them to all other DGs [45–47]. Notice that each DG needs to communicate with all other DGs under this distributed control structure. By averaging the values received from other DGs, a control signal can be generated as [47]

$$\delta u_i = K_i(s)\left(x^* - \frac{1}{N}\sum_{i\in N} x_i(t)\right) \tag{4.14}$$

where x is the variable of interest (e.g., DG output frequency, voltage amplitude, active power, reactive power, etc.) with a reference denoted as x^*. $K_i(s)$ denotes the controller that can be designed in various ways such as Proportional–integral (PI) and obviously can be tuned for dynamic performance. As explained previously, the reactive power sharing of the Q–V droop (or active power sharing of the P–V droop) is difficult to achieve as the voltage is not constant along the MG distribution line, as opposed to the frequency. Using this method, this problem can be easily addressed by averaging Q or P of each DG as the common variable and then generating the control signals for each DG by means of (4.14).

A more popular distributed control approach is based on consensus protocols that enable agents to converge toward consistency of the information shared in a distributed manner. In such cooperative control, each agent, or DG in MG applications, is endowed with its state variable and dynamics. A fundamental step in MAS on graph theory is the design of distributed protocols that guarantee consensus or synchronization in a way that the states of all the agents reach a common value. In distributed control of MASs for MGs, a number of DGs (as agents) coordinate together to cooperatively control the MG and fulfill a set of objectives. In this case, the performance of the MG relies on the agent (i.e., DG) dynamics and the topology of the adopted communication structure. Depending on whether there is a leader during the consensus or synchronization, consensus-based distributed secondary control can be further classified into two groups, i.e., cooperative regulator control and cooperative tracker control [48]. The distributed protocol of cooperative regulator control can be expressed as [47]

$$\delta u_i = K_i(s)\sum_{j\in N, j\neq i} \alpha_{ij}\left(x_j(t) - x_i(t)\right) \tag{4.15}$$

In this cooperative control, the local and neighboring information is collectively used to generate secondary control signals. Then in steady state, all the DGs will reach an agreement or consensus, i.e., $x_i = x_j$ for all i, j.

On the other hand, to control the DGs in an MG converging to a given reference value, the cooperative tracker control can be employed, which can be described by the following protocol [47]:

$$\delta u_i = -cK_i e_i \tag{4.16}$$

$$\delta u_i = \sum_{j \in N j \neq i} \alpha_{ij} \left(x_j \left(t \right) - x_i \left(t \right) \right) - g_i \left(x_i \left(t \right) - x^* \right) \quad (4.17)$$

where g_i is the pinning gain; x^* is the desired value of the cooperative control (e.g., frequency reference, voltage reference, etc.); c is the coupling gain; and K_i is the feedback control vector.

Over the past years, a variety of distributed secondary control methods have been developed for MGs. The majority of these approaches aim to achieve frequency regulation, and/or voltage control. For example, [49] introduces a fully distributed secondary control algorithm that achieves global frequency and voltage regulation as well as accurate active/reactive power sharing in droop-based MGs. A secondary distributed cooperative voltage control based on only its own and some neighbors' information was developed to improve the system reliability [50]. A distributed secondary control was proposed not only to restore frequency and voltage but also to ensure reactive power sharing [45]. A new cooperative distributed secondary controller was designed only using localized and nearest-neighbor communication without the knowledge of the MG topology, impedances, or loads [46]. A dynamic load equalization secondary control method has been adopted to converge droop coefficients within reasonable values in DC MGs [51]. A secondary controller was used to realize total harmonic distortion (THD) compensation of sensitive load bus and make DGs distribute their compensating efforts based on their rated capacity [52]. A distributed secondary control method was proposed based on Controller Area Network (CAN) bus sharing the integral output values, thus achieving a better dynamic power-sharing performance [53]. A pinning-based hierarchical and distributed cooperative control was developed for MG cluster (MGC), which includes DG-layer, MG-layer, and MGC-layer controls [54]. In this research, the DG-layer control, essentially a primary control strategy, regulates the local voltage/current of each DG unit and achieves load sharing. The MG-layer control, essentially a distributed secondary control mechanism, is performed for each MG, coordinating DG units in a cooperative manner through several sparse communication networks. This is to restore frequency and voltage within each MG. By treating each MG as an agent, the MGC-layer control coordinates MGs based on a higher-level peer-to-peer communication network among MG agents. The interaction between MG layer and the MGC layer is made possible by pinning some DG units of each MG to communicate with the MG agent. The MGC-layer control coordinates each MG to share active/reactive power among them and to regulate the system frequency and voltage in a distributed manner.

Meanwhile, distributed MPC has been developed at the secondary control level for MGs. In [55], an MPC strategy was applied in MGs to restore the system frequency. Compared to conventional methods including traditional PI approaches and an improved PI controller with Smith predictors (SPs), it is demonstrated that, after load changes, the frequency can return to nominal values with fewer oscillations in a shorter time. In [56], a distributed MPC secondary

control scheme for both voltage and frequency restoration was presented. Only local and neighboring information of DGs is needed to establish the prediction models while YALMIP toolbox and Gurobj optimizer are used as solvers. It is shown that the developed and distributed MPC is robust to perturbations and external disturbances. Similarly, in [57], MPC was utilized as a distributed strategy to implement secondary voltage control. It is necessary to emphasize here that, different from the voltage that varies along the power line because of the presence of line impedances, the frequency is a global variable in an ac MG. For individual MGs that operate separately, their voltages may have different frequencies. Regulating frequencies into a common value through secondary control is therefore necessary for multiple MGs interconnection into a MGC. In this context, in [58], a method using MPC was proposed to regulate the frequency among multiple MGs. It reveals that MPC shows superior performance than the traditional PI controllers when coping with various disturbances and communication delays. In [59], a distributed secondary frequency control based on an MPC algorithm was studied. It is aimed to regulate the frequency by managing the voltages of those voltage-sensitive loads by considering bus voltage constraints.

To date, there are still many open research challenges in this direction, such as DG pinning optimization, convergence rate, and communication structure optimization subject to changing MG physical configuration due to DG plug-and-play operations [60]. Besides, future extensive usage of open communication networks for secondary voltage control in autonomous MGs inherently introduces time delays, which would degrade the system performance or even cause instability. Existing literatures have largely ignored these communication delays between the MG central controller and primary local controllers [61].

4.2.2.3 Decentralized secondary control

In decentralized control, each DG restores its own frequency and voltage amplitudes to nominal values individually, while communication among DGs is not needed, as shown in Figure 4.5c. Recently, several decentralized control approaches have been developed. For example, to eliminate the impact of time delay caused by the low-bandwidth communication lines and restore the frequency and voltage amplitude to the rated values simultaneously, washout filter-based power-sharing strategies have been presented in [37, 62, 63] without any communication links. Washout filter-based power-sharing strategy is derived by combining the droop and secondary control methods. It is essentially an improved droop method by adding a band-pass filter formed by a low-pass filter and a high-pass filter. It is endowed with the capability to restore the frequency and voltage gaps caused by the droop control method while the communication-free and decentralized features can be retained.

4.2.3 Tertiary control

As the highest level in the hierarchy, tertiary control deals with economic

dispatching, operation scheduling, and power flow between the MG and the main grid. Notice that tertiary control is also referred to as the coordination of multiple MGs interacting with one another in networked MGs. Under the grid-connected operation, it is aimed to achieve interconnected power flows and maximize economic benefits.

Compared to primary control and secondary control, the research effort paid to tertiary control is relatively less. But this certainly does not mean tertiary control is not as important as the former two in MGs. Nowadays, most of the tertiary control strategies are focused on a very high level without considering power converter switchings and the MG actual circuitry topologies. Besides, the tertiary control strategies proposed are seldom incorporated with secondary control and primary control in actual implementation. For example, an optimization method was implemented to adjust the DG compensating efforts based on the voltage unbalance limits of local buses and DG terminals [64]. A scenario-based two-stage stochastic programming model was presented as the tertiary control taking into account some RES uncertainties and uncertain energy deviation prices [65]. A distributed two-level tertiary control is proposed to adjust the voltage setpoints and balance the loading among all sources, thus avoiding the single point of failure [66]. An interior-point optimization-based tertiary control was developed to coordinate the voltage source converters (VSCs) and the energy hub to minimize the voltage deviations by generating desired references [67]. A tertiary control using the receding horizon method was presented to provide the optimal power schedule based on the economic and environmental criteria [68].

Recently, there has been significant research interest in using MPC for MGs at the tertiary level. The main focuses are power flow optimization and operational benefit maximization. Considering the stochastic nature of renewable energy resources and daily load profiles, a challenging question is how to control effectively the power flow among DGs while taking into account the various DGs safety constraints, the storage dynamics, and the uncertainties coming from RESs and loads. In [69], the charging and discharging of battery energy storage systems in MGs are focused. The optimal use of energy storage systems (ESSs) is related to the network topology, constraints, objectives as well as state of charge (SoC) of the ESSs. The SoC limits are of high importance for battery ESSs. If overcharged or undercharged, ESSs would suffer significant lifetime deterioration. To address this concern, a new convex MPC strategy is proposed, which is based on a linear d–q reference frame voltage–current model and linearized power flow approximations for dynamic optimal flow between battery ESS units in an ac MG. In this method, the optimal power flows among ESSs are solved as a convex quadratically constrained quadratic program (QCQP). Thus, it can be implemented in a real-time manner as a receding horizon MPC. Since the local loads are powered by the local energy sources and ES systems within the MG, a natural objective is power network loss minimization in distribution lines, inverter LCL filter and battery charging/discharging, while maximizing the utilization of RESs. Network power quality requirements impose constraints on the VSC output voltages, while device operating limits are reflected on the constraints on the VSC

output currents and SoC of the batteries. These objective functions and constraints are then formulated into a finite-time optimal control problem. At each sampling period, a set of system states are predicted and updated, the optimal control problem is solved online, and the controller time horizon recedes by another step. Finally, this centralized MPC generates the voltage references for each distributed inverter, which will be implemented through the conventional cascaded voltage and current control loops. The proposed method does not assume that real and reactive power flows are decoupled, allowing line losses, voltage constraints, and converter current constraints to be addressed in the optimization. The proposed strategy was demonstrated on an islanded MG based on the IEEE 13 bus prototypical feeder, with distributed battery ESSs and intermittent PV generation.

In addition to the power loss minimization mentioned in Section 4.2.3, another major concern in MGs is the operational cost. Reference [70] presents a study on applying a MPC approach to the problem of efficiently optimizing MG operations while satisfying a time-varying request and operation constraints. It tackles the optimal operation planning of a MG. The proposed MPC controller aims at minimizing the overall MG operating costs to meet the predicted load demand of a certain period while satisfying complex operational constraints. Essentially, the MG optimal operational planning consists of taking decisions on how to optimally schedule internal production by generators, storage, as well as controllable loads, to cover the MG demand and minimize the generators' running costs and the cost of imported electricity from the utility grid in the next hours or day. To formulate the MPC problem, the mixed-integer linear programming (MILP) is used, which can be solved efficiently using commercial solvers without resorting to complex heuristics or decompositions techniques. As a result, the MILP formulation leads to significant improvements in solution quality and computational burden. In [71], a coordinated energy dispatch based on distributed model predictive control (DMPC) is presented, where the upper level provides optimal scheduling for energy exchange between the distribution network operator (DNO) and MGs while the lower level guarantees a satisfactory tracking between supply and demand. This DMPC strategy deals with the uncertainties in both supply and demand sides. With the proposed scheme, not only a supply-demand balance can be maintained economically, but also the renewable energy utilization of distributed MG systems can be improved.

Tertiary-level MPC has also been applied to networked MGs. To reduce the power purchased from the DNO, one interesting solution is to connect neighboring MGs in a network. One distinct advantage of networked MGs is that power shortfall in one MG can be compensated by the excess power available from its neighbors. In [72], a strategy is presented to coordinate the power flow among networked MGs. It aims to schedule and manage the energy exchanges at the network level by taking into account uncertainties from renewable resources and loads. To do this, an MPC-based scheme is developed to produce the scheduling of power exchanges among MGs and the charging/discharging operation of ESS within each MG. The MPC algorithm requires information on electricity prices and generation and load forecasts. This high-level algorithm

generates optimal setpoints for all DGs, ESSs, and power exchanges to maximize the network profit while power demand can be met. The implementation of this MPC-based power scheduling strategy can be elaborated as follows. At each control instant (t), a finite horizon (Nc) optimal control sequence, including the ESS charging/discharging, the amount of power exchanged among MGs, and the amount of power sold/bought to/from the DNO for the MG cluster, is determined. After that, only the first control action of the scheduling sequence is implemented. Then, the information available in each MG, i.e., ESS state, loads, renewable energy power generation, and energy price predictions, is updated for the next control period. Upon the completion of this control process, the control horizon moves one step forward, and the same implementation process is repeated to determine new control action. This MPC algorithm is implemented using Lingo optimization software. Similarly, a hierarchical distributed model predictive control strategy was developed in [73] to govern interconnected MGs with the purpose of increasing the overall infeed of RESs. The alternating direction method of multipliers (ADMM) is adopted to decompose and solve optimization problems in a distributed way. With the MG layer, local optimization problems are solved to obtain the reference of buying/selling power for each MG. Then, this information on energy buying/selling reference is collected and processed by a central controller on a higher layer, which will deliver the results back to individual MGs. In this way, the privacy of MGs can be protected to a large extent because individual MGs only communicate to the central entity about the power that they want to purchase or sell. Consequently, MGs maintain autonomy in their operation. Moreover, individual MGs can benefit from this networked operation as the shortfall of energy can be compensated by neighbors. Since the overall optimization problem is implemented in a distributed manner with every MG retaining its local controller, flexibility and scalability can be enhanced compared to centralized control.

References

[1] Hu J., Zhu J., Platt G. A droop control strategy of parallel-inverter-based microgrid. *Proceedings of IEEE International Conference on Applied Superconductivity and Electromagnetic Devices*, 14-16 Dec 2011; 2011. pp. 188–91.

[2] Wood A., Wollenberg B. *Power Generation, Operation, and Control*. New York, NY: Wiley; 1996.

[3] Guerrero J.M., Vasquez J.C., Matas J., de Vicuna L.G., Castilla M. 'Hierarchical control of droop-controlled AC and DC microgrids—a general approach toward standardization'. *IEEE Transactions on Industrial Electronics*. 2011, vol. 58(1), pp. 158–72.

[4] Han H., Hou X., Yang J., Wu J., Su M., Guerrero J.M. 'Review of power sharing control strategies for islanding operation of AC microgrids'. *IEEE Transactions on Smart Grid*. 2016, vol. 7(1), pp. 200–15.

[5] Chandorkar M.C., Divan D.M., Adapa R. 'Control of parallel connected

inverters in standalone AC supply systems'. *IEEE Transactions on Industry Applications*. 1993, vol. 29(1), pp. 136–43.

[6] Guerrero J.M., GarciadeVicuna L., Matas J., Castilla M., Miret J. 'A wireless controller to enhance dynamic performance of parallel inverters in distributed generation systems'. *IEEE Transactions on Power Electronics*. 2004, vol. 19(5), pp. 1205–13.

[7] Majumder R., Ghosh A., Ledwich G. Angle droop versus frequency droop in a voltage source converter based autonomous microgrid. *Proceedings of Power and Energy Society General Meeting*; Calgary, AB, Canada; 2009. pp. 1–8.

[8] Majumder R., Chaudhuri B., Ghosh A., Majumder R., Ledwich G., Zare F. 'Improvement of stability and load sharing in an autonomous microgrid using supplementary droop control loop'. *IEEE Transactions on Power Systems*. 2010, vol. 25(2), pp. 796–808.

[9] Hu J., Zhu J., Dorrell D.G., Guerrero J.M. 'Virtual flux droop method—a new control strategy of inverters in microgrids'. *IEEE Transactions on Power Electronics*. 2014, vol. 29(9), pp. 4704–11.

[10] Guerrero J.M., Chandorkar M., Lee T.-L., Loh P.C. 'Advanced control architectures for intelligent microgrids—Part I: decentralized and hierarchical control'. *IEEE Transactions on Industrial Electronics*. 2013, vol. 60(4), pp. 1254–62.

[11] Guerrero J.M., GarciadeVicuna L., Matas J., Castilla M., Miret J. 'Output impedance design of parallel-connected ups inverters with wireless load-sharing control'. *IEEE Transactions on Industrial Electronics*. 2005, vol. 52(4), pp. 1126–35.

[12] Chen T., Abdel-Rahim O., Peng F., Wang H. 'An improved finite control set-MPC-based power sharing control strategy for islanded AC microgrids'. *IEEE Access*. 2020, vol. 8, pp. 52676–86.

[13] Borup U., Blaabjerg F., Enjeti P.N. 'Sharing of nonlinear load in parallel-connected three-phase converters'. *IEEE Transactions on Industry Applications*. 2001, vol. 37(6), pp. 1817–23.

[14] Zhong Q.-C. 'Harmonic droop controller to reduce the voltage harmonics of inverters'. *IEEE Transactions on Industrial Electronics*. 2013, vol. 60(3), pp. 936–45.

[15] He J., Li Y.W., Guerrero J.M., Blaabjerg F., Vasquez J.C. 'An islanding microgrid power sharing approach using enhanced virtual impedance control scheme'. *IEEE Transactions on Power Electronics*. 2013, vol. 28(11), pp. 5272–82.

[16] Guerrero J.M., Matas J., Garcia de Vicuna L., Castilla M., Miret J., de Vicuña L.G. 'Decentralized control for parallel operation of distributed generation inverters using resistive output impedance'. *IEEE Transactions on Industrial Electronics*. 2007, vol. 54(2), pp. 994–1004.

[17] De Brabandere K., Bolsens B., Van den Keybus J., Woyte A., Driesen J., Belmans R. 'A voltage and frequency droop control method for parallel inverters'. *IEEE Transactions on Power Electronics*. 2007, vol. 22(4), pp.

1107–15.
[18] Moawwad A., Khadkikar V., Kirtley J.L. ‘A new P-Q-V droop control method for an interline photovoltaic (I-PV) power system’. *IEEE Transactions on Power Delivery*. 2013, vol. 28(2), pp. 658–68.
[19] Li Y., Kao C.N. ‘An accurate power control strategy for power electronic-interfaced distributed generation units operating in a low voltage multibus microgrid’. *IEEE Transactions on Power Electronics*. 2009, vol. 24(12), pp. 2977–88.
[20] Vasquez J.C., Guerrero J.M., Luna A., Rodriguez P., Teodorescu R. ‘Adaptive droop control applied to voltage-source inverters operating in grid-connected and islanded modes’. *IEEE Transactions on Industrial Electronics*. 2009, vol. 56(10), pp. 4088–96.
[21] Hanaoka H., Nagai M., Yanagisawa M. Development of a novel parallel redundant UPS. *Proceedings of 25th International IEEE Telecommunications Energy Conference*; Yokohama, Japan; 2003. pp. 493–8.
[22] Guerrero J.M., Vasquez J.C., Matas J., Castilla M., de Vicuna L.G. ‘Control strategy for flexible microgrid based on parallel line-interactive UPS systems’. *IEEE Transactions on Industrial Electronics*. 2009, vol. 56(3), pp. 726–36.
[23] Khayyer P., Ozguner U. ‘Decentralized control of large-scale storage-based renewable energy systems’. *IEEE Transactions on Smart Grid*. 2014, vol. 5(3), pp. 1300–7.
[24] Li Z., Chan K.W., Hu J., Guerrero J.M. ‘Adaptive droop control using adaptive virtual impedance for microgrids with variable PV outputs and load demands’. *IEEE Transactions on Industrial Electronics*. 2020, p. 1.
[25] Mahmood H., Michaelson D., Jiang J. ‘Accurate reactive power sharing in an islanded microgrid using adaptive virtual impedances’. *IEEE Transactions on Power Electronics*. 2015, vol. 30(3), pp. 1605–17.
[26] John B., Ghosh A., Zare F., Rajakaruna S. ‘Improved control strategy for accurate load power sharing in an autonomous microgrid’. *IET Generation, Transmission & Distribution*. 2017, vol. 11(17), pp. 4384–90.
[27] Zhang J., Shu J., Ning J., Huang L., Wang H. ‘Enhanced proportional power sharing strategy based on adaptive virtual impedance in low-voltage networked microgrid’. *IET Generation, Transmission & Distribution*. 2018, vol. 12(11), pp. 2566–76.
[28] Yang X., Hu H., Ge Y., Aatif S., He Z., Gao S. ‘An improved droop control strategy for VSC-based MVDC traction power supply system’. *IEEE Transactions on Industry Applications*. 2018, vol. 54(5), pp. 5173–86.
[29] Mi Y., Zhang H., Fu Y., Wang C., Loh P.C., Wang P. ‘Intelligent power sharing of DC isolated microgrid based on fuzzy sliding mode droop control’. *IEEE Transactions on Smart Grid*. 2019, vol. 10(3), pp. 2396–406.
[30] Zhou J., Tsai M.-J., Cheng P.-T. ‘Consensus-based cooperative droop control for accurate reactive power sharing in islanded AC microgrid’. *IEEE Journal of Emerging and Selected Topics in Power Electronics*. 2019, vol.

8(2), pp. 1108–16.
[31] Gao M., Chen M., Zhao B., Li B., Qian Z. ‘Design of control system for smooth mode-transfer of grid-tied mode and islanding mode in microgrid’. *IEEE Transactions on Power Electronics*. 2019, vol. 35(6), pp. 6419–35.
[32] Wei B., Guerrero J.M., Vásquez J.C., Guo X. ‘A circulating-current suppression method for parallel-connected voltage-source inverters with common DC and AC buses’. *IEEE Transactions on Industry Applications*. 2017, vol. 53(4), pp. 3758–69.
[33] Sun Y., Shi G., Li X., *et al*. ‘An f-P/Q]]> droop control in cascaded-type microgrid’. *IEEE Transactions on Power Systems*. 2018, vol. 33(1), pp. 1136–8.
[34] Golsorkhi M.S., Shafiee Q., Lu D.D.-C., Guerrero J.M. ‘Distributed control of low-voltage resistive AC microgrids’. *IEEE Transactions on Energy Conversion*. 2019, vol. 34(2), pp. 573–84.
[35] Wai R.-J., Zhang Q.-Q., Wang Y. ‘A novel voltage stabilization and power sharing control method based on virtual complex impedance for an off-grid microgrid’. *IEEE Transactions on Power Electronics*. 2019, vol. 34(2), pp. 1863–80.
[36] Shan Y., Hu J., Li Z., Guerrero J.M. ‘A model predictive control for renewable energy based AC microgrids without any PID regulators’. *IEEE Transactions on Power Electronics*. 2018, vol. 33(11), pp. 9122–6.
[37] Shan Y., Hu J., Liu M., Zhu J., Guerrero J.M. ‘Model predictive voltage and power control of islanded PV-battery microgrids with washout-filter-based power sharing strategy’. *IEEE Transactions on Power Electronics*. 2020, vol. 35(2), pp. 1227–38.
[38] Low K., Cao R. ‘Model predictive control of parallel-connected inverters for uninterruptible power supplies’. *IEEE Transactions on Industrial Electronics*. 2008, vol. 55(8), pp. 2884–93.
[39] Nguyen T., Yoo H., Kim H. Model predictive control of inverters in microgrids with constant switching frequency for circulating current suppression. *Proceedings of IEEE TENCON*; 2018. pp. 1566–71.
[40] Wang X., Zou J., Zhao J., *et al*. ‘A novel model predictive control strategy to eliminate zero-sequence circulating current in paralleled three-level inverters’. *IEEE Journal of Emerging and Selected Topics in Power Electronics*. 2019, vol. 7(1), pp. 309–20.
[41] Bidram A., Davoudi A. ‘Hierarchical structure of microgrids control system’. *IEEE Transactions on Smart Grid*. 2012, vol. 3(4), pp. 1963–76.
[42] Savaghebi M., Jalilian A., Vasquez J.C., Guerrero J.M. ‘Secondary control for voltage quality enhancement in microgrids’. *IEEE Transactions on Smart Grid*. 2012, vol. 3(4), pp. 1893–902.
[43] Savaghebi M., Jalilian A., Vasquez J.C., Guerrero J.M. ‘Secondary control scheme for voltage unbalance compensation in an islanded droop-controlled microgrid’. *IEEE Transactions on Smart Grid*. 2011, vol. 3(2), pp. 797–807.
[44] Mehrizi-Sani A., Iravani R. ‘Potential-function based control of a microgrid in Islanded and grid-connected modes’. *IEEE Transactions on Power*

Systems. 2010, vol. 25(4), pp. 1883–91.
[45] Shafiee Q., Guerrero J.M., Vasquez J.C. 'Distributed secondary control for islanded microgrids—a novel approach'. *IEEE Transactions on Power Electronics*. 2014, vol. 29(2), pp. 1018–31.
[46] Simpson-Porco J.W., Shafiee Q., Dörfler F., Vasquez J.C., Guerrero J.M., Bullo F. 'Secondary frequency and voltage control of islanded microgrids via distributed averaging'. *IEEE Transactions on Industrial Electronics*. 2015, vol. 62(11), pp. 7025–38.
[47] Khayat Y., Shafiee Q., Heydari R., *et al*. 'On the secondary control architectures of AC microgrids: an overview'. *IEEE Transactions on Power Electronics*. 2020, vol. 35(6), pp. 6482–500.
[48] Bidram A., Nasirian V., Davoudi A., Lewis F.L. *Cooperative Synchronization in Distributed Microgrid Control*. New York City, US: Springer; 2017.
[49] Shafiee Q., Nasirian V., Vasquez J.C., Guerrero J.M., Davoudi A. 'A multi-functional fully distributed control framework for AC microgrids'. *IEEE Transactions on Smart Grid*. 2018, vol. 9(4), pp. 3247–58.
[50] Bidram A., Davoudi A., Lewis F.L., Guerrero J.M. 'Distributed cooperative secondary control of microgrids using feedback linearization'. *IEEE Transactions on Power Systems*. 2013, vol. 28(3), pp. 3462–70.
[51] Wang P., Lu X., Yang X., Wang W., Xu D. 'An improved distributed secondary control method for DC microgrids with enhanced dynamic current sharing performance'. *IEEE Transactions on Power Electronics*. 2016, vol. 31(9), pp. 6658–73.
[52] Andishgar M.H., Gholipour E., Hooshmand Rahmat-Allah., Hooshmand R.-A. 'Improved secondary control for optimal total harmonic distortion compensation of parallel connected DGs in islanded microgrids'. *IET Smart Grid*. 2019, vol. 2(1), pp. 115–22.
[53] Wei B., Gui Y., Trujillo S., Guerrero J.M., Vasquez J.C., Marzabal A. 'Distributed average integral secondary control for modular UPS systems-based microgrids'. *IEEE Transactions on Power Electronics*. 2019, vol. 34(no. 7), pp. 6922–36.
[54] Wu X., Xu Y., He J., Wang X., Vasquez J.C., Guerrero J.M. 'Pinning-based hierarchical and distributed cooperative control for AC microgrid clusters'. *IEEE Transactions on Power Electronics*. 2020, vol. 35(9), pp. 9865–85.
[55] Ahumada C., Cárdenas R., Sáez D., Guerrero J.M. 'Secondary control strategies for frequency restoration in islanded microgrids with consideration of communication delays'. *IEEE Transactions on Smart Grid*. 2016, vol. 7(3), pp. 1430–41.
[56] Lou G., Gu W., Xu Y., Cheng M., Liu W. 'Distributed MPC-based secondary voltage control scheme for autonomous droop-controlled microgrids'. *IEEE Transactions on Sustainable Energy*. 2017, vol. 8(2), pp. 792–804.
[57] Guo Z., Li S., Zheng Y. Distributed model predictive control for secondary voltage of the inverter-based microgrid. *Chinese Control Conference CCC*;

2017. pp. 4630–4.
[58] Wang X., Zhao Q., He B., Wang Y., Yang J., Pan X. ‘Load frequency control in multiple microgrids based on model predictive control with communication delay’. *The Journal of Engineering*. 2017, vol. 2017(13), pp. 1851–6.
[59] Liu K., Liu T., Tang Z., Hill D.J. ‘Distributed MPC-based frequency control in networked microgrids with voltage constraints’. *IEEE Transactions on Smart Grid*. 2019, vol. 10(6), pp. 6343–54.
[60] Schiffer J., Dörfler F., Fridman E. ‘Robustness of distributed averaging control in power systems: Time delays & dynamic communication topology’. *Automatica*. 2017, vol. 80(3), pp. 261–71.
[61] Lou G., Gu W., Wang J., Sheng W., Sun L. ‘Optimal design for distributed secondary voltage control in islanded microgrids: Communication topology and controller’. *IEEE Transactions on Power Systems*. 2019, vol. 34(2), pp. 968–81.
[62] Yazdanian M., Mehrizi-Sani A. ‘Washout filter-based power sharing’. *IEEE Transactions on Smart Grid*. 2016, vol. 7(2), pp. 967–8.
[63] Han Y., Li H., Xu L., Zhao X., Guerrero J.M. ‘Analysis of washout filter-based power sharing strategy—an equivalent secondary controller for islanded microgrid without BC lines’. *IEEE Transactions on Smart Grid*. 2018, vol. 9(5), pp. 4061–76.
[64] Meng L., Tang F., Savaghebi M., Vasquez J.C., Guerrero J.M. ‘Tertiary control of voltage unbalance compensation for optimal power quality in islanded microgrids’. *IEEE Transactions on Energy Conversion*. 2014, vol. 29(4), pp. 802–15.
[65] Citores L., Corchero C., Heredia F.J. ‘A stochastic programming model for the tertiary control of microgrids’. *International Conference on Europen Energy Market EEM*. 2015, vol. 2015, pp. 1–6.
[66] Moayedi S., Davoudi A. ‘Distributed tertiary control of DC microgrid clusters’. *IEEE Transactions on Power Electronics*. 2017, vol. 31(2), pp. 1717–33.
[67] Mudaliyar S.R., Mishra S., Sharma R.K. ‘Tertiary load voltage control in an interconnected DC microgrid with energy hub’. *2017 7th International Conference on Power System ICPS*. 2018, vol. 2017, pp. 765–70.
[68] Delfino F., Ferro G., Robba M., Rossi M. ‘An architecture for the optimal control of tertiary and secondary levels in small-size islanded microgrids’. *International Journal of Electrical Power & Energy Systems*. 2018, vol. 103(4), pp. 75–88.
[69] Morstyn T., Hredzak B., Aguilera R.P., Agelidis V.G. ‘Model predictive control for distributed microgrid battery energy storage systems’. *IEEE Transactions on Control Systems Technology*. 2018, vol. 26(3), pp. 1107–14.
[70] Parisio A., Rikos E., Glielmo L. ‘A model predictive control approach to microgrid operation optimization’. *IEEE Transactions on Control Systems Technology*. 2014, vol. 22(5), pp. 1813–27.
[71] Du Y., Wu J., Li S., Long C., Onori S. ‘Coordinated energy dispatch of

autonomous microgrids with distributed MPC optimization'. IEEE Transactions on Industrial Informatics. 2019, vol. 6(5), pp. 2233–44.
[72] Ouammi A., Dagdougui H., Dessaint L., Sacile R. 'Coordinated model predictive-based power flows control in a cooperative network of smart microgrids'. *IEEE Transactions on Smart Grid*. 2015, vol. 6(5), pp. 2233–44.
[73] Hans C.A., Braun P., Raisch J., Grune L., Reincke-Collon C. 'Hierarchical distributed model predictive control of interconnected microgrids'. *IEEE Transactions on Sustainable Energy*. 2019, vol. 10(1), pp. 407–16.

Further reading

- Raza S.A., Jiang J. 'A benchmark distribution system for investigation of residential microgrids with multiple local generation and storage devices'. *IEEE Open Access Journal of Power and Energy*. 2020, vol. 7, pp. 41–50. doi:10.1109/OAJPE.2019.2952812
- Shi Z., Li J., Nurdin H.I., Fletcher J.E. 'Comparison of virtual oscillator and droop controlled islanded three-phase microgrids'. *IEEE Transactions on Energy Conversion*. 2019, vol. 34(4), pp. 1769–80. doi:10.1109/TEC.2019.2922447
- Lou G., Gu W., Lu X., Xu Y., Hong H. 'Distributed secondary voltage control in islanded microgrids with consideration of communication network and time delays'. *IEEE Transactions on Smart Grid*. 2020, vol. 11(5), pp. 3702–15. doi:10.1109/TSG.2020.2979503
- Fax R., Olfati-Saber J.A., Murray M. 'Consensus and cooperation in networked multi-agent systems'. *IEEE Proceedings*. 2020, vol. 95(1), pp. 215–33.
- Wang Y., Nguyen T.L., Syed M.H., *et al*. 'A distributed control scheme of microgrids in energy internet and its multi-site implementation'. *IEEE transactions on industrial informatics*.
- Zhang L., Zheng H., Hu Q., Su B., Lyu L. 'An adaptive droop control strategy for islanded microgrid based on improved particle swarm optimization'. *IEEE Access*. 2020, vol. 8, pp. 3579–93. doi:10.1109/ACCESS.2019.2960871
- Xu Y., Sun H., Gu W., Xu Y., Li Z. 'Optimal distributed control for secondary frequency and voltage regulation in an islanded microgrid'. *IEEE Transactions on Industrial Informatics*. 2019, vol. 15(1), pp. 225–35. doi:10.1109/TII.2018.2795584
- liu J. *'Studies on improving dynamic performance of microgrids by applying virtual synchronous generator control to distributed generators'*[Doctoral Dissertation]. Osaka University; 2016.
- Hamidi R.J., Livani H., Hosseinian S.H., Gharehpetian G.B. 'Distributed cooperative control system for smart microgrids'. *Electric Power Systems Research*. 2016, vol. 130(4), pp. 241–50. doi:10.1016/j.epsr.2015.09.012
- Nasirian V., Moayedi S., Davoudi A., Lewis F.L. 'Distributed cooperative control of DC microgrids'. *IEEE Transactions on Power Electronics*. 2015,

vol. 30(4), pp. 2288–303. doi:10.1109/TPEL.2014.2324579
- Silva W.W.A.G., Oliveira T.R., Donoso-Garcia P.F. 'An improved voltage-shifting strategy to attain concomitant accurate power sharing and voltage restoration in droop-controlled DC microgrids'. *IEEE Transactions on Power Electronics*. 2020, vol. 36(2), pp. 2396–406. doi:10.1109/TPEL.2020.3009619
- Yu C., Zhou H., Lai J., Lu X., Liu G.-P. 'Distributed optimal synchronization rate control for AC microgrids under event-triggered mechanism'. *IEEE Transactions on Power Systems* 1. doi:10.1109/TPWRS.2020.3035688
- Yi Z., Xu Y., Gu W., Fei Z. 'Distributed model predictive control based secondary frequency regulation for a microgrid with massive distributed resources'. *IEEE Transactions on Sustainable Energy*. in press.
- Cheng L., Zhang Z., Zhang F. 'Secondary voltage controls of virtual-droop-controlled bidirectional DC/DC converters in hybrid energy storage system'. *IET Power Electronics*. 2020, vol. 13(14), pp. 3018–25. doi:10.1049/iet-pel.2019.1566
- Sarrafan N., Rostami M.A., Zarei J., Razavi-Far R., Saif M., Dragicevic T. 'Improved distributed prescribed finite-time secondary control of inverter-based microgrids: design and real-time implementation'. *IEEE Transactions on Industrial Electronics* 1. doi:10.1109/TIE.2020.3031522
- Zaery M., Wang P., Huang R., Wang W., Xu D. 'Distributed economic dispatch for islanded DC microgrids based on finite-time consensus protocol'. *IEEE Access*. 2020, vol. 8, pp. 192457–68. doi:10.1109/ACCESS.2020.3032641
- Wong Y C., Lim C S., Cruden A., Rotaru M.D., Ray P K. 'A consensus-based adaptive virtual output impedance control scheme for reactive power sharing in radial microgrids'. *IEEE Transactions on Industry Applications*. *in press*.
- Keshavarz M., Doroudi A., Kazemi M.H., Dehkordi N.M. 'A novel adaptive distributed secondary voltage controller with high convergence rate for islanded microgrids'. *IEEE Systems Journal*. in press, pp. 1–11. doi:10.1109/JSYST.2020.3028778
- Espina E., Llanos J., Burgos-Mellado C., Cardenas-Dobson R., Martinez-Gomez M., Saez D. 'Distributed control strategies for microgrids: an overview'. *IEEE Access*. 2020, vol. 8, pp. 193412–48. doi:10.1109/ACCESS.2020.3032378
- Espina E., Cardenas-Dobson R., Simpson-Porco J.W., Saez D., Kazerani M. 'A consensus-based secondary control strategy for hybrid AC/DC microgrids with experimental validation'. *IEEE Transactions on Power Electronics*. *in press*.
- Xing L., Guo F., Liu X., Wen C., Mishra Y., Tian Y. 'Voltage restoration and adjustable current sharing for DC Microgrid with time delay via distributed secondary control'. *IEEE Transactions on Sustainable Energy*. *2021*, vol. 12(2), pp. 1068–77. doi: 10.1109/TSTE.2020.3032605
- Pullaguram D., Rana R., Mishra S., Senroy N. 'Fully distributed hierarchical control strategy for multi-inverter-based AC microgrids'. *IET Renewable*

Power Generation. 2020, vol. 14(13), pp. 2468–76. doi:10.1049/iet-rpg.2019.1117

- Rosero C.X., Velasco M., Marti P., Camacho A., Miret J., Castilla M. 'Active power sharing and frequency regulation in droop-free control for islanded microgrids under electrical and communication failures'. *IEEE Transactions on Industrial Electronics*. 2020, vol. 67(8), pp. 6461–72. doi:10.1109/TIE.2019.2939959
- Tucci M., Riverso S., Ferrari-Trecate G. 'Line-independent plug-and-play controllers for voltage stabilization in DC microgrids'. *IEEE Transactions on Control Systems Technology*. 2018, vol. 26(3), pp. 1115–23. doi:10.1109/TCST.2017.2695167
- Perez-Ibacache R., Silva C.A., Yazdani A. 'Linear state-feedback primary control for enhanced dynamic response of AC microgrids'. *IEEE Transactions on Smart Grid*. 2019, vol. 10(3), pp. 3149–61. doi:10.1109/TSG.2018.2818624
- Kammer C., Karimi A. 'Decentralized and distributed transient control for microgrids'. *IEEE Transactions on Control Systems Technology*. 2019, vol. 27(1), pp. 311–22. doi:10.1109/TCST.2017.2768421
- Peyghami S., Mokhtari H., Loh P.C., Davari P., Blaabjerg F. 'Distributed primary and secondary power sharing in a droop-controlled LVDC microgrid with merged AC and DC characteristics'. *IEEE Transactions on Smart Grid*. 2018, vol. 9(3), pp. 2284–94. doi:10.1109/TSG.2016.2609853
- Qian T., Liu Y., Zhang W., Tang W., Shahidehpour M. 'Event-Triggered updating method in centralized and distributed secondary controls for islanded microgrid restoration'. *IEEE Transactions on Smart Grid*. 2020, vol. 11(2), pp. 1387–95. doi:10.1109/TSG.2019.2937366
- Awal M.A., Yu H., Tu H., Lukic S.M., Husain I. 'Hierarchical control for virtual oscillator based grid-connected and islanded microgrids'. *IEEE Transactions on Power Electronics*. 2020, vol. 35(1), pp. 988–1001. doi:10.1109/TPEL.2019.2912152
- Xiao Z., Zhu M., Huang Y., Guerrero J.M., Vasquez J.C. 'Coordinated primary and secondary frequency support between microgrid and weak grid'. *IEEE Transactions on Sustainable Energy*. 2019, vol. 10(4), pp. 1718–30.
- Khayat Y. *Estimation-based consensus approach for decentralized frequency control of AC microgrids*. *Proceedings of European Conference on Power Electronics and Applications*; 2019. pp. 1–6.
- Hamzeh M., Mokhtari H., Karimi H. 'A decentralized self-adjusting control strategy for reactive power management in an islanded multi-bus MV microgrid'. *Canadian Journal of Electrical and Computer Engineering*. 2013, vol. 36(1), pp. 18–25. doi:10.1109/CJECE.2013.6544468
- Peng J., Fan B., Xu H., Liu W. 'Discrete-time self-triggered control of DC microgrids with data dropouts and communication delays'. *IEEE Transactions on Smart Grid*. 2020, vol. 11(6), pp. 4626–36. doi:10.1109/TSG.2020.3000138
- Rosero C.X., Velasco M., Marti P., Camacho A., Miret J., Castilla M. 'Active

power sharing and frequency regulation in droop-free control for islanded microgrids under electrical and communication failures'. *IEEE Transactions on Industrial Electronics*. 2020, vol. 67(8), pp. 6461–72. doi:10.1109/TIE.2019.2939959

- Sadabadi M.S., Shafiee Q., Karimi A. 'Plug-and-play voltage stabilization in inverter-interfaced microgrids via a robust control strategy'. *IEEE Transactions on Control Systems Technology*. 2017, vol. 25(3), pp. 781–91. doi:10.1109/TCST.2016.2583378
- Zamora R., Srivastava A.K. 'Multi-layer architecture for voltage and frequency control in networked microgrids'. *IEEE Transactions on Smart Grid*. 2018, vol. 9(3), pp. 2076–85.
- Wang Z., Liu F., Chen Y., *et al*. 'Multi-layer architecture for voltage and frequency control in networked microgrids'. *IEEE Transactions on Smart Grid*. 2019, vol. 10(1), pp. 1013–24.
- Ouammi A., Dagdougui H., Sacile R. 'Optimal control of power flows and energy local storages in a network of microgrids modeled as a system of systems'. *IEEE Transactions on Control Systems Technology*. 2015, vol. 23, (1), pp. 128–38. doi:10.1109/TCST.2014.2314474
- Marti P., Velasco M., Martin E.X., Vicuna L.G., Miret J., Castilla M. 'Performance evaluation of secondary control policies with respect to digital communications properties in inverter-based islanded microgrids'. *IEEE Transactions on Smart Grid*. 2018, vol. 9(3), pp. 2192–202.
- Hossain M.J., Pota H.R., Mahmud M.A., Aldeen M. 'Robust control for power sharing in microgrids with low-inertia wind and PV generators'. *IEEE Transactions on Sustainable Energy*. 2015, vol. 6(3), pp. 1067–77. doi:10.1109/TSTE.2014.2317801
- Sadabadi M.S., Shafiee Q., Karimi A. 'Robust control for power sharing in microgrids with low-inertia wind and PV generators'. *IEEE Transactions on Smart Grid*. 2018, vol. 9(6), pp. 6886–96.
- Tucci M., Riverso S., Ferrari-Trecate G. 'Line-independent plug-and-play controllers for voltage stabilization in DC microgrids'. *IEEE Transactions on Control Systems Technology*. 2018, vol. 26, (3), pp. 1115–23. doi:10.1109/TCST.2017.2695167
- Zuo S., Altun T., Lewis F.L., Davoudi A. 'Distributed resilient secondary control of DC microgrids against unbounded attacks'. *IEEE Transactions on Smart Grid*. 2020, vol. 11(5), pp. 3850–9. doi:10.1109/TSG.2020.2992118
- Kerdphol T., Rahman F.S., Mitani Y., Watanabe M., Kufeoglu S. 'Robust virtual inertia control of an islanded microgrid considering high penetration of renewable energy'. *IEEE Access*. 2017, vol. 6, pp. 625–36. doi:10.1109/ACCESS.2017.2773486
- Baghaee H. R., Mirsalim M., Gharehpetian G.B., Talebi H.A. 'Robust virtual inertia control of an islanded microgrid considering high penetration of renewable energy'. *IEEE Systems Journal*. 2018, vol. 12(4), pp. 3108–19.
- Golsorkhi M.S., Shafiee Q., Lu D.D.-C., Guerrero J.M. 'Distributed control of low-voltage resistive AC microgrids'. *IEEE Transactions on Energy*

Conversion. 2019, vol. 34(2), pp. 573–84. doi:10.1109/TEC.2018.2878690

- Delghavi M.B., Yazdani A. 'Sliding-mode control of AC voltages and currents of dispatchable distributed energy resources in master-slave-organized inverter-based microgrids'. *IEEE Transactions on Smart Grid*. 2019, vol. 10(1), pp. 980–91. doi:10.1109/TSG.2017.2756935
- Moayedi S., Davoudi A. 'Distributed tertiary control of DC microgrid clusters'. *IEEE Transactions on Power Electronics*. 2016, vol. 31(2), pp. 1717–33. doi:10.1109/TPEL.2015.2424672
- Nasser N., Fazeli M. 'Buffered-microgrid structure for future power networks; a seamless Microgrid control'. *IEEE Transactions on Smart Grid*. *in press*.
- Kerdphol T., Watanabe M., Hongesombut K., Mitani Y. 'Self-adaptive virtual inertia control-based fuzzy logic to improve frequency stability of microgrid with high renewable penetration'. *IEEE Access*. 2019, vol. 7, pp. 76071–83. doi:10.1109/ACCESS.2019.2920886
- Mokhtar M., Marei M.I., El-Sattar A.A. 'An adaptive droop control scheme for DC microgrids integrating sliding mode voltage and current controlled boost converters'. *IEEE Transactions on Smart Grid*. 2019, vol. 10(2), pp. 1685–93. doi:10.1109/TSG.2017.2776281
- Gomez L.A.G., Mokhtar M. I., Marei A.A., *et al*. 'An adaptive droop control scheme for DC microgrids integrating sliding mode voltage and current controlled boost converters'. *IEEE Access*. 2020, vol. 8, pp. 189298–312.
- Feng F., Zhang P. 'Enhanced microgrid power flow incorporating hierarchical control'. *IEEE Transactions on Power Systems*. 2020, vol. 35(3), pp. 2463–6. doi:10.1109/TPWRS.2020.2972131

Chapter 5
MPC of PV-wind-storage microgrids

5.1 Introduction

The global electrical power generation system has evolved gradually since the industrial revolution, and the growth of renewable power generation has accelerated considerably over the past years. In the next decades, large-scale transformation in electrical power generation, distribution, and consumption may be seen, particularly driven by global climate change. Wind energy is relatively clean and sustainable, and it has become one of the most promising and fastest-growing energy resources in the world. The global wind power cumulative installed capacity has increased from about 198 GW in 2010 to 651 GW in 2019, with strong continued growth foreseen across Europe, Asia, and Americas. In the year 2019 only, around 621 421 MW were generated from onshore installations, of which 54 206 MW belongs to new installation in that year [1]. Meanwhile, due to the on-going advancement in electronic technology and the incentives from governments and associations, the cost of electricity from wind energy has been reduced steadily.

Another promising renewable energy source (RES), solar power, has also attracted much attention. The global solar photovoltaic (PV) power capacity has increased rapidly, and it is expected to become a major contributor to the world's energy supply. The International Energy Agency (IEA) estimates that by 2050, solar PV power generation will contribute 16 percent of the world's electricity, and 20 percent of that capacity will come from residential installations [2]. Actually, among all low-carbon technology options, solar PV contributes to major CO_2 emissions reduction. This is mainly due to the significant deployment of solar power replacing traditional fossil-fuel power generation sources by utilizing solar panels with advanced technological solutions at better resource locations across various regions. According to International Renewable Energy Agency (IRENA), solar PV would contribute to 4.9 Gt of CO_2 emissions reductions in 2050, accounting for 21 percent of the overall energy-sector emissions reductions needed to meet Paris climate goals [3]. Base on the existing trend, IRENA's REmap analysis predicts that solar PV power installations could rise almost sixfold over the next decade, reaching a cumulative capacity of 2 840 GW globally by 2030 and increasing to 8 519 GW by 2050. At a global level, around

60 percent of total solar PV capacity in 2050 would be utility-scale [3]. At the same time, the deployment of rooftop solar PV systems with distributed storage has increased significantly in recent years in great measure because of supporting policies, attractive incentives, and falling costs. For example, behind-the-meter storage business models allow consumers to store the electricity generated by rooftop solar PV and consume it later when needed or sell it to the grid.

Though the cumulative installed capacity of wind power and solar power has increased rapidly, the grid integration of wind generators and solar PVs has been a worldwide challenge. Harvesting wind and solar energy is one thing, but how to effectively control and utilize the power generated from these distributed renewable energy sources (RESs) is another thing. To find a better way to realize the emerging potentials of distributed generations (DGs), a new paradigm known as microgrids (MGs) has been proposed [4–6]. As the building blocks of smart grids, MGs lay the foundation for the future smart grid system. A MG is a cluster of DGs and local loads that can offer many advantages to the current power grid in terms of power autonomy and the ability to incorporate renewable and non-RESs. A MG is a local power system integrated with multiple DGs and the associated power electronic devices for power control and measurement, thus, to meet various load demands. The main objectives of MGs are: (1) to exploit renewable energy efficiently and at the same time to smooth out the intermittent output of RESs with appropriate control methods; (2) to integrate various types of DGs into the power network effectively; (3) to reduce the burden of the traditional power system and provide ancillary services to the existing power grid; and (4) to supply electrical power to remote areas where utility power grid is not available.

One of the key components in a MG is energy storage. Energy storage provides a variety of technological solutions to manipulate the power supply to create a more resilient energy infrastructure that can be beneficial to both utilities and consumers [7–9]. From a more technical point of view, the energy storage systems (ESSs) play a critical role in stabilizing the voltage and frequency of the MG, particularly in islanded mode. They act as an energy buffer to compensate renewable intermittency, mitigate load uncertainties, and improve MG stability. By managing the power flow, the use of energy storage in the MG also enhances its efficiency in terms of power loss reduction through the distribution lines. Nowadays, different energy storage technologies have been developed, including batteries, thermal, mechanical storage, hydrogen, pumped hydropower, etc. Among them, batteries are the most popular and widely used ESSs in MG applications. Because of the intermittent nature of renewable energy, batteries are critical parts to absorb surplus energy during peak generation periods and provide insufficient power when peak demand occurs.

To integrate the RESs and ESSs mentioned in Section 5.1 into a reliable power network, the MG structure is an important consideration. In terms of voltage type, AC power has dominated the transmission and distribution network for many decades. This is also the case in MGs. It is noted that, recently, due to the increasing penetration of DC power sources such as PV, fuel-cell, battery energy storages, electric vehicles (EVs), modern DC loads, interests in various

MG configuration, particularly hybrid AC–DC MGs, are growing rapidly [8, 10–13]. As mentioned previously, generally MGs can be classified into three types of structures, namely AC-coupled, DC-coupled, and AC–DC-coupled MGs. Depending on the actual RESs and load types, appropriate MG structures can be designed and applied. Such hybrid AC–DC MG configurations, in which conventional AC power sources and electric appliances co-exist with DC power sources and modern DC loads, involve critical technical aspects.

Figure 5.1 shows a hybrid AC–DC MG. According to the classification presented in Chapter 1, this MG essentially belongs to the DC-coupled MG type. Solar PV panels and wind energy conversion systems are connected to a common DC bus through power electronic converters. The ESS is connected to the same DC bus through an AC–DC converter. The AC and DC buses are interconnected through a bidirectional AC–DC interlinking converter. Variable AC and DC loads are supplied by the AC and DC buses, respectively. Usually, a control center is needed to collect real-time information on the MG through a communication network. Such information will be processed, and then the control center delivers the control commands back to control the converters to regulate the power flow through the electric power link. This structure shown in Figure 5.1 can be applied when DC power sources are major power generation units in the MG. Note that in this structure, all the DGs and ESSs are connected to the DC bus. In this DC-coupled hybrid MG, some AC load can be connected directly to the AC bus, while other AC loads requiring variable frequency and variable amplitude can also be supplied with variable AC power as they can be connected to the DC bus through a DC–AC converter (to avoid the extra AC–DC rectification for AC bus connection). In this system, interlinking converters provide bidirectional power flow between AC and DC buses. Depending on the power exchange requirement such as power rating and reliability, more interlinking converters can be added in parallel between DC and AC buses. Even though it is not the main focus of this book, it is worth mentioning that, in future smart grid architecture, small MGs can be networked to each other via the distribution network operator (DNO). On top of that, a global central controller (GCC) is to coordinately control the networked MGs for flexible power exchange [14].

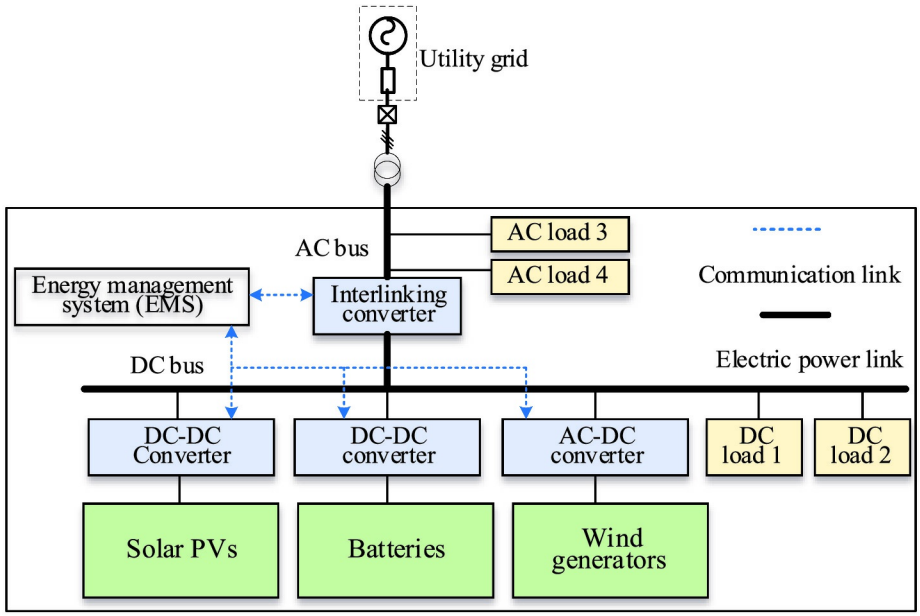


Figure 5.1 A hybrid AC–DC MG

Control of MGs with various loads and DGs has always been a challenging task. Unlike conventional power generation, RESs do not provide continuous electricity supply. Taking solar PV for example, usually, maximum solar irradiation occurs at around one o'clock with peak generation when the demand is not high for residential loads on a sunny day. On the other hand, the peak demand happens in the evening when there is no generation from PV systems. As a result, the usual peak production time and peak consumption time do not coincide, consequently affecting the system stability and degrading the overall system performance. With the increasing penetration of such renewable energy, the gap between generation and consumption will become more complicated.

The control of a hybrid AC–DC MG is still an open problem with on-going research. In such a MG, the common AC bus and the DC bus must be well maintained with stable voltages within acceptable ranges in terms of amplitude and frequency. To achieve this goal, effective system configurations associated with advanced control strategies are needed. In [15], a hybrid power network with various energy sources including wind, hydrogen and supercapacitor was proposed to manage the power exported into the grid. In this DC-coupled system, all the energy sources are interfaced to a common DC bus before connecting to the grid through the main inverter. The impact of variable load demand on the MG and the utility grid, however, is not studied. Another MG structure composed of fuel cells and PV arrays was studied in [16]. A coordinated operation of unit-power control and feeder-flow control was then designed to enhance system

stability and reduce the number of operating mode changes. A similar MG configuration was presented in [17]. In this work, a coordinated strategy for the battery, wind generator, and DC load management was proposed under variations of wind power generation and load. Hybrid AC–DC configurations where both AC bus and DC bus have distributed generation and loads have also been investigated [18].

Compared to the grid-connected mode, autonomous operation faces far more challenges. A critical requirement is to ensure the supply-demand balance within the MG. In [19], a hybrid AC–DC MG that can operate in grid-connected or islanded modes was studied. In islanded mode, the main AC–DC interlinking converter is controlled to generate stable AC voltage for the AC subgrid, while the DC-bus voltage in the DC subgrid is maintained by the bidirectional DC–DC converter. In grid-connected mode, the role of the AC–DC interlinking converter becomes maintaining a stable DC-link voltage and managing the power flows between the MG and the utility system. Since then, similar hybrid AC–DC MG topologies and power converters coordination control schemes have been adapted to achieve different control objectives [20–23]. The practical fluctuation nature of renewable energy resources, however, is not considered in this literature. More recently, a hybrid AC–DC MG comprised a DC MG and an AC MG interconnected through an interlinking converter is presented in [24]. Based on this structure, a V–I droop control scheme is applied in both DC and AC subgrids to improve system dynamics and mitigate frequency deviations while proportional load sharing can be achieved. In addition, a new voltage-voltage droop approach is developed for the interlinking converter to realize global power sharing with fast dynamic response. [25] presents a flexible testbed of a hybrid AC–DC MG. It consists of three AC DGs and six DC DGs that can be split into AC side, DC side, and interlinking side. This MG architecture allows to validate control schemes by experimental tests under various scenarios including load changes, plug-and-play and communication issues. In [26], a generic power flow algorithm is developed for unbalanced islanded hybrid AC–DC MGs. The proposed approach is based on the implicit Z_{BUS} method, showing fast convergence and robustness regardless of the R/X ratio of the lines. This research work focuses on a high-level power flow algorithm while the power converter coordination is not considered.

At the energy management level, many sophisticated energy management strategies have been developed and studied for different kinds of MGs. For example, an energy management and control system is proposed for a wind-PV-battery-based MG [27]. It enables stable operation of all subsystems within the MG under varying power demand and generation conditions. In [28], a distributed coordination control approach was developed to coordinate multiple converters interlinking the AC and DC subgrids for bidirectional power flows. A modular energy management system (EMS) based on mixed-integer linear programming is presented in [29] for in a PV-wind-battery-based MG. It can effectively reduce the operational costs and increase self-consumption based on 24-h ahead forecast data. Meanwhile, energy management schemes have also been studied for the control and optimization of microgrid clusters (MGCs). For instance, by taking

into account both network configuration and load dispatch, a power flow optimization scheme is introduced in [30] to reduce the total operational cost of a distribution network with interconnected MGs. In [31], a multiagent-based cooperative control is proposed to achieve user-defined objectives among the MG agents.

Despite the efforts mentioned above for hybrid AC–DC MGs, there are still technical problems that need to be solved before we can fully obtain the benefits brought by such hybrid MGs. First, as to the control of AC–DC interlinking converters, all the methods mentioned in Section 5.1 typically utilize an outer voltage loop and an inner current loop with proportional-integral-derivative (PID) controllers, leading to a relatively slow dynamic response. Besides, this structure requires complicated coordinate transformation, and much tuning effort is needed. To enhance system dynamic response ability, several alternative solutions including model predictive control (MPC) methods have been developed for inverters, either in grid-connected operation or islanded operation [32–35]. For example, a long-prediction model predictive current control is developed for grid-connected voltage source inverters with LCL filters [32]. The proposed method can achieve a constant switching frequency, which can ease the LCL filter design process. In [33], a strategy that incorporates selective harmonic elimination pulse width modulation (SHE-PWM) and a MPC for seven-level hybrid-clamped inverters is developed. Specifically, a unified SHE-PWM formulation is implemented for improved output waveform quality for high-power MV applications where low switching frequency is preferred. After the output voltage level signal from the SHE-PWM module is generated, an MPC controller is adopted for capacitor voltage balancing and fast dynamic response. In [34], an improved MPC is presented for stand-alone voltage source inverters. Instead of applying only one voltage vector in one control period, an optimal switching sequence with multiple vectors is chosen to reduce the output-voltage ripple with a constant switching frequency. In [35], a hierarchical MPC scheme is presented to autonomous operation and self-balancing cascaded multilevel inverters. The key idea is that the desired system performance is achieved by addressing each control objective hierarchically instead of formulating all control objectives in a single cost function. Thus, weight factors design can be eliminated. The recent advances of MPC discussed in Section 5.1 aim to obtain better system performance of inverters in terms of output voltages, currents, switching frequencies, computational burden, etc. However, they have not been designed for MGs where new challenges are the coordination of multiple power converters and variable power output from RESs. Second, the existing EMSs are designed mainly for either grid-connected mode or islanded mode. Yet, comprehensive EMSs considering different operating conditions have not been put forward. Third, grid synchronization and connection lack in-depth investigation. Without smooth grid synchronization and connection, power quality and system stability may be deteriorated, particularly during transients. Specifically, the main technical gaps to be addressed in this work are summarized as follows.

At the power converter level, as the electronic interfaces between the energy

resources and the common voltage buses, power converters should be able to fulfill proper power conversion accordingly. This can be achieved essentially by controlling the voltages and currents of the power converters. Since the AC–DC interlinking converter plays a significant role in power management and voltage regulation in an AC–DC hybrid MG, it will be focused on this work. Specifically, an MPC control strategy will be developed for the AC–DC interlinking converter for both islanded and grid-connected operations.

At the energy management level, the power balanced within the MG with various generation and loads should be kept so that stable operation of the system can be achieved. With this goal, an EMS on top will be designed, which will set the control demand for each power converter underneath to operate in a coordinated manner, considering different constraints such as state of charge (SoC) of batteries and fluctuating renewable power outputs.

5.2 Modeling of PV system and its control structure

The solar PV generator under study is shown in Figure 5.2. The solar modules are connected in series to form strings, which are further connected in parallel to form an array. The PV array supplies electrical power to the common DC link through a boost type DC–DC converter. The mathematical model of the solar module expressed by using output current and output voltage has been well established before in many literature such as [36]. Figure 5.3 shows the V–P characteristic of a SunPower Spr-305E-WHT-D solar array. It can be found that, under certain solar irradiance, the PV array outputs different power with different terminal voltages. Further, under different solar irradiance, the maximum power points of the power-voltage curves are corresponding to different terminal voltages. Therefore, to achieve maximum power point tracking (MPPT), we should adjust the PV output voltage accordingly, which can be done by using a boost DC–DC converter. It is noted that the ambient temperature also affects the PV outputs, although only the effect of solar irradiance is focused on in this study.

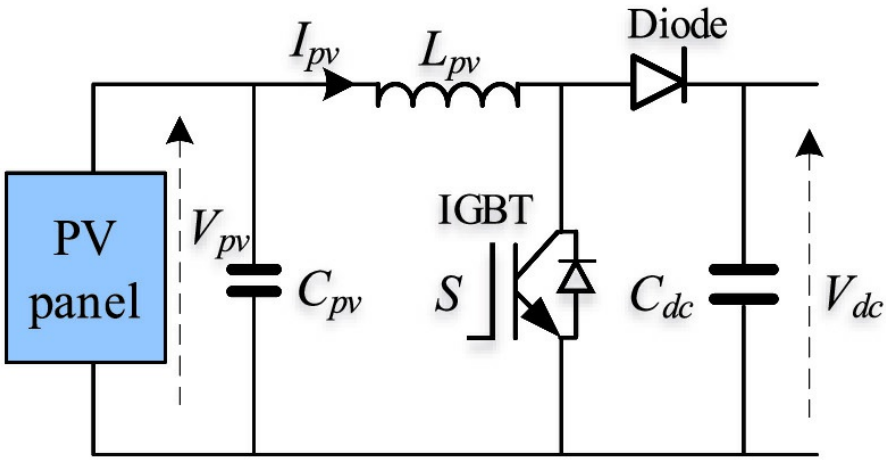


Figure 5.2 A solar PV power electronic system

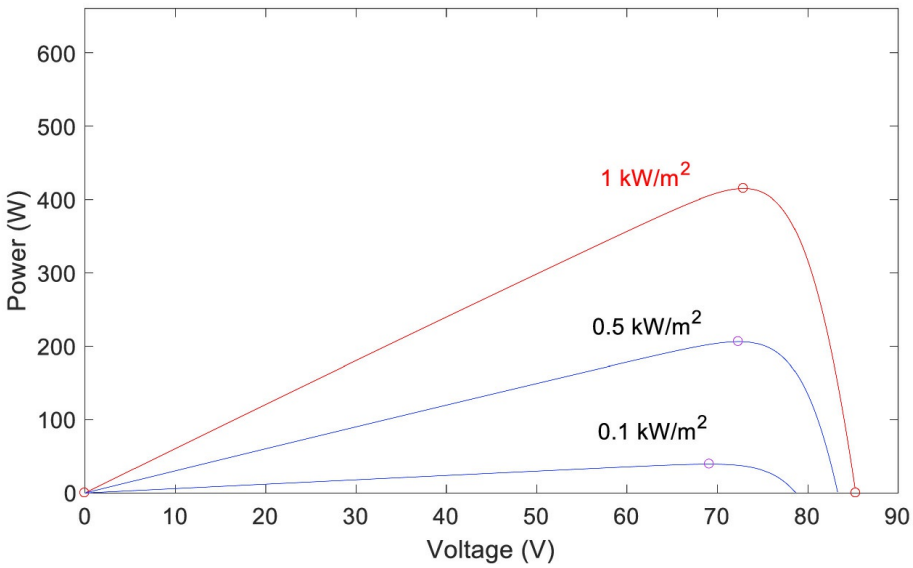


Figure 5.3 Output characteristics of a solar module

As explained previously, to obtain maximum power from the PV panel under various irradiance, the output voltage needs to be adjusted by controlling the boost DC–DC converter. The MPPT techniques of solar PV power generations have been widely developed and demonstrated, as discussed in Chapter 3. Here,

an incremental conductance method is utilized to track the maximum power point [37]. Notice that the boost converter should operate in either on-MPPT or off-MPPT by adjusting the duty cycle of the PWM signal, depending on the SoC of the battery and the power balance of the system. This will be further elaborated in Section 5.6.

5.3 Modeling of wind turbine system and its control structure

Figure 5.4 shows the structure of the wind energy conversion system in this study. The power captured by the wind turbine can be calculated by (3.1) and (3.2). Given a pitch angle, there is only one optimal value of λ that results in maximum C_p. Therefore, it is necessary to keep the shaft speed at an optimum value under a certain wind speed so as to produce maximum P_m. When the rotor rotates, it drives the permanent-magnet synchronous generator (PMSG) to spin so that three-phase AC voltage will be induced at the stator windings. It is noted that the optimal generator T_e–ω_r curve can be mapped based on the optimal turbine P_m–ω_m characteristic, where T_e is the generator electromagnetic torque and ω_r is the rotor speed. The mathematical models of the PMSG without saliency can be written as [27]

$$\begin{cases} \dfrac{di_{sd}}{dt} = -\dfrac{R_s}{L_d} i_{sd} + \dfrac{L_q}{L_d} p\omega_r i_{sq} + \dfrac{v_{sd}}{L_d} \\ \dfrac{di_{sq}}{dt} = -\dfrac{R_s}{L_q} i_{sq} - \dfrac{L_d}{L_q} p\omega_r i_{sd} - \dfrac{1}{L_q} p\omega_r \Phi_v + \dfrac{v_{sq}}{L_q} \end{cases} \tag{5.1}$$

where v_{sd} and v_{sq} are the *d*-*q* components of the stator voltage; i_{sd} and i_{sq} are the *d*-*q* components of the stator current; L_d and L_q are the *d*-*q* components of the stator inductance. R_s is the stator winding resistance. Φ_v is the magnetic flux linkage. p is the number of pole pairs. The electrical power is supplied from the PMSG to the DC bus through an electronic interface. For a small wind generator, a diode rectifier and a chopper with only one active switch are usually used. In high-power applications with large wind generators, full-scale voltage source PWM converters are commonly employed.

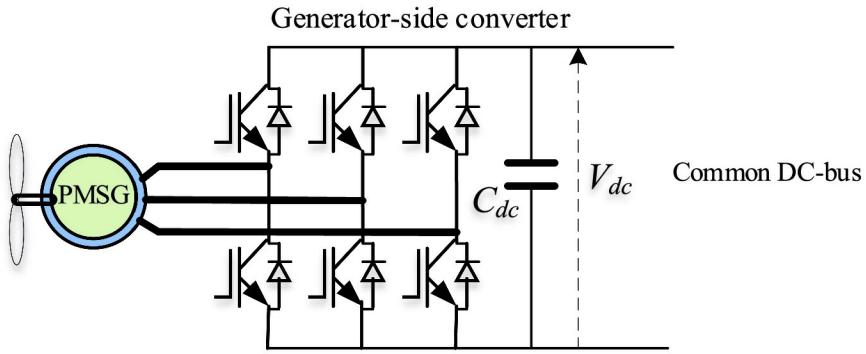


Figure 5.4 Wind power system structure

To extract maximum power from the wind energy, a control scheme without wind-speed sensor (anemometer) is used here. As pointed out in Chapter 3, different control methods have been developed for PMSGs in wind energy systems. Here, conventional cascaded linear control is adopted. Figure 5.5 helps describe the control principle. The generator torque reference is generated from the optimal T_e–ω_r curve according to the present rotor speed. The q component of the stator current will then be calculated from this torque reference together with inertia, pole pairs, and magnetic flux linkage of the generator. Subsequently, the stator voltage reference (i.e., required converter voltage) will be obtained according to (5.1) through PI control. Whether the generator accelerates or decelerates is determined by the error of the turbine torque and generator torque. If the optimal rotor speed is greater than the actual generator speed, the turbine torque will be larger than the generator torque, and the generator will speed up. On the other hand, the generator will decelerate if the required rotor speed for MPPT is lower than the generator rotating speed. Eventually, the turbine and generator torques settle down to the optimum torque point, and thus the wind turbine is controlled at the maximum power point. Similar to the solar PV system, the wind generator should operate in on-MPPT or off-MPPT, depending on the SoC of the battery and the power balance of the system.

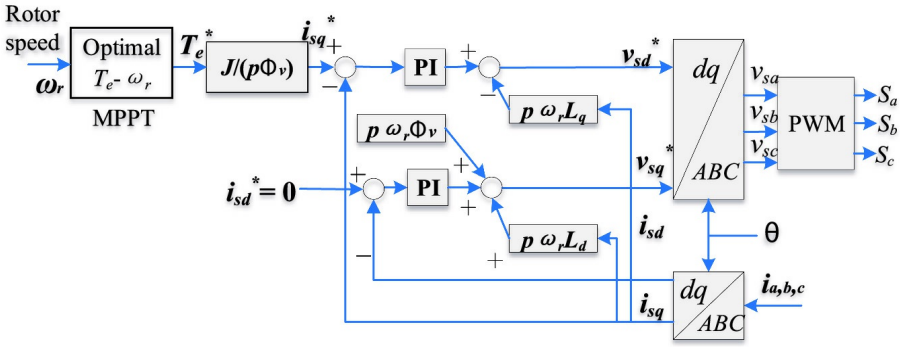


Figure 5.5 Control scheme of the generator-side converter

5.4 Modeling of ESS and its control structure

Figure 5.6 shows the ESS structure in the MG under study. Due to the intermittent nature of solar power and the variable load demand, ESS contributes to filling up the gap between power generation and consumption. Two useful and important parameters in a battery model are terminal voltage and SoC as [38].

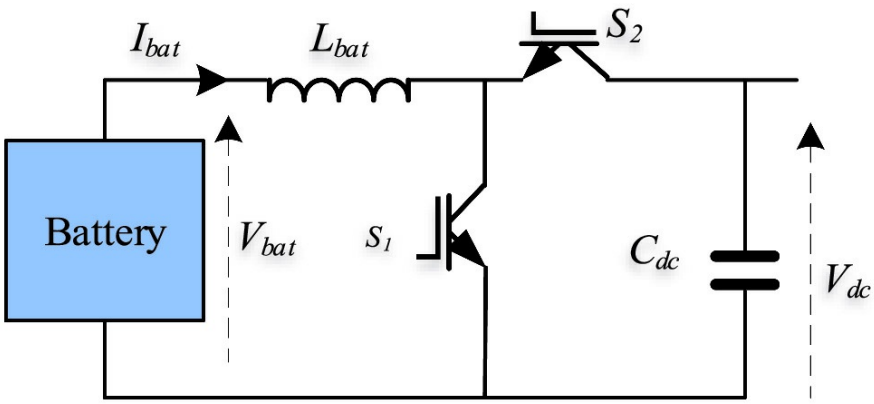


Figure 5.6 ESS

$$V_{bat} = V_o + R_{bat} I_{bat} - \frac{K Q_{bat}}{Q_{bat} + \int I_{bat} dt} + A_{bat} exp\left(B_{bat} \int I_{bat} dt\right) \quad (5.2)$$

$$SOC = 100\left(1 + \frac{\int I_{bat}dt}{Q_{bat}}\right) \tag{5.3}$$

where R_{bat} is the internal equivalent resistance of the battery, V_o the open-circuit voltage, I_{bat} the battery charging/discharging current, Q_{bat} the battery capacity, K the polarization voltage, A_{bat} the exponential voltage, and B_{bat} the exponential capacity. The battery current, whether charging or discharging, can be controlled by the bidirectional DC–DC converter.

The block diagram of the ESS control is shown in Figure 5.7. First, the battery current is measured and compared with the charging/discharging current reference. The error is then delivered to a PI controller to generate PWM switching signals. If the ESS is used to maintain the DC-bus voltage, then a two-loop control structure can be adopted by adding an outer loop to the original current loop [39]. The error between the measured DC-bus voltage and the reference is sent to a PI controller, the output of which is the reference current for the inner current loop. For better illustration, an example is provided here. When the DC-bus voltage is higher than the nominal level, a negative current reference will be generated from the outer voltage controller. Based on this negative current reference, the inner current loop then adjusts the PWM duty cycle to force the current flowing from the DC bus into the battery, leading to charging the battery. Subsequently, the DC-bus voltage will decrease to the reference as the excessive energy from the DC-link capacitor has been absorbed by the battery. During charging or discharging, attention should be paid to the SoC limits and the charging/discharging rates. These energy constraints of the battery can be described mathematically as

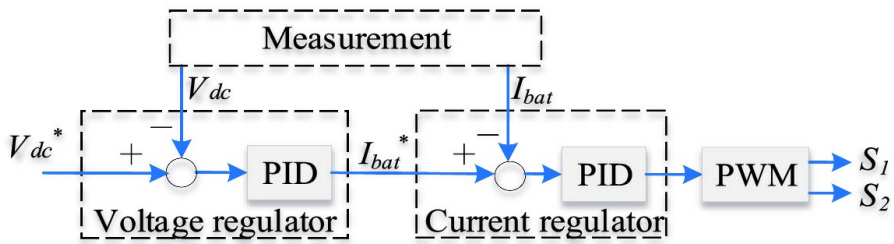


Figure 5.7 Control of the ESS

$$10\% \le SOC \le 90\% \tag{5.4}$$

$$-\frac{P_{Bat-N}}{V_{Bat}} \leq I_{bat} \leq \frac{P_{Bat-N}}{V_{Bat}} \tag{5.5}$$

where P_{Bat_N} is the battery rated powerand V_{Bat} the normal voltage.

5.5 Modeling of the AC subgrid and its control structure

Because of the merits like fast dynamic response and flexible inclusion of control objectives and constraints, MPC has been widely used to control bidirectional DC–DC converters and AC–DC converters [40, 41]. The major contribution of this work is to take one step further to develop a model predictive power and voltage control (MPPVC) approach for the AC–DC interlinking converter for hybrid AC–DC MG applications.

Figure 5.8 shows the AC-side circuitry of the MG. When the circuit breaker (CB) is turned ON and the bypass switch (BS) is switched OFF, the MG operates in grid-connected mode. The mathematical model based on this operation can be formulated as

$$\boldsymbol{V}_i = \boldsymbol{V}_g + \boldsymbol{I}_f R_f + L_f \frac{d\boldsymbol{I}_f}{dt} \tag{5.6}$$

where $\boldsymbol{V}_i$ and $\boldsymbol{V}_g$ are the converter voltage vector and the grid voltage vector, respectively; $\boldsymbol{I}_f$ the inductor current vector; R_f the line equivalent resistance; L_f the filter inductance. The output active and reactive powers supplied from the AC–DC interlinking converter to the utility grid can be computed as

$$P = \frac{3}{2} Re\left\{\boldsymbol{V}_g \boldsymbol{I}_f^*\right\} = \frac{3}{2}\left(V_{g\alpha} I_{f\alpha} + V_{g\beta} I_{f\beta}\right) \tag{5.7}$$

$$Q = \frac{3}{2} Im\left\{\boldsymbol{V}_g \boldsymbol{I}_f^*\right\} = \frac{3}{2}\left(V_{g\beta} I_{f\alpha} - V_{g\alpha} I_f\right) \tag{5.8}$$

Combining (5.6)–(5.8), the active and reactive powers at the end of the next sampling period can be predicted as

$$P^{k+1} = T_s\left[-\frac{R_f}{L_f} P^k - \omega Q^k + \frac{3}{2L_f}\left(|\boldsymbol{V}_g|^2 - Re\left(\boldsymbol{V}_g \boldsymbol{V}_i^*\right)\right)\right] + P^k \tag{5.9}$$

$$Q^{k+1} = T_s\left[\omega P^k - \frac{R_f}{L_f} Q^k - \frac{3}{2L_f} Im\left(\boldsymbol{V}_g \boldsymbol{V}_i^*\right)\right] + Q^k \tag{5.10}$$

where ω is the grid frequency in radians.

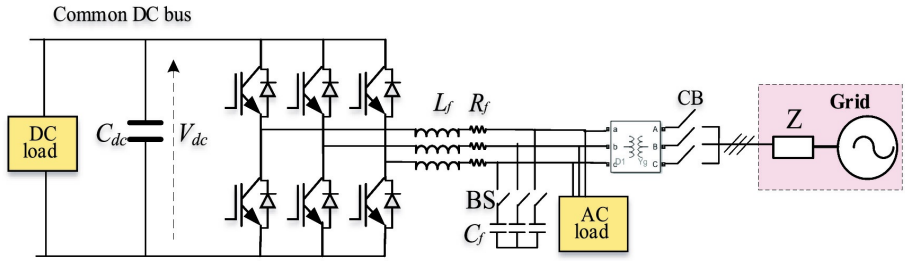


Figure 5.8 AC side of the MG

In grid-connected mode, the AC subgrid voltage is fixed by the utility grid rather than the interlink converter. Therefore, it can be used to regulate the power flow between the MG and the utility grid and to maintain a stable DC-bus voltage for DC loads. Since the active power flow between the AC and DC subgrids can be reflected on the DC-bus voltage, the active power reference is obtained from the outer voltage loop where a PI regulator is used to control the DC-bus voltage. When power source conditions or load demand change, the DC-bus voltage is maintained constant to keep the power balance within the system. Once the power references are determined, it is sent to the prediction model to estimate the power at the next sampling instant. A cost function is then formulated as a selection criterion to choose the optimum switching signals for the interlinking converter. Last, the switching option that can minimize the cost function is applied. Because the active and reactive powers injection into the grid are the control objectives in grid-tied mode, we can evaluate the effects of each control action on P and Q and through the cost function given below:

$$J_P = \left(P_{ref} - P^{k+1}\right)^2 + \left(Q_{ref} - Q^{k+1}\right)^2 \quad (5.11)$$

To isolate from the main grid, the CB is turned OFF and the BS is switched ON. In this case, the capacitor forms an LC filter together with the inductor for alleviating the harmonics in the converter output voltage. According to Kirchhoff's current law (KCL), the capacitor current can be obtained as

$$C_f \frac{d\boldsymbol{V}_C}{dt} = \boldsymbol{I}_f - \boldsymbol{I}_L \quad (5.12)$$

where C_f is the filter capacitance. $\boldsymbol{V}_C$ is the capacitor voltage vector (i.e., the load voltage vector). $\boldsymbol{I}_L$ is the load current vector. By applying Kirchhoff's voltage law

(KVL), the mathematical model of the AC subgrid can be written as

$$\boldsymbol{V}_i = \boldsymbol{I}_f R_f + L_f \frac{d\boldsymbol{I}_f}{dt} + \boldsymbol{V}_c \tag{5.13}$$

In islanded operation, the AC–DC interlinking converter is controlled to establish AC voltage in the AC subgrid. Thus, the task of maintaining the DC-bus voltage has to be carried out by the ESS. With this goal, the capacitor voltage should be the control objective of the model predictive voltage control (MPVC) controller. According to (5.12) and (5.13), the system model can be expressed as a state-space system

$$\frac{dx}{dt} = Ax + By \tag{5.14}$$

where

$$\mathrm{x} = \begin{bmatrix} \boldsymbol{V}_c \\ \boldsymbol{I}_f \end{bmatrix},\ \mathrm{y} = \begin{bmatrix} \boldsymbol{V}_i \\ \boldsymbol{I}_L \end{bmatrix},\ \mathrm{A} = \begin{bmatrix} 0 & 1/C_f \\ -1/L_f & -R_f/L_f \end{bmatrix}$$

$$\mathrm{B} = \begin{bmatrix} 0 & -1/C_f \\ 1/L_f & 0 \end{bmatrix}$$

(5.14) can be further expressed in discrete-time form by means of solving the linear differential equation, resulting in

$$x\left(k+1\right) = e^{T_S A} x\left(k\right) + A^{-1}\left(e^{T_S A} - \boldsymbol{I}_{2\times 2}\right) By\left(k\right) \tag{5.15}$$

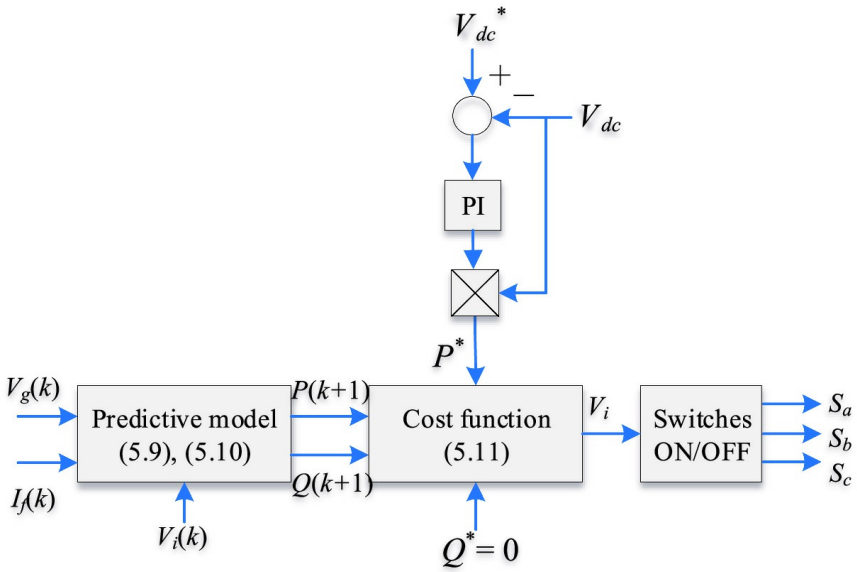
Therefore, the inductor current and capacitor voltage at (k+1)th instant can be predicted according to (5.15). To control the capacitor voltage tightly, the cost function is designed as

$$J_V = \left(V_{c\alpha}^{ref} - V_{c\alpha}^{k+1}\right)^2 + \left(V_{c\beta}^{ref} - V_{c\beta}^{k+1}\right)^2 \tag{5.16}$$

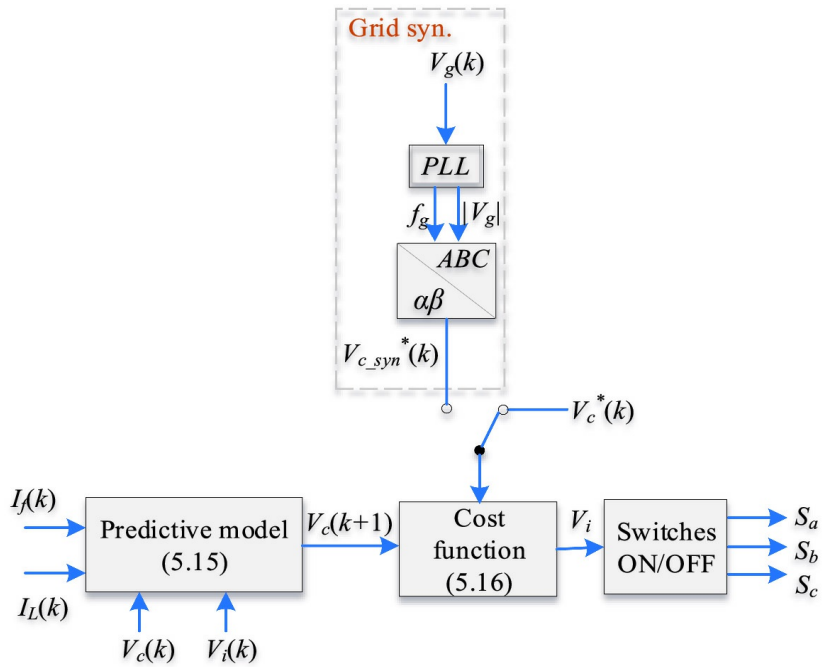
where V_c^{REf} is the nominal AC voltage of the AC subgrid. $V_{c\alpha}$ and $V_{c\beta}$ are the real and imaginary parts of the capacitor voltage vector, respectively. The voltage vector that can minimize (5.16) will be selected to control the converter for the next control period. Because the α and β components are controlled to track their sinusoidal references, respectively, the resulting voltage $\boldsymbol{V}_{\mathbf{c}}$ can present a stable and sinusoidal waveform.

When grid connection is necessary, grid synchronization proceeds. In Grid synchronization, phase-locked loop (PLL) is required to extract the grid information such as frequency and voltage magnitude. Then, a voltage with the same amplitude and a slightly lower frequency is set as V_c^{ref} in the cost function (5.16). As a result, the MG voltage will match the grid voltage in terms of amplitude, but apparently in a different angular speed. At instants when the phase angle of the MG AC voltage match that of the grid voltage, i.e., when the MG voltage phasor is aligned with the grid voltage phasor, grid connection can be carried out.

The block diagram of the proposed overall strategy is illustrated in Figure 5.9. To be specific, a model predictive power control (MPPC) for grid-connected operation and a MPVC for stand-alone operation and grid synchronization will be designed, respectively.


V_{dc}^*
+
−
V_{dc}
PI
P^*
$V_g(k)$
$I_f(k)$
Predictive model
(5.9), (5.10)
$P(k+1)$
$Q(k+1)$
$V_i(k)$
Cost function
(5.11)
V_i
$Q^* = 0$
Switches
ON/OFF
S_a
S_b
S_c

(a)


Grid syn.
$V_g(k)$
PLL
f_g
$|V_g|$
ABC
αβ
$V_{c_syn}^*(k)$
$V_c^*(k)$
$I_f(k)$
$I_L(k)$
Predictive model
(5.15)
$V_c(k)$
$V_i(k)$
$V_c(k+1)$
Cost
function
(5.16)
V_i
Switches
ON/OFF
S_a
S_b
S_c

(b)

Figure 5.9 Proposed control for the interlinking converter, (a) MPPC and (b) MPVC [4]

5.6 System level control

Previously, the power converter control, particularly MPC of the AC–DC interlinking converter, has been developed. Here, the system-level control is designed for energy management. The overall control strategy is depicted in Figure 5.10. For a hybrid AC–DC MG, different operation modes must be considered to ensure reliable power supply [4]. The power within the MG should be balanced as follows:

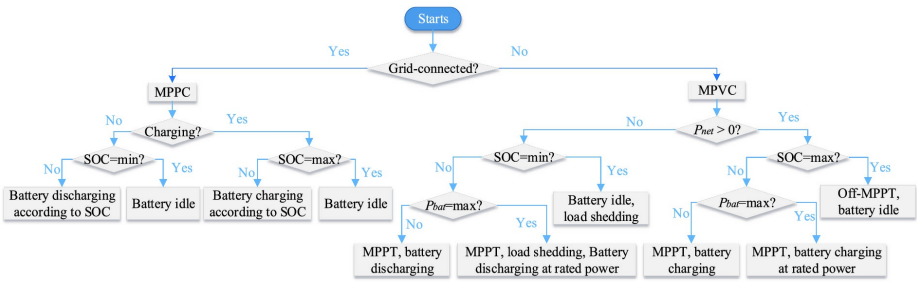


Figure 5.10 Energy management—system level control

$$P_{pv} + P_w + + P_{bat} + P_g - P_{loss} = P_{acL} + P_{dcL} \quad (5.17)$$

where P_{pv} and P_w are the power generated from solar PV and wind, respectively. P_{bat} is the power compensated by the battery; P_{loss} the total power loss; and P_g the power exchanged with utility. Positive P_{bat} indicates discharging while negative represents charging. Positive P_g means drawing power from utility whereas negative indicates injecting power to the utility. P_{acL} and P_{dcL} denote the power consumed by AC loads and DC loads, respectively. P_{net} is defined as P_{pv} and P_w subtracted by P_{acL}, P_{dcL} and P_{loss}.

5.6.1 Mode 1 operation

This mode refers to grid-connected operation. Any power deficit or power surplus within the MG is compensated by both ESS and the AC utility grid. In this case, obviously, the PV and wind generator should generate as much power as possible for the MG and the utility to increase revenue. With the support of the utility grid,

no load shedding is needed. The ESS can be charged or discharged by using closed current loop control. The AC–DC interlinking converter operates in the MPPC strategy to maintain the DC-bus voltage to enable power transfer between the DC subgrid and AC subgrid.

5.6.2 Mode 2 operation

For easy illustration, we denote the islanded mode as Mode 2 operation. Without the support from the main grid, the voltages at critical buses need to be maintained by DGs and the power balancing needs to be done within the MG. In this case, the DC-bus voltage is stabilized by the ESS through a two-loop control approach, while the AC-bus voltage is maintained by the AC–DC interlinking converter by using the proposed MPVC scheme, as detailed in Figures 5.7 and 5.9(b). Specifically, two scenarios need to be considered under this operation mode.

5.6.2.1 Low wind speed, low solar irradiation, and heavy load

Under this scenario, the power generated from PV and wind cannot meet the load demand. As a result, the ESS provides additional power by battery discharging while the PV and wind generator should continue to generate maximum power through MPPT. In an extreme situation when the power demand exceeds the power rating of the battery or the SoC hits the bottom, load shedding will be required for noncritical loads as the last resort to guarantee continuous power supply to critical loads.

5.6.2.2 High wind speed, high solar irradiation, and light load

On the other hand, if the generation from RESs is more than the power demand, the ESS is used to absorb the excess energy by charging the battery. If the battery has been fully charged or the charging current has reached the rated value, power curtailment from PVs and wind systems should be applied by deactivating MPPT.

5.6.3 Mode 3 operation

This mode covers the grid synchronization process prior to grid connection. Upon the grid connection demand is delivered from the control center, the grid synchronization process begins and the voltage across the AC subgrid terminal starts to follow the utility voltage. When the two voltages are aligned in terms of amplitude, phase angle, and frequency, the MG can be connected to the main grid. At any time before grid connection, this mode is still deemed as islanded mode, i.e, an extension of Mode 2. Similar to Mode 2, the DC-bus voltage is maintained by the ESS while the AC-bus voltage is established by the interlinking converter.

5.7 Case studies

The AC–DC hybrid MG shown in Figure 5.1 and the developed control method are verified in MATLAB/Simulink simulation. The generation and load parameters are listed in Table 5.1; 1 MW Load 1 and 0.5 MW Load 2 are constant resistances to represent linear load characteristics, while nonlinear loads are modeled by constant power type 1 MW Load 3 and 0.5 MW Load 4. The numerical simulation is studied in different operation modes under various generation and load conditions [4].

Table 5.1 Distributed generation and load parameters

Distributed generation	**Value**
Wind turbine	Base wind speed 12 m/s, R=31 m, C_p=0.47
PMSG	1.5 MW, L_d = L_q= 0.3 mH, Φ_V = 1.48 Wb, p = 48
Solar PV	SunPower Spr-305E-WHT-D, 2 MW
ESS	Lithium-ion battery, 1 MW, 300 V, 1.3 kA h
Power demand	**Value**
Linear loads	Critical Load 1—1 MW, noncritical Load 2—0.5 MW
Nonlinear loads	Critical Load 3—1 MW, noncritical Load 4—0.5 MW
Voltage level	**Value**
DC-bus voltage	1 200 V
DC-bus capacitor	6 mF
AC-bus voltage	0.69 kV
AC-bus LC filter	L = 0.6 mH, C = 1338 μF
Utility grid voltage	25 kV

5.7.1 Fluctuation output from renewable energy

The distributed renewable power generation units, solar PVs and the wind generator, are tested. First, the sunlight density is kept constant at 600 W/m^2, resulting in about 1.2 MW PV output. The wind speed steps down to 8 m/s at 5 s and steps up to 10 m/s at 15 s. Figure 5.11 shows the performance of the wind energy conversion system. Under variable wind velocity, it is observed that the rotating speed of the PMSG is adapted accordingly to maintain an optimal tip-speed ratio. As a result, the wind generator can capture the maximum wind energy and produce maximum electrical power.

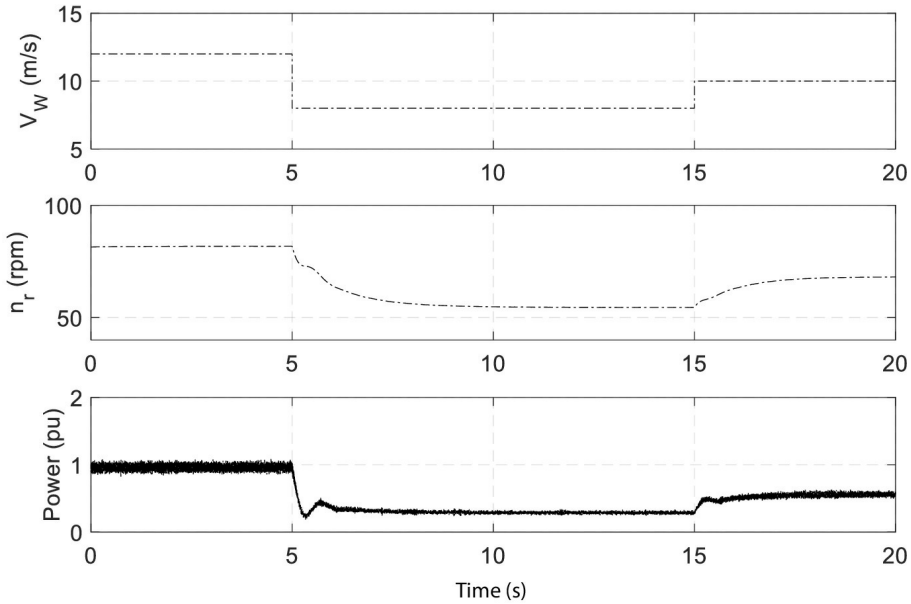


Figure 5.11 PMSG performance under wind speed variation

Then, wind speed is fixed at 10 m/s, while the solar irradiation increases from 400 W/m^2 to 1 000 W/m^2 and decreases afterward. The performance of the PV array is plotted in Figure 5.12. It is seen that the MPPT technique has been successfully implemented in the DC–DC boost converter. Specifically, the duty ratio of the PWM signals is controlled accordingly to adjust the PV terminal voltage so that the PV array can operate in MPP. Thus, it can be found that the PV output following the solar irradiance profile, increasing from about 0.8 MW to 2 MW and then decreasing gradually.

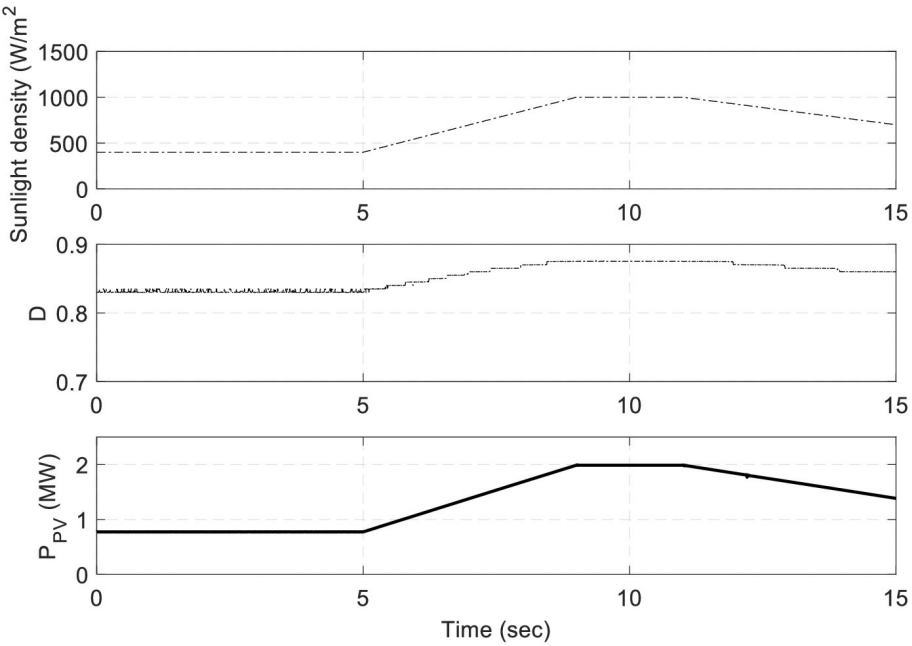


Figure 5.12 PV output under variable solar irradiation

5.7.2 Grid-connected operation

To demonstrate the effectiveness of the proposed control schemes and the reliable operation, a series of events have been imposed. In grid-connected mode, the solar irradiation level is kept constant at 600 W/m^2, resulting in about 1.2 MW power output. The wind generator produces fluctuating power, as shown in Figure 5.11. Loads 3, 2, 4, and 1 are switched on at 8 s, 11 s, 13 s, and 17 s, respectively. The system performance in different operation events is shown in Figure 5.13. Before the connection of Load 3 at 8 s, the power generated from the renewable energy resources exceed the load demand. In this case, the ESS absorbs about 0.5 MW power, as shown in Figure 5.13(b), while the excess is injected into the utility, as presented in Figure 5.13(d). Once Load 3 is switched in at 8 s, as the ESS is still controlled in a constant current charging mode, the power generated by PV and wind cannot meet the total power demand. As a result, additional power is drawn from the utility grid, leading to a reverse power flow, as demonstrated in Figure 5.13(d). After that, when Loads 2, 4, and 1 are further switched on subsequently, more power is imported from utility to the MG accordingly. It is noted that the voltage of the AC subgrid is supported by the stiff utility grid in the grid-connected operation, while DC subgrid voltage is maintained successfully by the AC–DC interlinking converter using the MPPC scheme, as shown in Figure 5.13(f).

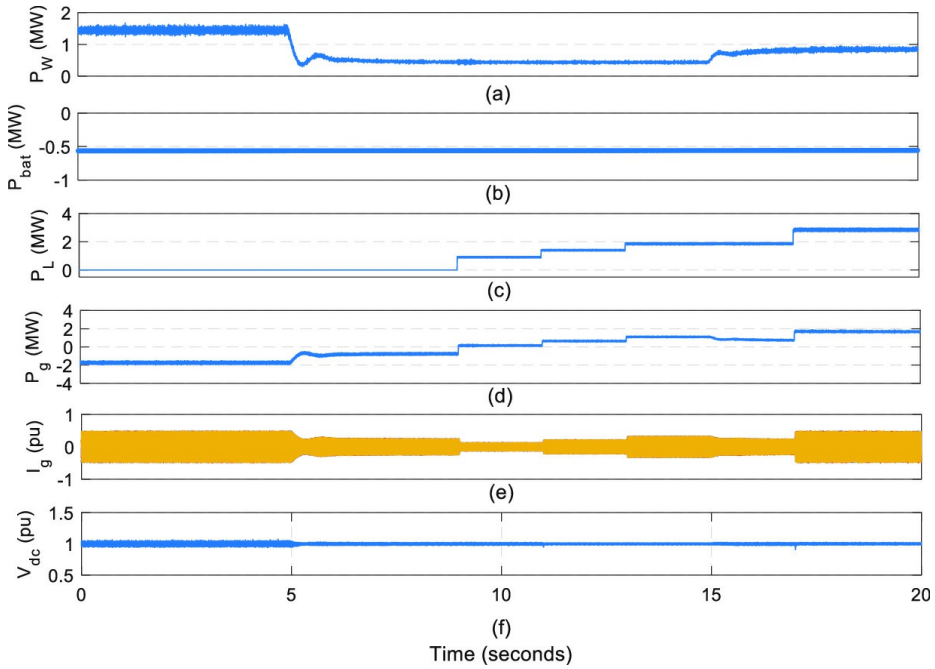


Figure 5.13 MG performance under variable wind power and load demand condition in grid-connected mode. The waveforms from top to bottom are (a) wind power, (b) battery power, (c) total load demand, (d) power exchanged between micro and utility grid, (e) current flow between micro and utility grid, and (f) DC-bus voltage.

5.7.3 Islanded operation

Without the support from the utility grid under islanded operation, the voltage will need to be established and the power balance will need to be maintained within the MG. In this scenario, the proposed MPVC method and the corresponding EMS strategy play an important role to achieve stable operation and provide high-quality power supply. To test the effectiveness of the proposed strategy, wind speed is fixed at 10 m/s, while the solar irradiation presents fluctuating feature shown in Figure 5.12. Load 3 (1 MW nonlinear load) is kept connected to the AC subgrid. Load variation sequence occurs as follows: Load 1 switched on at 9 s, Loads 2 and 4 switched on at 11 s.

The system performance of the MG is detailed in Figure 5.14. Before 11 s, the generation from PV and the wind generator is greater than power consumption. The surplus energy is absorbed by the ESS, leading to an increasing SoC. At 11 s, Loads 2 and 4 are connected simultaneously and the PV generation started to drop

due to the decrease in solar irradiance. The ESS responds quickly to bridge the power gap through discharging. At around 12 s, the ESS discharging current reaches the rated value, triggering the load shedding strategy. Thus, noncritical Load 4 is switched off.

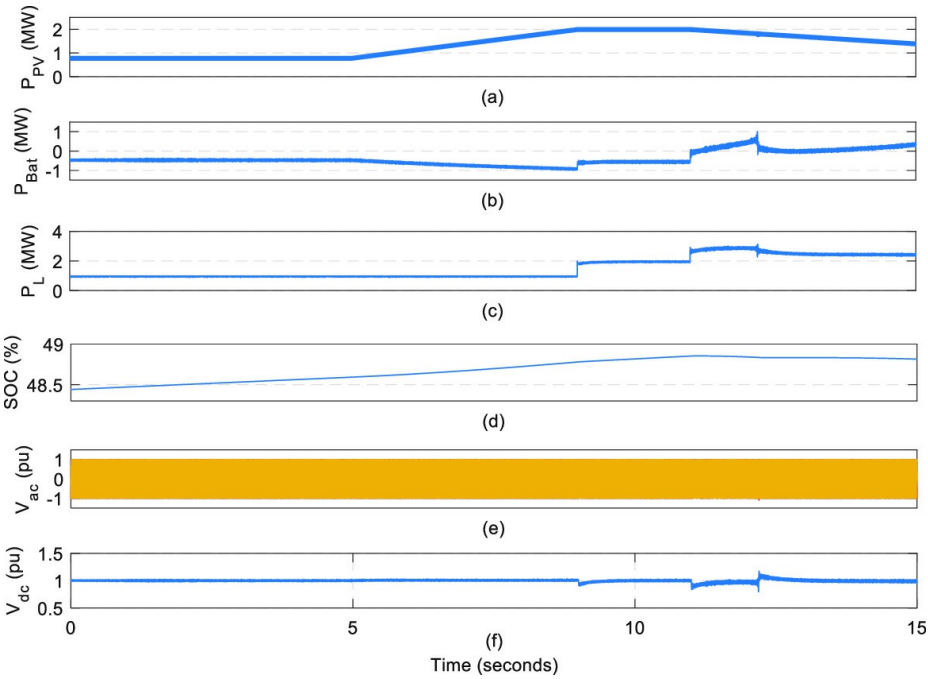


Figure 5.14 MG performance under variable PV power and load demand condition in islanded mode. The waveforms from top to bottom are (a) PV power, (b) battery power, (c) total load demand, (d) SOC, (e) AC-bus voltage, and (f) DC-bus voltage.

5.7.4 Grid-synchronization and connection

A smart MG should be endowed with fast grid synchronization and smooth transition from islanded operation to grid-connected mode. The AC–DC hybrid MG is tested here for such capability, as demonstrated in Figure 5.15. Initially, the MG is isolated from the main grid. Then the grid synchronization procedure begins at 0.05 s and the MG is connected to the utility grid at 0.2 s. Once the grid synchronization algorithm is activated, the AC–DC interlinking converter is controlled to enable the AC-subgrid voltage of the MG to track the utility grid voltage within 10 ms. Meanwhile, the DC-bus voltage is maintained at its reference during the whole process. It can be also seen that no overshoots in grid

current, AC-subgrid voltage and DC-subgrid voltage, proving a fast and safe grid connection process.

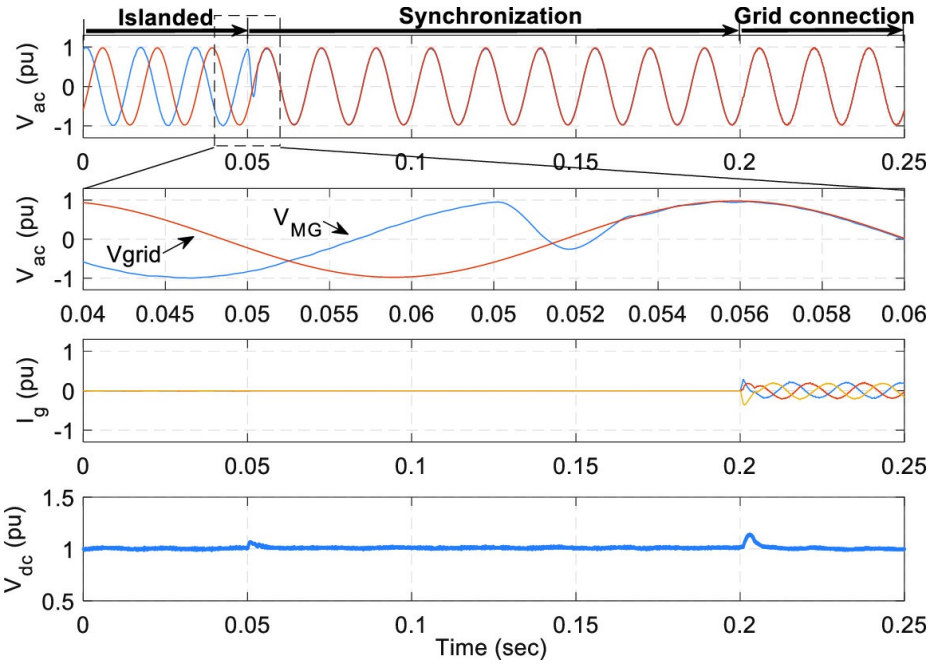


Figure 5.15 MG performance in grid synchronization and connection

5.8 Conclusion

In this research, a complete control strategy covering local-level power converter control and system-level energy management for a hybrid AC–DC MG with PV-wind-battery sources is developed. The main contribution of this work can be highlighted as follows. At the local level, the grid-interfaced power electronic converters are coordinated to cater to different operation modes and requirements. A model MPPVC method, which actually consists of a MPPC for grid-connected operation and a MPVC for islanded operation, is developed for the bidirectional converter interlinking the DC subgrid and AC subgrid, aiming to supply high-quality voltages at critical buses and to achieve fast and smooth grid synchronization and connection. At the system level, power balance under variable generation and consumption conditions is achieved by a sophisticated EMS. Satisfactory performance under various case studies has demonstrated the feasibility and effectiveness of the MG architecture and the proposed control strategy.

Despite the merits mentioned above, the following subsequent works can be done for possible further improvement.

1. As illustrated in the block diagram shown in Figure 5.9(a), even the cascade current loop has been eliminated in the proposed interlinking converter MPPC scheme for grid-connected operation, an outer voltage loop with PI regulators is still required to regulate the *d*-axis current or the active power flow that is reflected on the DC-bus voltage. Now the question is whether the function of this outer voltage loop can be integrated into the model predictive controller as well to form a fully cascade-less control structure.
2. Again, in grid-connected operation, the reactive power reference in the proposed MPPC scheme for interlinking converter can be utilized flexibly to provide grid support service according to actual grid requirement, rather than being set to zero.

References

[1] GWEC. *Global Wind Report*; 2019.
[2] International Energy Agency. *World Energy Outlook*; 2020.
[3] IRENA. *Future of solar photovoltaic – deployment, investment, technology, grid integration and socio-economic aspects*. International Renewable Energy Agency; 2019.
[4] Hu J., Shan Y., Xu Y., Guerrero J.M. 'A coordinated control of hybrid ac/dc microgrids with PV-wind-battery under variable generation and load conditions'. *International Journal of Electrical Power & Energy Systems*. 2019, vol. 104(6), pp. 583–92.
[5] Shan Y., Hu J., Chan K.W. Power sharing and V/f restoration of standalone AC microgrids using model predictive control. *Proceedings of 11th IET International Conference on Advances in Power System Control, Operation and Management*; 2018. pp. 1–5.
[6] Meng L., Luna A., Díaz E.R. 'Flexible system integration and advanced hierarchical control architectures in the microgrid research laboratory of Aalborg university'. *IEEE transactions on industry applications*. 2016, vol. 52(2), pp. 1736–49.
[7] Khaligh A. 'Battery, ultracapacitor, fuel cell, and hybrid energy storage systems for electric, hybrid electric, fuel cell, and plug-in hybrid electric vehicles: State of the art'. *IEEE Transactions on Vehicular Technology*. 2010, vol. 59(6), pp. 2806–14.
[8] Yi Z., Xu Y., Hu J., Chow M.-Y., Sun H. 'Distributed, neurodynamic-based approach for economic dispatch in an integrated energy system'. *IEEE Transactions on Industrial Informatics*. 2020, vol. 16(4), pp. 2245–57.
[9] Lam R.K., Yeh H.-G. 'PV ramp limiting controls with adaptive smoothing filter through a battery energy storage system'. *IEEE Green Energy and Systems Conference*. 2014, pp. 55–60.
[10] Nejabatkhah F., Li Y.W. 'Overview of power management strategies of

hybrid AC/DC microgrid'. *IEEE Transactions on Power Electronics*. 2015, vol. 30(12), pp. 7072–89.
[11] Kakigano H., Miura Y., Ise T. 'Low-voltage bipolar-type DC microgrid for super high quality distribution'. *IEEE Transactions on Power Electronics*. 2010, vol. 25(12), pp. 3066–75.
[12] Sahoo S.K., Sinha A.K., Kishore N.K. 'Control techniques in AC, DC, and hybrid AC-DC microgrid: a review'. *IEEE Journal of Emerging and Selected Topics in Power Electronics*. 2017, vol. 15(3), pp. 1238–50.
[13] Ouammi A., Dagdougui H., Dessaint L., Sacile R. 'Coordinated model predictive-based power flows control in a cooperative network of smart microgrids'. *IEEE Transactions on Smart Grid*. 2015, vol. 6(5), pp. 2233–44.
[14] Zhou T., Francois B. 'Energy management and power control of a hybrid active wind generator for distributed power generation and grid integration'. *IEEE Transactions on Industrial Electronics*. 2011, vol. 58(1), pp. 95–104.
[15] Khanh L.N., Seo J.-J., Kim Y.-S., Won D.-J. 'Power-management strategies for a grid-connected PV-FC hybrid system'. *IEEE Transactions on Power Delivery*. 2010, vol. 25(3), pp. 1874–82.
[16] Xu L., Chen D. 'Control and operation of a DC microgrid with variable generation and energy storage'. *IEEE Transactions on Power Delivery*. 2011, vol. 26(4), pp. 2513–22.
[17] Zhou H., Bhattacharya T., Tran D., Siew T.S.T., Khambadkone A.M. 'Composite energy storage system involving battery and ultracapacitor with dynamic energy management in microgrid applications'. *IEEE Transactions on Power Electronics*. 2017, vol. 26(3), pp. 923–30.
[18] Liu X., Wang P., Loh P.C. 'A hybrid AC/DC microgrid and its coordination control'. *IEEE Transactions on Grid*. 2011, vol. 2(2), pp. 278–86.
[19] Bhende C.N., Mishra S., Malla S.G. 'Permanent magnet synchronous generator-based standalone wind energy supply system'. *IEEE Transactions on Sustainable Energy*. 2011, vol. 2(4), pp. 361–73.
[20] Loh P.C., Li D., Chai Y.K., Blaabjerg F. 'Autonomous operation of hybrid microgrid with AC and DC subgrids'. *IEEE Transactions on Power Electronics*. 2013, vol. 28(5), pp. 2214–23.
[21] Loh P.C., Li D., Chai Y.K., Blaabjerg F. 'Autonomous control of interlinking converter with energy storage in hybrid AC–DC microgrid'. *IEEE Transactions on Industry Applications*. 2013, vol. 49(3), pp. 1374–82.
[22] Wang P., Jin C., Zhu D., Tang Y., Loh P.C., Choo F.H. 'Distributed control for autonomous operation of a three-port AC/DC/DS hybrid microgrid'. *IEEE Transactions on Industrial Electronics*. 2015, vol. 62(2), pp. 1279–90.
[23] Golsorkhi M.S., Heydari R., Savaghebi M. 'An adaptive droop control method for interlink converter N hybrid ac/dc microgrids'. *EPE'20 ECCE Europe*. 2020, pp. 1–10.
[24] Espina E., Burgos-Mellado C., Gomez J.S., *et al*. 'Experimental hybrid ac/dc microgrid prototype for laboratory research'. *EPE'20 ECCE Europe*. 2020, pp. 1–9.

[25] Pompodakis E.E., Kryonidis G.C., Demoulias C., Alexiadis M.C. 'A generic power flow algorithm for unbalanced islanded hybrid ac/dc microgrids'. *IEEE Transactions on Power Systems*, vol. 36(2), pp. 1107–20.
[26] Merabet A., Tawfique Ahmed K., Ibrahim H., Beguenane R., Ghias A.M.Y.M. 'Energy management and control system for laboratory scale microgrid based Wind-PV-battery'. *IEEE Transactions on Sustainable Energy*. 2017, vol. 8(1), pp. 145–54.
[27] Xia Y., Peng Y., Yang P., Yu M., Wei W. 'Distributed coordination control for multiple bidirectional power converters in a hybrid AC/DC microgrid'. *IEEE Transactions on Power Electronics*. 2017, vol. 32(6), pp. 4949–59.
[28] Luna A.C., Diaz N.L., Graells M., Vasquez J.C., Guerrero J.M. 'Mixed-Integer-linear-programming-based energy management system for hybrid PV-Wind-battery microgrids: modeling, design, and experimental verification'. *IEEE Transactions on Power Electronics*. 2017, vol. 32(4), pp. 2769–83.
[29] Tan S., Xu J.-X., Panda S.K. 'Optimization of distribution network incorporating distributed generators: An integrated approach'. *IEEE Transactions on Power Systems*. 2013, vol. 28(3), pp. 2421–32.
[30] Colson C.M., Nehrir M.H. 'Algorithms for distributed decision making for multiagent microgrid power management'. *Proceedings of IEEE Power Energy Society General Meeting*. 2011, pp. 1–8.
[31] Lim C.S., Goh H.H., Lee S.S. 'Long-prediction-horizon near-optimal model predictive grid current control for PWM-driven VSIs with *LCL* filters'. *IEEE Transactions on Power Electronics*. 2020, vol. 36(2), pp. 2246–57.
[32] Wu M., Tian H., Li Y.W., Konstantinou G., Yang K. 'A composite selective harmonic elimination model predictive control for seven-level hybrid-clamped inverters with optimal switching patterns'. *IEEE Transactions on Power Electronics*. 2020, vol. 36(1), pp. 274–84.
[33] Zheng C., Dragicevic T., Zhang Z., Rodriguez J., Blaabjerg F. 'Model predictive control of *LC*-filtered voltage source inverters with optimal switching sequence'. *IEEE Transactions on Power Electronics*, vol. 36(3), pp. 3422–36.
[34] Easley M., Shadmand M.B., Abu-Rub H. 'Hierarchical model predictive control of grid-connected cascaded multilevel inverter'. *IEEE Journal of Emerging and Selected Topics in Power Electronics*. 2020, pp. 1.
[35] Masters G.M. *Renewable and Efficient Electric Power Systems*. John Wiley & Sons; 2004.
[36] Banu I.V., Beniuga R., Istrate M. Comparative analysis of the perturb-and-observe and incremental conductance MPPT methods. *Proceedings of International Symposium on Advanced Topics in Electrical Engineering*; 2013. pp. 1–4.
[37] Tremblay O., Dessaint L.A., Dekkiche A.I. A generic battery model for the dynamic simulation of hybrid electric vehicles. *Proceedings of IEEE Vehicle Power and Propulsion Conference*; 2007. pp. 284–9.
[38] Hu J., Zhu J., Dorrell D.G. 'Model predictive control of grid-connected

inverters for PV systems with flexible power regulation and switching frequency reduction'. *Proceedings of IEEE Energy Conversion Congress and Exposition*. 2013, pp. 540–6.
[39] Ma T., Cintuglu M.H., Mohammed O.A. 'Control of a hybrid AC/DC microgrid involving energy storage and pulsed loads'. *IEEE Transactions on Industry Applications*. 2017, vol. 53(1), pp. 567–75.
[40] Hu J., Zhu J., Dorrell D.G. 'In-depth study of direct power control strategies for power converters'. *IET Power Electronics*. 2014, vol. 7(7), pp. 1810–20.
[41] Hu J., Zhu J., Zhang Y., Platt G., Dorrell D.G., Ma Q. 'Predictive direct control of doubly fed induction generator for grid synchronization in wind power generation'. *Proceedings of IEEE Energy Conversion Congress and Exposition*. 2011, pp. 2381–8.

Further reading

- Mahmud K., Rahman M.S., Ravishankar J., Hossain M.J., Guerrero J.M. 'Real-time load and ancillary support for a remote island power system using electric boats'. *IEEE Transactions on Industrial Informatics*. 2020, vol. 16(3), pp. 1516–28. doi:10.1109/TII.2019.2926511
- Wang L., Fu X., Wong M.-C.W. 'Operation and control of a hybrid coupled interlinking converter for hybrid AC/LVDC microgrids'. *IEEE Transactions on Industrial Electronics* 1. doi:10.1109/TIE.2020.3001802
- Gupta A., Doolla S., Chatterjee K. 'Hybrid AC–DC microgrid: Systematic evaluation of control strategies'. *IEEE Transactions on Smart Grid*. 2018, vol. 9(4), pp. 3830–43. doi:10.1109/TSG.2017.2727344
- Gupta A., Doolla S., Chatterjee K. 'Hybrid AC-DC microgrid: systematic evaluation of control strategies'. *IEEE transactions on smart grid*. 2018, vol. 9(4), pp. 3830–43.
- Mahmood H., Jiang J. 'Autonomous coordination of multiple PV/battery hybrid units in islanded microgrids'. *IEEE Transactions on Smart Grid*. 2017, vol. 9(6), pp. 6359–68. doi:10.1109/TSG.2017.2709550
- Li Z., Shahidehpour M. 'Small-signal modeling and stability analysis of hybrid AC/DC microgrids'. *IEEE Transactions on Smart Grid*. 2017, vol. 10(6), pp. 2080–95. doi:10.1109/TSG.2017.2788042
- Peyghami S., Mokhtari H., Blaabjerg F. 'Autonomous operation of a hybrid AC/DC microgrid with multiple interlinking converters'. *IEEE Transactions on Smart Grid*. 2018, vol. 9(6), pp. 6480–8.10.1109/TSG.2017.2713941
- Zhou Q., Shahidehpour M., Li Z., Che L., Alabdulwahab A., Abusorrah A. 'Compartmentalization strategy for the optimal economic operation of a hybrid AC/DC microgrid'. *IEEE Transactions on Power Systems*. 2019, vol. 35(2), pp. 1294–304. doi:10.1109/TPWRS.2019.2942273
- He L., Li Y., Guerrero J.M., Cao Y. 'A comprehensive inertial control strategy for hybrid AC/DC microgrid with distributed generations'. *IEEE Transactions on Smart Grid*. 2019, vol. 11(2), pp. 1737–47. doi:10.1109/TSG.2019.2942736

- Yoo H.-J., Nguyen T.-T., Kim H.-M. ‘Consensus-based distributed coordination control of hybrid AC/DC microgrids’. *IEEE Transactions on Sustainable Energy*. 2020, vol. 11(2), pp. 629–39. doi:10.1109/TSTE.2019.2899119
- Dabbaghjamanesh M., Kavousi-Fard A., Mehraeen S., Zhang J., Dong Z.Y. ‘Sensitivity analysis of renewable energy integration on stochastic energy management of automated reconfigurable hybrid AC–DC microgrid considering DLR security constraint’. *IEEE Transactions on Industrial Informatics*. 2020, vol. 16(1), pp. 120–31. doi:10.1109/TII.2019.2915089
- Zolfaghari M., Abedi M., Gharehpetian G.B. ‘Power flow control of interconnected AC–DC microgrids in grid-connected hybrid microgrids using modified UIPC’. *IEEE Transactions on Smart Grid*. 2019, vol. 10(6), pp. 6298–307. doi:10.1109/TSG.2019.2901193
- Tan K.T., Peng X.Y., So P.L., Chu Y.C., Chen M.Z.Q. ‘Centralized control for parallel operation of distributed generation inverters in microgrids’. *IEEE Transactions on Smart Grid*. 2012, vol. 3(4), pp. 1977–87. doi:10.1109/TSG.2012.2205952
- Bayhan S., Abu-Rub H. ‘Model predictive control based dual-mode controller for multi-source DC microgrid’. *Proceedings of 28th International Symposium on Industrial Electronics*. 2019, pp. 1–6.
- Poonahela I., Bayhan S., Abu-Rub H., Begovic M. ‘Implementation of finite control state model predictive control with multiple distributed generators in AC microgrids’. *IEEE 14th International Conference on Compatibility, Power Electronics and Power Engineering*. 2020, vol. 8-10, pp. 1–6.
- Sachs J., Sawodny O. ‘A two-stage model predictive control strategy for economic diesel-PV-battery island microgrid operation in rural areas’. *IEEE Transactions on Sustainable Energy*. 2016, vol. 7(3), pp. 903–13. doi:10.1109/TSTE.2015.2509031
- Pippia T., Sijs J., Schutter B.D. ‘A parametrized model predictive control approach for microgrids’. *IEEE Conference on Decision and Control*. 2018, vol. 17-19, pp. 1–6.
- Zheng Y., Li S., Tan R. ‘Distributed model predictive control for on-connected microgrid power management’. *IEEE Transactions on Control Systems Technology*. 2018, vol. 26(3), pp. 1028–39. doi:10.1109/TCST.2017.2692739
- Pahasa J., Ngamroo I. ‘Coordinated control of wind turbine blade pitch angle and PHEVs using MPCs for load frequency control of microgrid’. *IEEE Systems Journal*. 2016, vol. 10(1), pp. 97–105. doi:10.1109/JSYST.2014.2313810
- Lv Y., Yang P., Liu Z., Chen Y., Chen J. ‘Real-Time model predictive control for the regional autonomy multi-microgrids with three-phase/single-phase architecture’. *IEEE Conference on Innovative Smart Grid Technologies - Asia*. 2019, vol. 21-24, pp. 1–6.
- Morstyn T., Hredzak B., Aguilera R.P., Agelidis V.G. ‘Model predictive control for distributed microgrid battery energy storage systems’. *IEEE*

Transactions on control systems technology. 2018, vol. 26(3), pp. 1107–14. doi:10.1109/TCST.2017.2699159

- Zhao Y., Wu L., Song W., Ren W., Liu H. 'An evaluation index system for hybrid wind/PV/energy storage power generation system operating characteristics in multiple spatial and temporal scales'. *Proceedings of IET International Conference on Renewable Power Generation*. 2015, vol. 17-18, pp. 1–6.
- Xu M., Wu L., Liu H., Wang X. 'Multi-objective optimal scheduling strategy for wind power, PV and pumped storage plant in VSC-HVDC grid'. *The Journal of Engineering*. 2019, vol. 2019(16), pp. 3017–21. doi:10.1049/joe.2018.8435
- Puchalapalli S., Tiwari S.K., Singh B., Goel P.K. 'A microgrid based on wind-driven DFIG, DG, and solar PV array for optimal fuel consumption'. *IEEE Transactions on Industry Applications*. 2020, vol. 56(5), pp. 4689–99. doi:10.1109/TIA.2020.2999563
- Borowy B.S., Salameh Z.M. 'Methodology for optimally sizing the combination of a battery bank and PV array in a wind/PV hybrid system'. *IEEE Transactions on Energy Conversion*. 1996, vol. 11(2), pp. 367–75. doi:10.1109/60.507648
- Pradhan S., Singh B., Panigrahi B.K., Murshid S. 'A composite sliding mode controller for wind power extraction in remotely located solar PV–wind hybrid system'. *IEEE Transactions on Industrial Electronics*. 2019, vol. 66(7), pp. 5321–31. doi:10.1109/TIE.2018.2868009
- Nurunnabi M., Roy N.K., Hossain E., Pota H.R. 'Size optimization and sensitivity analysis of hybrid wind/PV microgrids -- A case study for Bangladesh'. *IEEE Access*. 2019, vol. 7, pp. 150120–40. doi:10.1109/ACCESS.2019.2945937
- Kellogg W.D., Nehrir M.H., Venkataramanan G., Gerez V. 'Generation unit sizing and cost analysis for stand-alone wind, photovoltaic, and hybrid wind/PV systems'. *IEEE Transactions on Energy Conversion*. 1998, vol. 13(1), pp. 70–5. doi:10.1109/60.658206
- Blakers A., Stocks M., Lu B., Cheng C., Stocks R. 'Pathway to 100% renewable electricity'. *IEEE Journal of Photovoltaics*. 2019, vol. 9(6), pp. 1828–33. doi:10.1109/JPHOTOV.2019.2938882
- Li X., Hui D., Lai X. 'Battery Energy Storage Station (BESS)-based smoothing control of photovoltaic (PV) and wind power generation fluctuations'. *IEEE Transactions on Sustainable Energy*. 2013, vol. 4(2), pp. 464–73. doi:10.1109/TSTE.2013.2247428
- Molla E.M., Kuo C.-C. 'Voltage sag enhancement of grid connected hybrid PV-wind power system using battery and SMES based dynamic voltage restorer'. *IEEE Access*. 2020, vol. 8, pp. 130003–13. doi:10.1109/ACCESS.2020.3009420
- Alharbi W., Bhattacharya K. 'Flexibility provisions from a fast charging facility equipped with DERs for wind integrated grids'. *IEEE Transactions on Sustainable Energy*. 2019, vol. 10(3), pp. 1006–14.

doi:10.1109/TSTE.2018.2857764
- Fathy A., Kaaniche K., Alanazi T.M. ‘Recent approach based social spider optimizer for optimal sizing of hybrid PV/wind/battery/diesel integrated Microgrid in Aljouf region’. *IEEE Access*. 2020, vol. 8, pp. 57630–45. doi:10.1109/ACCESS.2020.2982805
- Kalla U.K., Singh B., Murthy S.S., Jain C., Kant K. ‘Adaptive sliding mode control of standalone single-phase microgrid using hydro, wind, and solar PV array-based generation’. *IEEE Transactions on Smart Grid*. 2018, vol. 9(6), pp. 6806–14. doi:10.1109/TSG.2017.2723845
- Chishti F., Murshid S., Singh B. ‘Robust normalized mixed-norm adaptive control scheme for PQ improvement at PCC of a remotely located wind–solar PV-BES microgrid’. *IEEE Transactions on Industrial Informatics*. 2020, vol. 169(3), pp. 1708–21.
- Giraud F., Salameh Z.M. ‘Steady-state performance of a grid-connected rooftop hybrid wind-photovoltaic power system with battery storage’. *IEEE Transactions on Energy Conversion*. 2001, vol. 16(1), pp. 1–7. doi:10.1109/60.911395
- Arabali A., Ghofrani M., Etezadi-Amoli M., Fadali M.S. ‘Stochastic performance assessment and sizing for a hybrid power system of solar/wind/energy storage’. *IEEE Transactions on Sustainable Energy*. 2014, vol. 5(2), pp. 363–71. doi:10.1109/TSTE.2013.2288083
- Datta U., Kalam A., Shi J. ‘Battery energy storage system control for mitigating PV penetration impact on primary frequency control and state-of-charge recovery’. *IEEE Transactions on Sustainable Energy*. 2020, vol. 11(2), pp. 746–57. doi:10.1109/TSTE.2019.2904722
- Diab A.A.Z., Sultan H.M., Mohamed I.S., Kuznetsov O.N., Do T.D. ‘Application of different optimization algorithms for optimal sizing of PV/wind/diesel/battery storage stand-alone hybrid microgrid’. *IEEE Access*. 2019, vol. 7, pp. 119223–45. doi:10.1109/ACCESS.2019.2936656
- Caisheng W., Nehrir M.H. ‘Power management of a stand-alone wind/photovoltaic/fuel cell energy system’. *IEEE Transactions on Energy Conversion*. 2008, vol. 23(3), pp. 957–67. doi:10.1109/TEC.2007.914200
- Kusakana K. ‘Optimal scheduled power flow for distributed photovoltaic/wind/diesel generators with battery storage system’. *IET Renewable Power Generation*. 2015, vol. 9(8), pp. 916–24. doi:10.1049/iet-rpg.2015.0027
- Lin S., Wang Y., Liu M., Fan G., Yang Z., Li Q. ‘Stochastic optimal dispatch of PV/wind/diesel/battery microgrids using state‐space approximate dynamic programming’. *IET Generation, Transmission & Distribution*. 2019, vol. 13(15), pp. 3409–20. doi:10.1049/iet-gtd.2018.5840
- Ravada B.R., Tummuru N.R., Lingaiah B.N. ‘Photovoltaic-wind and hybrid energy storage integrated multi-source converter configuration-based grid-interactive microgrid’. *IEEE Transactions on Industrial Electronics*. 2021, vol. 68(5), pp. 4004–13.

Chapter 6
MPC of PV-ESS MGs with voltage support

This chapter investigates the impacts of microgrids (MGs) with high penetration of renewable energies on the distribution network. A model predictive power control (MPPC) scheme is presented to control and coordinate the DC–DC converter and inverter for grid-connected photovoltaic (PV) systems with energy storage system (ESS). By regulating the DC-bus voltage and controlling the active and reactive power flows, MPPC can support the power grid to maintain stable voltage and frequency and improve the power factor.

6.1 Introduction

The reduction of greenhouse gas emissions has been a significant task in global environment outlook. Recently, numerous government policies and incentives have been stipulated to promote the use of renewable energy sources (RESs). As one of the most popular and attractive RESs, the global accumulating solar PV power capacity has been increasing steadily. According to the International Energy Agency, solar PV power generation will contribute 16 percent of the world's electricity by 2050, 20 percent of which will come from residential installations [1].

Because of the intermittent solar irradiance and the variable load profile, PV systems are usually equipped with ESSs to fill the power gap between generation and consumption, and they can be further connected to the power grid for power injection [2]. In grid integration, power electronic converters serve as electronic interfaces between the power grid and RESs for power conversion [3, 4]. Solar PV systems can be classified into several operational configurations. Each configuration has the basic power electronic interfaces interconnecting the system to the utility grid [5]. As already described in Chapter 3, solar PV configurations can be generally categorized into centralized structures, string-array structures, and module structures. The centralized structure has been the most common option of PV installation over the past years. PV modules are connected in series and/or parallel before connected to a centralized DC/AC converter, i.e., inverter. The main advantage of this option is the reduced cost of power electronics

because only one inverter is needed. However, due to the mismatched solar output between PV modules and the utilization of string diodes, the power losses could be higher durating operation than other solutions. Another drawback is that this configuration presents a single point failure at the inverter, and thus is vulnerable to faults, leading to less reliability. As to string-array PV configuration, PV panels are connected in series to form strings. The main advantage of this topology is higher efficiency because no diodes are required and, hence, power losses during diode conduction can be avoided. More importantly, maximum power point tracking (MPPT) can be implemented on each PV string to maximize the solar power output. This is particularly useful when several strings are mounted on fixed surfaces in different operations. The shortcoming of this design is the increased cost due to the introduction of additional inverters. Another PV configuration is the module structure, in which each PV module is connected to a separate inverter. Obviously, this modular design facilitates the installation or removal of additional PV modules because each module has its own DC–AC inverter. The connection or disconnection to the utility can be easily done by connecting or disconnecting the inverter AC field wirings. The system reliability can experience an overall improvement because there is no single-point-of-failure. Compared to string-array option, the system overall efficiency can be even higher due to the possibility of MPPT operation on each PV module and the reduced mismatch among the modules.

In solar power generation, depending on the conditions and actual requirement, the PV converter topology can be various. So far, several proposed topologies have been studied and proved to be practically feasible [6, 7]. No matter what kind of topology is applied, eventually two major requirements must be satisfied, namely MPPT operation and power conversion (either DC–DC or DC–AC). Once again, as already mentioned in Section 6.1, the power electronics topologies in solar PV systems can be designed with a high degree of flexibility based on different factors, such as power rating, number of power processing stages, voltage level, the location of power decoupling capacitors, transformers used, and even the distribution feeder. Figure 6.1 shows a common PV-ESS configuration. The boost converter is used to regulate the PV panel terminal voltage for MPPT. The bidirectional DC–DC converter in the ESS is used to absorb excess energy by means of charging or to supply additional energy through discharging the battery. The grid-connected inverter converts the DC power into AC power for grid-connected operation.

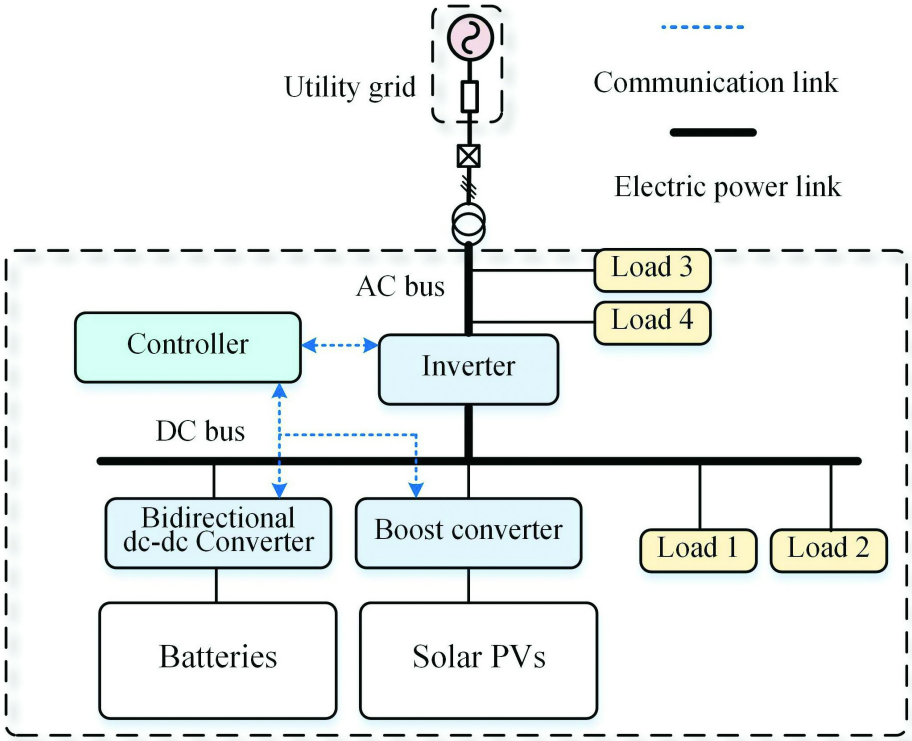


Figure 6.1 A PV-ESS configuration

There is ongoing research on the grid integration of PVs. However, large-scale grid integration of PVs is hindered by deployment, which faces its own distinct challenges in practice. On the one hand, variable energy generation of PVs because of stochastic sun radiation and, on the other hand, the mismatch between generation and load peaks in most of the network can cause voltage rise during the peak PV generation as well as voltage drop while meeting the peak load [8–10]. This problem would be more serious when PVs are connected in a low-voltage (LV) power grid at the distribution level. The ANSI C84.1 standard provides guidelines for the normal and emergency ranges of nominal 120 V power systems for both service and utilization cases [11]. According to the IEEE standard 1547, the maximum and minimum critical voltages are 1.1 p.u. and 0.88 p.u., respectively. Later, ±5 percent of nominal voltage is given by service voltage limits of IEEE Std 1547a-2014 [12, 13]. Many countries or regions around the world adopt these standards and specify their own requirement in voltage regulation.

So far, much effort has been paid by the research and industry communities to deal with voltage variations. The traditional approach to prevent the grid voltage variation is grid reinforcement or network upgrading [14]. Although this method

is effective, it is expensive. Another way is using the on-load tap changer (OLTC) transformers to raise the voltage at the distribution substation to keep the desired voltage along the feeder [15]. The major drawback of these conventional OLTCs is a high response time. The third traditional solution is placing capacitor banks along the feeder [16]. However, it is difficult to supply the exact reactive power demand by the use of switched capacitors. Flexible AC transmission system (FACTS) controllers [8], such as dynamic voltage restorer [17], static synchronous compensator [18], and unified power flow controller [19], can offer fast response characteristics by incorporating power electronics. Still, it is an expensive approach because of the large value of DC-bus capacitors and high-power switches.

Reinforcing the existing feeders or installing extra devices along the distribution network, as mentioned before, is typically expensive and takes additional time. Modifying a PV power system or operation is often the simplest solution. Curtailing the PV power generation can be applied during an overvoltage period [20]. In this method, the PV controllers stop applying MPPT algorithms and start curtailing real power to eliminate reverse power flow during the overvoltage period. However, it adversely affects PV owner revenues. Besides, this strategy is only effective during overvoltage period because curtailing PV outputs during undervoltage period would make things worse. Utilization of PV inverters' reactive power capability is one of the emerging technologies to address the voltage regulation issue in LV distribution networks with high PV penetrations. Different control schemes have been proposed using reactive power control. This method utilizes the ability of inverters to behave as small FACTS devices for voltage regulation. Based on this principle, decentralized grid voltage improvement approaches have been developed continuously in the last decade [21–24]. Actually, some commercial inverters such as SMA solar inverters have incorporated reactive capacity in industry applications [25, 26]. However, reactive power absorption requires higher current flow on distribution feeders, which leads to additional losses. Therefore, this approach must be implemented carefully by setting an accurate amount of reactive power for grid voltage regulation. Reactive and active power injection from solar PV inverters was proposed to mitigate overvoltages in [27]. It prioritizes the injection of reactive power, while the active power curtailment is performed only if overvoltage still exists after reactive power compensation.

Regarding PV inverter control, the cascaded linear control techniques have been commonly used for decades [28]. This control structure requires cascaded feedback loops as well as pulsewidth modulation, causing a relatively slow dynamic response. In a practical solar PV system, fluctuating power outputs from PV panels can cause oscillations in the DC-bus voltage, which, in turn, degrades the power quality on the AC side. As a result, traditional cascaded control may not be effective to alleviate this fluctuation. Another important aspect is the power flow between the utility grid and the PV system, which is usually managed by grid-connected inverters. Conventionally, the cascaded feedback loops with proportional-integral-derivative regulators are adapted to control the ESS DC–DC

converter and the grid-connected inverter [29–34]. In terms of controlling the ESS charging or discharging current, a simple inner current control loop can be employed [29–31]. For the grid-connected inverter, an outer voltage loop is used to maintain the DC-bus voltage with the *d*-axis current reference as the output, operating as a grid following inverter. In the inner current loop, the *d*-axis current is related to the active power flow, and the *q*-axis current is controlled to regulate the reactive power flow [32–34]. While the *d*-axis current reference is determined by the outer voltage loop, the setting of the *q*-axis current reference presents more flexibility. Usually, it can be set to zero for unity power factor operation. Using this conventional control method, the flexibility in power injection cannot be fully exploited because both the active and the reactive power flows between the PV system and the grid cannot be controlled in a straightforward manner. With the fast increase in penetration level of PVs in the LV distribution network, the voltage rise or drop has become a serious issue that deteriorates the power quality and grid stability [35, 36]. Flexible power regulation has become an important attribute of solar inverters to provide ancillary services.

To achieve fast power regulation, the PV system control method must be modified to directly control the active and reactive power injected into the point of common coupling (PCC) with the grid. Over the past few years, the model predictive control (MPC) scheme, in which the optimal switching state of the power converter is selected by evaluating all the possible control actions according to a specified cost function, has been applied to obtain better converter performance than conventional control methods [37–40]. So far, system-level algorithms have been developed to achieve a variety of objectives such as operational cost minimization [41], optimal power flow management [42], economic load dispatch [43], realizing voltage coordination [44], and stabilizing terminal voltages [45]. However, the MPC is rarely further investigated for power converter coordination in MGs. Also, flexible power injection by grid-connected solar inverters for voltage support (VS) has not yet been satisfactorily studied. At the device level, various MPC controllers for power converters are reviewed in [46, 47]. Examples include the following: as cascaded H-bridge (CHB) converters render reduced voltage stress on each power switch, they can be used to connect PV strings. Thus, [48] presents a phase-shifted MPC for CHB converters to achieve power balance under unbalanced power generation in different PV strings. In [49], a model predictive voltage control scheme is presented for three-level three-phase voltage source inverters (VSIs) for islanded PV systems. However, neither flexible power regulation nor VS is explored in this work. In [50], a MPC-based direct power-control method is presented for solar inverters in grid-connected applications. Although it can enable flexible active and reactive power injection into the grid, variable power outputs of solar PVs due to the fluctuating solar irradiance are ignored, which will affect the feasibility of the proposed controller. Besides, the root relationship between power flow and voltage deviation has not been revealed. Recently, an MPC strategy is developed to cope with the PV fluctuating output and stabilize the PCC voltage by controlling the ESS DC–AC converter [51]. Nevertheless, only the active power

regulation by ESS is exploited while the reactive capacity of the PV inverter is not utilized. In [52], an MPC algorithm is developed for a quasi-Z-source inverter in PV applications. The proposed controller can achieve maximum available power captured from the PV array. Also, it can decouple active and reactive power injection into the grid to ensure stable operation of the grid at the point of common coupling. In [53], a MPC scheme is incorporated with a PI control loop for DC–DC converters to step up voltages. Unfortunately, this method is not suitable for ESS charging and discharging, and the controller is not fully MPC-based. In [54], an MPC scheme is incorporated with the conventional droop method to control the parallel inverters in AC MGs. Once again, the fluctuating nature of renewable energy resources is not taken into account, and the grid-connected operation is not included when designing the controller. In [55], although the whole MG control is MPC-based, only stand-alone operation is focused, and the power regulation capability of the inverter is not exploited. In summary, to date, device-level control techniques of converters for flexible power regulation have not been satisfactorily developed for grid-connected PV systems.

In this work, a MPPC algorithm is developed for the control and coordination of the bidirectional DC–DC converter and inverter in a PV-ESS system shown in Figure 6.1. The active power is carefully chosen as the control objective for the bidirectional DC–DC converter, and both the active and the reactive power flows are set as the control objectives of the grid-connected inverter. The purpose of the proposed MPPC method is twofold. First, it can smooth the PV fluctuating output and maintain the stability of DC-link voltage through the ESS. Second, it can control the grid-connected inverter for flexible power flow between the PV-ESS system and the utility grid. Under grid voltage fluctuation, both the active and reactive power from the PV-ESS system can be used to support the grid.

In the field of power electronic converters development and application, the system parameters, including control parameters and physical circuitry parameters, have coupled effects on each other and, hence, on the system overall stability. Stability analysis has been a useful and necessary approach used by researchers and engineers to validate the feasibility of the developed control methods. Traditional stability analysis techniques, such as small-signal analysis, have been broadly studied and used for conventional control approaches. Nevertheless, the development of stability analysis of MPC methods is still at the beginning stage. Recently, MPC-based system-level stability has been reported [44, 56, 57]. However, to date, to our best knowledge, the robustness and stability analysis of converter-level MPC control have not yet been fully explored [46, 47]. One of the possible approaches is to conduct extensive simulations using different control parameters to evaluate the robustness and stability of the designed MPC controllers [46, 54]. Here in this research work, the robustness and stability of the proposed MPPC strategy are tested by gradually varying the LC filter settings. It is proved that the proposed MPPC scheme is highly stable and robust, as well as invulnerable to parameter variations. Obviously, this time-consuming stability analysis approach is not effective, especially for more complex MPC algorithm with many control parameters. Similar to small-signal techniques for conventional

linear control, systematic stability analysis technologies are highly desired for MPC.

6.2 Model predictive power control scheme

Conventionally, when a solar PV system equipped with energy storage is connected to the grid, its DC-bus voltage is controlled using an inverter, while an additional a buck-boost converter is required to regulate the ESS charging/discharging current according to the actual load demand and generation. After in-depth analysis, it can be found that this control structure presents limitations on the flexible power regulation capability because of the control requirement by the inverter for the DC-bus voltage. As a result, active and reactive power flows between the PV-ESS system and the grid cannot be fulfilled directly through the grid-connected inverter. The question now becomes whether it is possible to maintain the DC-bus voltage by controlling the DC–DC buck-boost converter rather than the inverter so that the inverter can be endowed with the control freedom on the bidirectional active and reactive power flows?

To address the above question and provide effective solutions, a comprehensive analysis of the system model is performed. Figure 6.2 shows the schematic configuration of the ESS, where a DC–DC converter is used to interface the battery with LV output with the high-voltage bus, also known as the DC-link. To facilitate the analysis, the schematic configuration of the ESS can be divided into two equivalent circuits, depending on the battery current direction, as shown in Figure 6.3. In boost operation, the battery supplies power to the DC-link through discharging, as depicted in Figure 6.3(a). By contrast, the battery absorbs power from the DC-link with I_B flowing into the battery. Notice that switches S_1 and S_2 operate in a complementary manner in both cases.

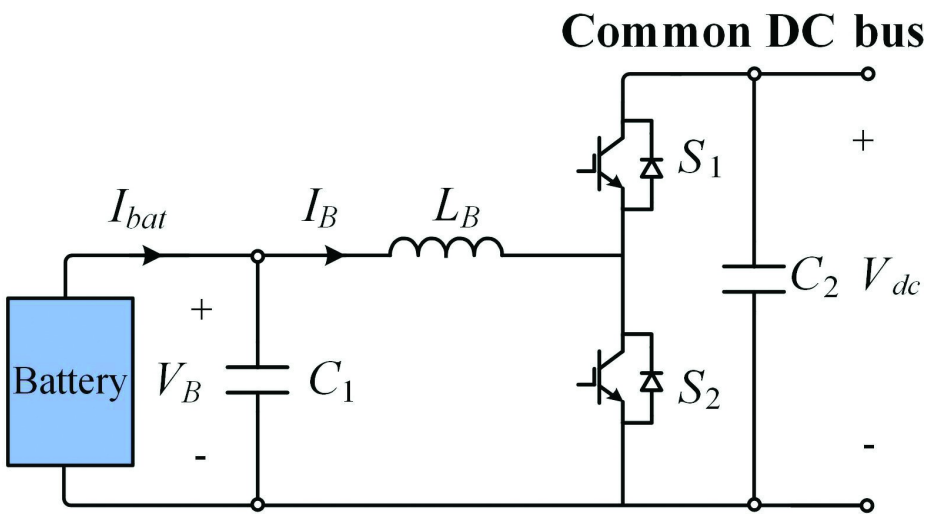


Figure 6.2 Schematic diagram of the ESS

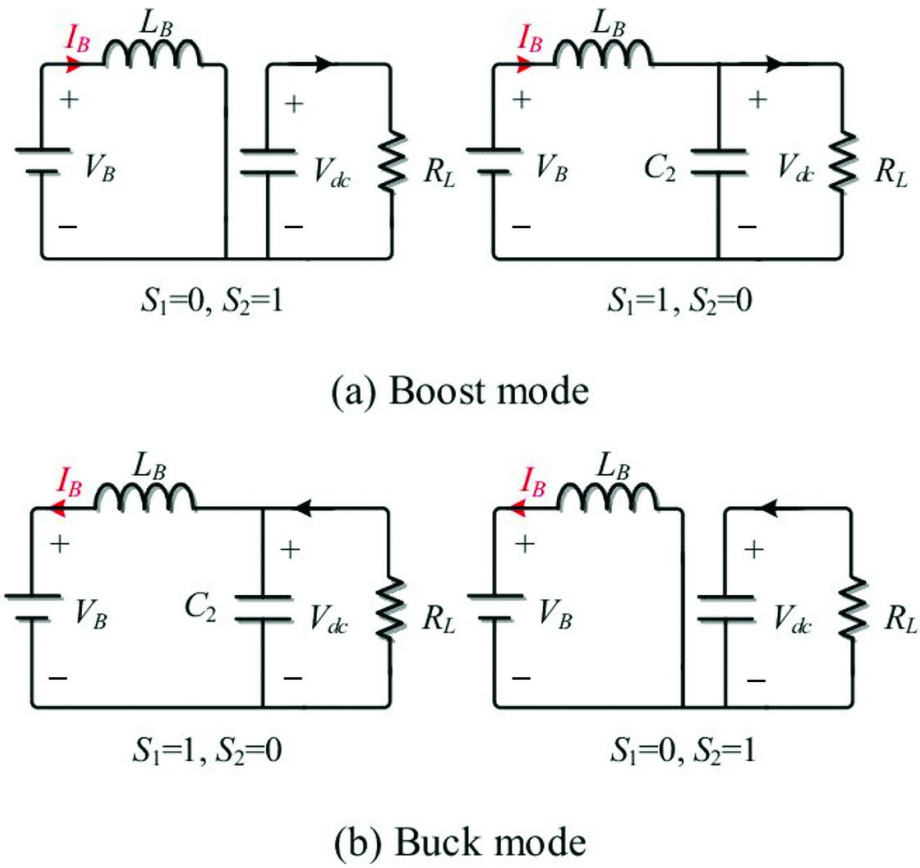


Figure 6.3 Equivalent circuits of (a) boost and (b) buck modes

According to Figure 6.3(a), the equivalent circuit in boost mode can be written mathematically as

$$\begin{cases} S_2 = 1,\ S_1 = 0: & L_B \dfrac{dI_B}{dt} = V_B \\ S_2 = 0,\ S_1 = 1: & L_B \dfrac{dI_B}{dt} = V_B - V_{dc} \end{cases} \tag{6.1}$$

Discretizing (6.1) with a sampling time T_S, the circuit model can be further expressed as

$$\begin{cases} S_2 = 1,\ S_1 = 0:\ I_B(k+1) = \frac{T_S}{L_B} V_B(k) + I_B(k) \\ S_2 = 0,\ S_1 = 1:\ I_B(k+1) = \frac{T_S}{L_B}\left(-V_{dc}(k) + V_B(k)\right) + I_B(k) \end{cases} \tag{6.2}$$

Correspondingly, the discrete-time models of the buck operation can be described as

$$\begin{cases} S_2 = 0,\ S_1 = 1:\ I_B(k+1) = \frac{T_S}{L_B}\left(V_{dc}(k) - V_B(k)\right) + I_B(k) \\ S_2 = 1,\ S_1 = 0:\ I_B(k+1) = -\frac{T_S}{L_B} V_B(k) + I_B(k) \end{cases} \tag{6.3}$$

Since charging and discharging processes are essentially determined by the battery current, it is necessary to establish the relationship of different currents flowing within the entire system. Figure 6.4 illustrates the current flows among the PV system, the ESS, and the rest of the MG (ROM).

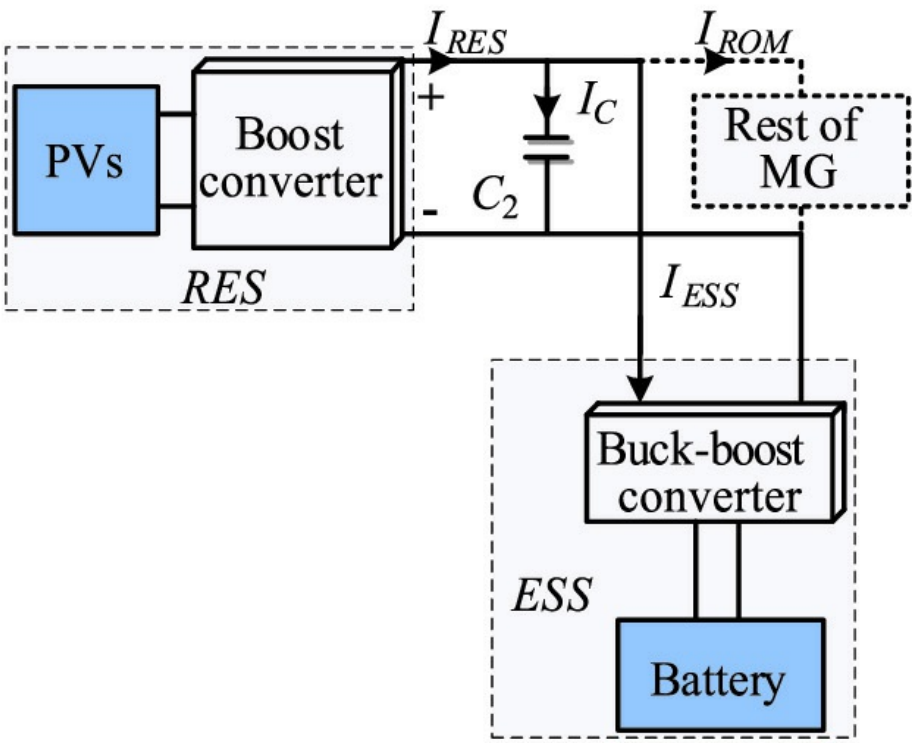


Figure 6.4 Currents flowing in the MG

According to Kirchhoff's Current Law, one can obtain

$$I_{ESS} = I_{RES} - I_C - I_{ROM} \tag{6.4}$$

where I_{ESS} is the current flowing into or out of the ESS being positive as charging and negative as discharging. I_{RES} is the current from the RES (PV system). I_C is the DC-bus capacitor current. I_{ROM} is the current flowing into the remaining parts of the MG, i.e., the current through the DC loads and the DC–AC VSI. As the power flow can be reflected on the DC-bus voltage across the capacitor, the required power from ESS to maintain the power balance of the system, and hence a constant DC-bus voltage, can be determined by

$$P^*_{ESS} = |I_{ESS} \cdot V^*_{dc}| \tag{6.5}$$

where $V_{dc}{}^*$ is the DC-bus voltage reference. In light of the relation between the current and voltage of a capacitor, here the DC-bus capacitor current at the (k+1)th time step can be predicted by

$$I_C\left(k+1\right) = \frac{1}{N}\left(\frac{C_2}{T_s}\left(V^*_{dc} - V_{dc}\left(k\right)\right)\right) \tag{6.6}$$

where N is an integer coefficient to limit the capacitor current [38], C_2 the capacitance of the DC-bus capacitor, and $V_{dc}(k)$ the DC-bus voltage at the kth time step. Substituting (6.6) into (6.4) with the assumption that both I_{RES} and I_{ROM} are unchanged during a short period T_s, one can predict the value of I_{ESS} at the next sampling instant as

$$I_{ESS}\left(k+1\right) = I_{RES}\left(k\right) - \frac{1}{N}\left(\frac{C_2}{T_s}\left(V^*_{dc} - V_{dc}\left(k\right)\right)\right) - I_{ROM}\left(k\right) \tag{6.7}$$

With the predicted ESS current, the required power from ESS in the next control instant for power balancing can now be computed according to (6.5) and (6.7) as

$$P^*_{ESS}\left(k+1\right) = \left|\left[I_{RES}\left(k\right) - \frac{1}{N}\left(\frac{C_2}{T_s}\left(V^*_{dc} - V_{dc}\left(k\right)\right)\right) - I_{ROM}\left(k\right)\right] \cdot V^*_{dc}\right| \tag{6.8}$$

Considering that the change in the battery voltage is relatively slow and the battery output current is equal to its inductor current in a steady state, the battery output power at the next time instant can be calculated as

$$P_{bat}\left(k+1\right) = \left|I_B\left(k+1\right) \cdot V_B\left(k\right)\right| \tag{6.9}$$

To achieve power balancing within the whole system, the power compensated by ESS is actually provided or absorbed by the battery. Consequently, the cost function of MPPC in ESS can be formulated as

$$\begin{aligned} J_P &= \left| P_{ESS}^{*}\left(k+1\right) - P_{bat}\left(k+1\right) \right| \\ s.t.\ SOC_{\min} &\le SOC \le SOC_{\max},\ I_{bat} \le \left| I_{bat\ rated} \right| \end{aligned} \tag{6.10}$$

where *SOC* is the state of charge and defined as

$$SOC = 1 - \frac{1}{Q_0}\int_0^t I_{bat}\left(t\right) dt$$

where Q_0 represents the total amount of charge in Ah stored in a battery, $I_{bat}(t)$ the battery current in A, and t the time in seconds. Now it can be seen that the measurement and prediction of the DC-bus voltage have been formulated in (6.8), while the tracking of the actual DC-bus voltage to its reference is implemented in (6.10).

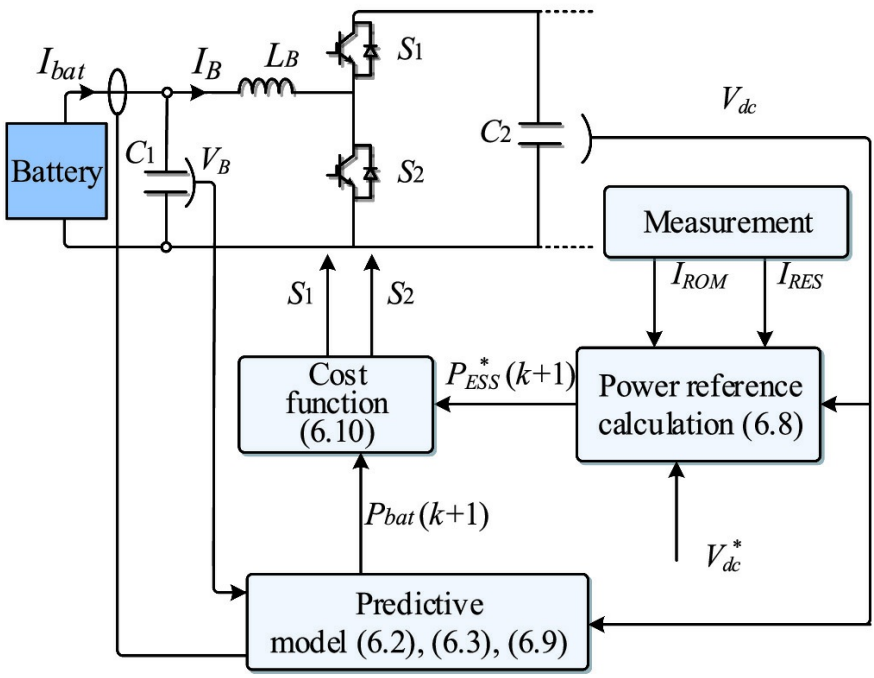


Figure 6.5 Block diagram of MPPC to control the DC–DC

bidirectional converter [58]

The proposed MPPC strategy for the buck-boost converter in the ESS is illustrated in Figure 6.5. The required ESS power can be calculated from the DC-bus voltage reference, V_{dc}^{*}, the PV system output current, I_{RES}, the DC-bus voltage, V_{dc}, the combination of DC load current and inverter input current, I_{ROM} according to (6.8). At the same time, the battery voltage and current and the actual DC-bus voltage will be used to predict the battery current $I_B(k+1)$, producing two possible values of $P_{bat}(k+1)$ by (6.2), (6.3), and (6.9). The optimal switching state that minimizes (6.10) will be selected to control the buck-boost converter. In this way, the DC-bus voltage across the capacitor can be maintained constant, which can function as the common DC-link for PV-ESS and also as the DC input for the grid-connected inverter.

Since the DC-bus voltage has been regulated using the bidirectional buck-boost DC–DC converter from the ESS, the grid-connected inverter or the DC–AC converter can now be endowed with more degrees of control freedom, e.g., to provide ancillary services on the grid side. As to the inverter operation, depending on the switching states of the six switches, there are totally eight voltage vectors as its outputs, which can be described in complex forms as

$$\boldsymbol{V}_i = \begin{cases} \frac{2}{3} V_{dc}^{*} e^{j(i-1)\frac{\pi}{3}} & (i = 1, 2, \ldots, 6) \\ 0 & (i = 0, 7) \end{cases} \tag{6.11}$$

Figure 6.6 presents the AC-side system. The mathematical model of the DC–AC converter can be expressed in the space phasor form as

$$\boldsymbol{V_i} = \boldsymbol{V_g} + \boldsymbol{I_f} R_f + L_f \frac{d\boldsymbol{I_f}}{dt} \tag{6.12}$$

where $\boldsymbol{V_g}$ and $\boldsymbol{V_i}$ are the grid voltage vector and the inverter output voltage vector, respectively, $\boldsymbol{I_f}$ denotes the inductor current vector, R_f being the equivalent resistance, and L_f being the filter inductance.

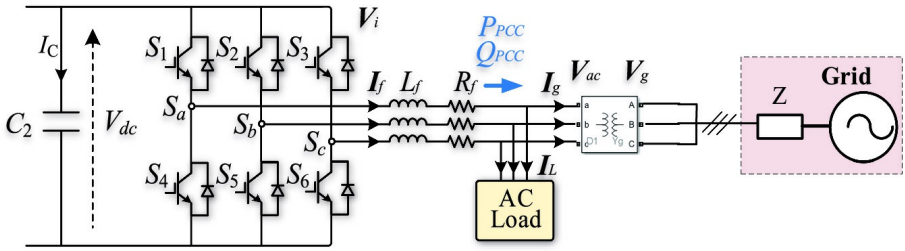


Figure 6.6 AC-side of MG

The output active and reactive power injected from the inverter into the AC common bus ($\boldsymbol{V}_{ac}$) or the PCC can be computed in the stationary $\alpha\beta$-plane as

$$P_{PCC} = \frac{3}{2}\mathrm{Re}\left\{\boldsymbol{V}_g\bar{\boldsymbol{I}}_f\right\} = \frac{3}{2}\left(V_{g\alpha}I_{f\alpha} + V_{g\beta}I_{f\beta}\right) \quad (6.13)$$

$$Q_{PCC} = \frac{3}{2}\mathrm{Im}\left\{\boldsymbol{V}_g\bar{\boldsymbol{I}}_f\right\} = \frac{3}{2}\left(V_{g\beta}I_{f\alpha} - V_{g\alpha}I_{f\beta}\right) \quad (6.14)$$

where $\bar{}$ denotes the complex conjugate, Re{} the real component, and Im{} the imaginary component. According to (6.11)–(6.14), the active and reactive power flows at the end of next sampling instant can be predicted as [58]

$$P_{PCC}(k+1) = T_s\left[-\frac{R_f}{L_f}P_{PCC}(k) - \omega Q_{PCC}(k) + \frac{3}{2L_f}\left(|\boldsymbol{V}_g|^2 - Re\left(\boldsymbol{V}_g\bar{\boldsymbol{V}}_i\right)\right)\right] + P_{PCC}(k) \quad (6.15)$$

$$Q_{PCC}(k+1) = T_s\left[\omega P_{PCC}(k) - \frac{R_f}{L_f}Q_{PCC}(k) - \frac{3}{2L_f}Im\left(V_g\bar{V}_i\right)\right] + Q_{PCC}(k) \quad (6.16)$$

where ω is the grid frequency in radians. Since the active and reactive power flows are the control objectives in the grid-connected PV system, the following cost function is designed to evaluate the effects of each voltage vector on P_{PCC} and Q_{PCC} as

$$J_P = \left(P_{ref} - P_{PCC}(k+1)\right)^2 + \left(Q_{ref} - Q_{PCC}(k+1)\right)^2 \quad (6.17)$$

The proposed MPPC scheme for the grid-connected inverter is explained in Figure 6.7. The inductor current vector, $\boldsymbol{I}_f$, the converter voltage vectors, $\boldsymbol{V}_i$, and the grid voltage, $\boldsymbol{V}_g$, are used to predict active and reactive powers. The switching state that can minimize (6.17) with the input active power reference P_{ref} and reactive power reference Q_{ref} will be selected, and the switches will be turned on

or off correspondingly to control the inverter. It is noted that a positive P_{ref} indicates the active power flows from the grid to the DC-bus, and vice versa. Similarly, a positive Q_{ref} indicates inductive reactive power injection into the grid, while a negative Q_{ref} means capacitive reactive power compensation. By specifying a flexible amount of P_{ref} and Q_{ref} within the system rated capacity, the PV-ESS can support and compensate the grid voltage to some degree.

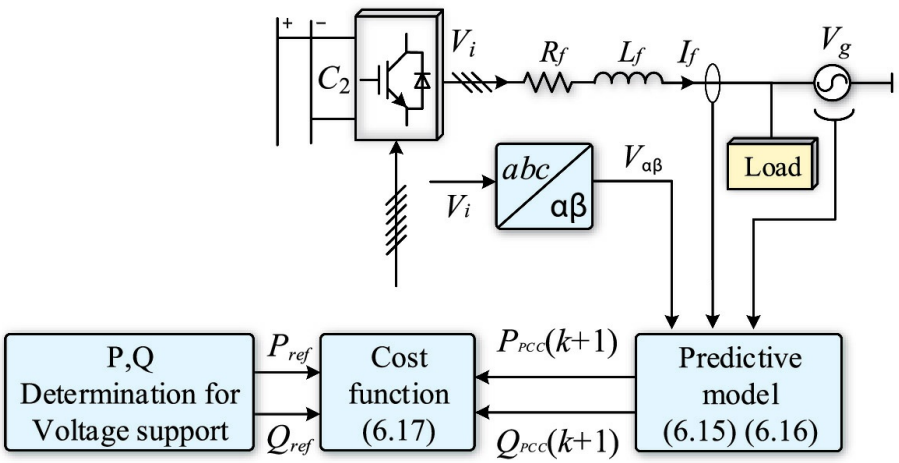


Figure 6.7 Block diagram of MPPC for the DC–AC converter connected to the grid [58]

6.3 Voltage support

In the Section 6.2, a MPPC algorithm has been developed for PV-ESS systems to offer a higher degree of control freedom for injecting active and reactive powers into the grid. Now, the remaining questions are how to fully utilize this flexible power injection capability and how this capability is limited by the PV-ESS power rating as well as the inverter capacity. In traditional power networks, the power flows in a one-way direction, from generation, transmission, distribution, to the end users. Under this power architecture, one common measure to stabilize the voltage is to install high-power voltage regulators at specified locations along the distribution network. This method has two limitations. First, such high-power voltage regulators are usually installed far away from the regional communities. As a result, the voltage at these residential areas, particularly small towns at the end of the feeder, is not well regulated. Second, in a power electronics-rich power grid, the voltage along the feeder can drop or rise in a time scale of a few seconds or even micro-seconds. Conventional voltage regulators, such as capacitor banks and OLTCs, may not be able to respond quick enough to compensate voltage

fluctuation. With the increasing penetration of RES and modern loads into the power grid, reverse power flows can make the voltage variation more complicated [59]. On the other hand, modifying the grid-connected distributed generation units near the customers or operating them in a decentralized manner is often the simplest but effective solution. One of the emerging techniques to address the voltage variation issue is to coordinate the active and reactive power injection of grid-connected solar inverters.

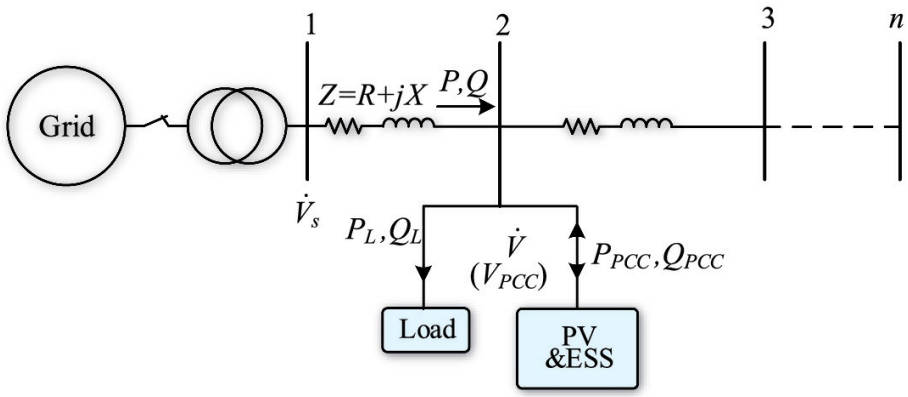


Figure 6.8 Single-line diagram of power flows

Figure 6.8 presents a single-line radial distribution feeder. The distribution transformer is located at Bus 1, the beginning of the feeder with voltage $\dot{V}_s$. Bus 2 is the AC common bus (i.e., the PCC) of the MG with voltage $\dot{V}$. $Z = R+jX$ denotes the impedance of the feeder, and P and Q, P_{PCC} and Q_{PCC}, and P_L and Q_L are the active and reactive powers from the feeder, the PV-ESS system, and the load, respectively. When Q_{PCC} is positive, the PV-ESS system supplies the inductive reactive power. Whereas if Q_{PCC} is negative, the PV-ESS system compensates the capacitive reactive power. Similarly, when P_{PCC} is positive, the PV-ESS system exports active power. Otherwise, the PV-ESS system imports active power from the grid.

Based on the basic theory of power flows, the voltage deviation from Bus 1 to Bus 2 can be expressed as

$$\Delta \dot{V} = \frac{RP+XQ}{\dot{V}} + j\frac{XP-RQ}{\dot{V}} \tag{6.18}$$

where the power exchange among the feeder, the PV-ESS system, and the local loads can be described as

$$P = P_L - P_{PCC} \tag{6.19}$$

$$Q = Q_L - Q_{PCC} \tag{6.20}$$

Considering the high R/X ratio in a LV distribution network, the voltage drop equals approximately the real part of (6.18) as [60]

$$V = V_s - \frac{R\left(P_L - P_{PCC}\right) + X\left(Q_L - Q_{PCC}\right)}{V} \tag{6.21}$$

According to (6.21), it can be revealed that Bus 2 voltage will change as the load changes. Especially, under a significant load variation, the voltage may fluctuate beyond the rated range, jeopardizing the safe operation of the grid. Necessary measures should be taken to mitigate the voltage deviation. To address this problem, a VS strategy by controlling both the active and the reactive power flows is proposed in this study. The real-time voltage at Bus 2 is measured. Once a voltage drop caused by the load is detected, the VS controller will send the power correction signals (ΔP and ΔQ) to the MPPC controller as power references (P_{ref} and Q_{ref}). The power compensation can be computed by [58]

$$\Delta P = P_{ref} = \left(V_{t+1} - V_{t-1}\right) \times 100\% \times m_W \tag{6.22}$$

$$\Delta Q = Q_{ref} = \left(V_{t+1} - V_{t-1}\right) \times 100\% \times m_{Var} \tag{6.23}$$

where $t + 1$ and $t - 1$ mean the sampling instants after and before the load change; m_W and m_{Var} denote the coefficients of the active and reactive power compensation, respectively. In this way, the PV-ESS system can provide corresponding active and reactive power compensation according to the actual PCC voltage variations. It is worth mentioning that (6.22) and (6.23) designed here is just a simplified mechanism to test the potential grid support capability of the PV-ESS system. In the actual implementation in a smart grid with high PV penetration, the amount of ΔP and ΔQ supplied by each PV-ESS unit should be calculated accurately by considering several factors such as inverter capacity, grid voltage variations, available P and Q from PV-ESS, and the transmission line R/X ratio.

After ΔP and ΔQ are determined by (6.22) and (6.23), they will be sent to the MPPC controller as the active and reactive power references, P_{ref}, Q_{ref}, as explained in Figure 6.7. Due to the feature of the MPPC control algorithm, once the voltage deviation is detected, the corresponding active and reactive power flows can be injected into the grid with a fast dynamic response to improve the voltage. Here, it is necessary to emphasize that a PV-ESS grid-connected inverter

is not an infinite source of real power or an infinite sink of reactive power. The amount of both active and reactive power flows is limited by the rated inverter capacity. This is illustrated in Figure 6.9 by a phasor diagram.

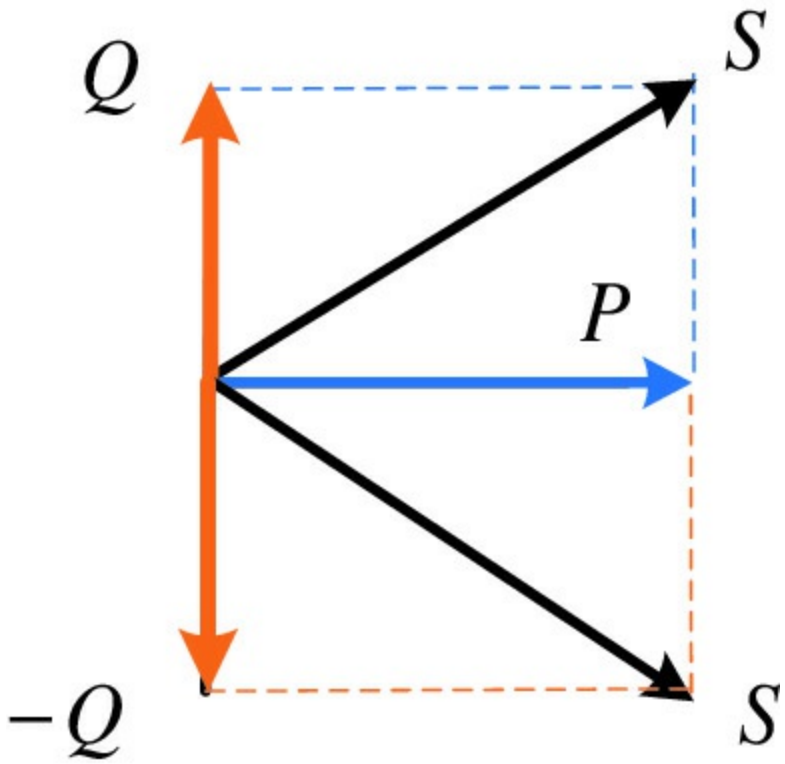


Figure 6.9 PV inverter active and reactive capacity

The range of allowable active power generation is given by

$$P \leq P_{ESS_max} + P_{PV_mpp} \tag{6.24}$$

where P_{ESS_max} is the power rating of the ESS, and P_{PV_mpp} the maximum PV power output. Once the actual active power is determined, the maximum amount of reactive power generation can be calculated by

$$|Q| \leq \sqrt{S^2 - P^2} \tag{6.25}$$

6.4 Verification

The PV-ESS system described in Figure 6.1 is numerically simulated in MATLAB®/Simulink environment. Since the solar PV boost converter and MPPT techniques have been presented and discussed in the Chapters 3 and 5, they will not be studied here. In this chapter, the effectiveness of the proposed MPPC scheme for the grid-connected inverter and the bidirectional DC–DC converter is tested. The system parameters are provided in Table 6.1 [58]. Loads 1 and 2 are made of constant resistors to model linear loads, whereas Loads 3 and 4 are constant power-type loads. For easy illustration, a negative current in ESS indicates the current flowing into the battery in a charging state. By contrast, the current flowing out of the battery in discharging state is defined as positive. The power exchanged between the PV-ESS system and the main grid are denoted as P_{PCC} and Q_{PCC}. A positive P_{PCC} and Q_{PCC} means that the power flows from the utility grid into the PV-ESS system.

Table 6.1 System parameters

Description	Value
Utility grid voltage	25 kV (phase–phase), 60 Hz
PCC voltage	0.69 kV (phase–phase), 60 Hz
DC-bus voltage	1.0 kV
Solar PV	SunPower Spr-305E-WHT-D, 2.5MW (STC)
ESS	Lithium-ion battery, 300 V, 2.3 kAh, $SOC_{\mathbf{max}}$ = 90%, $SOC_{\min}$ = 10%, $I_{\boldsymbol{bat_rated}}$ = 3.5 ka
DC-bus capacitor	C_2 = 50 mF
DC-side inductor	L_B = 0.17 mH
Inverter LC filter	L_f = 0.6 mH, R_f = 1.9 mΩ
Voltage support	$m_{\boldsymbol{W}}$ = −2.368 × 105, $m_{\boldsymbol{Var}}$ = −1.259×104

6.4.1 Flexible power injection from PV-ESS

Figure 6.10 shows the DC-side performance of the PV-ESS system using the proposed MPPC. Under fluctuating solar irradiation, the PVs generate variable electrical power with MPPT operation, as shown in Figure 6.10(a). The fluctuating PV output is absorbed and the DC-bus voltage is kept constant around its rated setpoint by the bidirectional DC–DC converter, as shown in Figure 6.10(b) and (c). The SOC keeps increasing as the battery is being charged by the

PVs, as shown in Figure 6.10(d).

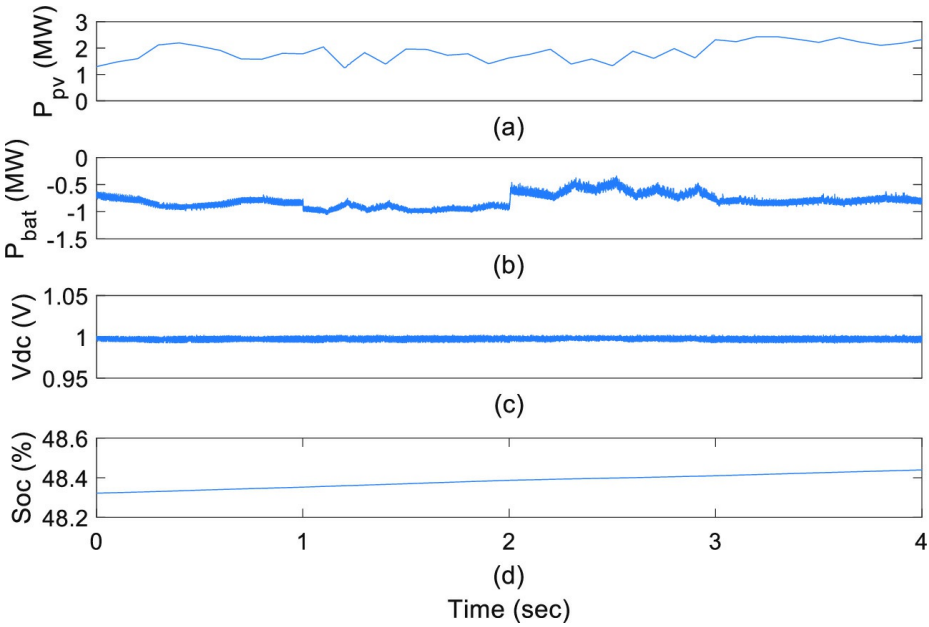


Figure 6.10 The performance of MPPC for DC–DC bidirectional converter under variable PV generation and load demand condition: (a) PV power, (b) battery power, (c) DC-bus voltage, (d) SOC

Figure 6.11 presents the AC-side performance of the PV-ESS system using the proposed MPPC strategy under the same solar irradiation profile. The AC load increases from 0.5 MW to 1.5 MW at 1 s and then reduces to 0.5 MW at 3 s. Initially, P_{ref} and Q_{ref} are set as 0, which means the inverter injects zero active and reactive powers to PCC. Then, P_{ref} varies in the sequence of 0.6 MW at 1 s and -0.6 MW at 2 s, while Q_{ref} increases to 0.4 M VAR at 2 s. It can be seen in Figure 6.11(a) and (b) that the actual active and reactive powers at the PCC are maintained close to their respective references. As the inverter did not provide power to the PCC before 1 s, the load is totally supplied by the utility grid. After 1 s, the PV-ESS system and the utility grid provide power to the load, resulting in the corresponding grid power and grid current, as shown in Figure 6.11(d) and (e).

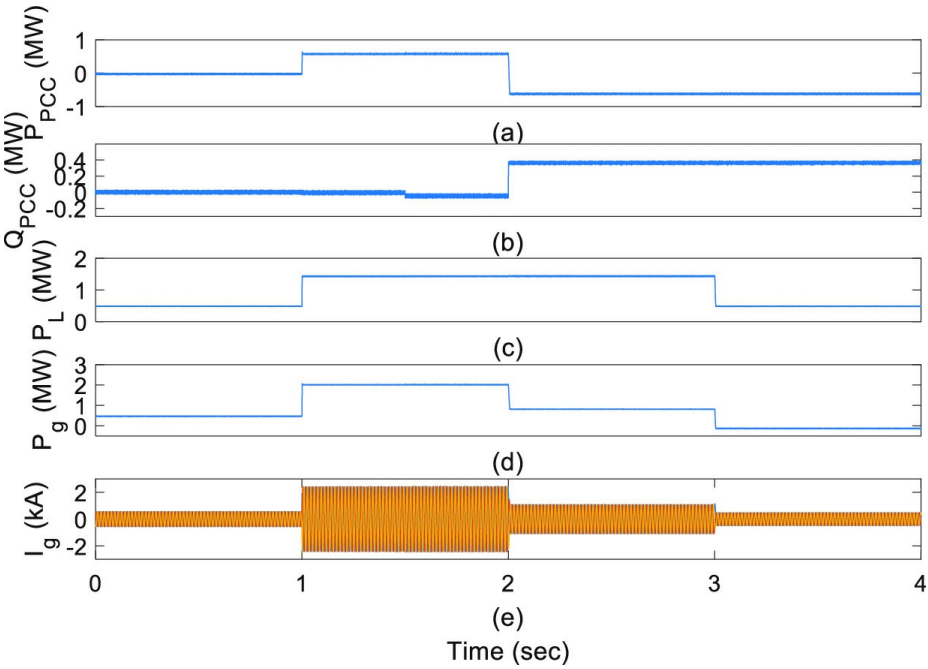


Figure 6.11 The performance of MPPC for grid-connected inverter under variable PV generation and load demand condition: (a) active power at PCC, (b) reactive power at PCC, (c) total load, (d) active power from grid, (e) grid current

6.4.2 Grid voltage support by PV-ESS

In the light of the aforementioned feature of flexible power regulation, VS can be applied. Since the active power regulation has a larger range than that of reactive power, VS can first employ active power regulation. Figure 6.12 presents the VS performance through active power and reactive power regulation. A 0.5 MW AC load is connected initially. At 1 s, a large AC load of 1 MW is switched in, leading to PCC voltage drop, which has been explained in Section 6.3. To better compare the performance of VS strategy, VS is activated both at 1.5 s. It is clear that the voltage has been boosted up by around 0.0022 pu in Figure 6.12 (a) and 0.0003 pu in Figure 6.12 (b). It is noted that the reactive power capacity is apparently smaller than that of active power. So, the voltage profile cannot be improved significantly by reactive power regulation. Whereas, with the improvement and high penetration of MGs, the coordinated reactive power regulation among these MGs can play a more important role to support the voltage significantly.

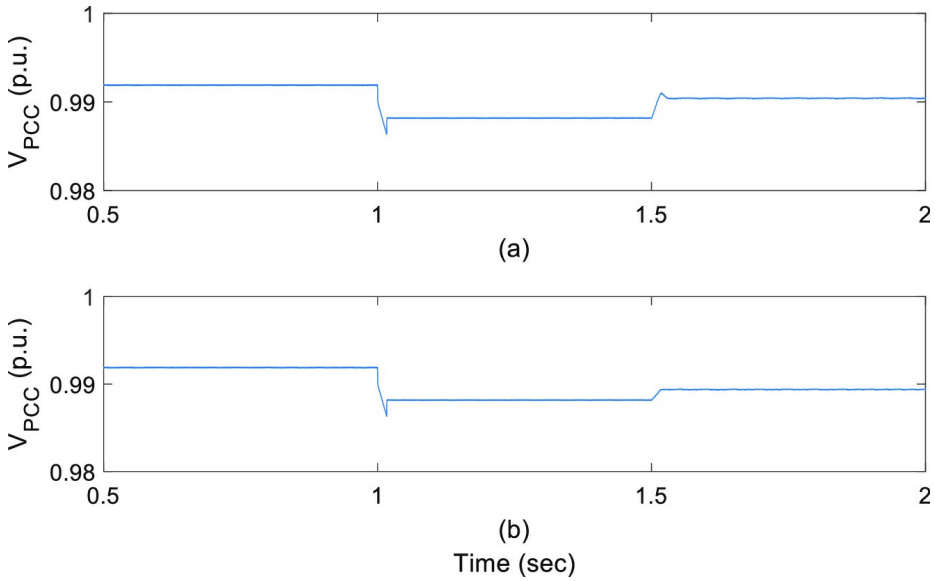


Figure 6.12 VS performance of the proposed method. (a) Using active power flow control. (b) Using reactive power flow control.

6.5 Conclusion

This research work proposes a MPPC scheme for grid-connected solar PVs with energy storage. The function of the MPPC is twofold. First, it aims to provide a stable and robust DC-bus voltage by controlling the DC–DC bidirectional converters. By doing this, the fluctuating PV output can be smoothed. Second, it can enable flexible active and reactive injection into the utility grid by controlling the grid-connected inverter. Under voltage dips caused by variable loads, a VS method is developed to restore the voltage.

References

[1] International Energy Agency. *World Energy Outlook*; 2020.

[2] Zhou H., Bhattacharya T., Tran D., Siew T.S.T., Khambadkone A.M. 'Composite energy storage system involving battery and ultracapacitor with dynamic energy management in microgrid applications'. *IEEE Transactions on Power Electronics*. 2011, vol. 26(3), pp. 923–30.

[3] Carrasco J.M., Franquelo L.G., Bialasiewicz J.T., *et al*. 'Power-electronic systems for the grid integration of renewable energy sources: a survey'. *IEEE Transactions on Industrial Electronics*. 2006, vol. 53(4), pp. 1002–16.

[4] Olivares D.E., Mehrizi-Sani A., Etemadi A.H., *et al*. 'Trends in microgrid control'. *IEEE Transactions on Smart Grid*. 2014, vol. 5(4), pp. 1905–19.
[5] Kramer W., Chakraborty S., Kroposki B., Thomas H. *Advanced power electronic interfaces for distributed energy systems, part 1: systems and topologies*technical report, NREL/TP-581-42672; 2008.
[6] Kjaer S.B., Pedersen J.K., Blaabjerg F. 'A review of single-phase grid-connected inverters for photovoltaic modules'. *IEEE Transactions on Industry Applications*. 2005, vol. 41(5), pp. 1292–306.
[7] Kouro S., Leon J.I., Vinnikov D., Franquelo L.G. 'Grid-connected photovoltaic systems: an overview of recent research and emerging PV converter technology'. *IEEE Industrial Electronics Magazine*. 2015, vol. 9(1), pp. 47–61.
[8] Haque M.M., Wolfs P. 'A review of high PV penetrations in LV distribution networks: present status, impacts and mitigation measures'. *Renewable and Sustainable Energy Reviews*. 2016, vol. 62(2), pp. 1195–208.
[9] Schittekatte T., Stadler M., Cardoso G., Mashayekh S., Sankar N. 'The impact of short-term stochastic variability in solar irradiance on optimal microgrid design'. *IEEE Transactions on Smart Grid*. 2018, vol. 9(3), pp. 1647–56.
[10] Walling R.A., Saint R., Dugan R.C., Burke J., Kojovic L.A. 'Summary of distributed resources impact on power delivery systems'. *IEEE Transactions on Power Delivery*. 2008, vol. 23(3), pp. 1636–44.
[11] American National Standard for Electric Power Systems and Equipment. *Voltage Ratings, C84.1*; 2006.
[12] IEEE. *Standard for interconnecting distributed resources with electric power systems, IEEE Std. 1547-2003*; 2003.
[13] IEEE. *Standard for interconnecting distributed resources with electric power systems – Amendment 1, IEEE Std. 1547a-2014* May; 2014. pp. 1–16.
[14] Shahnia F., Majumder R., Ghosh A., Ledwich G., Zare F. Sensitivity analysis of voltage imbalance in distribution networks with rooftop PVs. *Proceeding of IEEE on Power and Energy Society General Meeting*; 2010. pp. 1–8.
[15] Li X., Liao Q., Yin X., Xie J. A new on-load tap changing system with power electronic elements for power transformers. *In Proceeding of International Conference on Power System Technology*; 2002. pp. 556–9.
[16] Vinnal T., Janson K., Kalda H., Kutt L. Analyses of supply voltage quality, power consumption and losses affected by shunt capacitors for power factor correction. *Proceeding of IEEE Electric Power Quality and Supply Reliability Conference*; 2010. pp. 53–60.
[17] Bingsen W., Venkataramanan G. 'Dynamic voltage restorer utilizing a matrix converter and flywheel energy storage'. *IEEE Transactions on Industry Applications*. 2009, vol. 45(5), pp. 222–31.
[18] Kanchanaharuthai A., Chankong V., Loparo K.A. 'Transient stability and voltage regulation in multimachine power systems vis-à-vis STATCOM and battery energy storage'. *IEEE Transactions on Power Systems*. 2015, vol.

30(5), pp. 2404–16.
[19] Monteiro J., Silva J.F., Pinto S.F., Palma J. ‘Linear and sliding-mode control design for matrix converter-based unified power flow controllers’. *IEEE Transactions on Power Electronics*. 2014, vol. 29(5), pp. 3357–67.
[20] Gagrica O., Nguyen P.H., Kling W.L., Uhl T. ‘Microinverter curtailment strategy for increasing photovoltaic penetration in low-voltage networks’. *IEEE Transactions on Sustainable Energy*. 2015, vol. 6(2), pp. 369–79.
[21] Turitsyn K., Sulc P., Backhaus S., Chertkov M. ‘Options for control of reactive power by distributed photovoltaic generators’. *Proceedings of the IEEE*. 2011, vol. 99(6), pp. 1063–73.
[22] Kabir M.N., Mishra Y., Ledwich G., Dong Z.Y., Wong K.P. ‘Coordinated control of grid-connected photovoltaic reactive power and battery energy storage systems to improve the voltage profile of a residential distribution feeder’. *IEEE Transactions on Industrial Informatics*. 2014, vol. 10(2), pp. 967–77.
[23] Demirok E., González P.C., Frederiksen K.H.B., Sera D., Rodriguez P., Teodorescu R. ‘Local reactive power control methods for overvoltage prevention of distributed solar inverters in low-voltage grids’. *IEEE Journal of Photovoltaics*. 2011, vol. 1(2), pp. 174–82.
[24] Turitsyn K., Sulc P., Backhaus S., Chertkov M. ‘Options for control of reactive power by distributed photovoltaic generators’. *Proceedings of the IEEE*. 2011, vol. 99(6), pp. 1063–73.
[25] Available from http://www.sma.de.
[26] Available from https://solar.schneider-electric.com.
[27] Olivier F., Aristidou P., Ernst D., Van Cutsem T., Cutsem T.V. ‘Active management of low-voltage networks for mitigating overvoltages due to photovoltaic units’. *IEEE Transactions on Smart Grid*. 2016, vol. 7(2), pp. 926–36.
[28] Ang K.H., Chong G., Li Y. ‘PID control system analysis, design, and technology’. *IEEE Transactions on Control Systems Technology: a Publication of the IEEE Control Systems Society*. 2014, vol. 13(5), pp. 1813–27.
[29] Kwon M., Choi S. ‘Control scheme for autonomous and smooth mode switching of bidirectional DC–DC converters in a DC microgrid, *IEEE Transaction. on Power Electron*’. 2018, vol. 33(8), pp. 7094–104.
[30] Pirooz A., Noroozian R. ‘Model predictive control of classic bidirectional DC-DC converter for battery applications’. *2016 7th Power Electronics and Drive Systems Technologies Conference (PEDSTC)*; Tehran; 2016. pp. 517–22.
[31] Mei Y., Chen L., Li X., Sun K. ‘Model predictive control method for cascaded bi-directional DC-DC converter applied to a stand-alone photovoltaic energy storage system’. *2016 19th International Conference on Electrical Machines and Systems (ICEMS)*; Chiba; 2016. pp. 1–5.
[32] Merabet A., Tawfique Ahmed K., Ibrahim H., Beguenane R., Ghias A.M.Y.M. ‘Energy management and control system for laboratory scale

microgrid based wind-PV-battery'. *IEEE Transactions on Sustainable Energy*. 2017, vol. 8(1), pp. 145–54.
[33] Nejabatkhah F., Li Y.W. 'Overview of power management strategies of hybrid AC/DC microgrid'. *IEEE Transactions on Power Electronics*. 2015, vol. 30(12), pp. 7072–89.
[34] Ma T., Cintuglu M.H., Mohammed O.A. 'Control of a hybrid AC/DC microgrid involving energy storage and pulsed loads'. *IEEE Transactions on Industry Applications*. 2017, vol. 53(1), pp. 567–75.
[35] Molina-Garcia A., Mastromauro R.A., Garcia-Sanchez T., Pugliese S., Liserre M., Stasi S. 'Reactive power flow control for PV inverters voltage support in LV distribution networks'. *IEEE Transactions on Smart Grid*. 2017, vol. 8(1), pp. 447–56.
[36] Hu J., Li Z., Zhu J., Guerrero J.M. 'Voltage stabilization: a critical step toward high photovoltaic penetration'. *IEEE Industrial Electronics Magazine*. 2019, vol. 13(2), pp. 17–30.
[37] CortÉs P., RodrÍguez J., Antoniewicz P., Kazmierkowski M. 'Direct power control of an AFE using predictive control'. *IEEE Transactions on Power Electronics*. 2008, vol. 23(5), pp. 2516–23.
[38] Quevedo D.E., Aguilera R.P., Perez M.A., Cortes P., Lizana R. 'Model predictive control of an AFE rectifier with dynamic references'. *IEEE Transactions on Power Electronics*. 2012, vol. 27(7), pp. 3128–36.
[39] Shan Y., Hu J., Chan K.W. 'Power sharing and V/f restoration of standalone ac microgrids using model predictive control'. *Proceedings of 11th IET International Conference on Advances in Power System Control, Operation and Management (APSCOM 2018)*, 11-15 Nov; 2018. pp. 1–6.
[40] Hu J., Cheng K.W.E. 'Predictive control of power electronics converters in renewable energy systems'. *Energies*. 2017, vol. 10(4), pp. 1–14.
[41] Parisio A., Rikos E., Glielmo L. 'A model predictive control approach to microgrid operation optimization'. *IEEE Transactions on Control Systems Technology*. 2014, vol. 22(5), pp. 1813–27.
[42] Ouammi A., Dagdougui H., Dessaint L., Sacile R. 'Coordinated model predictive-based power flows control in a cooperative network of smart microgrids'. *IEEE Transactions on Smart Grid*. 2015, vol. 6(5), pp. 2233–44.
[43] Sundstrom C., Jung D., Blom A. 'Analysis of optimal energy management in smart homes using MPC'. *In Proceeding of European Control Conference*. 2016, pp. 2066–71.
[44] Moradzadeh M., Boel R., Vandevelde L. 'Voltage coordination in multi-Area power systems via distributed model predictive control'. *IEEE Transactions on Power Systems*. 2013, vol. 28(1), pp. 513–21.
[45] Moradzadeh M., Boel R., Vandevelde L.. 'Anticipating and coordinating voltage control for interconnected power systems'. *Energies*. 2014, vol. 7(2), pp. 1027–47.
[46] Vazquez S., Rodriguez J., Rivera M., Franquelo L.G., Norambuena M. 'Model predictive control for power converters and drives: advances and

trends'. *IEEE Transactions on Industrial Electronics*. 2017, vol. 64(2), pp. 935–47.
[47] Hu J., Zhu J., Platt G., Dorrell D.G. 'Model-predictive direct power control of ac/dc converters with one step delay compensation'. *Proceeding of Annual Conference on IEEE Industrial Electrics Society*; 2012.
[48] Cuzmar R.H., Pereda J., Aguilera R.P. 'Phase-shifted model predictive control to achieve power balance of Chb converters for large-scale photovoltaic integration'. *IEEE Transactions on Industrial Eectronics : a Publication of the IEEE Industrial Electronics Society*.
[49] Jin T., Shen X., Su T., Flesch R.C.C. 'Model predictive voltage control based on finite control set with computation time delay compensation for PV systems'. *IEEE Transactions on Energy Conversion*. 2019, vol. 34(1), pp. 330–8.
[50] Hu J., Zhu J., Dorrell D.G. Model predictive control of grid-connected inverters for PV systems with flexible power regulation and switching frequency reduction. *Proceeding of IEEE Energy Conversion Congress and Exposition*; 2013. pp. 540–6.
[51] Lei M., Yang Z., Wang Y., *et al*. 'An MPC-based ESS control method for PV power smoothing applications'. *IEEE Transactions on Power Electronics*. 2018, vol. 33(3), pp. 2136–44.
[52] Jain S., Shadmand M.B., Balog R.S. 'Decoupled active and reactive power predictive control for PV applications using a grid-tied quasi-z-source inverter'. *IEEE Journal of Emerging and Selected Topics in Power Electronics*. 2018, vol. 6(4), pp. 1769–82.
[53] Kim S.-K., Park C.R., Kim J.-S., Lee Y.I. 'A stabilizing model predictive controller for voltage regulation of a DC/DC boost converter'. *IEEE Transactions on Control Systems Technology*. 2014, vol. 22(5), pp. 2016–23.
[54] Dragicevic T. 'Model predictive control of power converters for robust and fast operation of AC microgrids'. *IEEE Transactions on Power Electronics*. 2018, vol. 33(7), pp. 6304–17.
[55] Shan Y., Hu J., Cheng K.W., Liu M. 'A universal model predictive control for practical AC microgrids with PVs and battery energy storage systems'. *Proceeding of IEEE Energy Conversion Congress and Exposition (ECCE)*, 23-27 Sept; 2018. pp. 1–6.
[56] Venkat A.N., Hiskens I.A., Rawlings J.B., Wright S.J. 'Distributed MPC strategies with application to power system automatic generation control'. *IEEE Transactions on Control Systems Technology*. 2008, vol. 16(6), pp. 1192–206.
[57] Olama A., Mendes P.R.C., Camacho E.F. 'Lyapunov-based hybrid model predictive control for energy management of microgrids'. *IET Generation, Transmission & Distribution*. 2018, vol. 12(21), pp. 5770–80.
[58] Shan Y., Hu J., Guerrero J.M. 'A model predictive power control method for PV and energy storage systems with voltage support capability'. *IEEE Transactions on Smart Grid*. 2020, vol. 11(2), pp. 1018–29.
[59] Maryam Hashemi N., Agelidis V. 'Evaluation of voltage regulation

mitigation methods due to high penetration of PV generation in residential areas'. *2013 International Conference on Renewable Energy Research and Applications (ICRERA)*; 2013. pp. 1180–9.

[60] Zeraati M., Hamedani Golshan M.E., Guerrero J.M. 'Distributed control of battery energy storage systems for voltage regulation in distribution networks with high PV penetration'. *IEEE Transactions on Smart Grid*. 2018, vol. 9(4), pp. 3582–93.

Further reading

- Zanella A., Bui N., Castellani A., Vangelista L., Zorzi M. 'Internet of things for smart cities'. *IEEE Internet of Things Journal*. 2014, vol. 1(1), pp. 22–32. doi:10.1109/JIOT.2014.2306328
- Bonfiglio A., Brignone M., Delfino F., Procopio R. 'Optimal control and operation of grid-connected photovoltaic production units for voltage support in medium-voltage networks'. *IEEE Transactions on Sustainable Energy*. 2014, vol. 5(1), pp. 254–63. doi:10.1109/TSTE.2013.2280811
- Molina-Garcia A., Mastromauro R.A., Garcia-Sanchez T., Pugliese S., Liserre M., Stasi S. 'Reactive power flow control for pv inverters voltage support in LV distribution networks'. *IEEE Transactions on Smart Grid*. 2017, vol. 8(1), pp. 447–56. doi:10.1109/TSG.2016.2625314
- Safayet A., Fajri P., Husain I. 'Reactive power management for overvoltage prevention at high pv penetration in low voltage distribution system'. *IEEE Transactions on Industry Applications*.
- Liu G., Guo L., Tao H., Zhu X., Wang W. 'PQ-U control method of grid-connected PV inverter under weak grid'. *Proceedings of IEEE Transportation Electrification Conference and Expo*; 2017.
- Lelis I.S., Drougakis I.A., Pompodakis E., Alexiadis M. 'Photovoltaic systems in low-voltage networks and overvoltage correction with reactive power control'. *IET Renewable Power Generation*. 2016, vol. 10(3), pp. 410–17.
- Braslavsky J.H., Collins L.D., Ward J.K. 'Voltage stability in a grid-connected inverter with automatic volt-watt and volt-var functions'. *IEEE Transactions on Smart Grid*. 2019, vol. 10(1), pp. 84–94. doi:10.1109/TSG.2017.2732000
- VallvéX., Graillot A., Gual S., Colin H. 'Micro storage and demand side management in distributed PV grid-connected installations'. *Electrical Power Quality and Utilisation. EPQU 2007. 9th International Conference*; 2007. pp. 1–6.
- Sugihara H., Yokoyama K., Saeki O., Tsuji K., Funaki T. 'Economic and efficient voltage management using Customer-Owned energy storage systems in a distribution network with high penetration of photovoltaic systems'. *IEEE Transactions on Power Systems*. 2013, vol. 28(1) 102–11. doi:10.1109/TPWRS.2012.2196529
- Marra F., Yang G., Traeholt C., Ostergaard J., Larsen E. 'A decentralized

storage strategy for residential feeders with photovoltaics'. *IEEE Transactions on Smart Grid*. 2014, vol. 5(2), pp. 974–81. doi:10.1109/TSG.2013.2281175

- Alam M., Muttaqi K., Sutanto D. 'Distributed energy storage for mitigation of voltage-rise impact caused by rooftop solar PV'. *Power and Energy Society General Meeting, 2012 IEEE*. 2012, pp. 1–8.
- Alam M.J.E., Muttaqi K.M., Sutanto D. 'Mitigation of Rooftop solar pv impacts and evening peak support by managing available capacity of distributed energy storage systems'. *IEEE Transactions on Power Systems*. 2013, vol. 28(4), pp. 3874–84. doi:10.1109/TPWRS.2013.2259269
- Alam M., Muttaqi K., Sutanto D. 'A novel approach for ramp-rate control of solar PV using energy storage to mitigate output fluctuations caused by cloud passing'. *IEEE Transactions on Energy Conversion*. 2014, vol. 29, pp. 507–18.
- Hashemi S., Ostergaard J., Yang G. 'A scenario-based approach for energy storage capacity determination in LV grids with high PV penetration'. *IEEE Transactions on Smart Grid*. 2014, vol. 5(3), pp. 1514–22. doi:10.1109/TSG.2014.2303580
- Yang Y., Li H., Aichhorn A.,*et al*. 'Sizing strategy of distributed battery storage system with high penetration of photovoltaic for voltage regulation and peak load shaving'. *IEEE Transactions on Smart Grid*. 2014, vol. 5(2), pp. 982–91. doi:10.1109/TSG.2013.2282504
- Ali A., Raisz D., Mahmoud K. 'Mitigation of voltage fluctuation in distribution system connected with PV and PHEVs using artificial bee colony algorithm'. *Proceedings of International Istanbul Smart Grids and Cities Congress and Fair*. 2018, pp. 144–8.
- Sahoo S.K., Sinha A.K., Kishore N.K. 'Control techniques in AC, DC, and hybrid AC–DC microgrid: a review'. *IEEE Journal of Emerging and Selected Topics in Power Electronics*, vol. 6(2), pp. 738–59; in press. doi:10.1109/JESTPE.2017.2786588
- Marra F., Yang G.Y., Fawzy Y.T., *et al*. 'Improvement of local voltage in feeders with photovoltaic using electric vehicles'. *IEEE Transactions on Power Systems*. 2013, vol. 28(3), pp. 3515–6. doi:10.1109/TPWRS.2013.2248959
- Foster J.M., Trevino G., Kuss M., Caramanis M.C. 'Plug-in electric vehicle and voltage support for distributed solar: theory and application'. *IEEE Systems Journal*. 2013, vol. 7(4), pp. 881–8. doi:10.1109/JSYST.2012.2223534
- Martinenas S., Knezovic K., Marinelli M. 'Management of power quality issues in low voltage networks using electric vehicles: experimental validation'. *IEEE Transactions on Power Delivery*. 2017, vol. 32(2), pp. 971–9. doi:10.1109/TPWRD.2016.2614582
- Alam M.J.E., Muttaqi K.M., Sutanto D. 'Effective utilization of available PEV battery capacity for mitigation of solar PV impact and grid support with integrated V2G functionality'. *IEEE Transactions on Smart Grid*. 2016, vol.

7(3), pp. 1562–71. doi:10.1109/TSG.2015.2487514
- Mahmud N., Zahedi A., Mahmud A. 'A cooperative operation of novel PV inverter control scheme and storage energy management system based on ANFIS for voltage regulation of grid-tied PV system'. *IEEE Transactions on Industrial Informatics*. 2017, vol. 13(5), pp. 2657–68. doi:10.1109/TII.2017.2651111
- Adhikari S., Li F. 'Coordinated v-f and p-q control of solar photovoltaic generators with MPPT and battery storage in microgrids'. *IEEE Transactions on Smart Grid*. 2014, vol. 5(3), pp. 1270–81. doi:10.1109/TSG.2014.2301157
- Kabir M.N., Mishra Y., Ledwich G., Dong Z.Y., Wong K.P. 'Coordinated control of grid-connected photovoltaic reactive power and battery energy storage systems to improve the voltage profile of a residential distribution feeder'. *IEEE Transactions on Industrial Informatics*. 2014, vol. 10(2), pp. 967–77. doi:10.1109/TII.2014.2299336
- Available from http://www.samlexsolar.com/learning-center/requirements-for-batteries.aspx.
- Wang L., Bai F., Yan R., Saha T.K. 'Real-time coordinated voltage control of PV inverters and energy storage for weak networks with high PV penetration'. *IEEE Transactions on Power Systems*. 2018, vol. 33(3), pp. 3383–95. doi:10.1109/TPWRS.2018.2789897
- Taylor Z., Akhavan-Hejazi H., Cortez E., *et al*. 'Customer-side SCADA-assisted large battery operation optimization for distribution feeder peak load shaving'. *IEEE Transactions on Smart Grid*. 2019, vol. 10(1), pp. 992–1004. doi:10.1109/TSG.2017.2757007
- Zhu X., Wang J., Lu N., Samaan N., Huang R., Ke X. 'A hierarchical VLSM-based demand response strategy for coordinative voltage control between transmission and distribution systems'. *IEEE Transactions on Smart Grid*, vol. 10(5), pp. 4838–47. doi:10.1109/TSG.2018.2869367
- Vogt M., Heckmann W., Hubert J.,*et al*. 'Local use of PV surplus – load control and thermal storage in a LV grid cell'. *7th International. Conference. on PV-Hybrids and Mini-grids*. 2014.
- Malik O., Havel P. 'Active demand-side management system to facilitate integration of RES in low-voltage distribution networks'. *IEEE Transactions on Sustainable Energy*. 2014, vol. 5(2), pp. 673–81. doi:10.1109/TSTE.2013.2288805
- Dedeoglu S., Konstantopoulos G.C., Paspatis A.G. 'Grid-supporting three-phase inverters with inherent RMS current limitation under balanced grid voltage sags'. *IEEE Transactions on Industrial Electronics*, vol. 5(2), p. 1. doi:10.1109/TIE.2020.3034860
- Gayatri M.T.L., Laxmi D.D., Saikumar N., Saivaraprasad N., Parimi A.M. 'Active power quality enhancement of wind microgrid supported by PV generation'. *IEEE-HYDCON*. 2020, pp. 1–6.
- Wu Y., Wu Y., Guerrero J., Vasquez J., Palacios-García E., Guan Y. 'IoT-enabled microgrid for intelligent energy-aware buildings: a novel hierarchical self-consumption scheme with renewables'. *Electronics*. 2020, vol. 9(550),

pp. 550–18. doi:10.3390/electronics9040550
- Mahmud K., Rahman M.S., Ravishankar J., Hossain M.J., Guerrero J.M. ‘Real-time load and ancillary support for a remote island power system using electric boats’. *IEEE Transactions on Industrial Informatics*. 2020, vol. 16(3), pp. 1516–28. doi:10.1109/TII.2019.2926511
- Perilla A., Rueda Torres J.L., Rakhshani E., *et al*. ‘Directional derivative-based method for quasi-stationary voltage support analysis of single-infeed VSC-HVDC units’. *High Voltage*. 2020, vol. 5(5), pp. 511–22. doi:10.1049/hve.2019.0420

Chapter 7
MPC of parallel PV-ESS microgrids

In this chapter, a control method consisting of a model predictive current control (MPCC) algorithm, a model predictive power control (MPPC) scheme, and a model predictive voltage control (MPVC) strategy is presented for microgrids (MGs) with parallel photovotaic energy storage systems (PV-ESS). The photovoltaic (PV) boost converter is controlled by the MPPC for maximum power point tracking (MPPT) operation. By controlling the bidirectional buck-boost converters of the battery energy storage systems (BESSs) based on the MPPC algorithm, the fluctuating output from the renewable energy sources (RESs) can be smoothed, while stable DC-bus voltages can be maintained as the inverter inputs. Then, the parallel inverters are controlled using a combination of the MPVC scheme and the droop method to ensure stable AC voltage output and proper power sharing.

7.1 Introduction

In the microgrids (MGs) studied in Chapters 5 and 6, all the distributed generations (DGs) and energy storage systems (ESSs) are connected to a common DC bus that is further interconnected to an AC bus through an AC–DC interlinking converter. In this chapter, a MG with multiple PV-ESS units connected to a common AC bus through parallel inverters is focused. The parallel operation of converters has been a challenging problem that is more complex than controlling a single DG unit. This is because every converter must incorporate to ensure proper load sharing and system stability in a MG with parallel converters. In this sense, appropriate control strategies for parallel-connected DGs are required.

Regarding the coordination of parallel inverters in MGs, many studies have been conducted over the past years to address the limitations of the droop scheme and improve the performance, as discussed previously in Chapter 4. For instance, by introducing power derivative-integral terms into the traditional droop control, faster transient response of power sharing can be achieved [1]. Reactive power sharing performance of nonlinear loads was improved using adaptive virtual impedance [2]. A modified angle droop control was described to remove the

dependence of real power sharing on the output inductance with lower but stable droop coefficients [3]. An enhanced proportional power-sharing method based on adaptive virtual impedance was presented to prevent power coupling [4]. The voltage-shifting and load current feedforward control methods were proposed to eliminate the voltage deviation due to the droop control and improve voltage control dynamics [5]. A new droop control method based on the Takagi–Sugeno (TS) fuzzy and sliding modes was proposed to improve the current-sharing performance and robustness against the network delays [6]. A novel consensus-based cooperative droop control was introduced to adaptively adjust the droop coefficients to improve the reactive power-sharing accuracy [7]. A new control scheme that includes the islanded, grid-connected, and transient controls was proposed to realize accurate power sharing and eliminate the steady-state voltage bias in islanded mode, and realize accurate power-flow control and restrain the harmonic current injected to grid in grid-connected mode, as well as realize a smooth mode-transfer between the above two modes [8]. The cross circulating current and zero-sequence circulating currents were considered and added to the traditional droop plus virtual impedance control to suppress both cross- and zero-sequence circulating currents [9]. The f–P/Q droop control was proposed to autonomously achieve power balance under both resistive-inductive and resistive-capacitive loads [10]. For low-voltage resistive MGs, a V–I droop method was adopted to alleviate traditional droop control shortcomings for the primary control in [11]. A novel voltage stabilization and power-sharing method based on the virtual complex impedance was studied to improve the voltage quality and achieve accurate power sharing without the impact of hardware parameters variations [12].

Although much research effort has been paid to improve the performance of primary control for MGs, no major change has been seen in the inner control loop, in which the conventional cascaded linear control has been broadly used. For many years, cascaded linear control has domination in power electronic control. However, this approach presents limitations [13]. First, this control structure contains multiple feedback loops and pulse width modulation (PWM), which leads to a relatively slow dynamic response. Second, much effort and time have to be paid to the tuning of proportional-integral-derivative (PID) parameters, which makes the controller not easy to implement. In reality, fluctuating output from RESs can cause oscillations in DC-bus voltage, which may be transferred and amplified to the AC side of the MG. As a result, the traditional cascaded control featuring relatively slow dynamics may not be sufficient to handle these oscillations. Besides, the performance of such cascaded linear control in the bottom level can significantly influence the effectiveness of higher-level control in the hierarchical control structure. This needs to be investigated thoroughly.

In contrast to the cascaded linear control, model predictive control (MPC) is based on the prediction of system future behavior over a finite time duration at each time step. The optimal control action of the power converter is selected according to the minimization of a predefined cost function. Due to its fast-dynamic response and flexible control scheme to accommodate various control

objectives and constraints, MPC has been widely applied in power converters, particularly inverters in either islanded operation or grid-connected operation [14–20]. It has also been recently used for parallel inverters of MGs. One of the trends is the droop-free MPC structure. In [21], a scheme for parallel operation of inverters is presented. First, a multiple-input–multiple-output state-space model is derived for the parallel-connected inverters system. Then, a MPC scheme is developed to control paralleled single-phase inverters. In this algorithm, two control objectives, i.e., voltage tracking and current sharing, are formulated into a weighted cost function. Both proper load sharing among inverters and plug-and-play capability can be achieved. The major limitation of this work is that it assumes no distribution lines between DGs and common voltage bus, and only one common resistor is used as the common load, which is usually not the case in practice. Even there are limitations, this work opens up a new research line in MG control. It is expected that the main challenge of this droop-free MPC is the development of an accurate multiple-input–multiple-output state-space model for parallel-connected inverters by considering various practical aspects such as distribution line impedance, resistor-inductor-capacitor (RLC) loads, nonlinear loads, etc. In [22], an improved MPC of inverters with output LC filter for constant switching frequency and circulating current suppression is presented. In the proposed control scheme, the virtual state vectors are generated in addition to the real state vectors, which are used for the estimation of the future states of voltage and current.

The MPC schemes discussed earlier, in which the optimal switching state of the power converter is determined according to a specified cost function, have been adopted in inverters to obtain better performance. Still, MPC is seldom reported in the coordinated control of multiple converters in MGs with different operation modes. Indeed, some system-level algorithms have been proposed to achieve a variety of goals such as minimizing system operating costs and economic load dispatch. The main focuses are power flow optimization and operational benefit maximization. For example, in [23], the charging and discharging of BESSs in MGs are focused. The optimal use of ESSs depends not only on the network topology, constraints, and objective but also the state of charge (SoC) of the ESSs. In [24], MPC approach is applied to solve the problem of efficiently optimizing MG operations while at the same time considering a time-varying request and operation constraints. It tackles the optimal operation planning of a MG. Under variable load profile, the proposed MPC controller aims at minimizing the overall MG operating costs while satisfying complex operational constraints. In [25], a MPC for optimal power exchange among networked MGs is proposed. Its purpose is to schedule and manage the energy exchanges at the network level by taking into account the uncertainties of renewable resources and loads. Actually, the MPC-based algorithm is used to not only determine the scheduling of power exchanges among MGs but also manage the charging/discharging of the ESS in each MG. To implement the MPC algorithm successfully, various information is required, including generation on the power source side, load forecasting on the demand side as well as electricity

prices. The high-level control generates optimal set points for all DGs, ESSs, and power exchanges to maximize the total network profit and to meet the load demand in each MG.

All these MPC algorithms discussed earlier are designed and implemented at the system level. Nevertheless, the physical electric structures of the MGs and the actual control of power converters have not been addressed. Now the question becomes that in renewable energy-based AC MGs with multiple power converters as electronic interfaces, would it be possible to implement MPC approaches instead of traditional cascade voltage or current feedback loops on the power converters given a MG with detailed circuit topology; and, to what extent, the overall system performance can be improved.

Another important point often ignored in existing MG research is that the inputs of the distributed inverters are usually connected to DC power sources rather than actual renewable energy resources. From the perspective of inverter control techniques development, it is acceptable and sufficient because this assumption can facilitate the design process. On the other hand, from a practical application point of view, the intermittent nature of such renewable energy resources must be taken into account. The fluctuating characteristics of RESs and hence, the variable electrical power outputs from DGs, are far more complicated than those simple DC sources in simulation and DC power sources in laboratories. To implement the coordination control of multiple DG converters and consider the fluctuating nature of distributed energy resources (DERs), an AC MG structure shown in Figure 7.1 is constructed and studied. The renewable energy resources could be solar, wind, etc. Here, a solar PV system is used as an example, which is not the main focus in this research. The whole system is composed of two subsystems: (1) parallel inverters with AC loads, and (2) PV-battery energy sources. On the basis of this configuration, a new control strategy using MPC algorithm is developed. Specifically, a MPCC is developed to control the PV boost converter. A MPPC is developed to maintain the DC-bus voltages and smooth the PVs outputs on the DC side of the MG with renewable energy and storage. Then on the AC side, a MPVC incorporated with the droop method is put forward to control the parallel inverters.

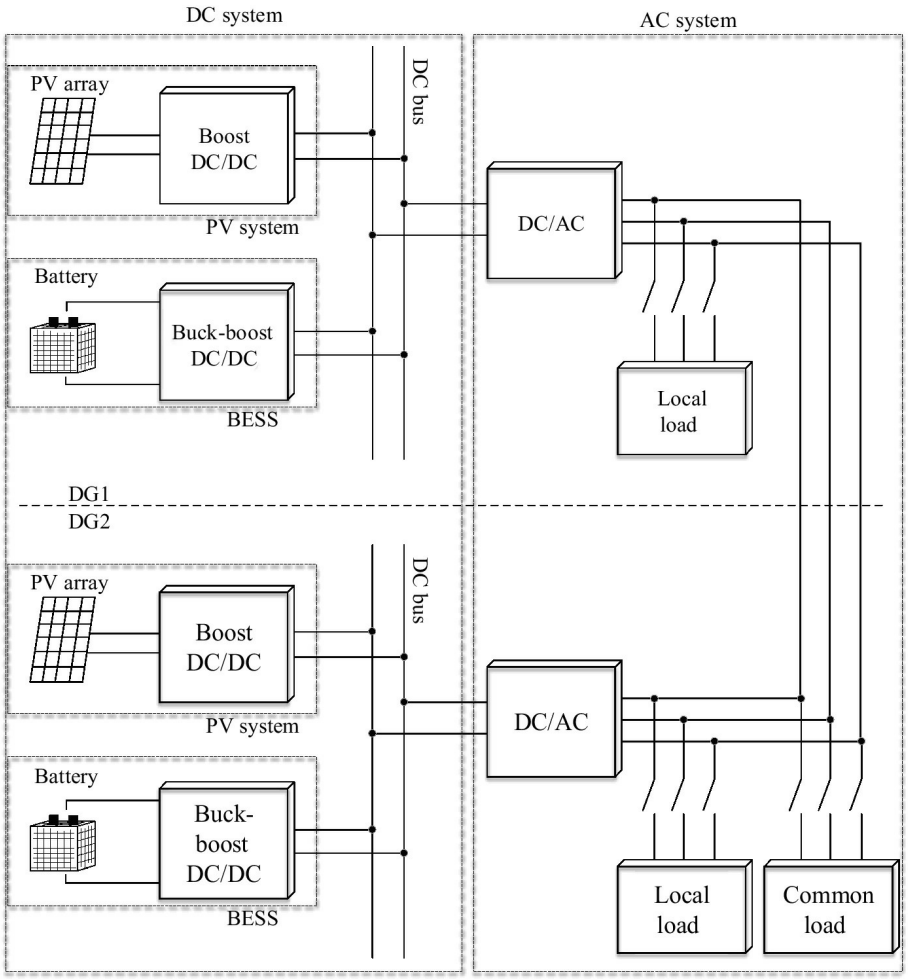


Figure 7.1 Topology of a PV-battery-based AC MG

7.2 MPCC for solar PVs

The PV power electronics are shown in Figure 7.2. There is only one controlled transistor of which gate signal is S (1 is ON and 0 is OFF) in DC–DC boost circuit. It is clear to draw the continuous-time expressions of the circuit using Kirchhoff's Voltage Law (KVL):

$S = 1$:

$$L\frac{dI_L}{dt} = V_{C1} \tag{7.1}$$

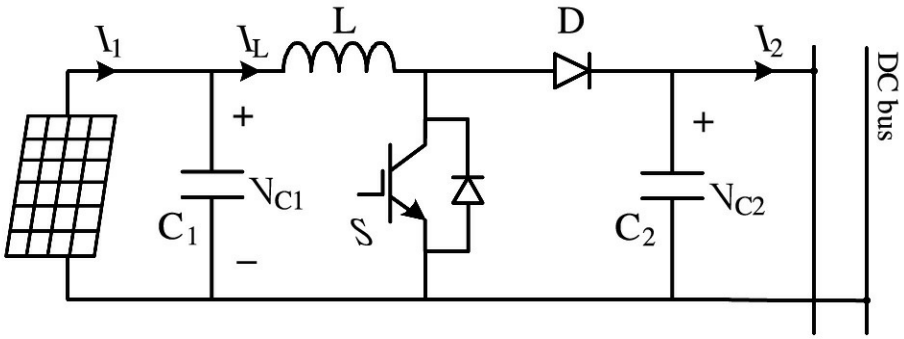


Figure 7.2 Simplified schematic of the PV DC–DC boost converter

$S = 0$:

$$L\frac{dI_L}{dt} = V_{C1} - V_{C2} \tag{7.2}$$

Applying Euler's forward law, the discrete-time model of the first-order system can be obtained by the approximation of derivatives:

$$\frac{dx}{dt} = \frac{x(k+1)-x(k)}{T_S} \tag{7.3}$$

where T_S is the sampling time. Then the discrete-time model of $S = 1$ and $S = 0$ can be rewritten as

$S = 1$:

$$I_L(k+1) = \frac{T_S}{L}(V_{C1}(k) - I_L(k) \tag{7.4}$$

$S = 0$:

$$I_L\left(k+1\right)=\frac{T_S}{L}\left(V_{C1}\left(k\right)-V_{C2}\left(k\right)\right)+I_L\left(k\right) \quad (7.5)$$

At steady state, the average current through capacitor C_1 is about zero. This means

$$I_1(k+1)\approx I_L(k+1) \quad (7.6)$$

Since the output current at the terminal of the PV array is the pre-control object, the cost function can be modified as

$$J=\left|I^*\left(k+1\right)-I_1\left(k+1\right)\right| \quad (7.7)$$

Finally, the optimal switching signal is selected by following the flowchart given in Figure 7.3. Figure 7.4 is the block diagram of the combination of MPPT and MPC techniques to control DC–DC boost converter. The link between MPPT and MPC is that MPPT provides the desired current command as the control objectives for the MPC to control the boost converter. MPPT techniques have been reviewed in Chapter 3, which will not be discussed in detail here. Under rapidly varying weather conditions, I_{pv} is a variable that only relates to the exterior solar irradiation and ambient temperature and can be the predicted reference value for the MPC.

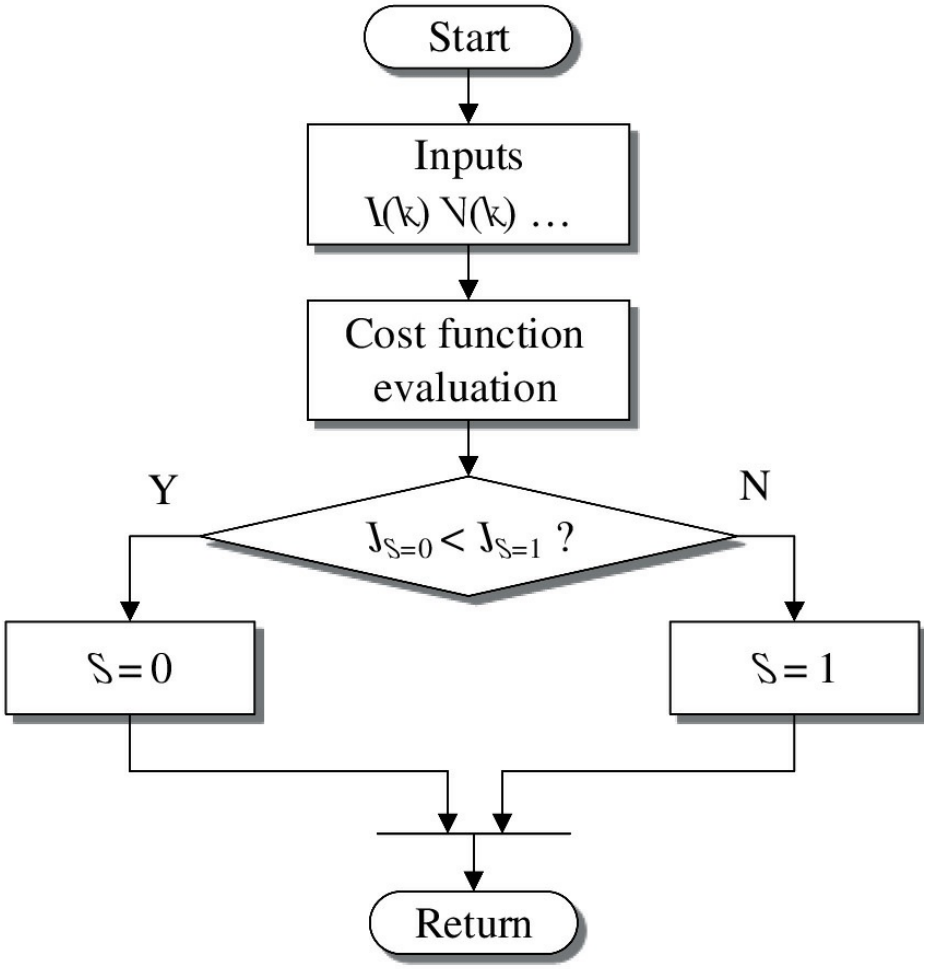


Figure 7.3 Simplified flowchart for selecting the optimal switching signal in MPCC-based DC–DC boost conversion

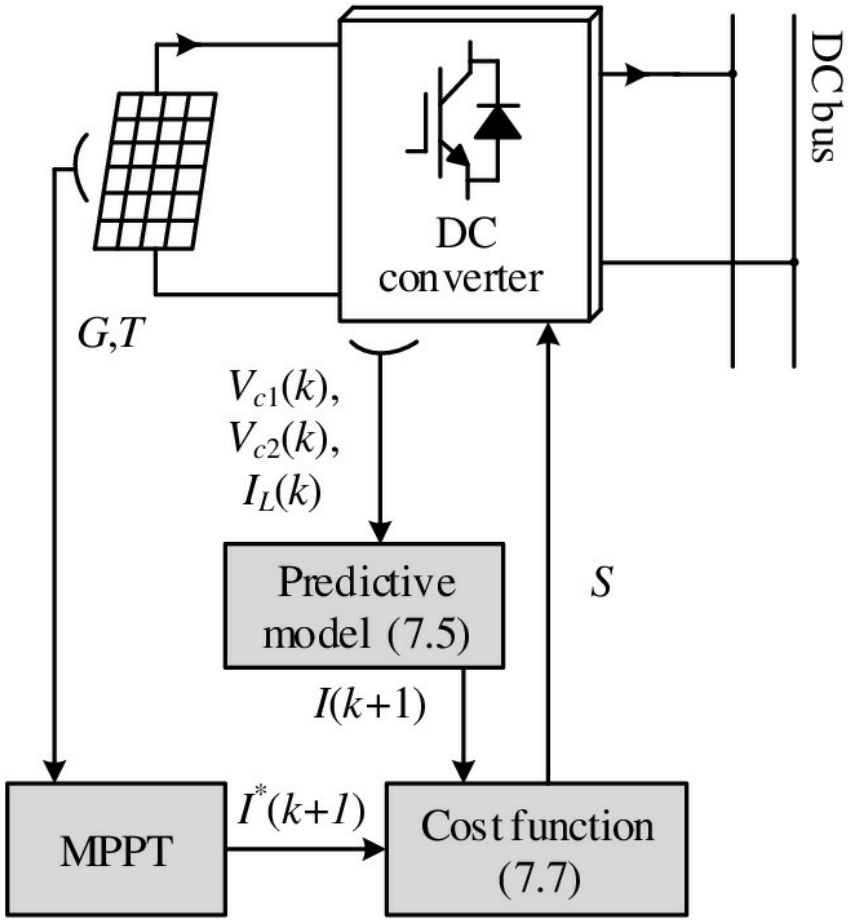


Figure 7.4 Block diagram of the combination of MPPT and MPCC to control the DC–DC boost converter

7.3 MPPC of BESS DC–DC converters

DC–DC converters are involved in providing easier interconnection and reliability of various DERs by stepping down or stepping up the voltage from the generated voltage of the power source to another voltage level. In MGs, the DC–DC converters mainly aim to interface various renewable energy resources to the DC bus or to the loads. Some popular types are boost converters, buck converters, and buck-boost converters [26]. Since most of the renewable energy resources are suitable for operating at low voltage, it is usually necessary to boost the low voltage obtained from the renewable source to the voltage suitable for the DC

bus, such as the solar PVs. As to the BESS, bidirectional buck-boost converters are commonly used as they allow bidirectional power flow, which makes them a natural fit for battery charging and discharging.

The aim of the BESS is to bridge the power gap caused by the PV output and the load demand by maintaining the DC-bus voltage. To supply or absorb active power by discharging or charging the battery, conventionally the battery current is regulated by controlling the bidirectional DC–DC converter. In this traditional method, the error of the current reference and the measurement is sent to a proportional–integral (PI) controller [27–29]. The output of the PI controller is then delivered to the pulse width modulator to generate the gate drive signals. Recently, there has been some work reported about the MPC of bidirectional DC–DC converters in BESS systems. For example, the MPC method developed in [30] is aimed to properly discharge the battery to increase bus voltage and charge the battery to decrease the bus voltage to maintain the DC-bus voltage within a predefined rated range. The converter discrete predictive models for buck mode and boost mode are derived, respectively. Based on these, two corresponding cost functions for buck operation and boost operation are designed with the DC-bus voltage as the controlled variable. In [31], an MPC method is developed for cascaded bidirectional DC–DC converters for high power-density requirements. Simulation and experimental results show that the proposed MPC approach can realize the stability of DC-bus voltage and the power balance between the PV, battery, and the load. More recently, an improved MPC strategy is presented for DC–DC single-ended primary-inductor converters [32]. Based on the relation between the inductor current ripple and switching frequency, an auto-tuning weighting factor scheme is developed to control the switching frequency with improved efficiency under input voltage variations. Once again, these recent advances of MPC in DC–DC converters discussed in Section 7.3 are within the scope of a single battery system or a simple PV-ESS system. Its application in MGs with variable power sources and multiple converters are yet to be explored.

Here, a MPPC is proposed, which includes a prediction model and control behavior optimization. The prediction model, which is derived based on the DC–DC converter circuit, will be used together with the current system status and the possible control behaviors to predict the future system status. The control behavior optimization, which is essentially a cost function, will be used to evaluate the effects of all possible control behaviors. Figure 7.5 provides insights into the current flow between the PV, BESS, and the AC side. To keep the power balance within the MG, the BESS plays an important role in power compensation through proper charging and discharging. Applying Kirchhoff's Current Law, the relationship of the currents can be described as

$$I_{DC} = I_{PV} - I_{C2} - I_{AC} \tag{7.8}$$

where I_{AC} means the current flowing into the inverter for AC loads. I_{DC} represents the current supplied or absorbed by the BESS. To keep the power balance within the MG, the power needed by the BESS can be computed as

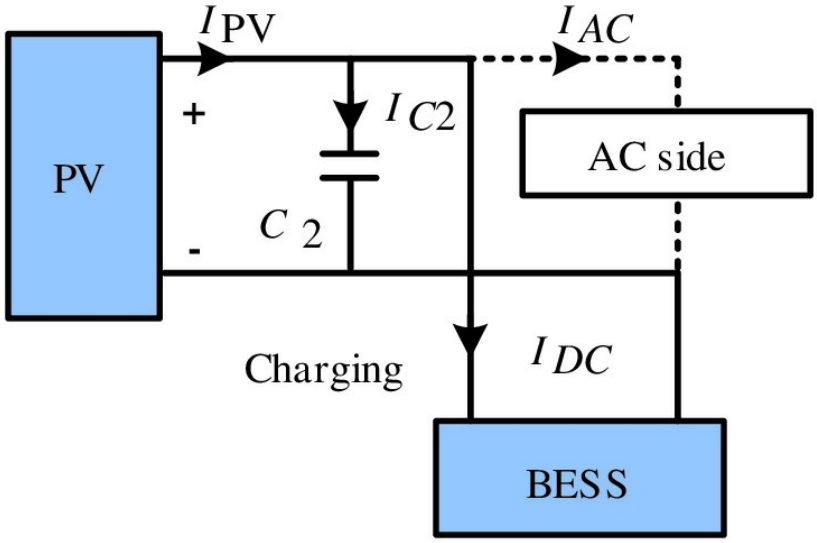
$$P^*_{BESS} = |I_{DC} . V^*_{DC}| \tag{7.9}$$

where V^*_{DC} is the DC-bus voltage reference. According to the capacitor dynamic characteristics, the current flowing through the DC-bus capacitor, C_2, can be predicted as

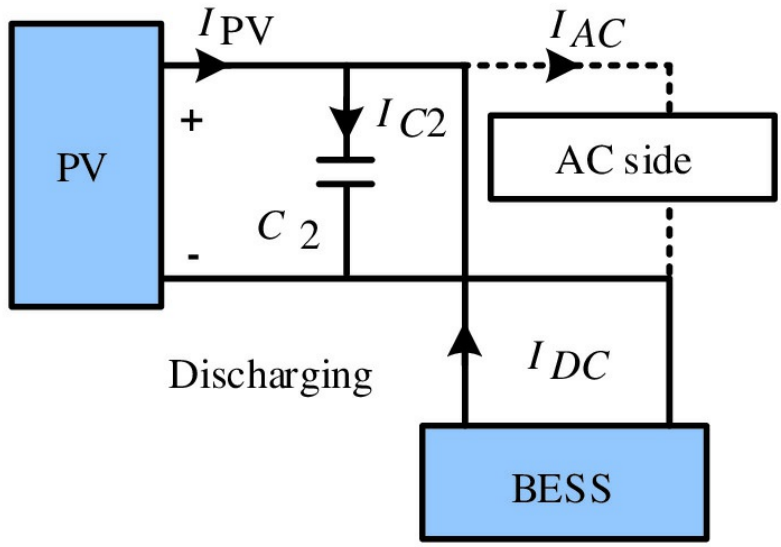
$$I_{C2}(k+1) = \frac{1}{N}\left(\frac{C_2}{T_s}\left(V^*_{DC} - V_{DC}(k)\right)\right) \tag{7.10}$$

where N is an integer coefficient used for capacitor's current limitation [33]. Combining (7.8)–(7.10), the required power by BESS to maintain power balance at the next control instant can be written as

$$P^*_{BESS}(k+1) = |I_{DC}(k+1) \cdot V^*_{DC}| \tag{7.11}$$


I_{PV}
I_{AC}
PV
+
I_{C2}
AC side
C_2
-
Charging
I_{DC}
BESS

(a)


I_{PV}
I_{AC}
PV
+
I_{C2}
AC side
C_2
-
Discharging
I_{DC}
BESS

(b)

Figure 7.5 Illustration of the current flow within the system. (a) Charging process, (b) discharging process

Since the power supplied or absorbed by BESS is actually controlled by the buck-boost converter, it is necessary to obtain the effect of its switching states on power absorbed/supplied. Figure 7.5 depicts the circuit topology of the BESS including the battery and the converter. If S_2 is switching (1 or 0) and S_1 is kept OFF, it operates in boost mode. The battery supplies power through discharging. By contrast, if S_1 is switching (1 or 0) and S_2 is maintained OFF, it operates in buck mode. The battery absorbs power through being charged. In boost mode, the model of the BESS circuit can be written as

$$\begin{cases} S_2 = 1,\ S_1 = 0: & L_B \dfrac{dI_B}{dt} = V_B \\ S_2 = 0,\ S_1 = 0: & L_B \dfrac{dI_B}{dt} = V_B - V_{DC} \end{cases} \tag{7.12}$$

The discrete-time model with a sampling time T_S can be expressed as

$$\begin{cases} S_2 = 1,\ S_1 = 0: & I_B(k+1) = \frac{T_s}{L_B} V_B(k) + I_B(k) \\ S_2 = 0,\ S_1 = 0: & I_B(k+1) = \frac{T_s}{L_B}\left(-V_{DC}(k) + V_B(k)\right) + I_B(k) \end{cases} \tag{7.13}$$

Using the same principle of electric circuit analysis, the discrete-time models of the converter in buck mode can be written as

$$\begin{cases} S_2 = 0,\ S_1 = 1: & I_B(k+1) = \frac{T_s}{L_B}\left(V_{DC}(k) - V_B(k)\right) + I_B(k) \\ S_2 = 0,\ S_1 = 0: & I_B(k+1) = -\frac{T_s}{L_B} V_B(k) + I_B(k) \end{cases} \tag{7.14}$$

In steady state, the battery terminal voltage almost keeps constant, and considering the approximate equality of battery output current and inductor current, the battery output power can be predicted as

$$P_{bat}(k+1) = \left| I_B(k+1) \cdot V_B(k) \right| \tag{7.15}$$

As the battery is the only energy storage device in the BESS, obviously, the power from the BESS calculated by (7.11) for power balancing with the MG needs to be provided by the battery through the buck-boost converter. Thus, the cost function should be designed as

$$J_P = \left| P^*_{BESS}\left(k+1\right) - P_{bat}\left(k+1\right) \right| \qquad (7.16)$$

The proposed MPPC strategy is illustrated in Figure 7.6. The actual DC-bus voltage V_{DC} and its reference V^*_{DC}, together with PV system output current, I_{PV}, inverter input current, I_{AC}, are first measured and used to determine the required BESS power. Meanwhile, the battery voltage and current, together with the actual DC-bus voltage, are utilized to predict the battery current $I_B(k+1)$, leading to four possible values of $P_{bat}(k+1)$ according to (7.13) and (7.14). Then, the switching behavior that minimizes the cost function (7.16) will be selected to control the buck-boost converter. In this way, the DC-bus voltages can be maintained stable as the input terminals for the parallel inverters on the AC side. Compared to traditional cascade control with PID regulators, it is noted that additional measurements of the PV current and the AC-side current are needed for the proposed MPPC approach. Hence, additional current sensors and communications are required within each PV-BESS unit. From the entire MG point of view, communication between parallel PV-BESS-inverter units can still be avoided because of the integration of droop method into the MPVC. The droop and the MPVC will be discussed in Section 7.4.

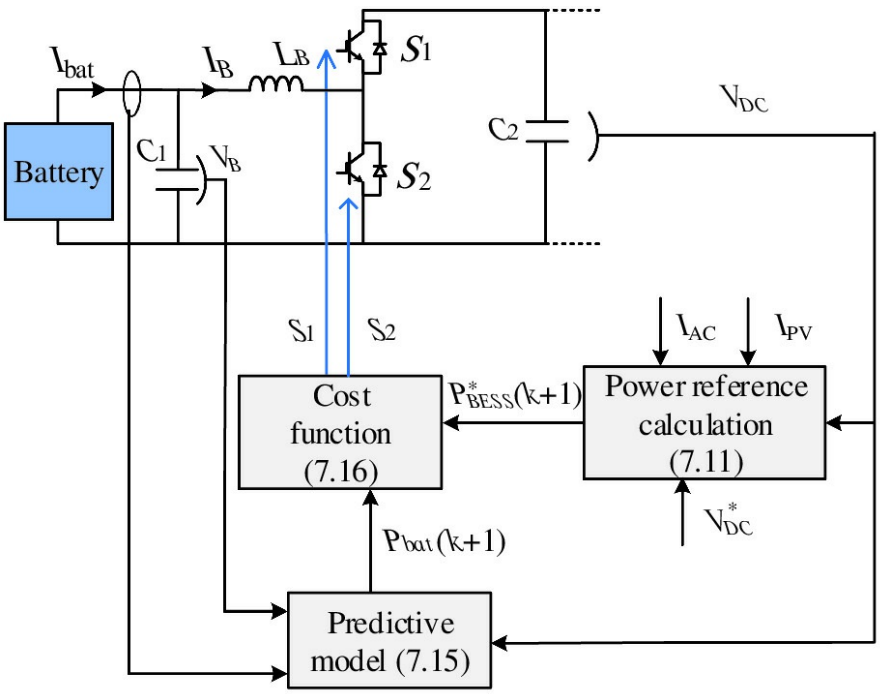


Figure 7.6 Block diagram of MPPC to control buck-boost

The optimal switching signal is selected by following the procedure of the flowchart presented in Figure 7.7, which involves an energy management procedure to coordinate the control of the converters in the whole system. Whether the battery's converter operates in discharging or charging mode depends on the power balance in the system. If there is a drop in the DC-bus voltage caused by the insufficient PV output power or excessive loads, the battery will discharge in boost mode to transfer power from the battery to the load, provided that SoC is greater than the minimum threshold. Otherwise, load shedding is usually required. On the other hand, if power generation is beyond the loads' need, DC-bus voltage increases along with the battery turning into buck mode (charging). If the battery is fully charged (SoC exceeds its maximum), MPPT should be deactivated to reduce the power generation.

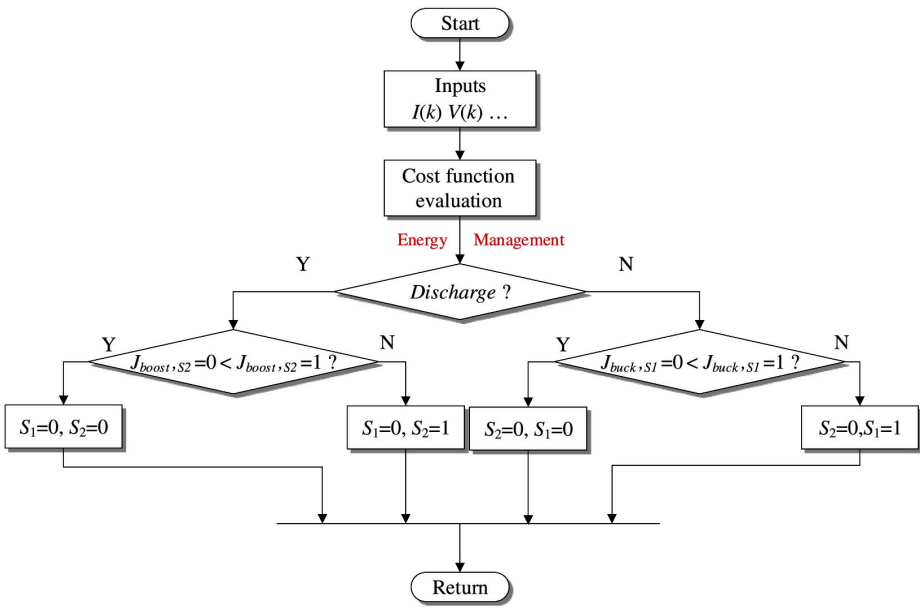


Figure 7.7 Simplified flowchart for selecting the optimal switching signal in MPC-based buck-boost conversion

7.4 MPVC of parallel inverters

For a single inverter-based local AC power system such as UPS, the target is to supply a stable and balanced output voltage for local loads. In MPVC, the voltage

across the filter capacitor is the control objective. According to the circuit shown in Figure 7.1, the dynamic behavior of the capacitor of the inverter LC filter can be expressed as

$$C\frac{d\boldsymbol{V_c}}{dt} = \boldsymbol{I_C} = \boldsymbol{I_f} - \boldsymbol{I_o} \tag{7.17}$$

Applying KVL, the voltage drop along the circuit can be expressed as

$$\boldsymbol{V_i} = \boldsymbol{I_f}R + L\frac{d\boldsymbol{I_f}}{dt} + \boldsymbol{V_c} \tag{7.18}$$

Combining (7.17) and (7.18), the above models can be expressed in a matrix form as

$$\frac{dx}{dt} = Ax + By \tag{7.19}$$

where

$$\text{x}=\begin{bmatrix}\boldsymbol{V_c}\\ \boldsymbol{I_f}\end{bmatrix},\ \text{y}=\begin{bmatrix}\boldsymbol{V_i}\\ \boldsymbol{I_0}\end{bmatrix},\ \text{A}=\begin{bmatrix}0 & 1/C\\ -1/L & -R/L\end{bmatrix},\ \text{B}=\begin{bmatrix}0 & -1/C\\ 1/L & 0\end{bmatrix}$$

By solving the linear differential equation (7.19), the following discrete-time form can be obtained:

$$x\left(k+1\right) = e^{T_S A}x\left(k\right) + A^{-1}\left(e^{T_S A} - \boldsymbol{I}_{2\times 2}\right)By\left(k\right) \tag{7.20}$$

where $\boldsymbol{I}_{2\times 2}$ is the identity matrix. Then, the capacitor voltage at the next (k+1)th instant can be predicted according to (7.20). To ensure tight tracking of the capacitor voltage to the reference, the cost function is formulated as

$$J_V = \left(V_{c\alpha}^{ref} - V_{c\alpha}^{k+1}\right)^2 + \left(V_{c\beta}^{ref} - V_{c\beta}^{k+1}\right)^2 \tag{7.21}$$

where $V_{c\alpha}$ and $V_{c\beta}$ are the real and imaginary components of the capacitor voltage, respectively. By applying all the possible inverter voltage vector into (7.20), different capacitor voltages can be predicted, leading to different values of the cost function (7.21). Then, the voltage vector that generates the least value of J_V will be selected to control the inverter. Because the α and β components are

both controlled to track their corresponding references, a stable and sinusoidal voltage can be established across the filter capacitor.

For parallel inverter-based AC power system, the droop method is commonly used to coordinate these inverters without interactive communication lines. The droop mechanism can be expressed in mathematical form as [34–36]

$$\begin{cases} f_j = f^* - m_j (P_j - P^*) \\ U_j = U^* - n_j (Q_j - Q^*) \end{cases} \tag{7.22}$$

where j is the index number of the inverters, f_j and U_j are the actual output frequency and voltage of the ith inverter, f^* and U^* indicate the nominal frequency and voltage, P^* and Q^* the nominal active and reactive power, P_j and Q_j the average active and reactive power, and m_j and n_j the droop gains.

Motivated by the effectiveness of the voltage control of MPVC and the load sharing capacity of the droop method, a new parallel inverter control strategy is developed here, as illustrated in Figure 7.8 [37]. The traditional voltage and current feedback loops have been replaced by the MPVC scheme. To obtain a better illustration, the overall block diagram of the proposed overall MPC strategy is depicted in Figure 7.9.

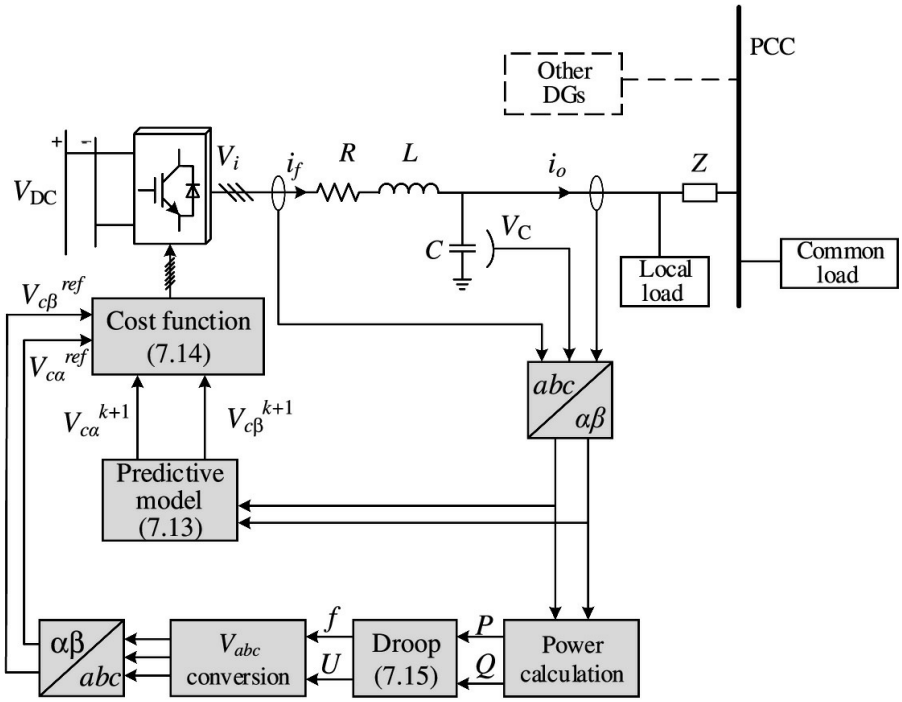


Figure 7.8 Block diagram of the combination of droop and MPVC for inverters [37]

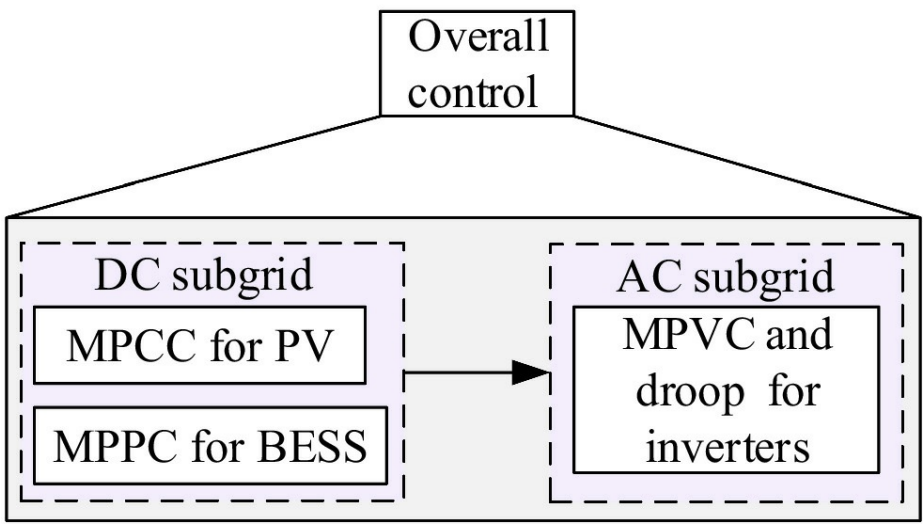


Figure 7.9 Overall control strategy for the parallel PV-ESS MG

7.5 Verification

The AC MG shown in Figure 7.1 is modeled and implemented in both MATLAB®/Simulink. The system parameters are listed in Table 7.1.

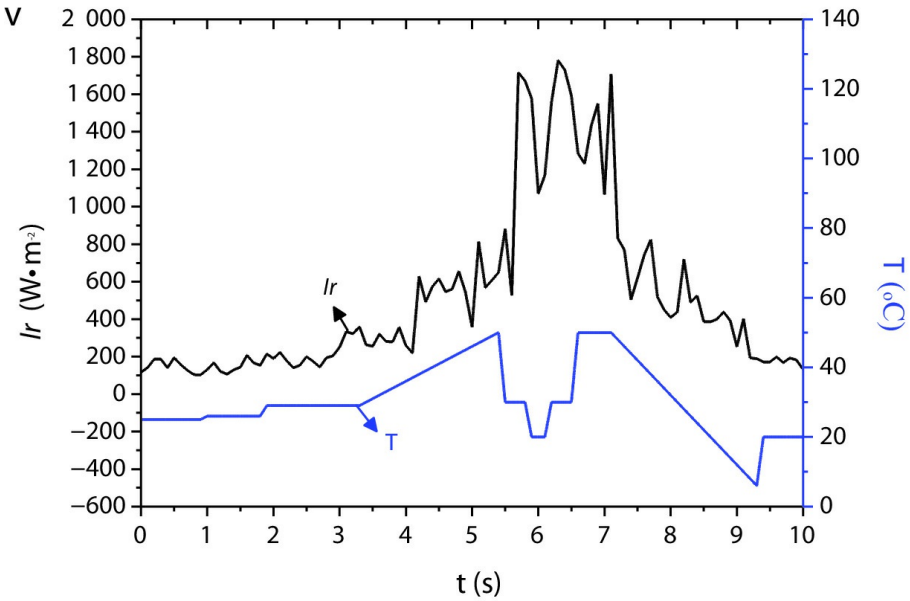
Table 7.1 System parameters

Parameters	Values
PV system	
Module maximum power (W)	305.226
Module open-circuit voltage V_{OC} (V)	64.2
Module short-circuit current I_{SC} (A)	5.96
Module voltage at maximum power point V_{mp} (V)	54.7
Module current at maximum power point I_{mp} (A)	5.58
Array parallel module strings	66
Array series-connected modules	10
BESS	
Nominal voltage (V)	500
Rated capacity (Ah)	1 600
Battery response time (s)	30
Initial SoC (%)	50
Internal resistance (Ohms)	0.003125
Integer coefficient N	2
Paralleled inverters	
DC-bus voltage V_{DC} (V)	1 000
Rated frequency f (Hz)	50
Filter inductance L (mH)	2
Filter capacitor C (μF)	250
Filter resistance R (Ohms)	0.04
DG1 and DG2 rating (kVA)	45, 42
Maximum voltage deviation (V)	10
Maximum frequency deviation (Hz)	1.5
Nominal phase-to-phase voltage V_{rms} (V)	380

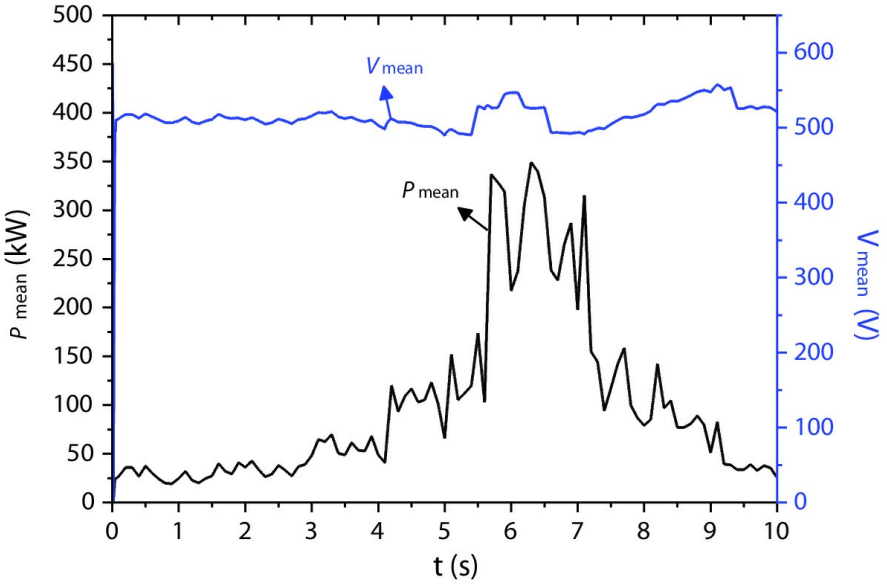
Line resistance R_{gl1} and R_{gl2} (Ohms)	0.005
Line reactance L_{gl1} and L_{gl2} (Ohms)	0.06
Line length of DG1 and DG2 (km)	10, 8
DG1 and DG2 load rated active power (kW)	18, 7
DG1 and DG2 load rated reactive power (kVAR)	7, 3.5
Common load rated active power (kW)	32
Common load rated reactive power (kVAR)	15
Sampling frequency (Hz)	25 k

7.5.1 MPPT of PV system

This case study verifies the ability of MPPT in PV systems under solar irradiation and ambient temperature variations. Figure 7.10 (a) shows the fluctuating irradiation and temperature curves, which covers the surge and slump situations happening in both PV systems of DG1 and DG2. The tracking results of DG1's can be seen from Figure 7.10 (b), considering the PV system output mean voltage and output mean power. It is seen that the proposed MPCC algorithm adjusts the boost converter input voltage accordingly under various temperature and irradiation conditions to achieve MPPT.



(a) Irradiation and temperature change



(b) PV system output mean voltage and power

Figure 7.10 PV system performance under variations of solar irradiation and ambient temperature

7.5.2 Charging and discharging processes of BESS

This case study verifies the capability of MPPC-based DC–DC buck-boost converter in BESS under the same irradiation and temperature changes as presented in Figure 7.10 (a). A DC load R_L=4 Ohms is switched into the DC-bus at 3 s. Operating in buck or boost mode is accompanied by the charging or discharging process of the battery, respectively. Figure 7.11 shows the charging and discharging processes of the battery in DG1 under environmental factors' changes and loads' changes. During approximately 0.5 s~3 s and 5.68 s~10 s, the value of SoC is increasing overall, which means the battery is being charged (buck mode), corresponding to the general negative current flowing from the DC bus into the battery and relatively high-level voltage at the battery output terminals. By contrast, during approximately 3 s~5.68 s, the battery mostly works in boost mode and the value of SoC is generally decreasing; this discharging process means a lower voltage level than that of charging.

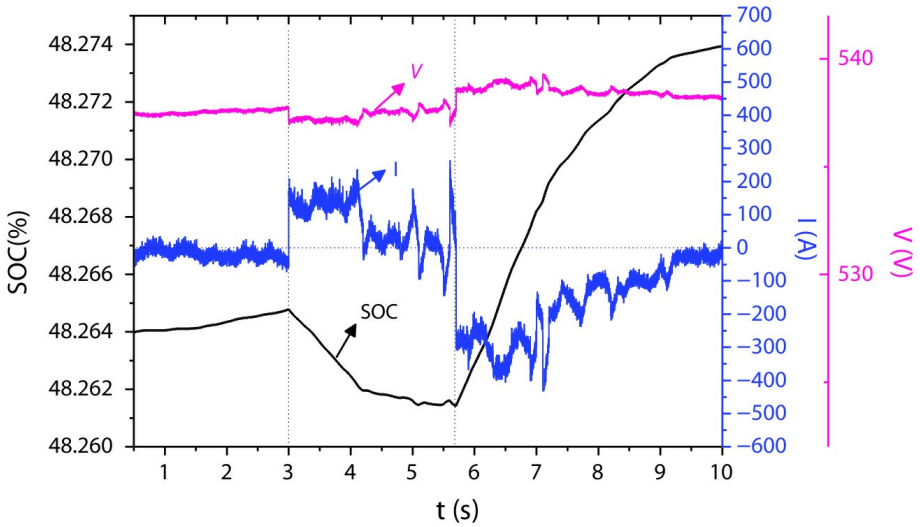


Figure 7.11 Charging and discharging processes of BESS

In this test, the dynamic response of the MPPC for the bidirectional DC–DC converter is evaluated, as shown in Figure 7.12. The system starts with a 1 000 V DC-bus reference. Then, at 3 s, DC-bus voltage reference decreases from 1 000 V to 800 V. Next, a step change in DC-bus voltage reference from 800 V to 1 200 V occurs at 6 s. From this figure, it demonstrates that the proposed MPC-based DC–DC conversion strategies achieve a fast response, a flexible regulation, and a small offset.

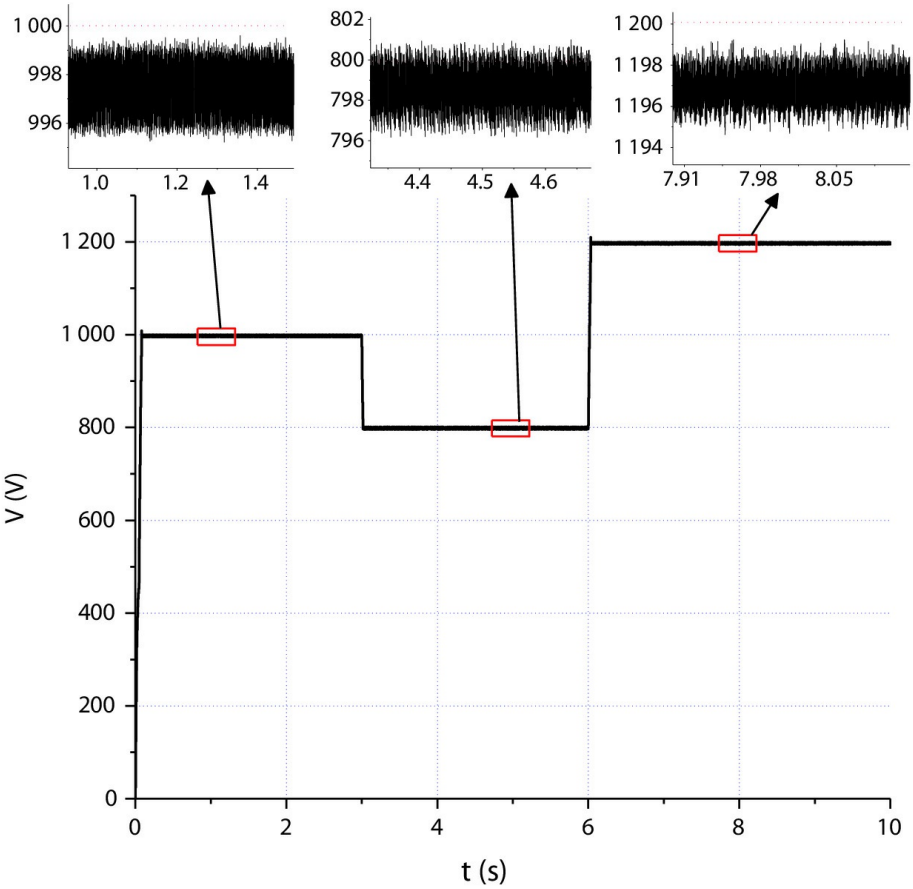


Figure 7.12 Step response of DC-bus voltage when changing DC bus references

The influences of environmental factors' changes and loads' changes on the DC-bus voltage are presented in Figure 7.13. It can be observed that the DC-bus voltage is well maintained, thanks to the voltage regulation ability of the bidirectional DC–DC converter. Specifically, under severe power consumption and generation situations such as large load connection at 3 s and rapid solar irradiation surge at 5.6 s, the DC-bus voltage is still tightly controlled, demonstrating the excellent control performance of the proposed MPPC method.

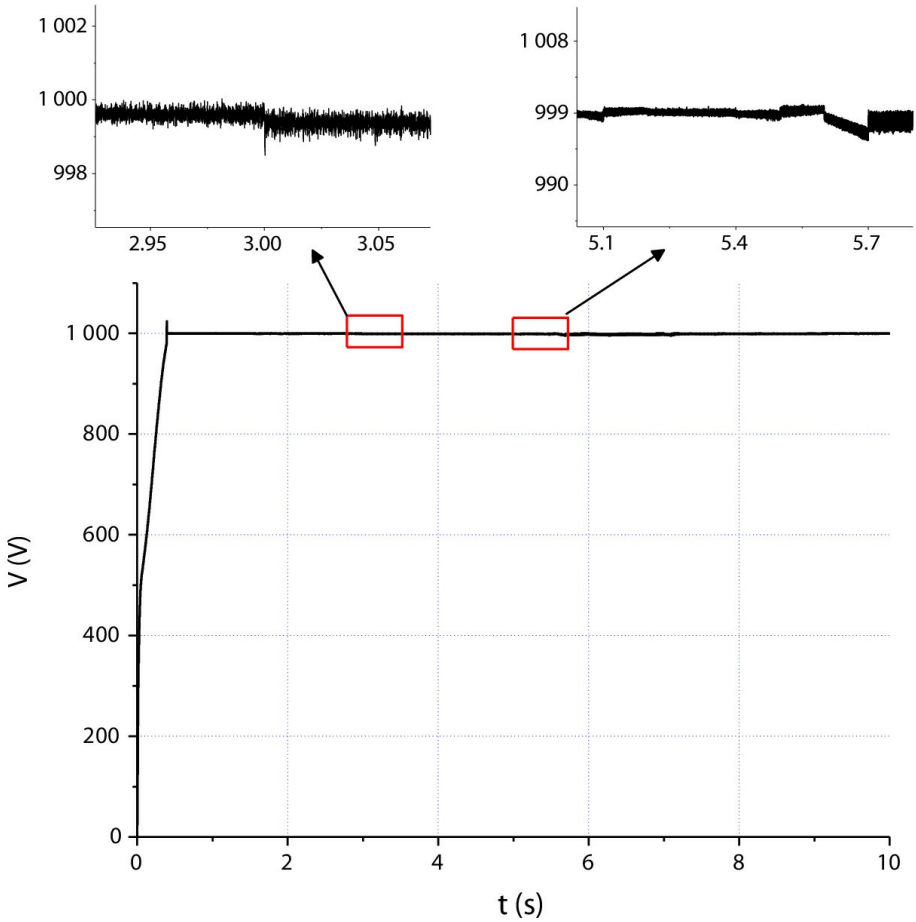


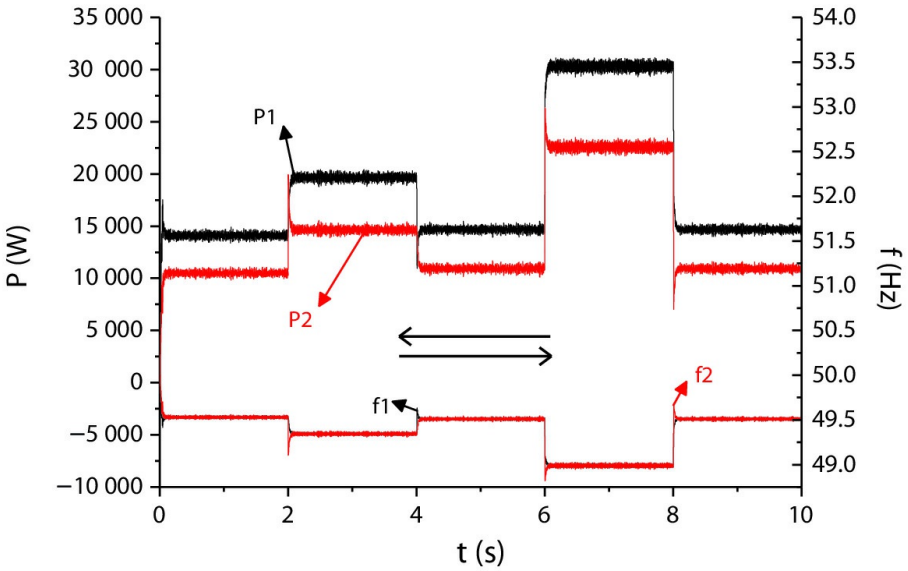
Figure 7.13 The DC-bus voltage under load variation and varying PV outputs

7.5.3 Power sharing between parallel inverters

This case study verifies the ability of the droop-MPC-combined method to control the parallel inverters of the two DGs. Voltage and frequency droop control is employed to provide the voltage references for each MPC, so it can balance the voltage and frequency in the standalone MG.

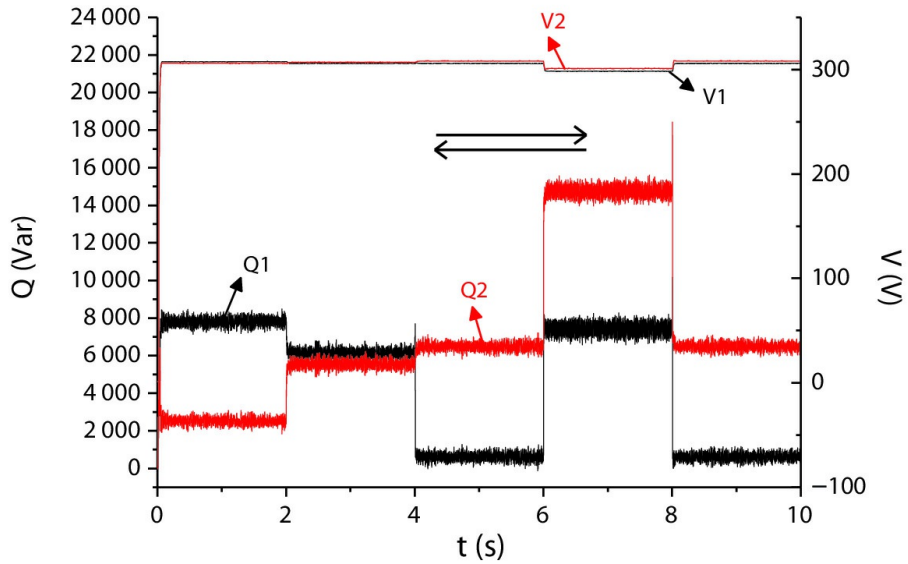
Figure 7.14 compares the changes of active power P and frequency f, reactive power Q and voltage V (magnitude) according to the loads' changes, as shown in Figure 7.14(a), (b), respectively. At 2 s, DG2 local load increases from 7 kW, 3.5 kVAR to 17 kW, 5 kVAR; at 4 s DG1 local load decreases from 18 kW, 7 kVAR to 9 kW, 2 kVAR. Then the common load is cut in at 6 s and cut off at 8 s. Since every DG has a different power rating, which means they have different droop

slopes, the power changes are provided proportional to their ratings. Each time the loads change, no matter local loads or common load, each DG contributes its own essential active and reactive power to compensate for the additional load increase, and vice versa. It can be seen that the power sharing between DGs is smooth and rapid-response.



(a) Active power and frequency

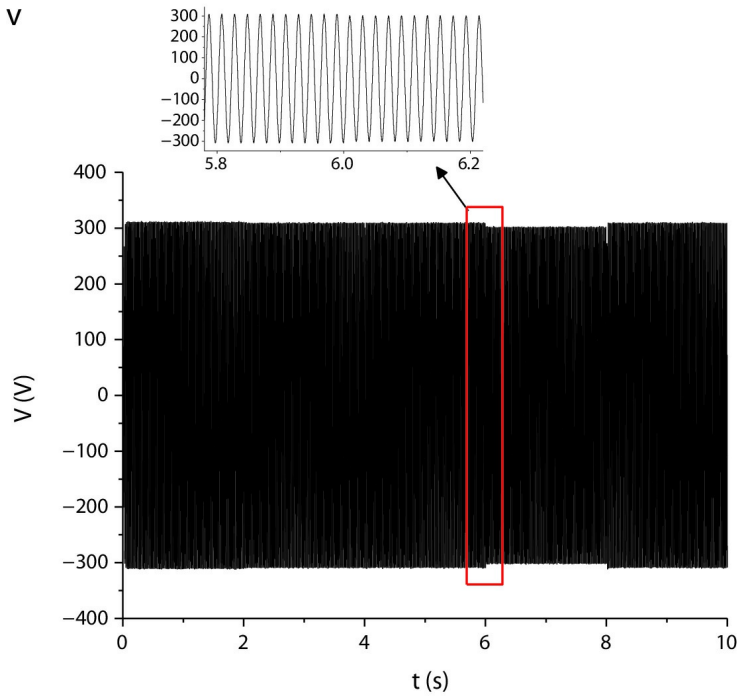
(b)



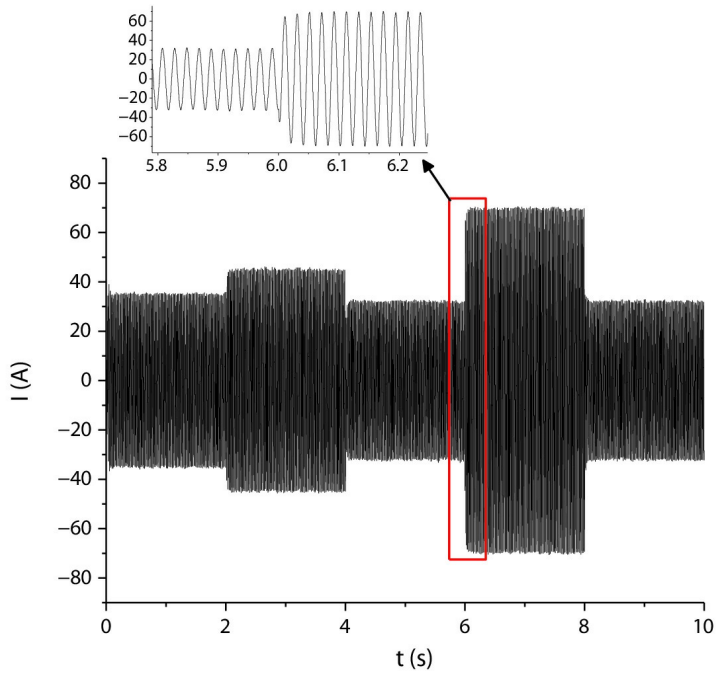
(b) Reactive power and voltage

Figure 7.14 MG response to load variations

Figure 7.15(a) and (b) present the corresponding changes of output a-phase voltage and current at PC1, respectively, under the same loads' changes in Figure 7.14. It can be seen from Figure 7.15, when loads increases, the voltage will be slightly decreased whereas the current will be obviously increased and vice versa. Although significant load changes, the whole transformation process is smooth.



(a) Output voltage



(b) Output current

Figure 7.15 DG output voltage and current

7.6 Conclusion

In this work, a MPC scheme for AC MGs with solar PVs and battery energy storage has been presented. This method addresses the problems of traditional cascade linear control including time-consuming PID tuning, complicated feedback loops, and slow dynamics. Specifically, a MPCC is used to control boost converters to achieve MPPT in solar PVs. A MPPC is developed for bidirectional DC–DC converters to maintain the DC-link voltage and mitigate the PV output fluctuation at the DC subgrid. Then a MPVC is incorporated with the droop method to control parallel inverters for load sharing at the AC subgrid. Testing results verified the effectiveness of the proposed overall control strategy, demonstrating its promising potentials in MG applications with fluctuating power generation and variable power demand.

References

[1] Guerrero J.M., GarciadeVicuna L., Matas J., Castilla M., Miret J. 'A wireless controller to enhance dynamic performance of parallel inverters in distributed generation systems'. *IEEE Transactions on Power Electronics*. 2004, vol. 19(5), pp. 1205–13.

[2] Mahmood H., Michaelson D., Jiang J. 'Accurate reactive power sharing in an islanded microgrid using adaptive virtual impedances'. *IEEE Transactions on Power Electronics*. 2015, vol. 30(3), pp. 1605–17.

[3] John B., Ghosh A., Zare F., Rajakaruna S. 'Improved control strategy for accurate load power sharing in an autonomous microgrid'. *IET Generation, Transmission & Distribution*. 2017, vol. 11(17), pp. 4384–90.

[4] Zhang J., Shu J., Ning J., Huang L., Wang H. 'Enhanced proportional power sharing strategy based on adaptive virtual impedance in low-voltage networked microgrid'. *IET Generation, Transmission & Distribution*. 2018, vol. 12(11), pp. 2566–76.

[5] Yang X., Hu H., Ge Y., Aatif S., He Z., Gao S. 'An improved droop control strategy for VSC-based MVDC traction power supply system'. *IEEE Transactions on Industry Applications*. 2018, vol. 54(5), pp. 5173–86.

[6] Mi Y., Zhang H., Fu Y., Wang C., Loh P.C., Wang P. 'Intelligent power sharing of DC isolated microgrid based on fuzzy sliding mode droop control'. *IEEE Transactions on Smart Grid*. 2019, vol. 10(3), pp. 2396–406.

[7] Zhou J., Tsai M.-J., Cheng P.-T. 'Consensus-based cooperative droop control for accurate reactive power sharing in islanded AC microgrid'. *IEEE Journal of Emerging and Selected Topics in Power Electronics*. 2019, vol. 8(2), pp. 1108–16.

[8] Gao M., Chen M., Zhao B., Li B., Qian Z. 'Design of control system for smooth mode-transfer of grid-tied mode and islanding mode in microgrid'. *IEEE Transactions on Power Electronics*. 2020, vol. 35(6), pp. 6419–35.
[9] Wei B., Guerrero J.M., Vásquez J.C., Guo X. 'A circulating-current suppression method for parallel-connected voltage-source inverters with common DC and AC buses'. *IEEE Transactions on Industry Applications*. 2017, vol. 53(4), pp. 3758–69.
[10] Sun Y., Shi G., Li X. 'An f-p/q droop control in cascaded-type microgrid'. *IEEE Transactions on Power Systems*. 2018, vol. 33(1), pp. 1136–8.
[11] Golsorkhi M.S., Shafiee Q., Lu D.D.-C., Guerrero J.M. 'Distributed control of low-voltage resistive AC microgrids'. *IEEE Transactions on Energy Conversion*. 2019, vol. 34(2), pp. 573–84.
[12] Wai R.-J., Zhang Q.-Q., Wang Y. 'A novel voltage stabilization and power sharing control method based on virtual complex impedance for an off-grid microgrid'. *IEEE Transactions on Power Electronics*. 2019, vol. 34(2), pp. 1863–80.
[13] Ang H., Chong G., Li Y. 'PID control system analysis, design, and technology'. *IEEE Transactions on Control Systems Technology: a Publication of the IEEE Control Systems Society*. 2014, vol. 13(5), pp. 1813–27.
[14] Lim C.S., Goh H.H., Lee S.S. 'Long-prediction-horizon near-optimal model predictive grid current control for PWM-driven VSIs with *LCL* filters'. *IEEE Transactions on Power Electronics*. 2021, vol. 36(2), pp. 2246–57.
[15] Liu M., Hu J., Chan K.W., *et al*. 'Dual cost function model predictive direct speed control with duty ratio optimization for PMSM drives'. *IEEE Access*. 2020, vol. 8, pp. 126637–47.
[16] Hu J., Li Y., Zhu J. 'Multi-objective model predictive control of doubly-fed induction generators for wind energy conversion'. *IET Generation, Transmission & Distribution*. 2019, vol. 13(1), pp. 21–9.
[17] Wu M., Tian H., Li Y.W., Konstantinou G., Yang K. 'A composite selective harmonic elimination model predictive control for seven-level hybrid-clamped inverters with optimal switching patterns'. *IEEE Transactions on Power Electronics*. 2021, vol. 36(1), pp. 274–84.
[18] Zheng C., Dragicevic T., Zhang Z., Rodriguez J., Blaabjerg F. 'Model predictive control of *LC* -filtered voltage source inverters with optimal switching sequence'. *IEEE Transactions on Power Electronics*. 2020, vol. 36(3), pp. 3422–36.
[19] Easley M., Shadmand M.B., Abu-Rub H. 'Hierarchical model predictive control of grid-connected cascaded multilevel inverter'. *IEEE Journal of Emerging and Selected Topics in Power Electronics* 1.
[20] Guo L., Li Y., Jin N., Dou Z., Wu J. 'Sliding mode observer-based AC voltage sensorless model predictive control for grid-connected inverters'. *IET Power Electronics*. 2020, vol. 13(10), pp. 2077–85.
[21] Low K., Cao R. 'Model predictive control of parallel-connected inverters for uninterruptible power supplies'. *IEEE Transactions on Industrial*

Electronics: A Publication of the IEEE Industrial Electronics Society. 2008, vol. 55(8), pp. 2884–93.

[22] Nguyen T., Yoo H., Kim H. 'Model predictive control of inverters in microgrids with constant switching frequency for circulating current suppression'. *In Proceeding of IEEE TENCON*. 2018, vol. 28-31, pp. 1566–71.

[23] Morstyn T., Hredzak B., Aguilera R.P., Agelidis V.G. 'Model predictive control for distributed microgrid battery energy storage systems'. *IEEE Transactions on Control Systems Technology*. 2018, vol. 26(3), pp. 1107–14.

[24] Parisio A., Rikos E., Glielmo L. 'A model predictive control approach to microgrid operation optimization'. *IEEE Transactions on Control Systems Technology*. 2014, vol. 22(5), pp. 1813–27.

[25] Ouammi A., Dagdougui H., Dessaint L., Sacile R. 'Coordinated model predictive-based power flows control in a cooperative network of smart microgrids'. *IEEE Transactions on Smart Grid*. 2015, vol. 6(5), pp. 2233–44.

[26] Dahale S., Das A., Pindoriya N.M., Rajendran S. 'An overview of DC-DC converter topologies and controls in DC microgrid'. *IEEE 7th International Conference on Power System*. 2017, pp. 1–6.

[27] Blaabjerg F., Teodorescu R., Liserre M., Timbus A.V. 'Overview of control and grid synchronization for distributed power generation systems'. *IEEE Transactions on Industrial Electronics*. 2006, vol. 53(5), pp. 1398–409.

[28] Kouro S., Leon J.I., Vinnikov D., Franquelo L.G. 'Grid-connected photovoltaic systems: An overview of recent research and emerging PV converter technology'. *IEEE Industrial Electronics Magazine*. 2015, vol. 9(1), pp. 47–61.

[29] Ma T., Cintuglu M.H., Mohammed O.A. 'Control of a hybrid AC/DC microgrid involving energy storage and pulsed loads'. *IEEE Transactions on Industry Applications*. 2017, vol. 53(1), pp. 567–75.

[30] Pirooz A., Noroozian R. 'Model predictive control of classic bidirectional dc-dc converter for battery applications'. *in Proceeding of 7th Power Electronics, Drive Systems & Technology Conference, Tehran*. 2016, pp. 517–22.

[31] Mei Y., Chen L., Li X., Sun K. 'Model predictive control method for cascaded bi-directional dc-dc converter applied to a stand-alone photovoltaic energy storage system'. *in Proceeding of 19th International Conference on Electrical Machines and Systems, Tehran*. 2016, pp. 1–5.

[32] Guler N., Biricik S., Bayhan S., Komurcugil H. 'Model predictive control of DC-DC SEPIC converters with auto-tuning weighting factor'. *IEEE Transactions on Industrial Electronics*, p. 1.

[33] Quevedo D.E., Aguilera R.P., Perez M.A., Cortes P., Lizana R. 'Model predictive control of an AFE rectifier with dynamic references'. *IEEE Transactions on Power Electronics*. 2012, vol. 27(7), pp. 3128–36.

[34] Guerrero J.M., GarciadeVicuna L., Matas J., Castilla M., Miret J. 'Output impedance design of parallel-connected ups inverters with wireless load-

sharing control'. *IEEE Transactions on Industrial Electronics*. 2005, vol. 52(4), pp. 1126–35.
[35] Han Y., Li H., Shen P., Coelho E.A.A., Guerrero J.M. 'Review of active and reactive power sharing strategies in hierarchical controlled microgrids'. *IEEE Transactions on Power Electronics*. 2017, vol. 32(3), pp. 2427–51.
[36] Li Z., Chan K.W., Hu J., Guerrero J.M. 'Adaptive droop control using adaptive virtual impedance for microgrids with variable PV outputs and load demands'. *IEEE Transactions on Industrial Electronics*. 2020.
[37] Shan Y., Hu J., Li Z., Guerrero J.M. 'A model predictive control for renewable energy based AC microgrids without any PID regulators'. *IEEE Transactions on Power Electronics*. 2018, vol. 33(11), pp. 9122–6.

Further reading

Energy storage in PVs; Battery sizing

- Barnes A.K., Balda J.C., Escobar-Mejia A. 'A semi-markov model for control of energy storage in utility grids and microgrids with PV generation'. *IEEE Transactions on Sustainable Energy*. 2015, vol. 6(2), pp. 546–56. doi:10.1109/TSTE.2015.2393353
- Afxentis S., Florides M., Machamint V., *et al*. 'Energy class dependent residential battery storage sizing for PV systems in Cyprus'. *The Journal of Engineering*. 2019, vol. 2019(18), pp. 4770–4. doi:10.1049/joe.2018.9338
- Yang Y., Ye Q., Tung L.J., Greenleaf M., Li H. 'Integrated size and energy management design of battery storage to enhance grid integration of large-scale PV power plants'. *IEEE Transactions on Industrial Electronics*. 2017, vol. 65(1), pp. 394–402. doi:10.1109/TIE.2017.2721878
- Fleischhacker A., Auer H., Lettner G., Botterud A. 'Sharing solar PV and energy storage in apartment buildings: resource allocation and pricing'. *IEEE Transactions on Smart Grid*. 2019, vol. 10(4), pp. 3963–73. doi:10.1109/TSG.2018.2844877
- Ahmadi M., Lotfy M.E., Shigenobu R., Howlader A.M., Senjyu T. 'Optimal sizing of multiple renewable energy resources and PV inverter reactive power control encompassing environmental, technical, and economic issues'. *IEEE Systems Journal*. 2019, vol. 13(3), pp. 3026–37. doi:10.1109/JSYST.2019.2918185
- PV projects worldwide. SunPower, *Fact Sheet | Solar Star Projects*. Available from https://us.sunpower.com/sites/default/files/media-library/case-studies/cs-solar-star-projects-fact-sheet.pdf [Accessed 08 Dec 2020].
- The world's biggest solar power plants. Available from www.power-technology.com/features/the-worlds-biggest-solar-power-plants [Accessed 08 Dec 2020].
- Wolfe P. An overview of the worlds' largest solar parks. Available from www.pv-magazine.com/2019/06/11/an-overview-of-the-worlds-largest-solar-parks [Accessed 08 Dec 2020].

- Australian Renewable Energy Agency, large-scale solar. Available from https://arena.gov.au/renewable-energy/large-scale-solar/ Control of PV-ESS [Accessed 08 Dec 2020].
- Ospina J., Gupta N., Newaz A., *et al*. 'Sampling-based model predictive control of PV-integrated energy storage system considering power generation forecast and real-time price'. *IEEE Power and Energy Technology Systems Journal*. 2019, vol. 6(4), pp. 195–207. doi:10.1109/JPETS.2019.2935703
- Alam M.J.E., Muttaqi K.M., Sutanto D. 'Alleviation of neutral-to-ground potential rise under unbalanced allocation of rooftop PV using distributed energy storage'. *IEEE Transactions on Sustainable Energy*. 2015, vol. 6(3), pp. 889–98. doi:10.1109/TSTE.2015.2415778
- Sharma R.K., Mishra S. 'Dynamic power management and control of a PV pem fuel-cell-based standalone AC/DC microgrid using hybrid energy storage'. *IEEE Transactions on Industry Applications*. 2018, vol. 54(1), pp. 526–38. doi:10.1109/TIA.2017.2756032
- Koh L.H., Wang P., Choo F.H., Tseng K.-J., Gao Z., Puttgen H.B. 'Operational adequacy studies of a PV-based and energy storage stand-alone microgrid'. *IEEE Transactions on Power Systems*. 2014, vol. 30(2), pp. 892–900. doi:10.1109/TPWRS.2014.2334603
- Rallabandi V., Akeyo O.M., Jewell N., Ionel D.M. 'Incorporating battery energy storage systems into multi-MW grid connected PV systems'. *IEEE Transactions on Industry Applications*. 2018, vol. 55(1), pp. 638–47. doi:10.1109/TIA.2018.2864696
- Bragard M., Soltau N., Thomas S., De Doncker R.W. 'The balance of renewable sources and user demands in grids: Power electronics for modular battery energy storage systems'. *IEEE Transactions on Power Electronics*. 2010, vol. 25(12), pp. 3049–56. doi:10.1109/TPEL.2010.2085455
- Stimoniaris D., Tsiamitros D., Dialynas E. 'Improved energy storage management and PV-active power control infrastructure and strategies for microgrids'. *IEEE Transactions on Power Systems*. 2016, vol. 31(1), pp. 813–20. doi:10.1109/TPWRS.2015.2389954
- Liu Y., Liang H. 'A three-layer stochastic energy management approach for electric bus transit centers with PV and energy storage systems'. *IEEE Transactions on Smart Grid*,1. doi:10.1109/TSG.2020.3024148
- Hashemi S., Ostergaard J., Yang G. 'A scenario-based approach for energy storage capacity determination in LV grids with high PV penetration'. *IEEE Transactions on Smart Grid*. 2014, vol. 5(3), pp. 1514–22. doi:10.1109/TSG.2014.2303580
- Zeraati M., Hamedani Golshan M.E., Guerrero J.M. 'Distributed control of battery energy storage systems for voltage regulation in distribution networks with high PV penetration'. *IEEE Transactions on Smart Grid*. 2018, vol. 9(4), pp. 3582–93. doi:10.1109/TSG.2016.2636217
- Zhou L., Zhang Y., Lin X., Li C., Cai Z., Yang P. 'Optimal sizing of PV and BESS for a smart household considering different price mechanisms'. *IEEE Access*. 2018, vol. 6, pp. 41050–9. doi:10.1109/ACCESS.2018.2845900

- Abdelrazek S.A., Kamalasadan S. ‘Integrated pv capacity firming and energy time shift battery energy storage management using energy-oriented optimization’. *IEEE Transactions on Industry Applications*. 2016, vol. 52(3), pp. 2607–17. doi:10.1109/TIA.2016.2531639
- Hashemi S., Ostergaard J. ‘Efficient control of energy storage for increasing the PV hosting capacity of LV grids’. *IEEE Transactions on Smart Grid*. 2018, vol. 9(3), pp. 2295–303.
- Hossain S.J., Biswas B.D., Bhattarai R., Ahmed M., Abdelrazek S., Kamalasadan S. ‘Operational value-based energy storage management for photovoltaic (PV) integrated active power distribution systems’. *IEEE Transactions on Industry Applications*. 2019, vol. 55(5), pp. 5320–30. doi:10.1109/TIA.2019.2920229
- van der Meer D., Chandra Mouli G.R., Morales-Espana Mouli G., Elizondo L.R., Bauer P., *et al*. ‘Energy management system with PV power forecast to optimally charge EVs at the workplace’. *IEEE Transactions on Industrial Informatics*. 2016, vol. 14(1), pp. 311–20. doi:10.1109/TII.2016.2634624
- Tran V.T., Muttaqi K.M., Sutanto D. ‘A robust power management strategy with multi-mode control features for an integrated PV and energy storage system to take the advantage of ToU electricity pricing’. *IEEE Transactions on Industry Applications*. 2018, vol. 55(2), pp. 2110–20. doi:10.1109/TIA.2018.2884622
- Wu D., Tang F., Dragicevic T., Vasquez J.C., Guerrero J.M. ‘Autonomous active power control for islanded AC microgrids with photovoltaic generation and energy storage system’. *IEEE Transactions on Energy Conversion*. 2014, vol. 29(4), pp. 882–92. doi:10.1109/TEC.2014.2358612
- Ranamuka D., Muttaqi K.M., Sutanto D. ‘Flexible AC power flow control in distribution systems by coordinated control of distributed solar-PV and battery energy storage units’. *IEEE Transactions on Sustainable Energy*. 2020, vol. 11(4), pp. 2054–62. doi:10.1109/TSTE.2019.2935479
- Liu N., Cheng M., Yu X., Zhong J., Lei J. ‘Energy-sharing provider for PV prosumer clusters: a hybrid approach using stochastic programming and stackelberg game’. *IEEE Transactions on Industrial Electronics*. 2018, vol. 65(8), pp. 6740–50. doi:10.1109/TIE.2018.2793181
- Di Piazza M.C., Luna M., La Tona G., Di Piazza A., Piazza M.C.D., Tona G.L. ‘Improving grid integration of hybrid PV-Storage systems through a suitable energy management strategy’. *IEEE Transactions on Industry Applications*. 2018, vol. 55(1), pp. 60–8. doi:10.1109/TIA.2018.2870348
- Thang T.V., Ahmed A., Kim C.-in., Park J.-H. ‘Flexible system architecture of stand-alone PV power generation with energy storage device’. *IEEE Transactions on Energy Conversion*. 2015, vol. 30(4), pp. 1386–96. doi:10.1109/TEC.2015.2429145
- Hafiz F., de Queiroz A.R., Husain I. ‘Coordinated control of PEV and PV-based storages in residential systems under generation and load uncertainties’. *IEEE Transactions on Industry Applications*. 2019, vol. 55(6), pp. 5524–32. doi:10.1109/TIA.2019.2929711

- Conte F., Massucco S., Saviozzi M., *et al*. 'Coordinated control of PEV and PV-based storages in residential systems under generation and load uncertainties'. *IEEE Transactions on Sustainable Energy*. 2018, vol. 9(3), pp. 1188–97.
- Kuleshov D., Peltoniemi P., Kosonen A., *et al*. 'Assessment of economic benefits of battery energy storage application for the PV‐equipped households in Finland'. *The Journal of Engineering*. 2019, vol. 2019(18), pp. 4927–31. doi:10.1049/joe.2018.9268
- Krata J., Saha T.K. 'Real-time coordinated voltage support with battery energy storage in a distribution grid equipped with medium-scale PV generation'. *IEEE Transactions on Smart Grid*. 2019, vol. 10(3), pp. 3486–97. doi:10.1109/TSG.2018.2828991
- Hafiz F., Awal M.A., Queiroz A.Rde., Husain I. 'Real-time stochastic optimization of energy storage management using deep learning-based forecasts for residential pv applications'. *IEEE Transactions on Industry Applications*. 2020, vol. 56(3), pp. 2216–26. doi:10.1109/TIA.2020.2968534
- Procopiou A.T., Petrou K., Ochoa L.F., Langstaff T., Theunissen J. 'Adaptive decentralized control of residential storage in PV-Rich MV–LV networks'. *IEEE Transactions on Power Systems*. 2018, vol. 34(3), pp. 2378–89.10.1109/TPWRS.2018.2889843
- 'Control of solar inverters'.
- Tummuru N.R., Mishra M.K., Srinivas S. 'Dynamic energy management of hybrid energy storage system with high-gain pv converter'. *IEEE Transactions on Energy Conversion*. 2014, vol. 30(1), pp. 150–60.10.1109/TEC.2014.2357076
- Goud P.C.D., Gupta R. 'Solar PV based nanogrid integrated with battery energy storage to supply hybrid residential loads using single‐stage hybrid converter'. *IET Energy Systems Integration*. 2020, vol. 2(2), pp. 161–9. doi:10.1049/iet-esi.2019.0030
- Mahmud N., Zahedi A., Mahmud A. 'A cooperative operation of novel PV inverter control scheme and storage energy management system based on ANFIS for voltage regulation of grid-tied PV system'. *IEEE Transactions on Industrial Informatics*. 2017, vol. 13(5), pp. 2657–68. doi:10.1109/TII.2017.2651111
- Sahu P.K., Manjrekar M.D. 'Controller design and implementation of solar panel companion inverters'. *IEEE Transactions on Industry Applications*. 2020, vol. 56(2), pp. 2001–11. doi:10.1109/TIA.2020.2965867
- Varma R.K., Rahman S.A., Vanderheide T. 'New control of PV solar farm as STATCOM (PV-STATCOM) for increasing grid power transmission limits during night and day'. *IEEE Transactions on Power Delivery*. 2015, vol. 30(2), pp. 755–63. doi:10.1109/TPWRD.2014.2375216
- Venkatramanan D., John V. 'A reconfigurable solar photovoltaic grid-tied inverter architecture for enhanced energy access in backup power applications'. *IEEE Transactions on Industrial Electronics*. 2020, vol. 67(12), pp. 10531–41. doi:10.1109/TIE.2019.2960742

- Nirmal Mukundan C.M., Jayaprakash P., Subramaniam U., Almakhles D.J. ‘Binary hybrid multilevel inverter-based grid integrated solar energy conversion system with damped SOGI control’. *IEEE Access*. 2020, vol. 8, pp. 37214–28. doi:10.1109/ACCESS.2020.2974773
- Varma R.K., Siavashi E.M. ‘Enhancement of solar farm connectivity with smart PV Inverter PV-STATCOM’. *IEEE Transactions on Sustainable Energy*. 2019, vol. 10(3), pp. 1161–71. doi:10.1109/TSTE.2018.2862405

Chapter 8
MPC of MGs with secondary restoration capability

In Chapter 7, a model predictive control (MPC) scheme has been incorporated with a droop method to control parallel photovoltaics-energy storage system - microgrids (MGs). Yet, there is still one problem that needs to be addressed, i.e., the voltage and frequency deviations. In this chapter, the drawbacks in the primary control layer are discussed. Then, secondary control is studied to restore the frequency and voltage. Specifically, a model predictive voltage control (MPVC) scheme taking into account the voltage changing trend is then developed to control the distributed inverters to improve the output voltage quality. A washout filter-based secondary control scheme with the plug-and-play capability is adopted to achieve proper load-sharing among parallel inverters and mitigate the voltage deviation.

8.1 Background and system configuration

MGs, formed by various distributed generations (DGs) such as solar photovoltaics (PVs), wind turbines, energy storages, and fuel cells have been broadly recognized as promising solution for future power grids featuring high renewable energy penetration and bidirectional power flow [1]. Depending on the voltage bus types, MGs can be classified into AC, DC, and hybrid types. Owing to the fact that most of the power is transferred through AC distribution networks, most of the MGs are AC and hybrid AC–DC types, though DC MGs have attracted increasing attention [2]. As the electronic interfaces between the power sources and the loads, power converters play a crucial role in MGs. For this reason, the development of advanced and high-performance control strategies for these power converters has become an ongoing research focus [3].

Unlike the grid-connected operation in which the voltage is strongly maintained by the stiff utility grid, it is critical to share the load demand properly while maintaining stable voltage and frequency in an islanded operation. Conventionally, the droop control method is used for power sharing [4–6]. However, it inherits several drawbacks. These include voltage frequency deviations subject to load variations, poor power quality in presence of nonlinear

loads [7], low power-sharing accuracy with mixed resistive and inductive transmission lines [8], and the trade-off between the voltage regulation and the power-sharing accuracy [9, 10].

To eliminate the voltage and frequency deviations caused by the droop control scheme, secondary control has been proposed, which can be classified into three groups: centralized, distributed, and decentralized. The majority of existing secondary control techniques are implemented centrally, e.g., those used for frequency and voltage restoration, reactive power-sharing, and voltage unbalance/harmonic compensation. In the centralized structure, a central controller coordinates the DGs and restores the frequency and voltage amplitudes. In this structure, all measured data, i.e., the voltage, current, and frequency are generally transmitted through a high-data-rate communication network. Active-power management, voltage control, reactive-power management, frequency restoration, and harmonic cancellation are the main features of centralized secondary control [11–14]. A centralized secondary control technique using proportional-integral-derivative regulators is studied in [15] to restore the frequency and voltage to the nominal level at the point of common coupling (PCC). In [16], a fuzzy-secondary-controller is proposed to regulate the voltage and frequency. Nevertheless, centralized secondary control suffers from its distinct centralized communication structure that requires point-to-point communication between the central controller and all DGs, which increases system complexity and compromises its scalability and reliability due to delay and data loss problems. Besides, it is usually costly in terms of both communication and computation when the number of DGs increases. Most importantly, the central controller exposes a single point-of-failure, i.e., any failure whether in the communication infrastructure or the central controller itself affects the overall stability and performance of the MG. Therefore, any deficiency in the communication network or failure degrades MG efficiency.

Considering the limitation of centralized secondary control, distributed control schemes have been recently developed as attractive solutions, given their sparse network structure, scalability, and improved resiliency to faults or unknown parameters. Those distributed secondary control approaches with reduced communication burden have become a competitive alternative. As units in an MG are heterogeneous and spatially distributed, it makes a natural fit for distributed control or multiagent system (MAS) network control to enhance MG stability and performance while addressing reliability and enhancing the scalability of MGs. In such kind of distributed control strategies, a local secondary control is designed for each DG to generate set points of the droop control to compensate the deviations produced by the primary control. Initially, an averaging-based structure was adopted, in which each DG measures its frequency and voltage amplitudes and then communicates them to all other DGs [17–19]. A more popular distributed control approach, distributed cooperative control, aims to force agents to converge to a consensus based on the information shared with neighbors. In cooperative control, each agent has its own state variable and dynamics. A fundamental concept in MAS is the design of distributed protocols based on graph

theory to guarantee consensus or synchronization in which all the agents reach the same value. In distributed control of MASs for MGs, a number of agents work together to achieve a set of objectives, e.g., voltage, frequency, and power. The effectiveness of achieving these objectives is related to the agent (i.e., DG) dynamics and the topology of the employed communication structure. Depending on whether there is a leader during the consensus or synchronization, consensus-based distributed secondary control can be further classified into two groups, i.e., cooperative regulator control and cooperative tracker control [20]. A pinning-based hierarchical and distributed cooperative control was recently proposed for microgrid cluster (MGC), which consists of three layers, i.e., DG-layer, MG-layer, and MGC-layer controls [21]. The DG-layer control is responsible for the local voltage/current of each DG unit as well as load sharing. The MG-layer control cooperatively manages DG units in each MG through several sparse communication networks. It attempts to restore frequency and voltage within each MG. Further, by treating each MG as an agent, the MGC-layer control coordinates MGs through a higher-level peer-to-peer communication graph. The MG-layer communication is interacted with the MGC-layer communication by pinning some DG units of each MG to communicate with the MG agent. The MGC-layer control coordinates each MG to share active or reactive power among them and to regulate the system frequency and voltage in a distributed manner.

In decentralized control, each DG restores its own frequency and voltage amplitudes to nominal values individually, while communication among DGs is not needed. Recently, several decentralized control approaches have been developed. For example, to eliminate the impact of time delay caused by the low-bandwidth communication lines and restore the frequency and voltage amplitude to the rated values simultaneously, washout filter-based power-sharing strategies have been presented in [22, 23] without any communication links. Washout filter-based power-sharing strategy stems from the combination of droop and secondary control methods. It is essentially an improved droop method by adding a band-pass filter formed by a low-pass filter and a high-pass filter. It is capable of restoring frequency and voltage back to the nominal values while the communication-free and decentralized features can be retained. For example, a washout filter-based power-sharing method was developed in [22] to restore the voltage and frequency to the nominal levels. In [23], it is proved that a washout filter-based power-sharing approach is actually equivalent to distributed secondary control in a stand-alone MG. The techniques presented in [22] and [23] have opened a promising research horizon in power sharing and voltage or frequency restoration in distributed inverter operation. However, the washout filter-based power-sharing methods developed so far also have their limitations. One of the concerns is the inconsistency in voltage restoration in different voltage buses and local load terminals, which actually is a common problem for many secondary control methods. In this sense, similar to other secondary control techniques, the washout filter-based methods still need to be further explored and improvements are still desired to fulfill the actual needs.

Indeed, as demonstrated by the ongoing research publications about primary

control and secondary control, many improved techniques have been developed to enhance the power-sharing accuracy and dynamics and to mitigate voltage deviations in MGs. All the effort made by researchers has provided a solid foundation for MG technologies to flourish. However, inverter control structure at the lowest bottom level of the hierarchy, or the inner control loops at Level 0, has not been investigated with enough research attention in the context of MG control. So far, conventional cascaded linear control has been applied in most of the MG control methods. As a matter of fact, as the Level 0 control layer in the bottom, such cascaded linear control techniques can significantly impact the effectiveness of higher-level control including Level 1—primary control, Level 2—secondary control, and Level 3—tertiary control. Their relationship and mutual impacts need to be thoroughly investigated, particularly from the perspective of MGs with fluctuating renewable energy and variable power demand.

Different from the cascaded linear control, MPC is based on the minimization of a predefined cost function by evaluating the predicted response of a power converter over a finite time horizon at each time step. Due to its fast dynamic response and flexibility in integrating various control objectives and constraints, MPC has been commonly utilized in the control of power converters. Examples include MPC of DC–AC inverters for islanded energy systems [24–27], AC–DC rectifiers to draw grid power and accommodate DC loads [28–30], bidirectional DC–DC converters for batteries charging/discharging [31, 32], DC–DC boost converters for solar PVs [33], and DC–DC buck converters for stepping down voltages [34]. Although these technologies have been applied in electric drives and individual DGs, they do not address large systems with multiple DGs and various power converters. In MGs with renewable energy sources and various types of loads, researchers face new challenges, especially renewable energy intermittency, power quality, proper load-sharing among DGs, etc. These are still open problems for MPC.

To fill the technical gap mentioned earlier, a new control scheme is proposed in this research for MGs with energy storage, local loads, and practical renewable energy resources to supply high-quality and reliable power. The system configuration of such as MG is shown in Figure 8.1. The control of the solar PVs with battery energy storage system (BESS) in the DC subgrid has been discussed in detail in Chapters 6 and 7. In this chapter, a MPVC incorporated with a washout filter-based power-sharing scheme is developed to control the parallel voltage source inverters (VSIs).

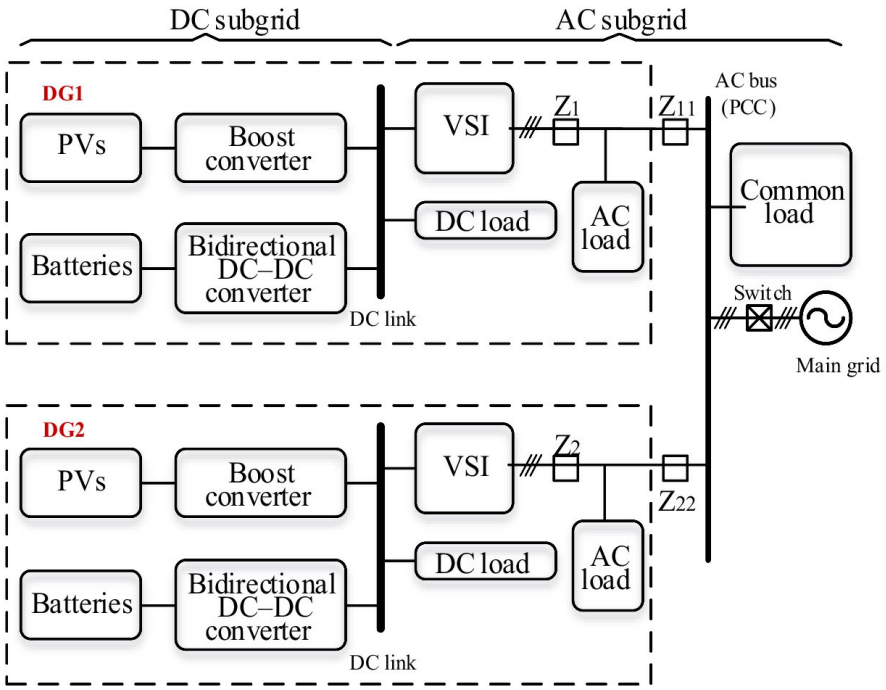


Figure 8.1 A MG with PV-BESS and multiple converters

8.2 Washout filter-based power-sharing method

- Droop-based power-sharing method

The power flow analysis within the PV-ESS systems and the control of bidirectional DC–DC converters using MPPC strategy have been studied in Chapters 6 and 7. They are therefore not discussed again here. After the PV output is buffered and the DC-bus voltage is maintained by the BESS, we can now proceed to control the AC subgrid of the MG. To coordinate the distributed power sources for voltage regulation and proper power-sharing, the well-known droop control method, which mimics the behavior of synchronous generators in traditional power plants, can be applied in this application without the requirement of communication among DGs. Its characteristic can be described as [4]

$$f = f^* - mP \tag{8.1}$$

$$E = E^* - nQ \tag{8.2}$$

where E and E^* are the measured and reference voltage values, respectively, f and f^* the measured and reference frequency values, m and n the droop coefficients, and P and Q the actual active and reactive powers contributed by a DG, respectively.

In load sharing based on the droop scheme, frequency and voltage deviations are inevitable due to the droop features expressed in (8.1) and (8.2). To address this issue, secondary control strategies are widely employed. For both frequency and voltage, the errors between the nominal values and the actual values are processed by PI controllers to generate the required compensations, which will be added to the original droop controller. This secondary control principle can be expressed in s-domain as [17]

$$f_c = k_{pf}\left(f^* - f\right) + \frac{k_{if}}{s}\left(f^* - f\right) \tag{8.3}$$

$$E_c = k_{pE}\left(E^* - E\right) + \frac{k_{iE}}{s}\left(E^* - E\right) \tag{8.4}$$

where f_C and E_C are the frequency and voltage compensation terms. k_{pf}, k_{if}, k_{pE}, and k_{iE} are the tuning parameters of the PI regulators for frequency and voltage compensation, respectively.

For this centralized secondary control structure, a central controller with low-bandwidth communication lines is required to establish the information connection between the central controller and the DGs. Such centralized secondary control suffers from inherent shortcomings of its communication mechanism, such as single point of failure, delay, and data loss. These problems can be addressed by introducing the washout filter-based power-sharing strategy in a decentralized manner.

- Relation between secondary control method and washout filter-based method

The washout filter-based power-sharing strategy can be derived based on the droop scheme and the secondary control method, as elaborated below [23].

Taking the frequency, f, as an example, one can rewrite the droop mathematical characteristic with the secondary control's compensation as

$$f = f^* - mP + f_c \tag{8.5}$$

By considering only the integration, i.e., setting $k_{pf} = 0$, (8.3) can be simplified as

$$f_c = \frac{k_{if}}{s}\left(f^* - f\right) \tag{8.6}$$

Substituting (8.5) into (8.6) yields

$$f_c = \frac{k_{if}}{s}\left(f^* - \left(f^* - mP + f_c\right)\right) = \frac{k_{if}}{s}\left(mP - f_c\right) \tag{8.7}$$

(8.7) can be rearranged as

$$f_c = \frac{k_{if}}{s + k_{if}} mP \tag{8.8}$$

Substituting (8.8) into (8.5), one can obtain

$$f = f^* - \frac{s}{s + k_{if}} mP \tag{8.9}$$

Compared to (8.1), (8.9) has an extra component $s/(s+k_{if})$. This is exactly the transfer function of a typical washout filter. This washout filter is actually a high-pass filter [35]. It can filter out DC components while letting transient components pass through, which renders the power sharing more robust against parameter uncertainties [36]. In a similar manner, (8.2) can be rewritten as

$$E = E^* - \frac{s}{s + k_{iE}} nQ \tag{8.10}$$

From this point of view, it can be seen that the washout filter-based power-sharing strategy expressed in (8.9) and (8.10) is endowed with the capability to eliminate the frequency and voltage gaps because of the droop scheme while at the same time the communication-free and decentralized features can be retained. This equivalence is subject to the following distinct attributes:

1. The frequency and voltage information are measured locally in the DGs, not from the PCC, which is different from the central-based secondary control.
2. The target voltage which is aimed to be restored is the filter capacitor's voltage of the inverter, i.e., the DG output voltage. This voltage can be regulated to the nominal value under the no-load condition. However, when a local load with high power demand is connected, the restoration will

deteriorate.

These restrictions limit the effectiveness of the washout filter functioning as the secondary controller to eliminate the deviations. These will be further analyzed, and a solution will be offered in the section below.

- Improved washout filter with PCC voltage compensation

In a MG, the frequency is a global quantity, independent of MG topologies and control strategies. If the droop control method is used, according to (8.1), any change in active power will affect the instantaneous frequency throughout the entire system. On the other hand, the situation is different when it comes to voltage. Due to the mixed impedance of distribution lines between the DGs and the PCC, the voltage will drop along these lines, leading to an unequal sharing of reactive power. According to (8.2), this kind of reactive power-sharing causes voltage drops complicatedly. The voltage drop along a line can be approximately computed by [37]

$$eE \approx \frac{XQ_e + RP_e}{E^*} \tag{8.11}$$

where eE indicates the voltage drop along the line; R and X are resistance and inductance of the line, Q_e and P_e the reactive and active powers passing through the line, respectively, and E^* is the reference voltage amplitude.

Equation (8.11) clearly reveals that though the washout filter method can restore the inverter output voltage to the rated value, the PCC voltage will still deviate from the rated value due to the line impedance. Since the PCC voltage is not directly controlled, it brings challenges to the grid-connection process. To further mitigate the voltage deviation and recover the PCC voltage, an additional coefficient, dv, can be added to eE. Hence, the voltage control will be eventually designed as

$$E = E^* - \frac{s}{s+k_{iE}} nQ + dv \cdot eE \cdot \underbrace{\frac{f_l}{s+f_l}}_{low-pass\ filter} \tag{8.12}$$

In the development of this improved washout filter-based secondary method, one concern is the information on X and R of the line impedance, since they are not always readily available. To get to know the impedance, given a power line, both offline and online methods can be applied. Offline methods use the original systematic states to evaluate the impedance [38]. On the other hand, online approaches rely on real-time measurements to estimate the impedance [39].

Another concern is the determination of dv, as the adjustment of dv can raise

the inverter output voltage to compensate the voltage drop at PCC. Regarding a DG as a local power generator and the power line as the distribution network, the electric power supply rules can also be applied in a MG. In this study, the voltage threshold φ is 10 percent. This threshold defines the upper approximation of dv as the following

$$dv \le \varphi \cdot E^* / \left(\frac{XQ_0 + RP_0}{E^*} \right) \tag{8.13}$$

where Q_0 and P_0 indicate the DG's capacity. By adding dv into (8.12), one can adjust flexibly dv to regulate the PCC voltage in a certain range to meet the actual requirements from the common loads and the possible utility grid connection.

8.3 Improved model predictive voltage control scheme

Subsequent to the determination of the voltage reference from the washout filter, the task is to control the inverters for proper power-sharing. The control algorithm can be implemented in the $\alpha\beta$ stationary orthogonal reference frame rather than the abc reference frame due to the advantage of less computation. The variable x (voltage or current) in the $\alpha\beta$ frame can be obtained by the Clarke transformation as

$$x_{\alpha\beta} = \frac{2}{3}\left[1 \; e^{(2\pi/3)j} \; e^{(4\pi/3)j}\right]\left[x_a \; x_b \; x_c\right]^{\mathrm{T}} = x_\alpha + jx_\beta \tag{8.14}$$

- The conventional MPVC method

The two-level three-phase VSI is one of the most common converters used in MGs to provide AC power supplies. It is therefore used in this study. A VSI can generate totally eight (2^3) possible switching states, which can be expressed as

$$\begin{cases} i = 1, 2, \ldots, 6: \; V_i = \frac{2}{3} V_{dc} e^{(i-1)(\pi/3)j} \\ i = 0, 7: \; V_i = \mathbf{0} \end{cases} \tag{8.15}$$

Accordingly, the gating signal combination ($S_a \; S_b \; S_c$) are 000, 100, 110, 010, 011, 001, 101, and 111, respectively. Figure 8.2 shows the equivalent circuit of the AC-subgrid.

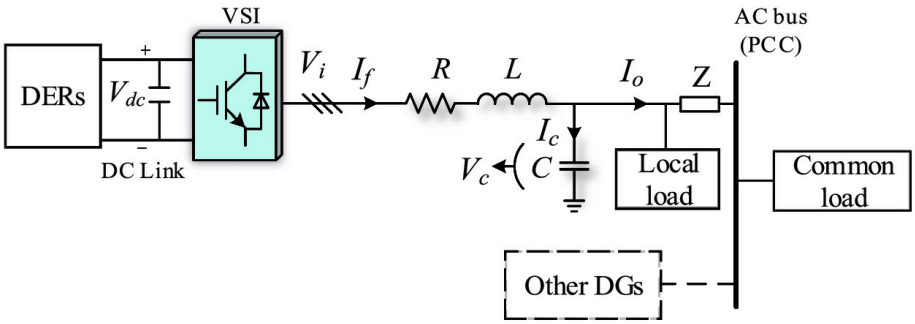


Figure 8.2 AC-subgrid circuitry

As shown in Figure 8.2, a VSI converts the DC power into AC power and supplies it to the local load and common load. An LC filter is used to eliminate the harmonics, where L is the inductance, C the capacitance, and R the resistance of the LC filter.

According to Kirchoff's Current Law and the capacitor dynamics, one can obtain

$$C\frac{dV_c}{dt} = I_C = I_f - I_o \tag{8.16}$$

where V_C and I_C are the capacitor voltage and current, respectively. I_f and I_O are the inductor and output currents, respectively.

Further, according to Kirchoff's Voltage Law, one obtains

$$L\frac{dI_f}{dt} = V_i - I_f R - V_c \tag{8.17}$$

Combining (8.16) and (8.17), a state-space model of the AC-subgrid can be written as [24, 26]

$$\frac{dx}{dt} = \boldsymbol{Ax} + \boldsymbol{By} \tag{8.18}$$

where

$$\boldsymbol{x}=\begin{bmatrix} V_c \\ I_f \end{bmatrix},\ \boldsymbol{y}=\begin{bmatrix} V_i \\ I_0 \end{bmatrix},\ \boldsymbol{A}=\begin{bmatrix} 0 & 1/C \\ -1/L & -R/L \end{bmatrix},\ \boldsymbol{B}=\begin{bmatrix} 0 & -1/C \\ 1/L & 0 \end{bmatrix}$$

Based on (8.18), the AC-subgrid can be discretized as

$$x\left(k+1\right)=e^{T_S A}x\left(k\right)+A^{-1}\left(e^{T_S A}-\boldsymbol{I}_{2\times 2}\right)By\left(k\right) \tag{8.19}$$

where $\boldsymbol{I}_{2\times 2}$ is the identity matrix. Using (8.19), the future capacitor voltage can be predicted. Conventionally, in to provide a stable and sinusoidal voltage supply, the cost function considering the voltage amplitude is designed as

$$J_V=\left(V_{c\alpha}^{*}-V_{c\alpha}\left(k+1\right)\right)^2+\left(V_{c\beta}^{*}-V_{c\beta}\left(k+1\right)\right)^2 \tag{8.20}$$

where $V_{c\alpha}(k+1)$ and $V_{c\beta}(k+1)$ are the real and imaginary parts of the predicted capacitor voltage, respectively. $V_{c\alpha}^{*}$ and $V_{c\beta}^{*}$ are the real and imaginary parts of the reference voltage, respectively. The voltage vector with its corresponding gating signal that can result in the least value of the cost function (8.20) will be chosen to control the VSI.

- The improved MPVC with voltage quality enhancement

From the conventional MPVC, the cost function J_V considers only the amplitude of the objective voltage. Unlike most of the MPC where the control reference is constant such as a constant power reference in grid-connected inverter system or a constant torque reference in electric drives, the control reference here is a perfect sinusoidal waveform. This means the reference values in the cost function vary with time, which brings in difficulties in tight amplitude tracking, and the vibrations around the reference trajectory are more likely to occur. As a result, it deteriorates the tracking accuracy.

To cope with the technical issue mentioned above, an improved MPVC scheme that takes into account the voltage changing trend for better voltage tracking is adapted here [40]. Figure 8.3 is shown to explain the idea behind this strategy. For an easy start, it is assumed that the voltage tracking errors at kth time instant are the same using conventional MPVC and improved MPVC, i.e., ΔE_0. Also, the trend of change, i.e., the slopes of trajectories, S_{con0} and S_{imp0}, is the same and equal to S_{ref0}. For the sake of simplicity, only two alternative predicted values, V_1 and V_2, are discussed, i.e., V_1 or V_2 will be selected in the future decision at the next step prediction horizon. At the $(k+1)$th instant as shown in Figure 8.3, V_1 and V_2 have the same error, ΔE_1, to the reference trajectory, the conventional and improved tracking methods can pass through either V_1 or V_2. In this case, just considering the voltage amplitude is not helpful, but once the slope is also included in the determination, the trajectory of the improved track is more

likely to be obtained with $S_{imp1} = S_{ref1}$. Otherwise, the conventional track may happen when $S_{con1} \neq S_{ref1}$, resulting in an inferior track.

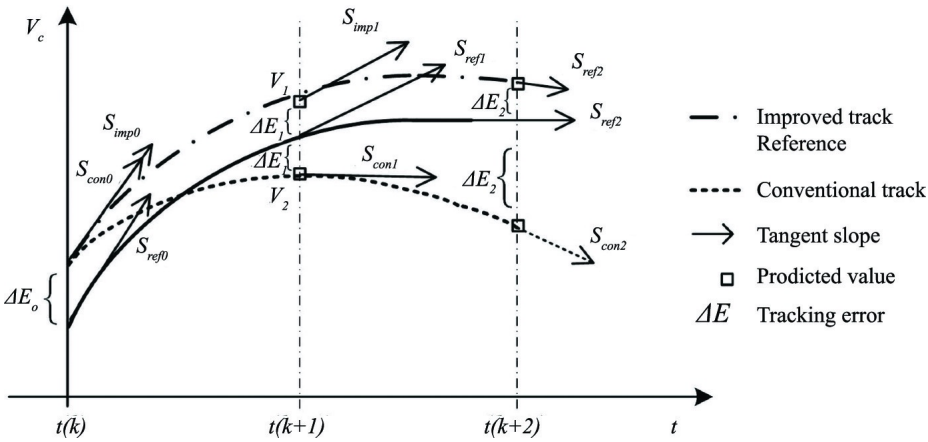


Figure 8.3 Voltage-tracking trajectory

This situation may aggravate if the (k+2)th time instant is considered for one-step delay compensation. Under the same error, ΔE_2, when the slope is respected ($S_{imp2} = S_{ref2}$), the improved tracking method can tightly follow the reference. Otherwise, when the slope is overlooked ($S_{con2} \neq S_{ref2}$), the tracking trajectory by the conventional method will deflect the reference, leading to higher harmonic distortion. To explain in a simple term, if the slope (i.e., the trend of change) is also considered in the determination (i.e., the cost function), the tracking trajectory (i.e., the improved track) will approach the reference as closely as possible.

In the improved MPVC scheme, one of the key steps is to obtain the "slope," which can be calculated by taking the derivative of the capacitor voltage. Since the cost function (8.20) contains two terms, the derivative operation needs to be applied to both voltage reference and actual values.

To get the referenced derivative value, we start with the expression of the capacitor voltage reference, i.e.,

$$\begin{aligned} V_c^* &= V_{c\alpha}^* + jV_{c\beta}^* \\ &= V_c sin\left(\omega t\left(k\right)\right) + jV_c cos\left(\omega t\left(k\right)\right) \end{aligned} \tag{8.21}$$

where ω is the angular frequency.

Taking derivatives of (8.21) yields

$$\frac{dV_c^*}{dt} = \omega V_c cos\left(\omega t\left(k\right)\right) - j\omega V_c sin\left(\omega t\left(k\right)\right) = \omega V_{c\beta}^* - j\omega V_{c\alpha}^* \tag{8.22}$$

The predicted derivative value of V_c based on the discrete-time model of (8.16) can then be calculated as [41]

$$\frac{dV_c\left(k+1\right)}{dt} = \frac{I_f\left(k+1\right) - I_o\left(k\right)}{C} = \frac{I_{f\alpha}\left(k+1\right) - I_{o\alpha}\left(k\right)}{C} + j\frac{I_{f\beta}\left(k+1\right) - I_{o\beta}\left(k\right)}{C} \tag{8.23}$$

where $I_{f\alpha}\left(k+1\right)$ and $I_{f\beta}\left(k+1\right)$ are obtained from (8.19).

To minimize both the real and imaginary tracking errors between the references of (8.22) and the predicted values of (8.23), the following cost function can be formulated

$$J_{VD} = \left(\omega V_{c\beta}^* - \left(\frac{i_{f\alpha}\left(k+1\right) - i_{o\alpha}\left(k\right)}{C}\right)\right)^2 + \left(\omega V_{c\alpha}^* + \left(\frac{i_{f\beta}\left(k+1\right) - i_{o\beta}\left(k\right)}{C}\right)\right)^2 \tag{8.24}$$

Finally, the complete improved cost function can be expressed as [41]

$$J = aJ_V + bJ_{VD} \tag{8.25}$$

where *a* and *b* are the weighting coefficients. The first term is used to track the voltage amplitude and the second term to track the voltage changing trend. This cost function will be used to evaluate the effect of each possible voltage vector. The optimal switching state that minimizes *J* is selected and applied to control the inverter.

- Overall control strategy

For better comparison, the conventional droop method with cascaded inner feedback loops and the proposed overall control strategy are depicted in Figures

8.4 and 8.5, respectively. For the proposed strategy, first, P and Q can be computed by

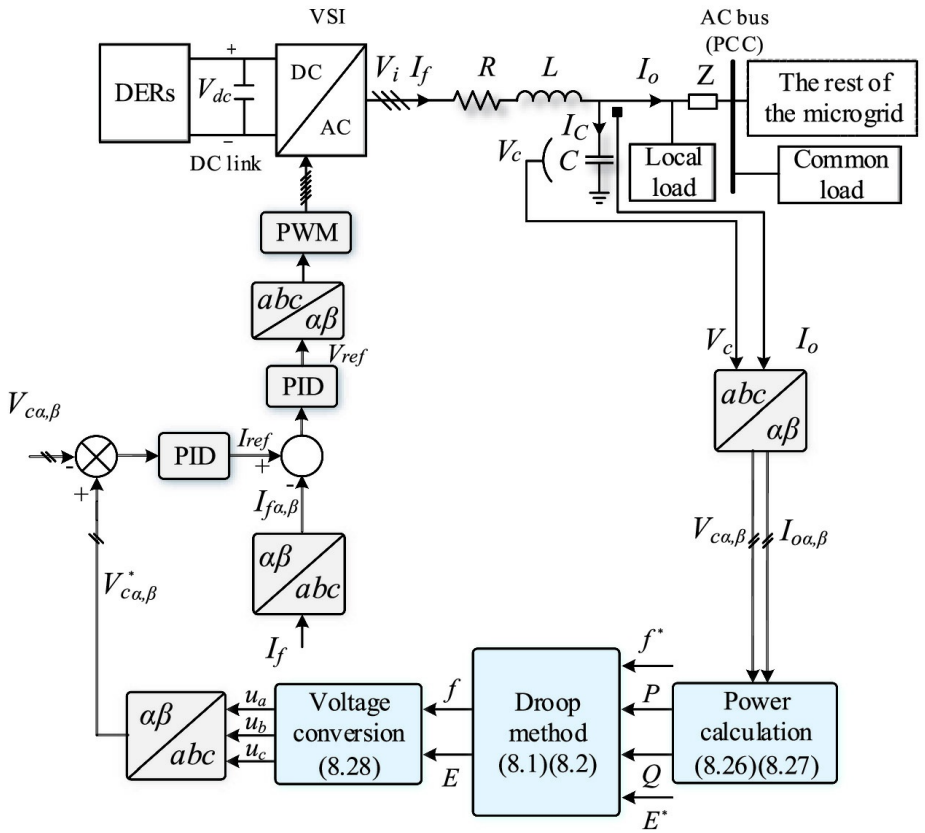


Figure 8.4 Block diagram of the conventional overall control scheme

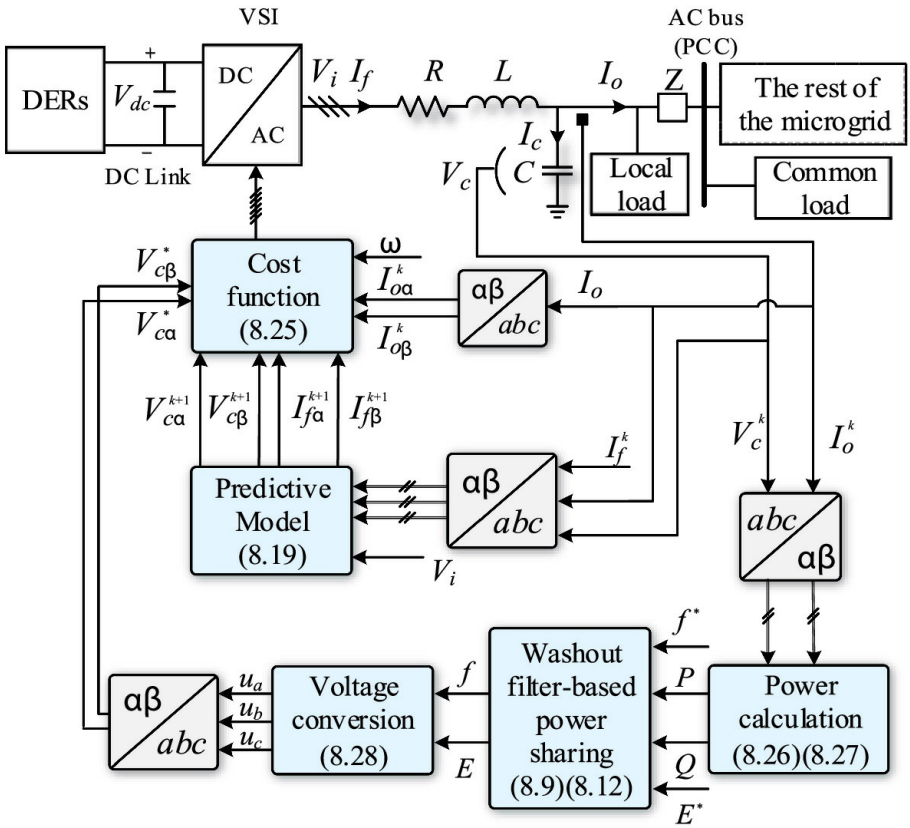


Figure 8.5 Proposed overall control strategy of inverters (improved MPVC and improved washout filter-based power-sharing strategy) [41]

$$P = \frac{3}{2}\left(V_{c\alpha}I_{o\alpha} + V_{c\beta}I_{o\beta}\right) \cdot \underbrace{\frac{f_l}{s + f_l}}_{low\text{-}pass\ filter} \tag{8.26}$$

$$Q = \frac{3}{2}\left(V_{c\beta}I_{o\alpha} - V_{c\alpha}I_{o\beta}\right) \cdot \underbrace{\frac{f_l}{s + f_l}}_{low\text{-}pass\ filter} \tag{8.27}$$

where f_l is the cutoff frequency of the low-pass filter.

Next, the washout filter-based power-sharing method will generate the frequency and voltage references. Three-phase voltage conversion is then required to transform this frequency and voltage into three-phase sinusoidal voltages through

$$\begin{cases} u_a = E\sin\left(2\pi f + 0\right) \\ u_b = E\sin\left(2\pi f - 2\pi/3\right) \\ u_c = E\sin\left(2\pi f + 2\pi/3\right) \end{cases} \tag{8.28}$$

where u_a, u_b, and u_c are the three-phase voltages. Further transferred into $\alpha\beta$ reference frame, these voltage references will then be delivered to the inner MPVC controller.

8.4 Results

The proposed control method depicted in Figure 8.5 is validated based on the MG configuration shown in Figure 8.1. The system data and control parameters are listed in Table 8.1 [41]. Two identical DGs, namely DG1 and DG2, are used in the test. A diode-bridge rectifier with a combination of a capacitor and a resistor at the DC side is used as a nonlinear load. Initially, both AC and DC loads are connected to DG 1 and DG2 locally. Then, a sequence of events described in Table 8.2 occurs, respectively, to examine the effectiveness of the proposed control strategy [41].

Table 8.1 System parameters

Voltage level	Value
AC-bus voltage	380 V (p-p, rms), 50 Hz

DC-rated voltage	1 000 V
Circuit	**Value**
AC-bus LC filter	R = 0.02 Ω, L = 3.6 mH, C = 200 μF
DC-side circuit	L_{Bf} = 50 μH, L_B = 170 μH, L_B = 80 mH, C_1 = 50 mF, C_2 = 26 mF, C_3=100 μF
Line impedance	R_{line} = 0.1 Ω, L_{line} = 2.4 mH
Generation	**Value**
Solar PV	SunPower Spr-305-WHT, 200 kW (STD)
Battery	Lithium-ion, 500 V, 1.6 kAh
Load	**Value**
Initial DC loads	DG1: 20 kW, DG2: 20 kW
Initial AC loads	DG1: (50 kW, 0 kVAR), DG2: (50 kW, 0 kVAR)
AC common load	(40 kW, 10 kVAR)
Nonlinear AC load	R_{nl} = 75 Ω, C_{nl} = 20 mF
Control	**Value**
MPPC	N = 1
Power sharing	$_m$ = 1.25e−5, $_n$ = 8.33e−5, k_{if} = 15, k_{iE} = 10, $_{fl}$ = 6.25 Hz
Washout filter	dv =1.84 during ~1 sto3 s, other time: 1.62
MPVC	Improved: (a = 0.8, b = 0.2), conventional: (a = 1, b = 0)
Sampling interval	20 μs

Table 8.2 Load profile

Sequence	Operations	Time (s)
AC side		
1	AC common load increases from 40 kW, 10 kVAR to 80 kW, 20 kVAR	1
3	AC common load decreases from 80 kW, 20 kVAR to 40 kW, 10 kVAR	3
4	Nonlinear AC load switches in	5

6	Nonlinear AC load switches out	7
DC side		
2	Each DG's DC load increases from 20 kW to 40 kW	2
5	Each DG's DC load decreases from 40 kW to 20 kW	6

Figure 8.6 presents the performance of the DC side of the MG using the proposed control strategy under varying solar irradiation and ambient temperature profiles and subject to a series of events specified in Table 8.2. From the result, a fluctuant PV output power is observed due to the resultant effects of fluctuating solar irradiation and ambient temperature, as shown in Figure 8.6c. Thanks to the MPPC scheme for PV-ESS, which has been detailed in Chapter 7, a stable DC-link voltage supply is maintained as shown in Figure 8.6d. Compared to the result of conventional cascaded loops control structure as shown in Figure 8.7e, the MPPC scheme leads to a smoother and more stable DC-link voltage with much fewer voltage ripples.

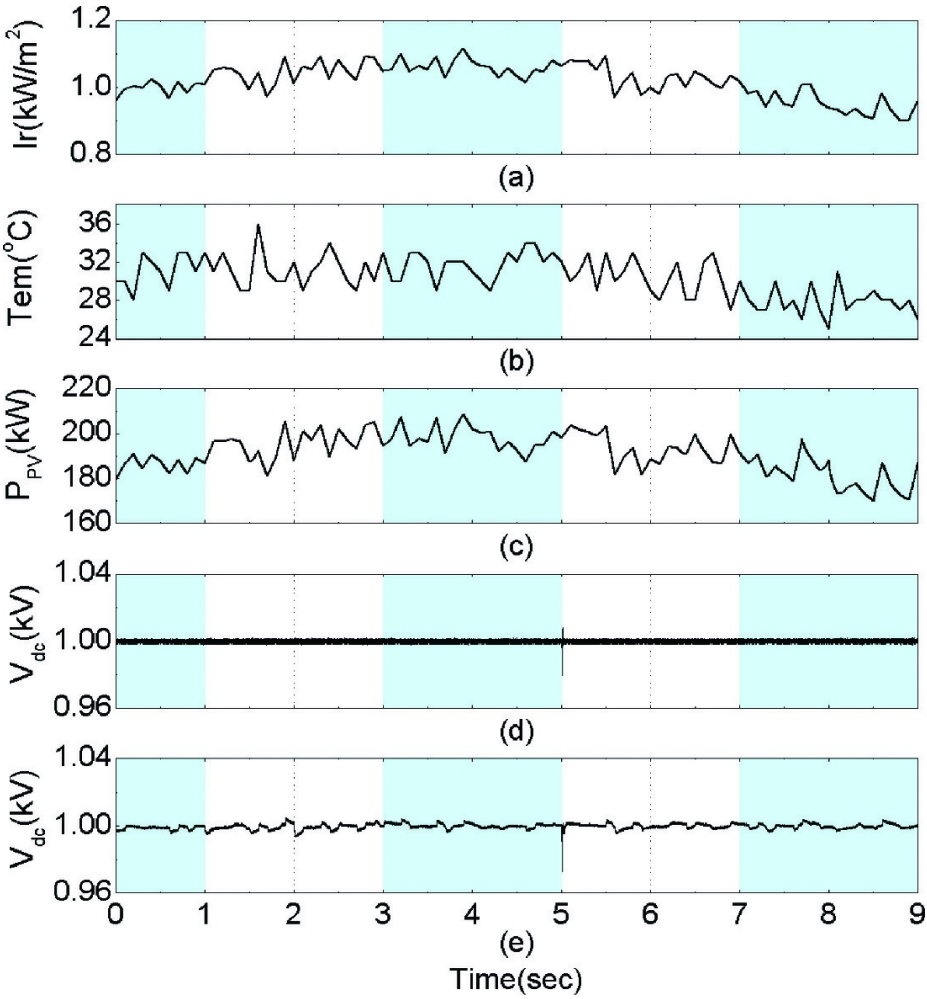


Figure 8.6 Performance of the DC side of the MG using the proposed control strategy under varying solar irradiation and ambient temperature and variable load demand. (a) Solar irradiation, (b) ambient temperature, (c) electrical power generated by PVs, (d) DC-link voltage by using MPPC scheme, (e) DC-link voltage using conventional cascaded loops control structure.

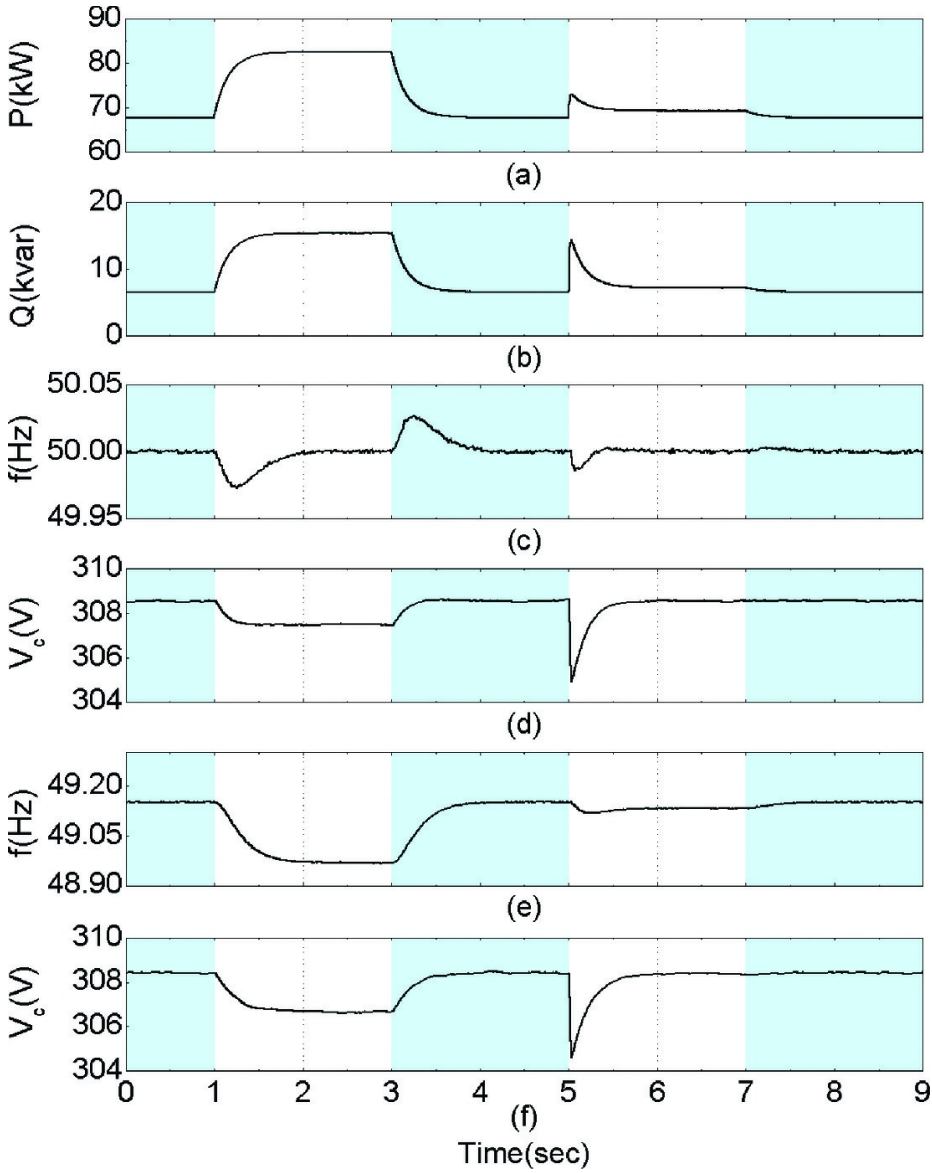
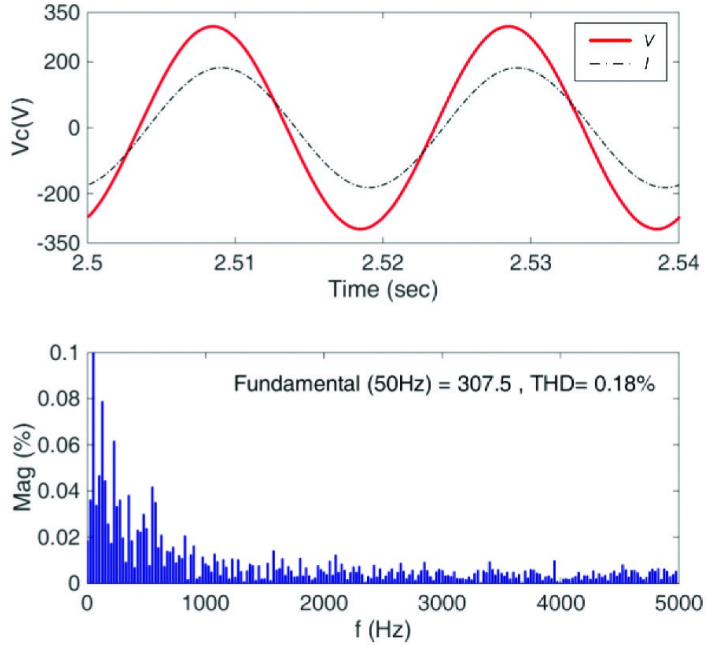


Figure 8.7 Performance of AC side of the MG using the proposed control strategy. (a) DG1 active power output, (b) DG1 reactive power output, (c) DG1 frequency using proposed washout filter-based power-sharing method, (d) DG1 output voltages using proposed washout filter-based power-sharing method, (e) DG1 frequency using conventional droop control,

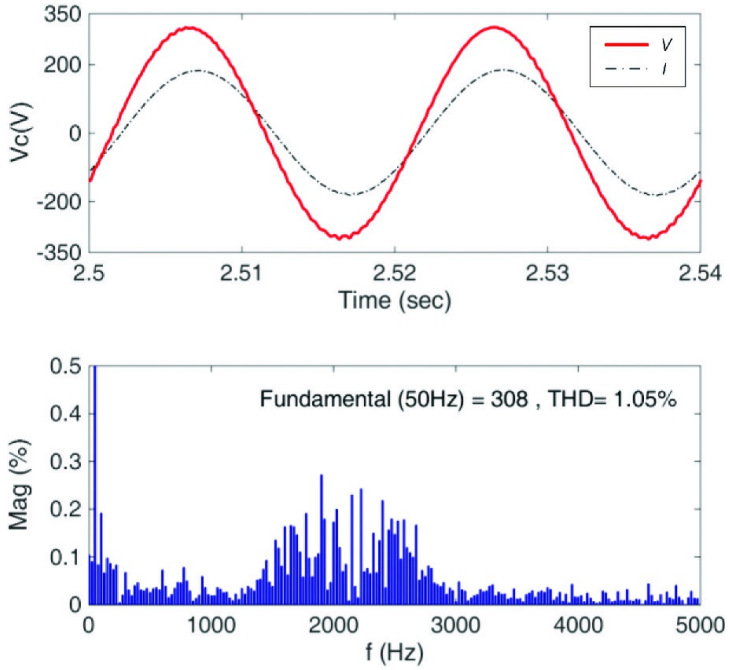
(f) DG1 output voltage using conventional droop control.

After the PV outputs have been smoothed and DC-bus voltages can be maintained in the DC-subgrid, the performance of the AC-subgrid will be evaluated. As listed in Table 8.2, a series of events are taking place to evaluate the performance of the proposed washout filter-based power-sharing strategy with the improved MPVC scheme. Figure 8.7 shows the power-sharing performance of the washout filter with improved MPVC cost function under the same PV profile shown in Figure 8.6 and the same load profile in Table 8.2. Figure 8.7a and b show that the washout filter-based power-sharing method can well respond to the changing load demands. Figure 8.6c presents the frequency response of the proposed method. It can be seen that the frequency can track the nominal level subsequence to load variations in 1 s, 3 s, 5 s, and 7 s, showing a robust frequency restoration capability. This actually appears to be a consequence of central secondary control as shown in [4], and it demonstrates the equivalence between secondary control and washout filter-based power-sharing method. In contrast, obvious frequency deviation can be observed in Figure 8.6e without using the washout filter-based power-sharing scheme, particularly between 1 s and 3 s when AC common load is increased. Figure 8.6e and f compares the voltage performance. It is found that the proposed strategy can also compensate the voltage amplitude deviation.

It is noted that, in the proposed overall control strategy in this work, an improved MPVC scheme is incorporated with the washout filer-based power-sharing strategy. To validate the advantage of the improved MPVC algorithm, the AC-side performance of the MG is further studied and analyzed. Figure 8.8 shows the voltage quality when the MG supplies linear loads. Comparing Figure 8.8a and b, MPVC with improved cost function (8.25) shows a better voltage quality and a lower total harmonic distortion (THD) value than MPVC with conventional cost function (8.20). Figure 8.9 shows the voltage quality when the MG supplies nonlinear loads. Due to nonlinear loads, the THD values increase. However, the performance of MPVC with improved cost function is still superior to MPVC with a conventional cost function.

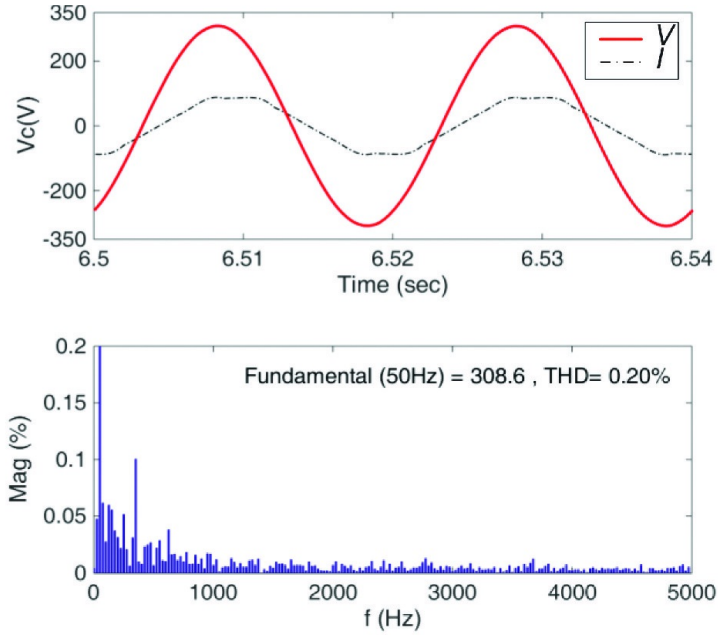

V
I
Vc(V)
Time (sec)
Fundamental (50Hz) = 307.5 , THD= 0.18%
Mag (%)
f (Hz)

(a)

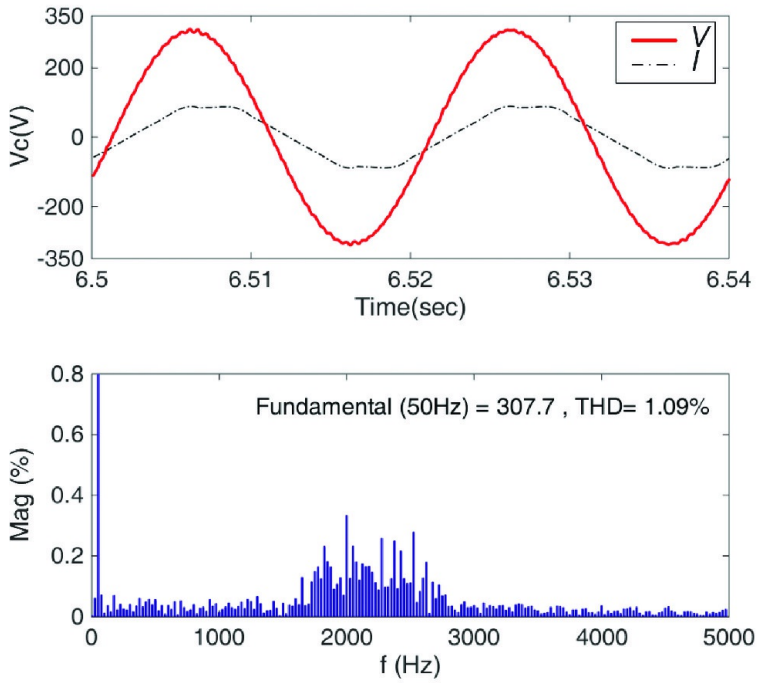

V
I
Vc(V)
Time (sec)
Fundamental (50Hz) = 308 , THD= 1.05%
Mag (%)
f (Hz)

(b)

Figure 8.8 Voltage quality when the MG supplies linear loads [41]. (a) DG1 output voltage using improved cost function (8.25), (b) DG1 output voltage using conventional cost function (8.20).


V
I
Vc(V)
Time (sec)
Fundamental (50Hz) = 308.6 , THD= 0.20%
Mag (%)
f (Hz)

(a)


V
I
Vc(V)
Time(sec)
Fundamental (50Hz) = 307.7 , THD= 1.09%
Mag (%)
f (Hz)

(b)

Figure 8.9 Voltage quality when the MG supplies nonlinear loads [41]. (a) DG1 output voltage using improved cost function (8.25), (b) DG1 output voltage using conventional cost function (8.20).

8.5 Conclusion

This research work aims to address the voltage deviation problem in a decentralized manner without involving a heavy communication burden. Specifically, a washout filter-based power-sharing strategy is developed to ensure proper load sharing. It can not only restore the voltage and frequency to the nominal levels but also enable plug-and-play capability for individual DGs within the MG. Furthermore, an improved MPVC technique is incorporated with the washout filter-based power-sharing approach. The purpose is to further improve the AC voltage quality with less THD under both linear and nonlinear loads.

References

[1] Huang J., Jiang C., Xu R. 'A review on distributed energy resources and microgrid'. Renewable and Sustainable Energy Reviews. 2008, vol. 12(9), pp. 2472–83.

[2] Yang P., Xia Y., Yu M., Wei W., Peng Y. 'A decentralized coordination control method for parallel bidirectional power converters in a hybrid AC–DC microgrid'. *IEEE Transactions on Industrial Electronics*. 2018, vol. 65(8), pp. 6217–28.

[3] Dai K., Liu P., Wang G., Duan S., Chen J. 'Practical approaches and novel control schemes for a three-phase three-wire series-parallel compensated universal power quality conditioner'. *The 19th Annual IEEE Applied Power Electronics Conference and Exposition, 2004 (APEC04), Anaheim, CA, USA*. 2004, vol. 1, pp. 601–6.

[4] Guerrero J.M., Vasquez J.C., Matas J., de Vicuna L.G., Castilla M. 'Hierarchical control of droop-controlled AC and DC microgrids—a general approach toward standardization'. *IEEE Transactions on Industrial Electronics*. 2011, vol. 58(1), pp. 158–72.

[5] Li X., Guo L., Zhang S., *et al*. 'Observer-based DC voltage droop and current feed-forward control of a DC microgrid'. *IEEE Transactions on Smart Grid*. 2018, vol. 9(5), pp. 5207–16.

[6] Sun Y., Hou X., Yang J., Han H., Su M., Guerrero J.M. 'New perspectives on droop control in AC microgrid'. *IEEE Transactions on Industrial Electronics*. 2017, vol. 64(7), pp. 5741–5.

[7] Deng Y., Tao Y., Chen G., Li G., He X. 'Enhanced power flow control for

grid-connected droop-controlled inverters with improved stability'. *IEEE Transactions on Industrial Electronics*. 2017, vol. 64(7), pp. 5919–29.
[8] John B., Ghosh A., Zare F. 'Load sharing in medium voltage islanded microgrids with advanced angle droop control'. *IEEE Transactions on Smart Grid*. 2018, vol. 9(6), pp. 6461–9.
[9] Micallef A., Apap M., Spiteri-Staines C., Guerrero J.M., Vasquez J.C. 'Reactive power sharing and voltage harmonic distortion compensation of droop controlled single phase islanded microgrids'. *IEEE Transactions on Smart Grid*. 2014, vol. 5(3), pp. 1149–58.
[10] Guan Y., Guerrero J.M., Zhao X., Vasquez J.C., Guo X. 'A new way of controlling parallel-connected inverters by using synchronous-reference-frame virtual impedance loop—Part I: control principle'. *IEEE Transactions on Power Electronics*. 2016, vol. 31(6), pp. 4576–93.
[11] Bidram A., Davoudi A. 'Hierarchical structure of microgrids control system'. *IEEE Transactions on Smart Grid*. 2012, vol. 3(4), pp. 1963–76.
[12] Savaghebi M., Jalilian A., Vasquez J.C., Guerrero J.M. 'Secondary control for voltage quality enhancement in microgrids'. *IEEE Transactions on Smart Grid*. 2012, vol. 3(4), pp. 1893–902.
[13] Savaghebi M., Jalilian A., Vasquez J.C., Guerrero J.M. 'Secondary control scheme for voltage unbalance compensation in an islanded droop controlled microgrid'. *IEEE Transactions on Smart Grid*. 2011, vol. 3(99), pp. 1–11.
[14] Mehrizi-Sani A., Iravani R. 'Potential-function based control of a microgrid in islanded and grid-connected modes'. *IEEE Transactions on Power Systems*. 2010, vol. 25(4), pp. 1883–91.
[15] Guerrero J.M., Vasquez J.C., Matas J., de Vicuna L.G., Castilla M. 'Hierarchical control of droop-controlled AC and DC microgrids—a general approach toward standardization'. *IEEE Transactions on Industrial Electronics*. 2011, vol. 58(1), pp. 158–72.
[16] Andalib-Bin-Karim C., Liang X., Zhang H. 'Fuzzy-secondary-controller-based virtual synchronous generator control scheme for interfacing inverters of renewable distributed generation in microgrids'. *IEEE Transactions on Industry Applications*. 2018, vol. 54(2), pp. 1047–61.
[17] Shafiee Q., Guerrero J.M., Vasquez J.C. 'Distributed secondary control for islanded microgrids—a novel approach'. *IEEE Transactions on Power Electronics*. 2014, vol. 29(2), pp. 1018–31.
[18] Simpson-Porco J.W., Shafiee Q., Dörfler F., Vasquez J.C., Guerrero J.M., Bullo F. 'Secondary frequency and voltage control of islanded microgrids via distributed averaging'. *IEEE Transactions on Industrial Electronics*. 2015, vol. 62(11), pp. 7025–38.
[19] Schiffer J., Dörfler F., Fridman E. 'Robustness of distributed averaging control in power systems: time delays & dynamic communication topology'. *Automatica*. 2017, vol. 80(3), pp. 261–71.
[20] Bidram A., Nasirian V., Davoudi A., Lewis F.L. *Cooperative Synchronization in Distributed Microgrid Control*. Berlin/Heidelberg: Springer; 2017.

[21] Wu X., Xu Y., He J., Wang X., Vasquez J.C., Guerrero J.M. 'Pinning-based hierarchical and distributed cooperative control for AC microgrid clusters'. *IEEE Transactions on Power Electronics*. 2020, vol. 35(9), pp. 9865–85.
[22] Yazdanian M., Mehrizi-Sani A. 'Washout filter-based power sharing'. *IEEE transactions on smart grid*. 2016, vol. 7(2), pp. 967–8.
[23] Han Y., Li H., Xu L., Zhao X., Guerrero J.M. 'Analysis of washout filter-based power sharing strategy—an equivalent secondary controller for islanded microgrid without Lbc lines'. *IEEE Transactions on Smart Grid*. 2018, vol. 9(5), pp. 4061–76.
[24] Cortes P., Ortiz G., Yuz J.I., Rodriguez J., Vazquez S., Franquelo L.G. 'Model predictive control of an inverter with output LC filter for UPS applications'. *IEEE Transactions on Industrial Electronics*. 2009, vol. 56(6), pp. 1875–83.
[25] Preindl M., Bolognani S. 'Model predictive direct speed control with finite control set of PMSM drive systems'. *IEEE Transactions on Power Electronics*. 2013, vol. 28(2), pp. 1007–15.
[26] Hu J., Xu Y., Cheng K.W., Guerrero J.M. 'A model predictive control strategy of PV-battery microgrid under variable power generations and load conditions'. *Applied Energy*. 2018, vol. 221(6), pp. 195–203.
[27] Ipoum-Ngome P.G., Mon-Nzongo D.L., Flesch R.C.C., Song-Manguelle J., Wang M., Tao J. 'Model-free predictive current control for multilevel voltage source inverters'. *IEEE Transactions on Industrial Electronics*, p. 1.
[28] Zhang Y., Li Z., Xu W., Hu J., Zhu J. 'Grid synchronization of DFIG using model predictive direct power control'. *In Proceedings of International Conference on Electrical Machines and Systems*. 2011, pp. 1–6.
[29] Hu J., Cheng K.W.E. 'Predictive control of power electronics converters in renewable energy systems'. *Energies*. 2017, vol. 10(4), pp. 515–14.
[30] Pourmahdi-Torghabe M., Ghazi R. 'Fuzzy-based model predictive control for three-phase rectifier'. *Proceedings of 11th Power Electronics, Drive Systems, and Technologies Conference*. 2020, pp. 1–6.
[31] Gong Z., van de Ven B.A.C., Gupta K.M., *et al*. 'Distributed control of active cell balancing and low-voltage bus regulation in electric vehicles using hierarchical model-predictive control'. *IEEE Transactions on Industrial Electronics*. 2020, vol. 67(12), pp. 10464–73.
[32] Shan Y., Hu J., Cheng K.W., Liu M. 'A universal model predictive control for practical AC microgrids with PVS and battery energy storage systems'. *In Proceedings of IEEE Energy Conversion Congress and Exposition (ECCE)*. 2018, pp. 6257–62.
[33] El Islam Remache S., Barra K. 'Performance comparison among boost and multi level boost converters for photovoltaic grid connected system using finite set model predictive control'. *The 9th International Renewable Energy Congress (IREC)*. 2018, pp. 1–6.
[34] Liu Z., Xie L., Bemporad A., Lu S. 'Fast linear parameter varying model predictive control of buck DC-DC converters based on FPGA'. *IEEE Access*.

2018, vol. 6, pp. 52434–46.
[35] Guerrero J.M., Matas J., Garcia De Vicunagarcia De Vicuna L., Castilla M., Miret J. 'Wireless-control strategy for parallel operation of distributed-generation inverters'. *IEEE Transactions on Industrial Electronics*, vol. 53(5), pp. 1461–70.
[36] Hassouneh M.A., Lee H.-C., Abed E.H. 'Washout filters in feedback control: benefits, limitations and extensions'. *Proceedings of American Control Conference, Boston, MA, USA*. 2004, pp. 3950–5.
[37] He J., Li Y.W. 'An enhanced microgrid load demand sharing strategy'. *IEEE Transactions on Power Electronics*. 2012, vol. 27(9), pp. 3984–95.
[38] Mahmood H., Michaelson D., Jiang J. 'Accurate reactive power sharing in an islanded microgrid using adaptive virtual impedances'. *IEEE Transactions on Power Electronics*. 2015, vol. 30(3), pp. 1605–17.
[39] Ritzmann D., Wright P.S., Holderbaum W., Potter B. 'A method for accurate transmission line impedance parameter estimation'. *IEEE Transactions on Instrumentation and Measurement*. 2016, vol. 65(10), pp. 2204–13.
[40] Dragičević T. 'Model predictive control of power converters for robust and fast operation of Ac microgrids'. *IEEE Transactions on Power Electronics*. 2018, vol. 33(7), pp. 6304–17.
[41] Shan Y., Hu J., Liu M., Zhu J., Guerrero J.M. 'Model predictive voltage and power control of islanded PV-battery microgrids with washout-filter-based power sharing strategy'. *IEEE Transactions on Power Electronics*. 2020, vol. 35(2), pp. 1227–38.

Further reading

Secondary control

- Rey J.M., Marti P., Velasco M., Miret J., Castilla M. 'Secondary switched control with no communications for islanded microgrids'. *IEEE Transactions on Industrial Electronics*. 2017, vol. 64(11), pp. 8534–45. doi:10.1109/TIE.2017.2703669
- Kammer C., Karimi A. 'Decentralized and distributed transient control for microgrids'. *IEEE Transactions on Control Systems Technology*. 2019, vol. 27(1), pp. 311–22. doi:10.1109/TCST.2017.2768421
- Romero M.E., Seron M.M. 'Ultimate boundedness of voltage droop control with distributed secondary control loops'. *IEEE Transactions on Smart Grid*. 2019, vol. 10(4), pp. 4107–15. doi:10.1109/TSG.2018.2849583
- Dou C., Yue D., Zhang Z., Ma K. 'MAS-based distributed cooperative control for DC microgrid through switching topology communication network with time-varying delays'. *IEEE Systems Journal*. 2017, vol. 13(1), pp. 615–24. doi:10.1109/JSYST.2017.2726081
- Li Z., Cheng Z., Liang J., Si J., Dong L., Li S. 'Distributed event-triggered secondary control for economic dispatch and frequency restoration control of

droop-controlled AC microgrids'. *IEEE Transactions on Sustainable Energy*. 2020, vol. 11(3), pp. 1938–50. doi:10.1109/TSTE.2019.2946740
- Liu B., Wu T., Liu Z., Liu J. 'A Small-AC-signal injection-based decentralized secondary frequency control for droop-controlled islanded microgrids'. *IEEE Transactions on Power Electronics*. 2020, vol. 35(11), pp. 11634–51. doi:10.1109/TPEL.2020.2983878
- Li Z., Zang C., Zeng P., Yu H., Li S. 'Fully distributed hierarchical control of parallel grid-supporting inverters in islanded AC microgrids'. *IEEE Transactions on Industrial Informatics*. 2018, vol. 14(2), pp. 679–90. doi:10.1109/TII.2017.2749424
- Shen X., Wang H., Zhang D., Li J., Wang R., Su Q. 'Distributed finite-time secondary voltage restoration of droop-controlled islanded microgrids'. *IEEE Access*. 2020, vol. 8, pp. 118183–91. doi:10.1109/ACCESS.2020.3004340
- Tapia G., Tapia A., Ostolaza J.X. 'Proportional–integral regulator-based approach to wind farm reactive power management for secondary voltage control'. *IEEE Transactions on Energy Conversion*. 2007, vol. 22(2), pp. 488–98. doi:10.1109/TEC.2005.858058
- Zhao C., Sun W., Wang J., Li Q., Mu D., Xu X. 'Distributed cooperative secondary control for islanded microgrid with markov time-varying delays'. *IEEE Transactions on Energy Conversion*. 2019, vol. 34(4), pp. 2235–47. doi:10.1109/TEC.2019.2935501
- Manaffam S., Talebi M.K., Jain A.K., Behal A. 'Synchronization in networks of identical systems via pinning: application to distributed secondary control of microgrids'. *IEEE Transactions on Control Systems Technology*. 2017, vol. 25(6), pp. 2227–34. doi:10.1109/TCST.2016.2635587
- Shahgholian S., Keyvani-Boroujeni G., Fani B. 'A distributed secondary control approach for inverter-dominated microgrids with application to avoiding bifurcation-triggered instabilities'. *IEEE Journal of Emerging and Selected Topics in Power Electron*. 2020, vol. 8(4), pp. 3361–71.
- Wu X., Xu Y., He J., *et al*. 'Delay-dependent small-signal stability analysis and compensation method for distributed secondary control of microgrids'. *IEEE Access*. 2019, vol. 7, pp. 170919–35. doi:10.1109/ACCESS.2019.2955090
- Su H.-Y., Liu T.-Y. 'Enhanced worst-case design for robust secondary voltage control using maximum likelihood approach'. *IEEE Transactions on Power Systems*. 2018, vol. 33(6), pp. 7324–6. doi:10.1109/TPWRS.2018.2868172
- Schiffer J., Seel T., Raisch J., Sezi T. 'Voltage stability and reactive power sharing in inverter-based microgrids with consensus-based distributed voltage control'. *IEEE Transactions on Control Systems Technology*. 2015, vol. 24(1), pp. 96–109. doi:10.1109/TCST.2015.2420622
- Weitenberg E., Jiang Y., Zhao C., Mallada E., De Persis C., Dorfler F. 'Robust decentralized secondary frequency control in power systems: merits and tradeoffs'. *IEEE Transactions on Automatic Control*. 2019, vol. 64(10), pp. 3967–82. doi:10.1109/TAC.2018.2884650

- Li Q., Peng C., Wang M., Chen M., Guerrero J.M., Abbott D. 'Distributed secondary control and management of islanded microgrids via dynamic weights'. *IEEE Transactions on Smart Grid*. 2019, vol. 10(no. 2), pp. 2196–207. doi:10.1109/TSG.2018.2791398
- Chen G., Guo Z. 'Distributed secondary and optimal active power sharing control for islanded microgrids with communication delays'. *IEEE Transactions on Smart Grid*. 2019, vol. 10(2), pp. 2002–14. doi:10.1109/TSG.2017.2785811
- Jiang K., Su H., Lin H., He K., Zeng H., Che Y. 'A practical secondary frequency control strategy for virtual synchronous generator'. *IEEE Transactions on Smart Grid*. 2020, vol. 11(3), pp. 2734–6. doi:10.1109/TSG.2020.2974163
- Abdolmaleki B., Shafiee Q., Seifi A.R., Arefi M.M., Blaabjerg F. 'A zeno-free event-triggered secondary control for AC microgrids'. *IEEE Transactions on Smart Grid*. 2020, vol. 11(3), pp. 1905–16. doi:10.1109/TSG.2019.2945250
- Peyghami S., Mokhtari H., Loh P.C., Davari P., Blaabjerg F. 'Distributed primary and secondary power sharing in a droop-controlled LVDC microgrid with merged AC and DC characteristics'. *IEEE Transactions on Smart Grid*. 2018, vol. 9(3), pp. 2284–94. doi:10.1109/TSG.2016.2609853
- Qian T., Liu Y., Zhang W., Tang W., Shahidehpour M. 'Event-triggered updating method in centralized and distributed secondary controls for islanded microgrid restoration'. *IEEE Transactions on Smart Grid*. 2020, vol. 11(2), pp. 1387–95. doi:10.1109/TSG.2019.2937366
- Shuai Z., Huang W., Shen X., Li Y., Zhang X., Shen Z.J. 'A maximum power loading factor (MPLF) control strategy for distributed secondary frequency regulation of islanded microgrid'. *IEEE Transactions on Power Electronics*. 2019, vol. 34(3), pp. 2275–91. doi:10.1109/TPEL.2018.2837125
- Cheng L., Zhang Z., Zhang F. 'Secondary voltage controls of virtual-droop-controlled bidirectional DC/DC converters in hybrid energy storage system'. *IET Power Electronics*. 2020, vol. 13(14), pp. 3018–25. doi:10.1049/iet-pel.2019.1566

Frequency and voltage stabilization

- Joung K.W., Kim T., Park J.-W. 'Decoupled frequency and voltage control for stand-alone microgrid with high renewable penetration'. *IEEE Transactions on Industry Applications*. 2019, vol. 55(1), pp. 122–33. doi:10.1109/TIA.2018.2866262
- Serban E., Ordonez M., Pondiche C. 'Voltage and frequency grid support strategies beyond standards'. *IEEE Transactions on Power Electronics*. 2016, vol. 32(1), pp. 298–309. doi:10.1109/TPEL.2016.2539343
- Wai R., Zhang Q., Wang Y., Serban E., Ordonez M., Pondiche C. 'Voltage and frequency grid support strategies beyond standards'. *IEEE Transactions on Power Electronics*. 2019, vol. 34(3), pp. 2327–38.

- Thakallapelli A., Nair A.R., Biswas B.D., Kamalasadan S. ‘Frequency regulation and control of grid-connected wind farms based on online reduced-order modeling and adaptive control’. *IEEE Transactions on Industry Applications*. 2020, vol. 56(2), pp. 1980–9. doi:10.1109/TIA.2020.2965507
- Bae Y., Vu T.-K., Kim R.-Y. ‘Implemental control strategy for grid stabilization of grid-connected PV system based on german grid code in symmetrical low-to-medium voltage network’. *IEEE Transactions on Energy Conversion*. 2013, vol. 28(3), pp. 619–31. doi:10.1109/TEC.2013.2263885
- Davari M., Mohamed Y.A.-R.I. ‘Robust droop and DC-bus voltage control for effective stabilization and power sharing in VSC multiterminal DC grids’. *IEEE Transactions on Power Electronics*. 2018, vol. 33(5), pp. 4373–95. doi:10.1109/TPEL.2017.2715039
- Hafezi H., Faranda R. ‘Dynamic voltage conditioner: A new concept for smart low-voltage distribution systems’. *IEEE Transactions on Power Electronics*. 2018, vol. 33(9), pp. 7582–90. doi:10.1109/TPEL.2017.2772845
- Gonçalves A.F.Q., Aguiar C.R., Bastos R.F., Pozzebon G.G., Machado R.Q. ‘Voltage and power control used to stabilise the distributed generation system for stand‐alone or grid‐connected operation’. *IET Power Electronics*. 2016, vol. 9(3), pp. 491–501. doi:10.1049/iet-pel.2015.0071

Chapter 9
MPC of MGs with tertiary power flow optimization

In this chapter, the tertiary control strategy is discussed for economic dispatch and power flow optimization. The model predictive control (MPC)-based algorithm is used to determine the scheduling of power exchanges between the microgrid and the main grid. By considering the power prices, power generation and load forecasts, it enables a supply–demand balance in an economic way.

9.1 Tertiary control of MGs and MPC

As already highlighted in Chapter 4, hierarchical control is a common and effective solution to govern a complex energy system, and it has now been applied in microgrids (MGs) and widely recognized as a standard control framework. In a typical MG with multiple converter-interfaced distributed generations (DGs) and diverse bus types as well as various operating modes, a three-level control structure including primary, secondary, and tertiary control can be utilized to coordinate different units [1, 2]. These three levels are differentiated by specified control objectives and bandwidths, as depicted in Figure 9.1. Each level has its own control goals and provides supervisory control over lower-level systems.

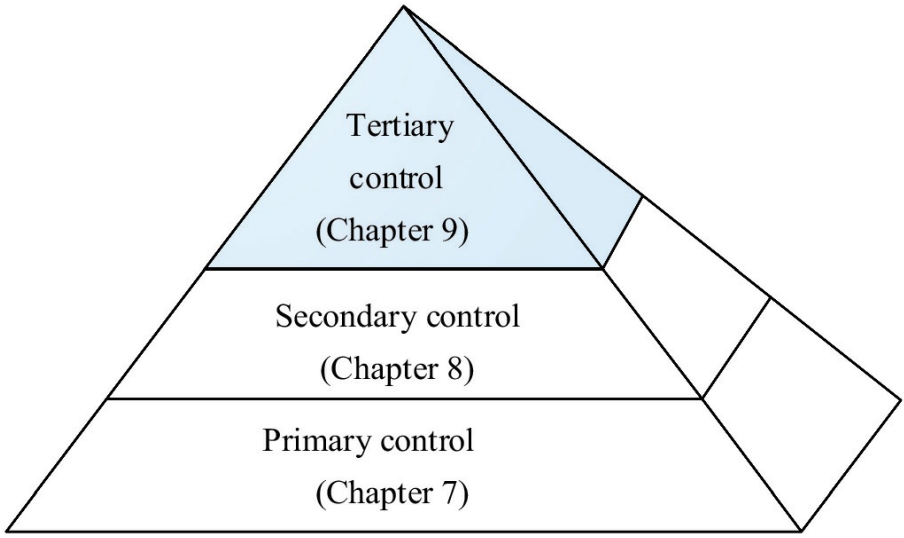


Figure 9.1 Hierarchical control pyramid of a MG [3, 4]

Primary control, as the name suggests, is the underlying level that stabilizes the whole system in terms of voltage and frequency within acceptable ranges, while at the same time, enables load sharing among DGs with fast response. Under the circumstances that the droop control method is used in the primary control, the output voltages of DGs change with respect to load variations, leading to frequency/voltage deviations. In the steady state, secondary control can restore the deviated frequency/voltage to their rated values. Grid synchronization loop can also be integrated into the secondary controller for grid connection. Upon the MG meets the synchronization requirement, it can connect to the main grid. Tertiary control focuses on regulating the power imported to or exported from the MG. Moreover, associated economic and cost optimization, as well as power planning are all included in the tertiary control regime. In general, regardless of control levels, all these approaches can be divided into three categories: centralized, distributed, and decentralized. So far, many studies have been conducted for the hierarchical control of MGs, particularly for primary control and secondary control.

As the highest level in the hierarchy, tertiary control deals with economic dispatching, operation scheduling, and power flow between the MG and the main grid. Notice that tertiary control is also referred to as the coordination of multiple MGs interacting with one another in networked MGs. Under the grid-connected operation, it is aimed to achieve interconnected power flows and maximize economic benefits.

Nowadays, most of the tertiary control strategies are focused on a very high level considering neither the power converter switching patterns nor the MG

actual circuitry topologies. Besides, tertiary control strategies proposed are seldom incorporated with secondary control and primary control in actual implementation to form a complete and holistic strategy. For example, a scenario-based two-stage stochastic programming model was presented as the tertiary control taking into account renewable energy source (RES) uncertainties and uncertain energy deviation prices [5]. Components considered in this particular MG include a solar photovoltaic (PV) module, a wind generator, an electric vehicle (EV), and three types of loads (critical, adjustable, and shiftable). The developed model can provide an optimal schedule of the components in the MG and an optimal bidding strategy for day-ahead market to minimize operational cost.

In some research works about tertiary control, power converters and actual circuitry topologies are actually considered. In [6], an optimization method was developed to adjust the DG compensating efforts according to the acceptable voltage unbalance range at different voltage buses and DG terminals. The motivation of this work is the consideration of unbalanced voltage issues in three-phase power systems in which the transmission lines are unsymmetrical or single-phase loads are connected, which may result in additional power losses and deteriorate the system stability. In this work, primary and secondary controllers are used to share the load demand according to DGs capacity and at the same time, to compensate voltage unbalance at critical buses. Then, tertiary control, which essentially is an optimization algorithm, is applied to adjust the compensating contribution of each DG by taking into account the voltage unbalance limits at DG terminals and in local buses. In [7], an important issue that is usually ignored in MG research is addressed. Voltage deviations caused by droop control at the primary level can be mitigated by introducing secondary control. This has been widely studied. However, secondary voltage control at different buses cannot ensure voltage quality at critical load buses because secondary control directly regulates DG output voltages rather than point of common coupling (PCC) voltages. To solve this problem, an interior-point optimization-based tertiary control was developed to coordinate the voltage source converters (VSCs) and the energy hub to minimize the voltage deviations by generating desired references. The proposed method runs an interior-point optimization algorithm and reroutes the power distribution in the network and hence, mitigate the load voltage deviations.

As the foundation of MG tertiary control, reliable power flow analysis is critically important to explore the potential of MGs as primary resilience resources. Power flow of islanded MG, however, remains an open problem. In [8], a generalized microgrid power flow (GMPF) is developed to enable incorporating hierarchical control schemes into MG power flow. GMPF introduces an adaptive structure where the power outputs of DGs are adjusted incrementally until they satisfy the control objectives. In [9], a DC MG consisting of PV array, storage, power grid connection, and DC load is presented. Based on this, an optimization method is developed for DC MG power flow by means of a multi-layer supervision control, including energy management layer and operation

layer. This proposed multi-layer supervision control can deal with instantaneous power balancing subsequent to the power flow optimization while providing a communication interface with the utility grid. The optimization includes a forecast of load consumption and solar PV power generation, while satisfying various constraints such as grid power limitations, storage capability, electricity pricing, and grid peak hour. The supervision subsystem, as an interface between the power subsystem and the smart grid, optimizes local power flow, with respect to grid requirements and element constraints, to reduce energy cost, avoid undesired power loss, and reduce peak grid power supply. The supervision subsystem is supposed to exchange data with the smart grid and to deal with end-user demand and data forecast. Energy management layer optimizes power flow off-line, few hours ahead, and the operation layer controls power flow and ensures self-correcting capability. The optimization is executed by mixed integer linear programming. It can respond to issues of performing peak shaving, avoiding undesired injection, and making full use of locally produced energy with respect to rigid element constraints.

Another promising method called MPC, also referred to as receding horizon control, has been widely used in power converters for its flexible control scheme in which different constraints and multiple control objectives can be easily formulated [10–14]. The optimal control behavior is determined according to a cost function. Thus, the control system becomes much simpler but reliable with improved dynamic response. As already discussed in Chapter 2, two important branches have been widely used, namely finite control set (FCS)-MPC and continuous control set (CCS)-MPC. The key principle is to derive a predictive model that is used to predict the system future behavior and to design a cost function that is used to determine the optimal control set.

While these techniques have been applied in power electronic converters and autonomous distributed generations, they can also address large systems, which is usually known as system-level MPC, or grid-level MPC [15, 16]. It is similar to converter-level MPC in terms of control structure. The system-level MPC also consists of a predictive model, cost function, and solving algorithm. System-level MPC functions as an optimization algorithm that is suitable to optimize the performance of constrained systems with multiple objectives. Nevertheless, system-level MPC aims to control system-level operations rather than power electronic converter switching states, e.g., power flows within a MG or among networked MGs, energy storage system (ESS) capacity, load management, etc.

In large-scale energy systems with RESs, researchers need to face new challenges in the development of MPC, including the intermittency of RESs, load sharing accuracy, circulating currents, grid stability, etc. The unique features of MPC make it a natural fit in MG tertiary control as MPC problems incorporate prediction models and consider operation and security constraints. Besides, the MPC has the capability in the prediction of future behaviors of the system, which are very attractive for renewable-based MGs and load forecasting. At each control step, the most updated information on load forecasts, power generation, and electricity prices are used over a rolling horizon. Thus, the control is robust

against external uncertainties. As detailed in Chapter 4, tertiary control aims to manage the power exchange among interconnected/networked MGs and to control the power flow between the MG and utility grid. Therefore, addressing power flow for optimal economic dispatch is the major objective for this highest control level. In this sense, system-level MPC is mostly utilized to solve optimization problems under various constraints. Figure 9.2 illustrates two main areas that are addressing by tertiary control, together with possible control objectives and constraints. In the remaining of this chapter, MPC is referred to system-level MPC.

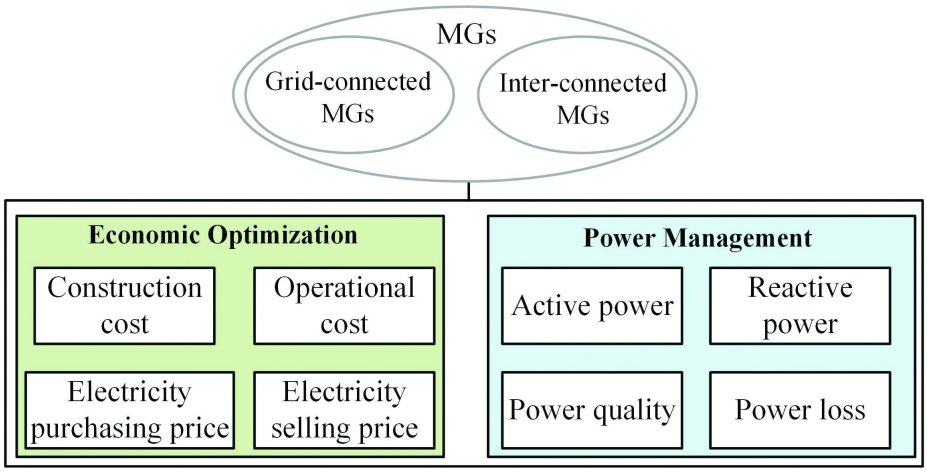


Figure 9.2 Considerations in MG tertiary control

9.2 MPC for economic dispatch and optimal power flow in MGs

To explain the application of MPC in tertiary control in MGs, a MG structure is presented in Figure 9.3 for easy illustration. It consists of a wind generator and a solar PV array as renewable power generation sources, a fuel cell as backup power sources, a battery bank as energy storage, and a household as the electric load. Specifically, electric loads can be categorized into three types, namely crtical loads, adjustable loads, and shiftable loads. The fuel cell system supplies additional power as a backup power generation unit in case of insufficient generation from RESs. The battery bank bridges the fluctuating gap between power generation and power consumption. All the DGs are connected to the common voltage bus, at which the MG communicates with the main grid through a static transfer switch (STS). The power converters act as power electronic interfaces between distributed energy resources (DERs) and the grid to stabilize the voltage and achieve power conversion. The DGs communicate with each

other or even with the control center via plug-and-play wireless connectivity modules.

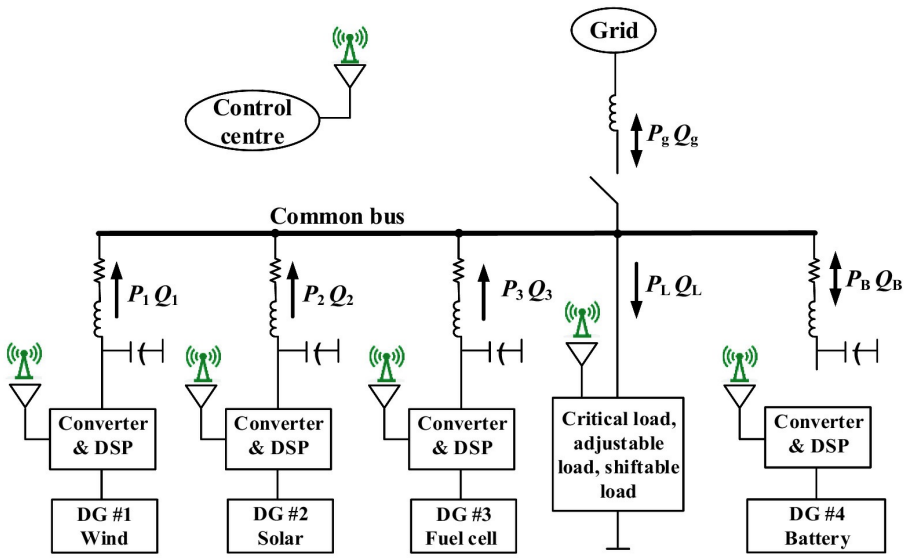


Figure 9.3 A MG structure with various DERs and different types of loads

Taking the advantages of the MPC scheme, control strategies for MGs using MPC at the tertiary level can be developed, which is depicted in Figure 9.4. With generation and load forecasting, the MPC controller flexibly includes different constraints in the cost function to generate set points for battery, fuel cell, and power flow exchanged with utility grid to achieve various objectives [17].

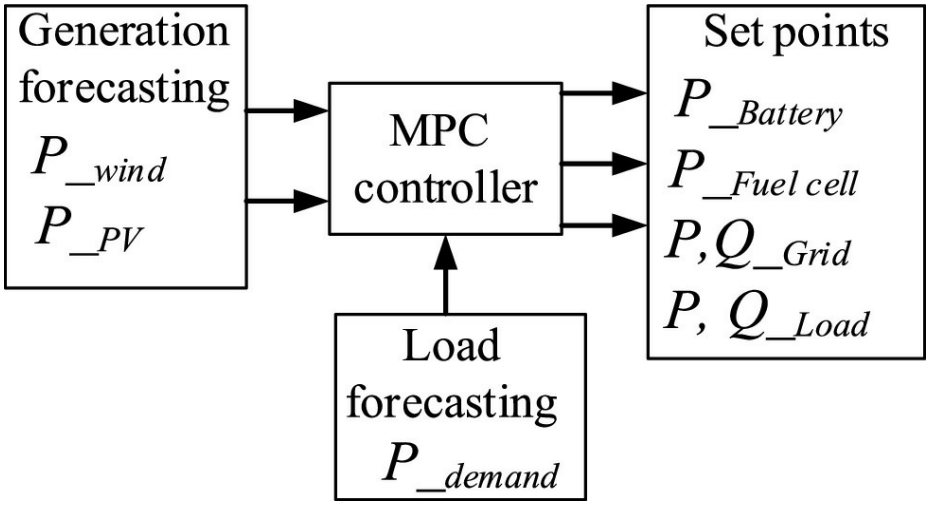


Figure 9.4 Schematic illustration of the tertiary level MPC for MGs

The main control objectives of the MG system from the system perspective can be illustrated in Figure 9.5, which can be summarized in four major aspects.

- It would make no sense to construct a MG if high-quality electrical power cannot be generated for the loads, regardless of variable load profiles and fluctuating power generations. Therefore, the first task of the MPC controller is to regulate the voltages at different critical buses and load terminals within a specified range.
- Due to the intermittent nature of the RESs and the time-varying load profile, the power generation and consumption vary with respect to time. It is expected that the load demand can be met locally by means of energy storage or by nearby RESs through an optimal route. Unnecessary power transfer will lead to additional power losses in the lines. With this in mind, the power flow within the MG should be optimized to minimize the power loss along the lines.
- It is usually necessary to use ESS to fill the gap between power generation and power consumption within the MG. Over-discharging and over-charging, as well as frequent operation, will degrade the performance and shorten the lifespan of these expensive energy storage devices. Thus, an important aspect is to protect the battery bank.
- Since power outages and disturbances usually take place along the distribution network, ancillary services offered by distributed generation systems become a significant attribute to successfully integrate RESs into the grid. New grid codes from the transmission system operator (TSOs) allow DERs to remain connected to the grid so that DERs can contribute to grid

voltage support through power compensation. Hence, power flow optimization, either active power or reactive power control at the tertiary level, should take into account the grid requirements.

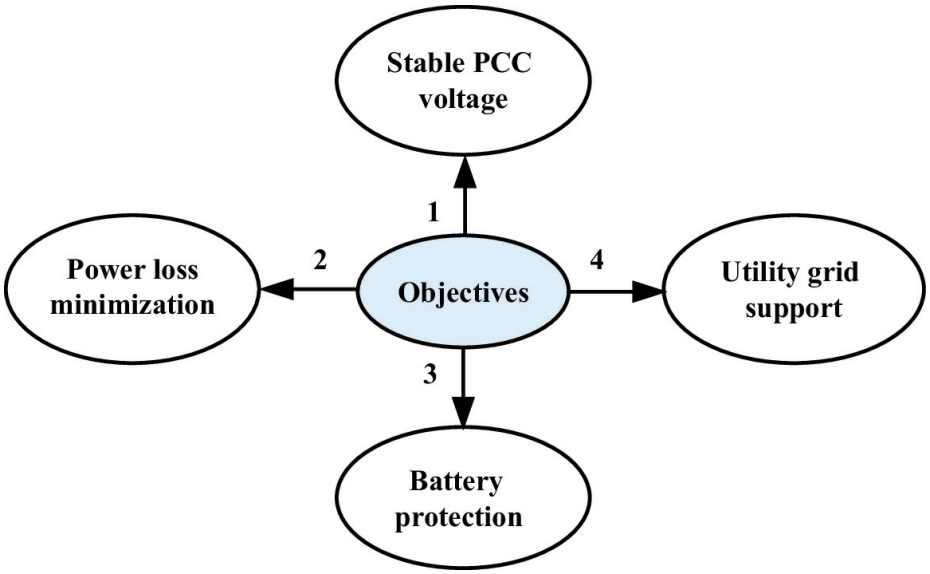


Figure 9.5 Control objectives of the tertiary level MPC in MGs

To apply system-level MPC methods, the first step is to establish an accurate predictive model shaped by various uncertainties and constraints. To do this, an integrated mathematical representation of all concerned aspects in a MG is required. After that, a time series-based method is needed to formulate a future-value oriented receding equation, which predicts the future status based on existing current states. Key considerations and important constraints will be formulated into the cost function in which power flow optimization, operating cost minimization, and system efficiency maximization are reflected. Generally, forecasting information on DG outputs, electricity prices, and load demands will be involved. The power flow management and economic dispatch address the questions about how the load demands should be shared among various power sources and/or energy storages, while taking into account the trade-off between power loss minimization, power generation maximization, and power storage optimization. As different objectives and constraints are involved in the MPC algorithm, leading to a complex optimization problem, which is usually solved using a specific solver toolbox.

The block diagram of a system-level MPC is illustrated in Figure 9.6. The prediction model, established upon the system model, formulates an expression for the future state prediction based on current/past states and possible forecasts. In other words, the predictive model is used to predict the future plant outputs,

based on past and current values and the proposed optimal future control actions. More specifically, the forecasts/predictions of the predictive model can be various system variables on a certain time-interval basis, such as electricity prices, PV generations, load demands, etc. These optimal control actions are calculated by an optimizer taking the cost function (where the future tracking error is considered) as well as the constraints into account. Since the optimizer generates control actions, it is a fundamental part of the strategy. If the cost function is quadratic, its minimum can be obtained as an explicit linear function of past inputs and outputs and the future reference trajectory. In the presence of inequality constraints, the control actions can be obtained by more computationally efficient algorithms.

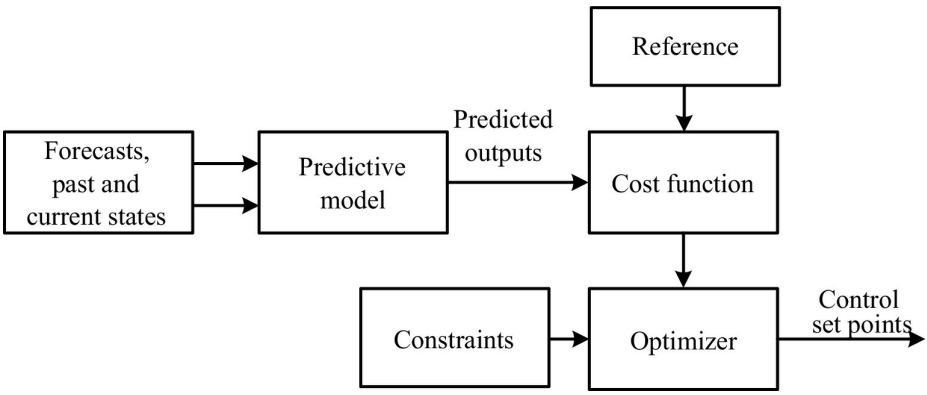


Figure 9.6 System-level MPC

The control objectives together with system constraints should be reflected in the cost function design. Thus, the predictions generated from the predictive model and possible desired targets are formulated into this cost function. Generally, the terms formulated in a cost function reflect the multiple control objectives and optimization targets. During each control period, the optimal control/command sequence over a certain time horizon is computed by considering all the constraints. Then, a group of system states is refreshed, resulting in an updated control sequence, waiting for another round of calculation to move the horizon one step forward.

In MGs, constraints involved in RESs, power converters, power electronic components, power lines, and the utility grid should be considered. Once the constraints are well formulated, the system will be able to operate within or near the constraint boundaries safely while obtaining satisfactory system performance. With the time horizon window moving forward, the optimization problems taking constraints into account will then be continuously solved, and the optimization problem will be updated once new predictions are available. The sampling interval Δt of a system-level MPC is often larger than that of converter-level MPC, ranged from several seconds, several hours to days. The time horizon is

often determined according to the actual situation. For instance, if the PV power output is measured on a 1-min period basis, while the PV generation is predicted every 30 min. In this case, the sampling interval for the MPC is expected to be multiples of 30 min for a better match and precision.

The steps to implement the system-level MPC can be summarized as follows [16]:

- System mathematical model and control objectives with past and present states are utilized to establish a receding model.
- Compute the optimal control/command sequence over a certain control horizon.
- Implement the first control action of the sequence.
- Update all system states for the next period while moving one step forward and repeating the optimization.

The benefits of utilizing MPC for tertiary control in MGs can be summarized as follows.

- Various objectives can be integrated in an intuitive and a direct way into the cost function with a straightforward quadratic summation.
- Various constraints can be comprehensively considered with suitably limited ranges.
- An effective specific toolbox with a powerful solver can be used to facilitate the algorithm solving process, which is particularly useful in tertiary-level control with complex formulations and various constraints.
- System-level MPC can provide a receding prediction horizon with a feedback mechanism that effectively reduces the impacts of uncertainties, thus making it more robust to disturbances.

The operation of an islanded MG is usually complex due to the uncertain and intermittent nature of renewable energies as well as the concern of operating cost and economic benefit. Therefore, a system-level optimization for islanded MGs is necessary. In the scheduling of power flows inside or outside MGs, specific conditions must be considered. Among them, maximizing economic benefit is a prominent requirement. This economic optimization related to power management is common when dealing with the interaction between DGs, either RESs or conventional nonrenewable power sources, with the main grid. For example, in [18], an optimization based on MPC was developed for the power flow optimization of a grid-connected MG. Five cost-related parts are formulated in the cost function, as expressed in (9.1), including buying and selling prices of electricity (1st and 2nd terms), fuel consumption cost (3rd term), generator start-up cost (4th term), and the cost involved in battery ESS (5th term) [18].

$$J^*\left(\zeta\left(k\right),\bar{\boldsymbol{P}}_{PV}\left(k\right),\bar{\boldsymbol{P}}_{L}\left(k\right),\bar{c}_{Imp}\left(k\right),\bar{c}_{Exp}\left(k\right)\right)=$$
$$min\sum_{i=0}^{N-1}[\underbrace{\Delta T\bar{c}_{Imp,i}P_{eImp}\left(k+i\right)}_{1st}-\underbrace{\Delta T\bar{c}_{Exp,i}P_{eExp}\left(k+i\right)}_{2nd}$$
$$+\underbrace{\Delta Tc_G\boldsymbol{F}^{\boldsymbol{T}}\boldsymbol{k}_G\left(k+i\right)}_{3rd}+\underbrace{c_sc_Gk_s\left(k+i\right)}_{4th}]-\underbrace{c_BV_{nom}Q\zeta\left(k+N\right)}_{5th} \tag{9.1}$$

where $\zeta\left(k\right)$ is the state of charge (SoC) of the battery, $\bar{\boldsymbol{P}}_{PV}\left(k\right)$ the PV generation forecasts, $\bar{\boldsymbol{P}}_{L}\left(k\right)$ the load demand forecasts, $\bar{c}_{Imp}\left(k\right)$ the electricity purchasing price forecasts, $\bar{c}_{Exp}\left(k\right)$ the electricity selling price forecasts, N the number of samples, ΔT the sampling time, P_{eImp} the power imported from the grid, P_{eExp} the power exported to the grid, c_G the cost of generator fuel, c_S the penalty of start-up fuel, c_B the stored energy value of the battery, V_{nom} the nominal voltage of the battery, and Q the battery capacity.

So far, in addition to the example of MPC in MGs with focus on economic optimization as shown in (9.1), other types of MPC approaches have been developed to achieve various goals in MGs. To achieve better economic dispatch, a MG considering energy storages and power demands was modeled in [19] to build the MPC predictive model. A distributed MPC power management scheme was proposed in [20]. Both economic and environmental impacts are reflected in the cost function. In [21], by considering comprehensive aspects, including the cost/benefit of energy sources, the cost due to imbalance between power supply and load demand, the cost of the power exchange with the main grid, and the operation cost/benefit of batteries, a distributed MPC was designed and implemented to achieve an overall economic optimization. In [22], a novel distributed economic MPC approach was proposed to maximize MG owner's benefits by formulating the cost of buying energies from or selling energies to the MG into the cost functions. In [23], a stochastic MPC method was investigated to figure out the optimal power references for wind generators and EVs.

Other MPC methods have also been seen in recent years. In [24], a two-layer MPC strategy was developed for the optimization of an islanded MG. To obtain an accurate and reliable predictive model, a seasonal auto regression integrated moving average model and exponential smoothing technique are applied. After that, discrete dynamic programming is used to solve the optimization program. In [25], a MPC method was proposed for power flow optimization in a MG. Different aspects and constraints, such as load consumption, power line loss, and battery discharge/charge are formulated in the cost function. Due to its complexity, the algorithm is solved using YALMIP toolbox with CPLEX solver. A two-layer distributed MPC scheme was reported in [26] to control an islanded DC MG. The upper-layer MPC coordinates parallel DC–DC converters among

DGs, while the lower-layer MPC control the wind generators at the power source side. Similarly in [27], MPC was utilized to control power flows coordinating by ESS in an islanded MG. The power losses from lines, filters, and batteries are also integrated into the cost function as the minimization objective. Finally, the optimization problem is solved using CPLEX solver and YALMIP toolbox.

In [28], a holistic control strategy based on a MPC algorithm is proposed. Specifically, at each optimization step, using a receding horizon approach, the tertiary control provides the optimal power schedule for the MG on the basis of economic and environmental criteria. Then, the secondary control, to provide set points for primary control, uses another objective function that minimizes the quadratic deviation from the reference values provided by the tertiary level and the desired frequency for good performances. The proposed MG control architecture is illustrated in Figure 9.7.

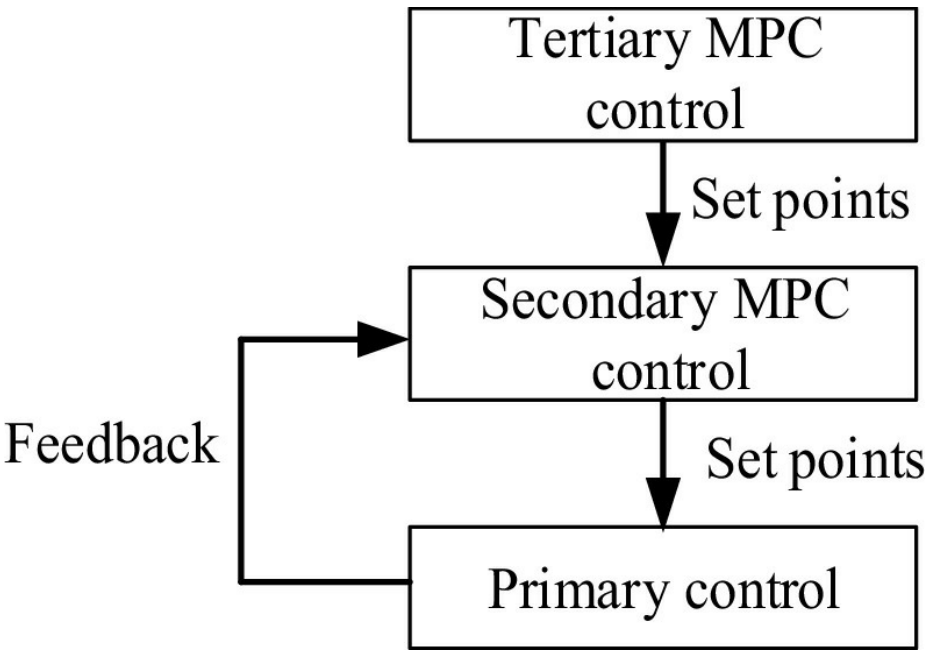


Figure 9.7 Hierarchical control architecture in [28]

In this holistic control strategy, the tertiary level problem is addressed using a MPC approach (and, in particular, a receding horizon control scheme has been adopted). The objective function includes operating costs, while constraints are given by the storage system state equation, the capability curve of each component, and the balance for active and reactive power in the MG. The resulting solution (i.e., the optimal values of the decision variables that are here represented by power production from the diesel engine and power exchange with

the storage) provides set points that are given to the secondary control level, whose goal is to minimize another objective function. The goal of the developed secondary control is to manage the power injections from each source according to the set points coming from the tertiary control, to create reference patterns to limit the frequency oscillations caused by the variation of the PV unit. The electrical load is a forecasted parameter supposed to be known in the short term. Renewable resources also are forecasted parameters, but the power produced by the renewable generators can be curtailed at the desired level (as in the tertiary control). The secondary level solves a multi-objective control problem to regulate the system's frequency and track the upper-level references. In particular, under a MPC scheme, at each run of the tertiary control, after having received the references for the first 15 min, secondary control tracks the optimal values for an optimization horizon of 10 s.

Recently, hybrid MGs have attracted increasing interest in residential households. For this, the home energy management system (HEMS) together with optimization and control techniques combining other concepts such as demand-side management has played an important role in the search for solutions [29]. The proposed optimization model consists of RESs, two different storage devices and loads commonly found in the household of Brazilian consumers. In particular, we present a formulation that includes the cost of the electricity, the aging of the components, and the operational constraints. The MPC techniques allow satisfying user demand, maximizing the economical benefit of the MG, minimizing the electricity purchased from the power grid, as well as extend the lifespan of each storage device, fulfilling the different system constraints contributing to the demand-side management. The proposed model results in the minimization of the energy consumption of the power grid reducing the value of the tariff paid by the prosumer as well as the control of the SoC of the two ESSs, extending the lifespan and contributing to the stability of supply/storage. In [30], the proposed approach allows minimizing the usage of the traditional electric grid for supplying the power to the building's loads using as much as possible the power generated by RES while optimizing the storage devices' operations. A MPC strategy is proposed to balance the power flow in a MG system. The deployed strategy controls the charge/discharge current of the battery depending on RES production, and load consumption variability. Novickij [31] proposes an improved MPC-based approach for managing the DERs of a MG. MPC-based energy management systems are computationally intensive and can become too slow for online optimization. The main aim of this approach is to improve on the computational time and scalability of the current MPC-based control schemes. This is done by decoupling the unit commitment and economic dispatch problems, and solving them separately. The control scheme takes into account the current and predicted prices of electricity, the forecasts of loads and the availability of renewable energy. The proposed approach is compared to an MPC approach commonly found in literature. It performed better in terms of computation time and scalability, with a slight trade-off in cost minimization while respecting the constraints of the MG. MPC is a well-established form of

receding horizon control in engineering. It allows for the control of multi-variable systems with constraints on both the states and control inputs. Its ability to handle stochastic processes and its closed-loop control makes it a great candidate for managing renewable resources.

9.3 MPC for networked MGs

Converter-level MPC techniques are relatively mature as they have been widely used in power electronics and also applied in the primary control in MGs, as introduced in Chapters 7 and 8. Meanwhile, grid-level MPC in the tertiary layer dealing with power flow and economic operation has also been reported, as just discussed in Section 9.2 in this chapter. As centralized generating facilities are giving way to DERs, under future smart grid framework, small MGs that are geographically adjacent to each other can be interconnected to form MG clusters with additional flexibility for resilient operations. As an autonomous energy system owned by private equity or individuals, each MG in the network is able to decide when to be interconnected and how much power to be exchanged with others. Figure 9.8 shows a configuration of MGs interconnected through physical power highway and digital highway. Efficient top-level control, usually referred to operation control or energy management, is needed to govern such complex power networks. It mainly aims to achieve overall economic dispatch by allowing the best utilization of DERs.

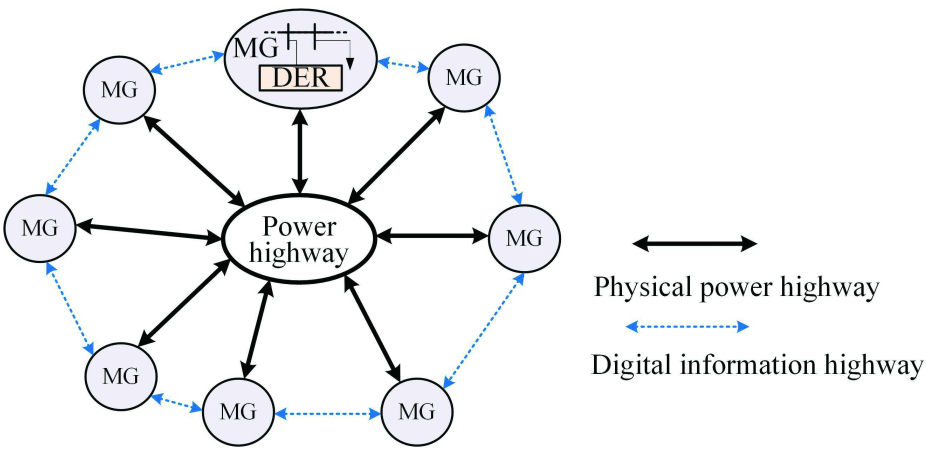


Figure 9.8 Physical connection and digital communication of networked MGs

Networked MGs, or a cluster of electrically interconnected MGs, as shown in Figure 9.8, have now become a promising measure to efficiently accommodate more RESs and loads. The excess power generation from one MG can be stored

in the storage system or supplied to the nearby MGs. On the other hand, the deficit power of an MG can be supplied by any other MG with sufficient energy. Thus, this power architecture enables mutual power support among small AC–DC MGs and promotes renewable power generation [32]. To facilitate this interaction, distribution energy management systems regulate power flows while distribution network operator (DNO) is usually necessary to transmit these control commands. Different from a single MG, the power coordination of networked MGs poses a higher demand for more efficient power optimization.

In [33], a distributed two-level tertiary control is proposed to adjust the voltage set points and balance the loading among all sources, thus avoiding the single point of failure. Similar to the operation of a single MG, load sharing among DGs within a DC MG is managed through primary and secondary controllers. The difference here is that the tertiary control level is designed to provide a higher-level load sharing among MGs within a cluster. Flexible power exchange between MGs can maximize the utilization of renewable sources and releases the stress of the network, which improves system reliability and availability and reduces the maintenance costs due to aging components and network upgrading. In the proposed control method, the power flow among DGs is governed by adjusting voltage set points for individual MGs through a cooperative approach. In other words, the voltage adjustment copes with the load sharing among MGs within the MG cluster. In this way, loading mismatch among neighboring MGs can be addressed. In [34], a centralized MPC scheme was developed to coordinate the power flow within networked MGs. The predictive model is constrained with an upper limit and a lower limit by considering the power capacity along the distribution lines and the power capacities of MGs. The energy sold or purchased is formulated into the cost function. The first term optimizes the power flow with adjacent MGs, while the second term determines the amount of energy exchanged with the utility grid. In [35] and [36], MPC was used to minimize the operating cost and maintain power balance simultaneously under fluctuating power generation and power demand conditions. The dynamic receding-horizon procedure of the MPC enables the selection of the most suitable control actions to address various constraints. Different from [34] where a centralized MPC approach is presented, a distributed MPC was proposed in [37] to maximize the economic benefit and simultaneously minimize the degradation of ESSs with the consideration of diverse constraints such as SoC. The optimization problem is solved using TOMLAB/CPLEX solver.

9.4 Future trend

The traditional power system is experiencing steady transformation from centralized-control bulky power systems to decentralized and distributed energy networks formed by fundamental building blocks—MGs. These new trends and directions indicate new requirements for superior control schemes. MPC is a promising option to meet the urgent need of a future grid featuring high penetration of renewable energy and bidirectional power flow. The unique

features of MPC that can incorporate prediction models and consider operation and security constraints, together with its capability in the prediction of future behavior of the system, make it a natural fit in MGs with renewable energy and load forecasts. Specifically, the field of focus will likely be narrowed to the following aspects in the coming years.

9.4.1 New mathematical formulation

The prediction model lays the foundation for the whole MPC controller. Its accuracy and completeness affect system performance. To derive the system mathematical model for MPC, several expression formats can be used, including impulse response form, transfer function form, and state-space form [38]. So far, most of the predictive models in MPC are expressed in state-space forms. Actually, other alternatives can be used to rewrite the model state, depending on the actual needs. For example, using Laguerre functions, the established predictive model requires less number of optimization variables while the system transient response is not compromised [39]. For the grid-level MPC, the selection of an appropriate modeling method can be even more crucial. In [40], a future-value receding model is employed to produce steps-ahead prediction for multiple-input multiple-output systems. In [41], the input-output feedback linearization method is used to facilitate the predictive model design without the need to consider the prior steady-state operating point. Steady-state offsets between the actual value and the reference have been a challenge in MPC-based control system. To eliminate these steady-state offsets, steady state constrained autoregressive with exogenous terms model (SSARX) model can be utilized to design an adaptive scheme for this purpose [42]. In case of a system featuring nonlinear characteristics in nature, nonlinear MPC modeling may be needed to obtain a more accurate prediction model [43, 44].

9.4.2 Holistic and intelligent MPC approaches

In existing MPC of MGs, two clear research streams have been witnessed. On the one hand, the control and operation of power converters are focused, but the system-level energy management and the impact of the utility grid are seldom considered. On the other hand, system-level power flow control and load management with a MG or among interconnected MGs have been studied from a high level. However, the details of power electronic topologies and their control methods remain unsolved. Currently, there is still a gap in MPC of MGs between converter-level operation and system-level optimization. There is an urgent need to develop holistic MPC approaches that can cope with power converter control in the bottom and the power flow on top. Meanwhile, other intelligent methods such as fuzzy logic control and multi-agent system algorithm can incorporate with MPC to achieve more control flexibility and a higher degree of intelligence.

9.4.3 MPC in DC MGs

With the proliferation of DC generation and DC loads, DC distribution has become more and more popular over the past years. As already mentioned in Chapter 1, DC MGs offer many advantages over AC MGs, including higher efficiency and reliability, easy grid synchronization, and no control requirement for reactive power and frequency regulation [25, 26, 34]. These advantages facilitate plug and play operation and enable simpler grid integration of RESs. In this context, DC MGs and the associated MPC methods tend to be a major MG research area in the next decades. For example, in a PV-dominant DC MG, the voltages at various DC buses can be maintained and the power flow can be controlled using converter-level MPC. Then the set points of PV outputs and ESS charging/discharging can be determined using grid-level MPC.

9.4.4 Distributed and decentralized control

Assigning the control task to different units based on operation in different time frames is what constitutes the idea of control hierarchy (primary, secondary, and tertiary controls). The use of centralized control is very effective to control a network of MGs with one owner, given that all the relevant information is gathered at a single point. However, if MGs are owned by different owners, centralized control is not applicable. On the other hand, distributed control techniques consider the interactions between units [45, 46]. Within the higher control levels (secondary and tertiary), the need for distributed approaches arises because of the desire and need for higher reliability, security, and situational awareness. Besides, physical and communication structures of MGs can be time-varying because of the desired plug-and-play capability of MGs. From this perspective, the distributed control structure provides a robust control framework that appropriately operates in the presence of time-varying, restricted, and unreliable communication networks [47].

9.5 Conclusion

This chapter looks into the potential use of MPC in MGs at the tertiary level and explores the possibilities of smart MG architecture and innovative control concepts for future grids. The power flow and energy management at the tertiary control level are discussed for both individual MGs and networked MGs. The latest developments of grid-level MPC in these applications are reviewed. The future trend of MPC in MGs is also pointed out.

References

[1] Guerrero J.M., Vasquez J.C., Matas J., de Vicuna L.G., Castilla M. ‘Hierarchical control of droop-controlled AC and DC microgrids—A general approach toward standardization’. *IEEE Transactions on Industrial Electronics*. 2011, vol. 58(1), pp. 158–72.

[2] Han H., Hou X., Yang J., Wu J., Su M., Guerrero J.M. ‘Review of power

sharing control strategies for Islanding operation of AC microgrids'. *IEEE Transactions on Smart Grid*. 2016, vol. 7(1), pp. 200–15.
[3] Guerrero J.M., GarciadeVicuna L., Matas J., Castilla M., Miret J. 'A wireless controller to enhance dynamic performance of parallel inverters in distributed generation systems'. *IEEE Transactions on Power Electronics*. 2004, vol. 19(5), pp. 1205–13.
[4] Guerrero J.M., Chandorkar M., Lee T.-L., Loh P.C. 'Advanced control architectures for intelligent microgrids—Part I: decentralized and hierarchical control'. *IEEE Transactions on Industrial Electronics*. 2013, vol. 60(4), pp. 1254–62.
[5] Citores L., Corchero C., Heredia F.J. 'A stochastic programming model for the tertiary control of microgrids'. *International Conference on the European Energy Market*. 2015, pp. 1–6.
[6] Meng L., Tang F., Savaghebi M., Vasquez J.C., Guerrero J.M. 'Tertiary control of voltage unbalance compensation for optimal power quality in islanded microgrids'. *IEEE Transactions on Energy Conversion*. 2014, vol. 29(4), pp. 802–15.
[7] Mudaliyar S.R., Mishra S., Sharma R.K. 'Tertiary load voltage control in an interconnected DC microgrid with energy hub'. *2017 7th International Conference on Power System (ICPS)*. 2018, vol. 2017, pp. 765–70.
[8] Ren L., Zhang P. 'Generalized microgrid power flow'. *IEEE Transactions on Smart Grid*. 2018, vol. 9(4), pp. 3911–13.
[9] Sechilariu M., Wang B.C., Locment F., Jouglet A. 'DC microgrid power flow optimization by multi-layer supervision control: design and experimental validation'. *Energy Conversion and Management*. 2014, vol. 82(March), pp. 1–10.
[10] Vazquez S., Rodriguez J., Rivera M., Franquelo L.G., Norambuena M. 'Model predictive control for power converters and drives: advances and trends'. *IEEE Transactions on Industrial Electronics*. 2017, vol. 64(2), pp. 935–47.
[11] Cortes P., Kazmierkowski M.P., Kennel R.M., Quevedo D.E., Rodriguez J. 'Predictive control in power electronics and drives'. *IEEE Transactions on Industrial Electronics*. 2008, vol. 55(12), pp. 4312–24.
[12] Li K., Hu J., Chen M. 'Model predictive control of parallel distributed generation inverters in smart microgrids'. *Proceedings of IEEE 8th International Power Electronics and Motion Control Conference*. 2016, pp. 3414–18.
[13] Hu J., Zhu J., Dorrell D.G. 'Model predictive control of grid-connected inverters for pv systems with flexible power regulation and switching frequency reduction'. *Proceedings of IEEE Energy Conversion Congress and Exposition*. 2013, pp. 540–6.
[14] Hu J., Zhu Y., Zhang G., Platt D.G. 'Predictive direct control of doubly fed induction generator for grid synchronization in wind power generation'. *Proceedings of IEEE Energy Conversion Congress and Exposition*. 2011, pp. 2381–8.

[15] Camacho E.F., Bordons C. *Model predictive control*. Berlin/Heidelberg: Springer; 2013.
[16] Hu J., Shan Y., Guerrero J.M., Ioinovici A., Chan K.W., Rodriguez J. 'Model predictive control of microgrids — an overview'. *Renewable and Sustainable Energy Reviews*. 2021, vol. 136, pp. 1–12.
[17] Hu J., Zhu J., Guerrero J.M. 'Model predictive control of smart'. *Proceedings of 17th International Conference on Electrical Machines and Systems*. 2014, pp. 2815–20.
[18] Clarke W.C., Manzie C., Brear M.J. 'An economic MPC approach to microgrid control. 2016 Aust'. *Control Conference AuCC*. 2017, vol. 2016, pp. 276–81.
[19] Nassourou M., Puig V., Blesa J., Ocampo-Martinez C. 'Economic model predictive control for energy dispatch of a smart micro-grid system'. *2017 4th International Conference on Control, Decision and Information Technologies*. 2017, vol. 2017, pp. 944–9.
[20] Zheng Y., Li S., Tan R. 'Distributed model predictive control for On-Connected Microgrid power management'. *IEEE Transactions on Control Systems Technology*. 2018, vol. 26(3), pp. 1028–39.
[21] Jia Y., Dong Z.Y., Sun C., Chen G. 'Distributed economic model predictive control for a wind-photovoltaic-battery microgrid power system'. *IEEE transactions on sustainable energy*. 2019, pp. 1–1.
[22] Zhang X., Bao J., Wang R., Zheng C., Skyllas-Kazacos M. 'Dissipativity based distributed economic model predictive control for residential microgrids with renewable energy generation and battery energy storage'. *Renewable Energy*. 2017, vol. 100(4B), pp. 18–34.
[23] Kou P., Feng Y., Liang D., Gao L. 'A model predictive control approach for matching uncertain wind generation with PEV charging demand in a microgrid'. *International Journal of Electrical Power & Energy Systems*. 2019, vol. 105(1), pp. 488–99.
[24] Sachs J., Sawodny O. 'A two-stage model predictive control strategy for economic diesel-PV-battery island microgrid operation in rural areas'. *IEEE Transactions on Sustainable Energy*. 2016, vol. 7(3), pp. 903–13.
[25] Morstyn T., Hredzak B., Agelidis V.G. 'Dynamic optimal power flow for DC microgrids with distributed battery energy storage systems. ECCE 2016 — IEEE energy convers'. *Congress and Exposition Proceedings*. 2016.
[26] Kou P., Liang D., Gao L. 'Distributed coordination of multiple PMSGs in an islanded DC microgrid for load sharing'. *IEEE Transactions on Energy Conversion*. 2017, vol. 32(2), pp. 471–85.
[27] Morstyn T., Hredzak B., Aguilera R.P., Agelidis V.G. 'Model predictive control for distributed microgrid battery energy storage systems'. *IEEE Transactions on Control Systems Technology*. 2018, vol. 26(3), pp. 1107–14.
[28] Delfino F., Ferro G., Robba M., Rossi M. 'An architecture for the optimal control of tertiary and secondary levels in small-size islanded microgrids'. *International Journal of Electrical Power & Energy Systems*. 2018, vol. 103(4), pp. 75–88.

[29] Freire V.A. ‘Home energy management for a AC/DC microgrid using model predictive control’. *International Conference on Smart Energy Systems and Technologies*. 2019, pp. 1–6.
[30] Elmouatamid A. ‘A model predictive control approach for energy management in micro-grid systems’. *International Conference on Smart Energy Systems and Technologies*. 2019, pp. 1–6.
[31] Novickij I. ‘Model predictive control based approach for microgrid energy management’. *IEEE Canadian Conference of Electrical and Computer Engineering*. 2019, pp. 1–6.
[32] Zhou X., Zhou L., Chen Y., *et al*. ‘A microgrid cluster structure and its autonomous coordination control strategy’. *International Journal of Electrical Power & Energy Systems*. 2018, vol. 100(1), pp. 69–80.
[33] Hajar K., Hably A., Bacha S., Elrafhi A., Obeid Z. ‘An application of a centralized model predictive control on microgrids’. *2016 IEEE Electrical Power Energy Conference*. 2016, pp. 1–6.
[34] Moayedi S., Davoudi A. ‘Distributed tertiary control of DC microgrid clusters’. *IEEE Transactions on Power Electronics*. 2017, vol. 31(2), pp. 1717–33.
[35] Yang X., He H., Zhang Y., Chen Y., Weng G. ‘Interactive energy management for enhancing power balances in multi-microgrids’. *IEEE Transactions on Smart Grid*. 2019, vol. 10(6), pp. 6055–69.
[36] Yang X., Zhang Y., He H., Ren S., Weng G. ‘Real-time demand side management for a microgrid considering uncertainties’. *IEEE transactions on smart grid*. 2019, vol. 10, pp. 3401–14.
[37] Garcia-Torres F., Bordons C., Ridao M.A. ‘Optimal economic schedule for a network of microgrids with hybrid energy storage system using distributed model predictive control’. *IEEE Transactions on Industrial Electronics*. 2019, vol. 66(3), pp. 1919–29.
[38] Aldaouab I., Daniels M., Ordonez R. ‘Model predictive control energy dispatch to optimize renewable penetration for a microgrid with battery and thermal storage’. *In 2018 IEEE Texas Power and Energy Conference*. 2018, vol. 2018, pp. 1–6.
[39] Puvvula Sri Rama Venkata Ranga Sai V., Kesanakurthy S.S. ‘Model predictive control approach for frequency and voltage control of standalone micro-grid’. *IET Generation, Transmission & Distribution*. 2018, vol. 12(14), pp. 3405–13.
[40] Jayachandran M., Ravi G. ‘MPC based secondary control strategy for an Islanded AC microgrid under linear loads’. *Proc 4th International Conference on Electrical Energy Systems ICEES*. 2018, vol. 2018, pp. 644–51.
[41] Lou G., Gu W., Sheng W., Song X., Gao F. ‘Distributed model predictive secondary voltage control of islanded microgrids with feedback linearization’. *IEEE Access*. 2018, vol. 6, pp. 50169–78.
[42] Perez A., Yang Y. ‘Adaptive model predictive control based on the steady state constrained ARX model’. *In 2018 IEEE Green Energy and Smart*

Systems Conference. 2018, pp. 1–6.
[43] Hausberger T., Kugi A., Deutschmann A., Eder A., Kemmetmüller W. 'A nonlinear MPC strategy for AC/DC-converters tailored to the implementation on FPGAs'. *IFAC-PapersOnLine*. 2019, vol. 52(16), pp. 376–81.
[44] Karthikeyan A., Previsic M., Scruggs J., Chertok A. 'Non-Linear model predictive control of wave energy converters with realistic power Take-off configurations and loss model'. *CCTA 2019 — 3rd IEEE Conference on Control Technology and Applications*. 2019, pp. 270–7.
[45] Yazdanian M., Mehrizi-sani A. 'Distributed control techniques in microgrids'. *IEEE transactions on smart grid*. 2014, vol. 5(6), pp. 2901–9.
[46] Hans C.A., Braun P., Raisch J., Grune L., Reincke-Collon C. 'Hierarchical distributed model predictive control of interconnected Microgrids'. *IEEE Transactions on Sustainable Energy*. 2019, vol. 10(1), pp. 407–16.
[47] Shan Y., Hu J., Chan K., Islam S. 'A unified model predictive voltage and current control for microgrids with distributed fuzzy cooperative secondary control'. *IEEE Transactions on Industrial Informatics*. in press.

Further readings

- Camponogara E., Jia D., Krogh B.H., Talukdar S. 'Distributed model predictive control'. *IEEE Control Systems Magazine*. 2002, vol. 22(1), pp. 44–52.
- Ouammi A., Dagdougui H., Dessaint L., Sacile R. 'Coordinated model predictive-based power flows control in a cooperative network of smart microgrids'. *IEEE Transactions on Smart Grid*. 2015, vol. 6(5), pp. 2233–44. doi:10.1109/TSG.2015.2396294
- Shi Y., Tuan H.D., Savkin A.V., Duong T.Q., Poor H.V. 'Model predictive control for smart grids with multiple electric-vehicle charging stations'. *IEEE Transactions on Smart Grid*. 2019, vol. 10(2), pp. 2127–36. doi:10.1109/TSG.2017.2789333
- Parisio A., Rikos E., Glielmo L. 'A model predictive control approach to microgrid operation optimization'. *IEEE Transactions on Control Systems Technology*. 2014, vol. 22(5), pp. 1813–27. doi:10.1109/TCST.2013.2295737
- Liu G., Starke M.R., Ollis B., Xue Y. 'Networked microgrids scoping study'. *Oak Ridge National Laboratory Report, ORNL/TM-2016/294*. 2016.
- Teimourzadeh S., Tor O.B., Cebeci M.E., Bara A., Oprea S.V. 'A three-stage approach for resilience-constrained scheduling of networked microgrids'. *Journal of Modern Power Systems and Clean Energy*. 2019, vol. 7(4), pp. 705–15. doi:10.1007/s40565-019-0555-0
- Golsorkhi M.S., Hill D.J., Karshenas H.R. 'Distributed voltage control and power management of networked microgrids'. *IEEE Journal of Emerging and Selected Topics in Power Electronics*. 2018, vol. 6(4), pp. 1892–902. doi:10.1109/JESTPE.2017.2773138
- Liu K., Liu T., Tang Z., Hill D.J. 'Distributed MPC-based frequency control

in networked microgrids with voltage constraints'. *IEEE Transactions on Smart Grid*, vol. 10(6), pp. 6343–54. doi:10.1109/TSG.2019.2902595

- Shahnia F., Bourbour S., and Ghosh A. 'Coupling neighboring microgrids for overload management based on dynamic multicriteria decision-making'. *IEEE Transactions on Smart Grid*. 2017, vol. 8(2), pp. 969–83.
- Gao H., Liu J., Wang L., Wei Z. 'Decentralized energy management for networked microgrids in future distribution systems'. *IEEE Transactions on Power Systems*. 2018, vol. 33(4), pp. 3599–610. doi:10.1109/TPWRS.2017.2773070
- Xu Y., Sun H., Gu W. 'A novel discounted min-consensus algorithm for optimal electrical power trading in grid-connected DC Microgrids'. *IEEE Transactions on Industrial Electronics*. 2019, vol. 66(11), pp. 8474–84. doi:10.1109/TIE.2019.2891445
- Alam M.N., Chakrabarti S., Ghosh A. 'Networked microgrids: state-of-the-art and future perspectives'. *IEEE Transactions on Industrial Informatics*. 2019, vol. 15(13), pp. 1238–50. doi:10.1109/TII.2018.2881540
- Li P., Ji H., Wang C., *et al*. 'Coordinated control method of voltage and reactive power for active distribution networks based on soft open point'. *IEEE Transactions on Sustainable Energy*. 2017, vol. 8(4), pp. 1430–42. doi:10.1109/TSTE.2017.2686009
- Lagorse J., Paire D., Miraoui A. 'A multi-agent system for energy management of distributed power sources'. *Renewable Energy*. 2010, vol. 35(1), pp. 174–82. doi:10.1016/j.renene.2009.02.029
- Cao W., Wu J., Jenkins N., Wang C., Green T. 'Operating principle of soft open points for electrical distribution network operation'. *Applied Energy*. 2016, vol. 164(9), pp. 245–57. doi:10.1016/j.apenergy.2015.12.005
- López E., Monteiro J., Carrasco P., Sáenz J., Pinto N., Blázquez G. 'Development, implementation and evaluation of a wireless sensor network and a web-based platform for the monitoring and management of a microgrid with renewable energy sources'. *International Conference on Smart Energy Systems and Technologies (SEST), 9-11 Sept*. 2019, pp. 1–6.
- Harmon E., Ozgur U., Cintuglu M.H., de Azevedo R., Akkaya K., Mohammed O.A. 'The internet of microgrids: a cloud-based framework for wide area networked microgrids'. *IEEE Transactions on Industrial Informatics*. 2018, vol. 14(3), pp. 1262–74. doi:10.1109/TII.2017.2785317
- Rahmani-Andebili M. 'Analyzing the effects of problem parameters on the operation cost of the networked microgrids'. *Proceedings of IEEE Kansas Power and Energy Conference (KPEC), 13-14*. 2020, pp. 1–6.
- Li Z., Shahidehpour M., Aminifar F., Alabdulwahab A., Al-Turki Y. 'Networked microgrids for enhancing the power system resilience'. *Proceedings of the IEEE*. 2017, vol. 105(7), pp. 1289–310. doi:10.1109/JPROC.2017.2685558
- Zhao Y., Yu J., Ban M., Liu Y., Li Z. 'Privacy-preserving economic dispatch for an active distribution network with multiple networked microgrids'. *IEEE Access*. 2018, vol. 6, pp. 38802–19. doi:10.1109/ACCESS.2018.2854280

- Tang Z., Zhang P., Krawec W.O., Jiang Z. 'Programmable quantum networked microgrids'. *IEEE Transactions on Quantum Engineering*. 2020, vol. 1, pp. 1–13. doi:10.1109/TQE.2020.3019738
- Li Y., Zhang P., Luh P.B. 'Formal analysis of networked microgrids dynamics'. *IEEE Transactions on Power Systems*. 2017, vol. 33(3), pp. 3418–27. doi:10.1109/TPWRS.2017.2780804
- Zamora R., Srivastava A.K. 'Multi-layer architecture for voltage and frequency control in networked microgrids'. *IEEE Transactions on Smart Grid*. 2018, vol. 9(3), pp. 2076–85.
- Nasser N., Fazeli M. 'Buffered-microgrid structure for future power networks; A seamless microgrid control'. *IEEE Transactions on Smart Grid*. 2021, vol. 12(1), pp. 131–40.10.1109/TSG.2020.3015573
- Wang Y., Mondal S., Deng C., Satpathi K., Xu Y., Dasgupta S. 'Cyber-resilient cooperative control of bidirectional interlinking converters in networked AC/DC microgrids'. *IEEE Transactions on Industrial Electronics* 1. doi:10.1109/TIE.2020.3020033
- Wan W., Bragin M.A., Yan B., *et al*. 'Distributed and asynchronous active fault management for networked microgrids'. *IEEE Transactions on Power Systems*. 2020, vol. 35(5), pp. 3857–68. doi:10.1109/TPWRS.2020.2976044
- Che L., Shahidehpour M., Alabdulwahab A., Al-Turki Y. 'Hierarchical coordination of a community microgrid with AC and DC microgrids'. *IEEE Transactions on Smart Grid*. 2015, vol. 6(6), pp. 3042–51. doi:10.1109/TSG.2015.2398853
- Liu S., Liu R., Zheng J., Liu X. 'Predictive function control in tertiary level for power flow management of DC microgrid clusters'. *Electronics Letters*. 2020, vol. 56(13), pp. 675–6. doi:10.1049/el.2020.0108
- Davari M., Nafisi H., Nasr M.-A., Blaabjerg F. 'A novel IGDT-based method to find the most susceptible points of cyberattack impacting operating costs of VSC-based microgrids'. *IEEE Journal of Emerging and Selected Topics in Power Electronics*, p. 1; in press. doi:10.1109/JESTPE.2020.3015447
- Delfino F., Rossi M., Ferro G., Minciardi R., Robba M. 'MPC-based tertiary and secondary optimal control in islanded microgrids'. *Proceedings of IEEE International Symposium on Systems Engineering, 28-30 Sept*. 2015, pp. 1–6.
- Yu X., Ni X., Huang A. 'Multiple objectives tertiary control strategy for solid state transformer interfaced DC microgrid'. *Proceedings of IEEE Energy Conversion Congress and Exposition (ECCE), 14-18 Sept*. 2014, pp. 1–6.
- Arefi A., Shahnia F. 'Tertiary controller-based optimal voltage and frequency management technique for multi-microgrid systems of large remote towns'. *IEEE Transactions on Smart Grid*. 2018, vol. 9(6), pp. 5962–74. doi:10.1109/TSG.2017.2700054
- Zhou Q., Shahidehpour M., Li Z., Xu X. 'Two-layer control scheme for maintaining the frequency and the optimal economic operation of hybrid AC/DC microgrids'. *IEEE Transactions on Power Systems*. 2019, vol. 34(1), pp. 64–75. doi:10.1109/TPWRS.2018.2864285
- Morstyn T., Savkin A.V., Hredzak B., Tuan H.D. 'Scalable energy

management for low voltage microgrids using multi-agent storage system aggregation'. *IEEE Transactions on Power Systems*. 2018, vol. 33(2), pp. 1614–23. doi:10.1109/TPWRS.2017.2734850

- Cintuglu M.H., Youssef T., Mohammed O.A. 'Development and application of a real-time testbed for multiagent system Interoperability: a case study on hierarchical microgrid control'. *IEEE Transactions on Smart Grid*. 2018, vol. 9(3), pp. 1759–68. doi:10.1109/TSG.2016.2599265
- Adineh B., Keypour R., Davari P., Blaabjerg F. 'Review of harmonic mitigation methods in microgrid: from a hierarchical control perspective'. *IEEE Journal of Emerging and Selected Topics in Power Electronics*,1; in press. doi:10.1109/JESTPE.2020.3001971
- Abhishek A., Ranjan A., Devassy S., Kumar Verma B., Ram S.K., Dhakar A.K. 'Review of hierarchical control strategies for DC microgrid'. *IET Renewable Power Generation*. 2020, vol. 14(10), pp. 1631–40. doi:10.1049/iet-rpg.2019.1136
- Babazadeh-Dizaji R., Hamzeh M. 'Distributed hierarchical control for optimal power dispatch in multiple DC microgrids'. *IEEE Systems Journal*. 2020, vol. 14(1), pp. 1015–23. doi:10.1109/JSYST.2019.2937836
- Awal M.A., Yu H., Tu H., Lukic S.M., Husain I. 'Hierarchical control for virtual oscillator based grid-connected and islanded microgrids'. *IEEE Transactions on Power Electronics*. 2020, vol. 35(1), pp. 988–1001. doi:10.1109/TPEL.2019.2912152
- Zaery M., Wang P., Wang W., Xu D. 'Distributed global economical load sharing for a cluster of DC microgrids'. *IEEE Transactions on Power Systems*. 2020, vol. 35(5), pp. 3410–20. doi:10.1109/TPWRS.2020.2975378
- Espina E., Llanos J., Burgos-Mellado C., Cardenas-Dobson R., Martinez-Gomez M., Saez D. 'Distributed control strategies for microgrids: an overview'. *IEEE Access*. 2020, vol. 8, pp. 193412–48. doi:10.1109/ACCESS.2020.3032378

Index

adaptive droop control concept 104–5
alternating current-coupled microgrids 4–5
alternating current–direct current (AC–DC)-coupled hybrid microgrids 6 *see also* hybrid alternating current–direct current microgrids
alternating current (AC) subgrid
  capacitor current 136
  cost function 136, 137
  grid-connected mode 136
  grid synchronization 137
  mathematical model 135, 136
  output active and reactive powers 135
  state-space system 136
alternating direction method of multipliers (ADMM) 114
average load sharing (ALS) approach 48–50

battery energy storage station (BESS) DC–DC converters 189
  bidirectional buck-boost converters 183
  buck-boost converter control 186–7
  charging and discharging process 192–4
  converter discrete predictive models 183–4
  cost function 186
  discrete-time model 185
  Kirchhoff's Current Law 184
  power balance 184
  single-ended primary-inductor converters 184
beta method 81–2
brushless doubly fed twin stator induction generator (BDFTSIG) 69

cascaded H-bridge (CHB) converters 157
centralized control, parallel inverters 45–6
centralized secondary control technique 206
circular chain control, parallel inverter 46–7
Clarke transformation 212
consensus-based cooperative droop control 105, 178
constant speed constant frequency (CSCF) system 65–6

constant voltage method 81
Controller Area Network (CAN) 110
conventional droop control 51
cross circulating current 178
Curie point 68
current source inverters (CSIs) 23

deadbeat-based predictive control approach
  AC–DC conversion system 32–4
  advantages 31–2
  DFIG-based wind power system 31
  switching table-based direct power control 32, 33
  working principle 31
direct current-alternating current (DC–AC) converters 22–3
  circuitry topologies 22–3
  grid-feeding inverters 24
  grid-forming inverters 23
  grid-supporting power inverter 24
  multilevel inverters 23
direct current-coupled microgrids
  vs. AC MGs 7
  advantage 7
  drawbacks 8
  renewable energy sources 7
  structure 5–6
direct current-direct current (DC–DC) converters
  distributed energy resource-fed DC 21
  high-voltage-gain 22
  isolated converters 21
  multiport 22
  non-isolated converters 21
  selection 21
direct power control (DPC) 27, 28, 71–2
direct torque control (DTC) 71
discrete-time model 181
distributed energy resources (DERs) 4, 180
distributed generation (DG) 1
  advantages 61
  configurations 61–2
  solar PV system 62
  technical challenges 63
  wind energy conversion system 62
distributed model predictive control (DMPC) 113
distributed renewable power generation
  distributed generation (DG) 61–3
  solar photovoltaics generation: *see* solar photovoltaics generation

wind power generation 63–74
distributed secondary control approaches 206
distributed two-level tertiary control 112
distribution network operator (DNO) 113
doubly fed induction generator (DFIG) 68–9
doubly-fed induction generator (DFIG)-based wind power system 31, 61, 62
direct power control 71–2
direct torque control 71
finite-state model predictive control technique 72
grid synchronization 72
droop-based power-sharing method 208–10
droop mechanism
MG primary control
adaptive droop control concept 104–5
adaptive virtual impedance 105
limitations 101
low-voltage resistive MGs 105
MIMO state-space model 106
mismatch and unknown line impedances 103–4
model predictive control 106
nonlinear loads 103
P–f droop 101
power-sharing method 105
principle 100
Q–V droop 101
renewable energy resources 104
traditional cascaded linear control 105–6
voltage and frequency deviations 102
voltage regulation and load sharing accuracy 102–3
zero common-mode voltage method 106
parallel inverter-based AC power system 188

energy storage 14–15
energy storage systems (ESSs) 1, 14–15, 126, 158–9
control structure 134
modeling 133–5

finite control set-MPC (FCS-MPC) 41–3
finite-control set MPC-based MPPT 83
flexible AC transmission system (FACTS) controllers 155
Fuzzy logic control 27–9

generalized microgrid power flow (GMPF) 233
grid-feeding inverters 24
grid-forming inverters 23
grid-level MPC 43, 44

grid-supporting power inverter 24

hierarchical control architecture
  primary control
    droop coefficients 100
    droop mechanism 100–6
    parallel operation 100
    requirements 99–100
  secondary control
    centralized secondary control 107
    decentralized secondary control 111
    distributed secondary control 107, 109–11
    grid synchronization 107
  tertiary control
    distributed two-level 112
    DMPC strategy 113
    energy storage systems 112
    interior-point optimization-based tertiary control 112
    MPC strategy 112–14
    networked MGs 113
    network power quality requirements 112
    operational cost 113
    scenario-based two-stage stochastic programming model 112
hierarchical control pyramid 232
high-voltage-gain DC–DC converters 22
hill-climb searching algorithm 71
home energy management system (HEMS) 241
hybrid alternating current–direct current (AC–DC) microgrids
  energy management level 129, 130
  grid-connected mode 128
  hierarchical MPC scheme 130
  hybrid power network 128
  power converter level 130
  power exchange requirement 127
  SHE-PWM module 129–30
  structure 127
  technical problems 129
  unit-power control and feeder-flow control 128
  V–I droop control scheme 128–9
  voltage-voltage droop approach 129

information and communication technologies 15–16
insulated-gate bipolar transistor (IGBT) bridges 32
interior-point optimization-based tertiary control 112
International Energy Agency (IEA) 125
International Renewable Energy Agency (IRENA) 125

Kirchhoff's current law (KCL) 136, 160
Kirchhoff's voltage law (KVL) 136

low-voltage distribution networks 98
low-voltage resistive microgrids 178

master-slave control, parallel inverter 47–8
maximum power point tracking (MPPT)
  solar module 131–2
  solar photovoltaics (PVs) system 190–1
    beta method 81–2
    constant voltage method 81
    finite-control set MPC-based MPPT 83
    fixed duty cycle 81
    MPP locus characterization 81
    P&O method 82
    system oscillation and ripple correlation 82
    temperature method 82
  string-array PV configuration 154
microgrid central controller (MGCC) 2
microgrid clusters (MGCs) 129, 207
microgrids (MGs)
  AC–DC-coupled hybrid 6
  AC subgrid modeling 135–7
  alternating current-coupled 4–5
  cascaded linear control 178
  control flexibilities 4
  direct current-coupled 5–8
  distributed energy resource 4, 180
  distributed generation (DG) units 3
  energy storage 14–15, 126
  f–P/Q droop control 178
  hierarchical control architecture: *see* hierarchical control architecture
  hybrid AC–DC MG 127–9
  information and communication technologies 15–16
  inverter control techniques development 180
  laboratory 3
  lack of systematic approaches 13–14
  large-scale grid integration 14
  microgrid central controller 2–3
  modeling 97–8
  multiple-input–multiple-output state-space model 178–9
  networked 8–9
  new semiconductor devices 12
  objectives 2, 126
  operating modes 3

operation considerations
power balancing 10
power quality 10–11
power sharing 9–10
seamless mode transition 11
system stability 11–12
optimal power exchange 179
physical electric structures 179
power electronic converters and control 12–13
power stations 4
primary control 178
renewable intermittency 13
smart sensors 15
static transfer switch 3–4
structure 2, 126
system-level algorithms 179
mixed-integer linear programming (MILP) 113, 129
model predictive control (MPC) 72
AC–DC conversion 39, 41
characteristics 44
cost function 39, 44
DC MGs 244–5
disadvantages 44–5
distributed and decentralized control 245
droop-free MPC structure 178
droop mechanism 106
finite control set-MPC (FCS-MPC) 41–3
fluctuation output 141
grid-connected operation 141–3
grid-level MPC 43, 44
grid-synchronization and connection 143–5
holistic and intelligent approaches 244
islanded operation 142–3
new mathematical formulation 244
parameter design 39
photovoltaic-energy storage system microgrids: *see* photovoltaic-energy storage system microgrids
PMSG-based wind systems 73–4
power converter control 138
AC subgrid 135–7
energy storage systems (ESSs) 133–5
solar module 130–2, 131
wind turbine system modeling 132–3
principle 39, 40
system level control

energy management 139
mode 1 operation 139
mode 2 operation 139–40
mode 3 operation 140
system-level MPC 43
system predictive model 39
tertiary control strategy: *see* tertiary control strategy
tertiary-level 113
model predictive power control (MPPC), 138
DC–AC converter, 163
DC–DC bidirectional converter control, 162
photovoltaic-energy storage system (PV-ESS) microgrids 158–63
model predictive voltage control (MPVC) 136
Clarke transformation 212
conventional MPVC method 212–13
conventional overall control scheme 215–16
improved MPVC 213–15
three-phase voltage conversion 215–16
modular energy management system (EMS) 129
multiagent system (MAS) 206
multiple-input–multiple-output (MIMO) state-space model 106, 178
multiport DC–DC converters 22

networked microgrids 8–9
neutral-point-clamped (NPC) inverter 73–4
neutral point potentials (NPP) perturbation-based zero sequence circulating current (ZSCC) feedback control method 106

on-load tap changer (OLTC) 155
operational cost 113

permanent-magnet synchronous generator (PMSG) 67–8, 73–4, 132, 141
photovoltaic-energy storage system (PV-ESS) microgrids
bidirectional DC–DC converter 157
boost converter 154
cascaded feedback loop 156
centralized structure 153
conventional control method 156
flexible AC transmission system controllers 155
flexible power injection 167–8
grid-connected inverter 156
grid integration 154
grid voltage support 168–9
maximum power point tracking 154
model predictive control scheme 156–7
model predictive power control scheme

AC-side system 162
buck-boost converter 159–61
DC–AC converter 162, 163
DC–DC bidirectional converter 167
energy storage systems 158, 159
grid-connected inverter 168
on-load tap changer 155
operational configurations 153
predictive voltage control scheme 157
PV converter topology 154
PV inverters' reactive power capability 155
SMA solar inverters 156
string-array PV configuration 154
variable energy generation 154
verification 166–9
voltage support
conventional voltage regulators 164
power compensation 165
power exchange 165
power flows 164
PV inverter active and reactive capacity 165–6
traditional power networks 164
plug-and-time-shift charge strategy 15
point of common coupling (PCC) 2
power electronic converters
control methods 25
DC–AC converters 22–3
DC–DC converters 21–2
parallel inverters
average load sharing (ALS) approach 48–50
centralized control 45–6
circular chain control 46–7
droop control 50–2
master-slave control 47–8
single converter control
direct control strategy 27
Fuzzy logic control 27–9
predictive control 30–45
sliding mode control 29–30
voltage-oriented control 25–7
power-sharing method 105
primary control 231
pulse width modulation (PWM) 24

quadratically constrained quadratic program (QCQP) 112

renewable energy sources (RESs) 1

scenario-based two-stage stochastic programming model 112, 232
secondary control technique
  centralized 206
  decentralized control 207
  distributed control schemes 206
  improved model predictive voltage control 212–16
  microgrid cluster (MGC)-layer control 207
  multiagent system network control 206
  solar irradiation 219
  voltage quality 221–2
  washout filter-based power-sharing strategy 208–12
selective harmonic elimination pulse width modulation (SHE-PWM) module 129–30
Sensformer 15
single- phase multiple-stage PV power electronics 78–9
single-phase single-stage PV power electronics 78
sliding mode control (SMC) 29–30
smart sensors 15
solar photovoltaic (PV) power system 1
  cost function 181
  global power generation 125
  grid-side inverter control 83–4
  maximum power point tracking (MPPT) control 80–3
  model predictive current control algorithm
    BESS DC–DC converters 183–7
    DC–DC boost converter 182–3
  parallel inverters
    control strategy 189
    cost function 188
    discrete-time form 188
    droop mechanism 188
    dynamic behavior, capacitor 188
    power sharing 193–6
    system parameters 190
  principle and configuration
    centralized PV configuration 74–6
    current *vs.* voltage characteristic 74, 75
    module inverters 77
    power output performance 74, 75
    principle and configuration 74–7
    string-array PV systems 76–7
  PV-battery-based AC MG 181
  single-phase multiple-stage 78–9
  single-phase single-stage 78

solar module
mathematical model 130–1
maximum power point tracking 131–2
output characteristics 131
three-phase single-stage 79–80
squirrel cage induction generator (SCIG) system 69
static transfer switch (STS) 3–4
steady state constrained autoregressive with exogenous terms model (SSARX) model 206
string-array PV systems 76–7
SunPower Spr305E-WHT-D solar array 131
switching table-based direct power control (SDPC) 27, 32, 33
system-level MPC 43, 237–8

tertiary control strategy
considerations 234
generalized microgrid power flow (GMPF) 233
islanded MG 239
MPC
benefits 238–9
control objectives 235–7
economic optimization 239–40
holistic control strategy 240
networked MGs 242–3
schematic illustration 235, 236
system-level MPC methods 234, 237–8
two-layer MPC strategy 240
unbalanced voltage issues 232
voltage deviations 233
optimal control actions 238
optimization method 232
receding horizon control 233
scenario-based two-stage stochastic programming model 232
three-phase photovoltaics (PVs) topology 79–80
tip speed ratio (TSR) 64
traditional power grid 1
transmission system operator (TSOs) 237
two-stage decentralized energy management framework 8
two-vector-based low-complexity model predictive DPC 72

uninterruptable power supply (UPS) 26

variable speed constant frequency (VSCF) wind generators
advantages 66–7
comparison 70
doubly fed induction generator 68–9

permanent-magnet synchronous generator 67–8
squirrel cage induction generator 69
wound field synchronous generator 67
vector-sequence-based predictive control (VPC)
active and reactive power derivatives 36
concatenated voltage vectors 32–3
controller performance 36
improved 37
principle 33–5
symmetric 3+3 vectors sequence 36
system performance 37–9
vector selection criteria 34–5
voltage-oriented control (VOC)
block diagram 25, 26
linear control technique 26–7
merits 25
uninterruptable power supply 26
voltage reference 25
voltage-tracking trajectory 214
voltage-voltage droop approach 129

washout filter-based power-sharing strategy
droop-based power-sharing method 208–10
load profile 218
overall control strategy 217
PCC voltage compensation 211–12
secondary control method 210
wind energy
cumulative installed capacity 126
global wind power 125
wind power generation
constant speed constant frequency system 65–6
cost distribution 64
grid synchronization 72–3
grid voltage 73
power flow path 63
power regulation 72–3
power signal feedback 71
variable speed constant frequency system 66–70
wind and rotor speed 70–1
wind energy 63
wind turbine 64–5
wind turbine system
generator-side converter 133
modeling 132–3
permanent-magnet synchronous generator 132

stator voltage reference 133
structure 132
wound field synchronous generator (WFSG) 67

zero sequence circulating current (ZSCC) feedback control method 106
zero-sequence circulating currents 178

Model Predictive Control for Microgrids
From power electronic converters to energy management

Microgrids have emerged as a promising solution for accommodating the integration of renewable energy resources. But the intermittency of renewable generation is posing challenges such as voltage/frequency fluctuations, and grid stability issues in grid-connected modes. Model predictive control (MPC) is a method for controlling a process while satisfying a set of constraints. It has been in use for chemical plants and in oil refineries since the 1980s, but in recent years has been deployed for power systems and electronics as well.

This concise work for researchers, engineers and graduate students focuses on the use of MPC for distributed renewable power generation in microgrids. Fluctuating outputs from renewable energy sources and variable load demands are covered, as are control design concepts. The authors provide examples and case studies to validate the theory with both simulation and experimental results and review the shortcomings and future developments.

Chapters treat power electronic converters and control; modelling and hierarchical control of microgrids; use of MPC for PV and wind power; voltage support; parallel PV-ESS microgrids; secondary restoration capability; and tertiary power flow optimization.

About the Authors

Jiefeng Hu is an associate professor in power converters and smart microgrids, and the program coordinator (electrical engineering) with Federation University Australia.

Josep Guerrero is a full professor with the Department of Energy Technology, Aalborg University, Denmark.

Syed Islam is a professor and the dean for the School of Engineering, Information Technology and Physical Sciences at Federation University Australia.

ISBN 978-1-83953-397-6

9 781839 533976 >

The Institution of Engineering and Technology
theiet.org
978-1-83953-397-6